Singular Eigenfunctions in Hydrodynamic Stability : The Roles of Rotation, Stratification and Elasticity

A Thesis
Submitted for the Degree of
Doctor of Philosophy

by

Anubhab Roy

Engineering Mechanics Unit
Jawaharlal Nehru Centre for Advanced Scientific Research
(A Deemed University)
Bangalore – 560 064

MARCH 2013

Katul, Rivu and My Parents

DECLARATION

I hereby declare that the matter embodied in the thesis entitled "**Singular Eigenfunctions in Hydrodynamic Stability : The Roles of Rotation, Stratification and Elasticity**" is the result of investigations carried out by me at the Engineering Mechanics Unit, Jawaharlal Nehru Centre for Advanced Scientific Research, Bangalore, India under the supervision of Prof. Ganesh Subramanian and Prof. Rama Govindarajan and that it has not been submitted elsewhere for the award of any degree or diploma.

In keeping with the general practice in reporting scientific observations, due acknowledgment has been made whenever the work described is based on the findings of other investigators.

Anubhab Roy

CERTIFICATE

We hereby certify that the matter embodied in this thesis entitled "**Singular Eigenfunctions in Hydrodynamic Stability**" has been carried out by Mr. Anubhab Roy at the Engineering Mechanics Unit, Jawaharlal Nehru Centre for Advanced Scientific Research, Bangalore, India under our supervision and that it has not been submitted elsewhere for the award of any degree or diploma.

Prof. Ganesh Subramanian
(Research Supervisor)

Prof. Rama Govindarajan
(Research Supervisor)

Acknowledgements

This thesis has seen the light of day due to contributions and encouragements of several individuals.

First amongst all, I would like to thank *Ganesh Subramanian* for being a mentor extraordinaire. His uncompromising attitude for doing science and insistence on thinking deeply about problems has helped me grow immensely as a researcher. I am grateful to him for being extremely perseverant with me, when things weren't smooth sailing, and always attentively listening to the various ideas I barraged him with, how much soever naive and raw they may be. In my years as a graduate student if there is something that I can never complain about, would be a complete freedom to choose my problems. I would like to thank him for that.

For guiding me through challenges from my first day in JNC to this day of completion, I am immensely grateful to *Rama Govindarajan*. Besides being a supervisor who showed exemplary patience and immense faith in my abilities, she has has been an enviable counselor in making life decisions. Her constant encouragement and allowing me to work the way I wanted, has been instrumental in my appreciating the delights of teaching.

I am grateful to *K. R. Sreenivas* and *Santosh Ansumali* for their valuable discussions and insights at various stages of my research and *Diptiman Sen*, *Chandan Dasgupta*, *Joseph Mathew* and *Debasis Sengupta* for the insightful courses they offered and, in the process, exciting me about topics beyond my research area.

I would like to thank Woods Hole Oceanographic Institute for giving me the opportunity to spend three wonderful months in the summer program; with special mention for my supervisors - Neil Balmforth and Colm-cille Caulfield.

JNCASR, DST, APS and WHOI are gratefully acknowledged for providing financial support for attending conferences and workshops.

During the course of my stay in JNC there have been innumerable friends who have made research exciting and life joyous. I would like to thank -

Kaushik, Pinaki, Ratul for my first introduction to research life; an attitude of skepticism, curiosity and unabashed zest for life - I owe it to them, *Harish* for being an amazing comrade in expeditions both in the mountains and the world of fluid dynamics alike, *Devranjan*

and *Ashish* for the fun times in JNC and adventures in Europe, *Vivekanand* and *Bishakh* for the 'good times' during my MS days and always being at beck and call for sending across papers after they left, *Mukund* for his discourses on 'life, universe and everything', *Sumesh* for his lessons on birds and life, *Ponnu* and *Dhiraj* for their company and merriment all along my PhD, *Vinod, Sameen, Kirti, Vijay, Priyanka, Rajapandiyan, Gayathri, Aditya, Rakshith, Vivek, Rahul, Vinay, Ujjayan, Dinesh, Vishwanath, Srikanth, Saikishan, Rohith, Navaneeth, Prashanth, Rajesh, Shahjahan, Jose, Mamta, Milind, Divya, Shashank, Vybhav, Rohan, Sunil, Croor, Deepak, Siddharth, Shiwani, Abhishek, Krithika* for making EMU a vibrant place.

Vikas, Saikat, Saransh, Shrimant, Ashutosh, Anupam, Parijat, Priyank and *Mintu*, the *Banarasi junta*, who always provided encouragement and support to pursue research.

Finally none of this would have been possible without the support of *my parents*. I am thankful to my brother, uncle and grandmother, who have at various stages propelled me and helped me achieve whatever I have managed to achieve today. My surviving through PhD and continuing to believe in myself has happened only because of the sacrifices and selfless contributions of my wife, *Senjuti*.

And yes, *so long and thanks for all the fish*!

Abstract

Hydrodynamic stability, an important branch of fluid mechanics, owes its popularity to the successful prediction of the transition of (unstable) laminar states in a wide class of flows. While the traditional approach has been reliant on an analysis within a modal framework, the merits of a nonmodal approach have been recognized in the last two and a half decades particularly in the context of shearing flows. Although the non-modal approach typically involves the solution of an initial value problem, the resulting temporal response, for short times and at large Reynolds numbers (Re), may also be understood in terms of the dynamics of the underlying inviscid continuous spectra (CS). The equations governing the evolution of small-amplitude perturbations in shearing flows in this limit are usually singular, and the continuous spectra owe their origin to such singular points. The thesis is mainly concerned with the structure of the singular eigenfunctions comprising such inviscid continuous spectra in rotating flows, and to a lesser extent, with the singular eigenfunctions in homogeneous and stratified parallel shearing flows, and rotational flows in the presence of elasticity. The manner in which such eigenfunctions may be superposed to obtain a solution of the initial value problem is also considered. The detailed analysis is devoted to the singular modes of a Rankine vortex both in two and three dimensions; an analytically soluble problem that nevertheless offers insight into the singular eigenfunctions associated with more general vorticity profiles. The Rankine analysis is then extended to smooth vortices. In three dimensions, such an extension is made by drawing an analogy with (stably) stratified shear flows and the associated continuous spectra. The final part of the thesis discusses the continuous spectrum of an elastic vortex column in the limit of high Reynolds and Deborah numbers. Further, a novel two-dimensional instability of an elastic vortex column, that arises from the resonant interaction of elastic shear waves, is analyzed in detail both numerically and via an asymptotic analysis valid in the limit of weak elasticity.

Effects of Rotation and Stratification

The motivation to study singular eigenfunctions in rotating flows is, in part, to understand the response of a vortex column to imposed vortical disturbances, the vortical disturbance here being regarded as a surrogate for ambient turbulence. Vortices are ubiquitous in nature and range from massive tropical cyclones, large trailing vortices shed by aircrafts down to the tiny whorls in a coffee cup. At high Reynolds numbers, vortices offer an economical description of fluid motion and a clear understanding of their dynamics aids better prediction and control in fluid dynamical problems of both engineering and geophysical interest.

The Rankine vortex is the simplest canonical vortical structure, consisting of a core of rigidly rotating fluid surrounded by an irrotational exterior. On account of Coriolis forces, the vortex

column supports an intricate array of oscillations eponymously known as the Kelvin modes, and that comprise the discrete spectrum. The Kelvin modes possess vorticity only inside and at the edge of the core, and are thus incapable of representing the effect of an exterior vortical disturbance. However, recent numerical investigations have highlighted the algebraic growth of vortex columns subject to appropriate exterior disturbances (optimal perturbations). The incompleteness of the discrete spectrum is, in fact, a generic feature of shearing flows, and a complete basis is obtained only on inclusion of the appropriate CS-eigenfunctions. Accordingly, the work in the thesis, on one hand, develops an extended modal picture that includes the CS-eigenfunctions capable of representing vortical disturbances outside the core; and simultaneously solves the Cauchy initial value problem on the other. The CS-modes in two dimensions have a twin-vortex-sheet structure, the vortex sheets being threaded by axial vortex lines. In three dimensions, the CS-modes have core vorticity and belong to one of two families depending on the nature of the singular structure at the critical radius. The Λ_1 family is an extension of the 2D CS-modes since the singularity is again a vortex-sheet now threaded by helical lines; the Λ_2 family has a localized axial jet riding at the critical radius leading to a dipole-singularity in the perturbation vorticity field. It is shown, for a Rankine vortex, that the modal representation for the evolution of an arbitrary initial vorticity field, including both discrete and continuous spectra, is identical to the solution of the initial value problem, thereby resolving the issue of completeness of the eigenfunction expansion. The solution of the initial value problem also identifies three mechanisms that in isolation, and when acting in consonance, lead to short-time algebraic growth. These involve the stretching-tilting of perturbation vorticity by the mean shear (termed the anti-lift up effect), the transverse alignment of perturbations with an initial favorable tilt that allows for an extraction of energy from the mean shear (the Orr mechanism), and resonant interactions of the discrete and continuous spectra. The growth rates obtained for the Rankine vortex appear to be consistent with the recent numerical findings.

Having characterized the spectrum of a Rankine vortex in its entirety, we examine smooth vorticity profiles corresponding to more realistic vortices. The structure of the 2D CS-modes for this case are developed based on a recipe already known for homogeneous plane parallel flows with curved velocity profiles. The eigenfunctions depart from those of a Rankine vortex in having a non-local PV-singular contribution arising from the base-state vorticity gradient. The modal superposition of the 2D CS-modes, again developed in a manner similar to that for parallel flows, allows for the identification of an exponentially damped solution known as a *quasi-mode*. The resulting solution of the initial value problem in two dimensions exhibits exponential asymptotics in an intermediate time regime. This *quasi-mode* regime precedes the inevitable algebraic decay associated with the long-time dephasing of the 2D CS-modes. Analysis of the 3D CS-modes associated with a smooth vortex is more complicated. A local analysis, in the vicinity of the critical radius, highlights the similarity between the 3D CS-modes and the CS-modes in stratified shear flow, allowing one to define analogs of the Λ_1 and Λ_2 families for a smooth vortex. The 3D CS-modes of a smooth vortex are generalized functions that require a Hadamard-finite-part interpretation. Further, based on the analogy between the role of buoyancy forces in stratified flows, and Coriolis forces in rotational flows, we develop analytically soluble stratified flow analogs of both a Rankine and a smooth vortex. The soluble analogs highlight

the approach of the modal superposition for a stratified shear flow towards the more familiar form for the homogeneous case.

Effects of Elasticity

Here, we focus on the singular eigenfunctions associated with an elastic vortex column in two dimensions. The parameter regime considered corresponds to high Reynolds and Deborah numbers (De) and is relevant to rapid swirling flows of elastic liquids (dilute polymer solutions). Inertia and elasticity are the dominant physical factors, and their relative importance is determined by the ratio of the aforementioned parameters known as the elasticity number (E = De/Re). The singular eigenfunctions comprising the 2D CS-spectrum now have a pair of singularities corresponding to forward and backward propagating (pre-stressed) elastic shear waves. Next, we analyze a novel instability of an elastic vortex column whose physical origin may be traced to the resonant interaction of a pair of transverse shear waves at the edge of the vortex core - a backward travelling wave at the vortex edge has the same velocity as a forward travelling wave located at a distance $O(\sqrt{\mathrm{E}})$ from the edge. The unstable mode is determined numerically using two complementary techniques. The first technique adopted for solving the boundary value problem is a shooting method using a 'carpet-bombing' approach. The second technique is a Chebyshev collocation based compound matrix method for solving the governing nonlinear eigenvalue problem. An analytical approach, involving a (multiple)-boundary layer analysis, shows that the growth rate in the limit of small but finite E is transcendentally small. The difficulties in both numerical and analytical approaches, in the small E limit, arise due to the close approach of the unstable mode towards the continuous spectrum with the marginally stable mode being a singular one; this is unlike classical inviscid theory wherein the marginal mode is a regular S-wave.

List of Figures

List of Tables

Contents

Chapter 1

Introduction

"... not every solution of the equations of motion, even if it is exact, can actually occur in Nature. The flows that occur in Nature must not only obey the equations of fluid dynamics, but also be stable."

- Landau & Lifshitz [1987]

This has been a question that has perplexed fluid dynamicists for centuries. The ubiquitous nature of turbulence, and the inability to offer a universal theory of it, led many to try tackling what was perceived as a simpler problem: of transition from a laminar state to a turbulent one. In the last two centuries, such efforts have offered remarkable insights many-a-times and have helped in making successful predictions. The description has undergone major reforms from time to time, progressing from the early experiments of Osborne Reynolds and G I Taylor to the sophisticated machinery of control theory used presently. Interested reader can find excellent references in the form of both monographs (Lin [1955], Chandrasekhar [1961], Drazin & Reid [1981], Craik [1985], Schmid & Henningson [2001], Charru [2011]) and reviews (Bayly *et al.* [1988],Huerre & Rossi [1998],Huerre [2000], Chomaz [2005], Schmid [2007]).

Early studies in hydrodynamic stability arose from the theory of water waves, with Newton

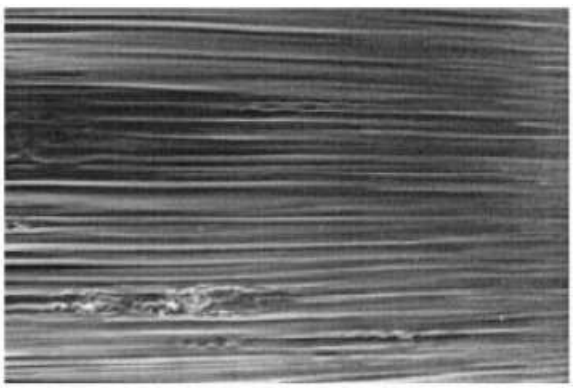

Figure 1.1: Experimental observations of streaky structures in boundary layers (Matsubera & Alfredsson [2001])

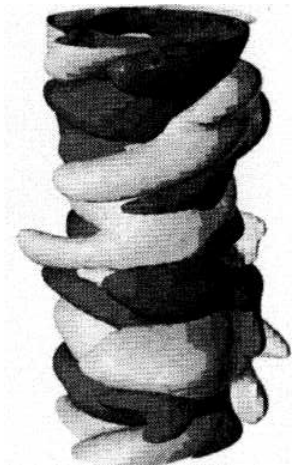

Figure 1.2: Direct numerical simulations (DNS) depicting vortex interaction with fine-scale homogeneous, isotropic turbulent field (Melander & Hussain [1994])

followed by seminal works by Laplace, Cauchy, Poisson and later, by Stokes. Incidentally most of the early work was done before the world got acquainted with Fourier series, although Cauchy employed de facto Fourier transforms (Craik [2004],Craik [2005]). The advent of harmonic analysis facilitated the study of stability of mechanical systems by introducing the notion of

normal modes. A normal mode is a pattern of oscillations in which the entire system oscillates in space/ time with the same wave-length/ frequency. A coupled pendulum with two degrees of freedom has two normal modes whereas a vibrating string has infinitely many normal modes, often labelled as harmonics in musical instruments. The beauty of normal modes lies in their ability to offer a complete description for the evolution of any arbitrary disturbance in *most* cases. We mention *most* because the normal modes usually referred to, constitute the discrete

(a) Trailing vortices (http://www.myskymom.com/)

(b) Numerical evidence of 'bursting' of a trailing vortex (Moet *et al.* [2005])

(c) Jupiter's Giant Red Spot (source: Wikipedia)

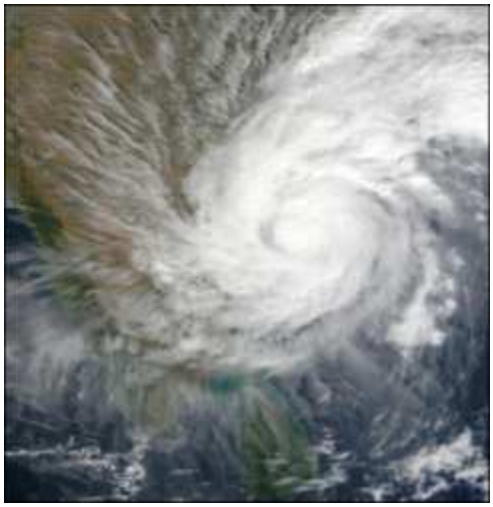

(d) Tropical cyclone approaching Andhra Pradesh, India on Dec. 17, 2003 (nasa.gov)

Figure 1.3: Vortices in various engineering and geophysical scenarios.

spectrum of the linearized stability operator. As it turns out, problems in hydrodynamic stability of shearing flows are exceptional in the above sense in that the governing operator almost always has an associated continuous spectrum. Among other things, a continuous spectrum arises due to an unbounded domain, or due to the operator having singular points in the (possibly bounded) domain of interest[1]. Continuous spectrum for shear flows is mathematical manifestation of

[1]Strictly speaking, a differential operator has a purely discrete spectrum if the associated integral operator happens to be compact. An operator $K \in L(\mathcal{H})$ ($\mathcal{H}$ is a Hilbert space and $L(\mathcal{H})$ are bounded operators on $\mathcal{H}$) is said to

filamentation process to small scales. The continuous spectra that arise due to the former reason (for instance, the viscous continuous spectrum for the Blasius boundary layer - Grosch & Salwen [1978]) will not be investigated in the present dissertation. The focus in this thesis will thus be on the continuous spectra that arise due to the latter reason, namely , the governing differential operator possesses singular points in the flow domain. Although the first reference to such singular eigenfunctions in the context of hydrodynamic stability can be found as early as Rayleigh [1945], the role of the continuous spectrum in various problems of transport theory received a major impetus from the works of Eliassen *et al.* [1953] and Case [1960] in hydrodynamic stability and Van Kampen [1955] and Case [1959] in the context of plasma oscillations. The framework developed in the present thesis, for analyzing singular eigenfunctions, is largely motivated by the above efforts. Despite being known for such a long time, singular eigenfunctions have remained relatively obscure entities to classical hydrodynamics stability practitioners, in part due to exponential stability theory finding them to be mostly neutrally stable (such singular modes may also be damped on occasion; this is the case for complex fluids such as dilute polymer solutions (Gorodtsov & Leonov [1967]) and bacterial suspensions (Subramaniam & Nott [2011]), when one accounts for the finite relaxation time of the underlying microstructure). An equally important reason for this obscurity is the notion that a superposition of such singular eigenfunctions would always exhibit an algebraic decay for long times due to the de-cohering action of differential shear. This belief has, however, undergone a change with a revival of interest in non-modal stability theory in the last two decades (Trefethen *et al.* [1993], Schmid [2007])[2]. In the specific context of turbulence, this revival (Farrell [1984], Farrell [1987]) has led to the notion of the transition route to turbulence being generalized to include one involving an algebraic instability in addition to the more traditional exponential instability route. Figures 1.1 and 1.2 show nonlinear manifestations of non-modal behavior in two systems - streak formation (a consequence of the most dangerous initial condition in shear flows as predicted by non-modal stability theory) in a boundary layer and an isolated vortex, an exponentially stable structure, that can respond to external disturbances (a turbulent field as shown in the DNS) via non-modal dynamics (to be discussed in detail in this thesis).

This thesis studies the nature of the singular eigenfunctions comprising the continuous spectra in the shear flow problems involving rotation, stratification and elasticity. Physically these singular eigenfunctions occur due to the allowance for arbitrarily large cross-stream gradients in the absence of diffusion of vorticity/momentum (due to viscosity in Newtonian fluids) or diffusion of stress (due to macromolecular diffusion in complex fluids).

A major portion of this thesis tries to address evolution of disturbances in swirling flows. Besides being one of the most easily identifiable objects in any turbulent flow, vortices/coherent structures are objects of immense engineering and geophysical interest (figure 1.3). Efforts in understanding aircraft trailing vortices (Widnall [1975], Spalart [1998]) or geophysical vortices

be compact if for every bounded sequence, z_n, of vectors of $\mathcal{H}$, the sequence, Kz_n, has a convergent subsequence. In finite dimensions, by Bolzano-Weierstrass theorem this is automatically true. In infinite dimensions this is not necessarily true. E.g - an infinite sequence of orthonormal basis functions in a Hilbert space is bounded but fails to contain a convergent subsequence.

[2]It would be unfair to portray non-modal stability theory as a recent development in hydrodynamic stability theory. Orr [1907] can easily be attributed to be the first to provide a comprehensive explanation for non-modal behavior of disturbances in shear flows. One can find an excellent literature review in this regard in Monin & Yaglom [1997].

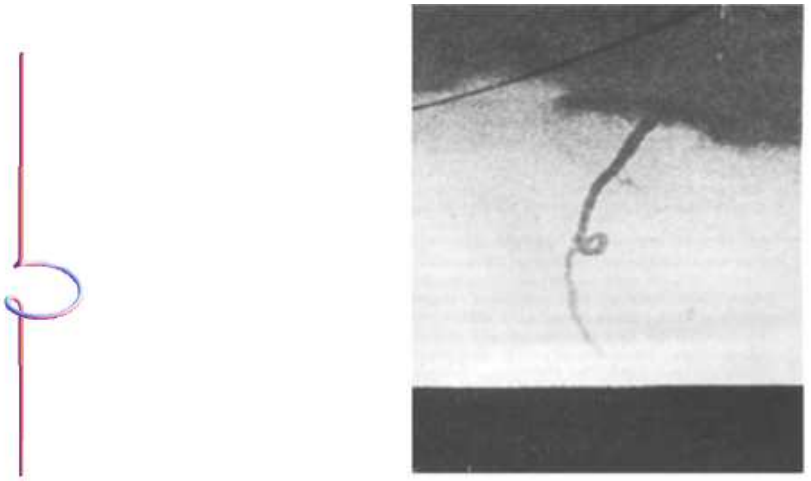

(a) (b)

Figure 1.4: Bending waves in vortices - (a) A nonlinear bending wave (a 'soliton') in a vortex filament, (b) A tornado exhibiting bending waves (Aref & Flinchem [1984]).

like Jupiter's giant red spot and tropical cyclones (Montgomery & Kallenbach [1997]) have been instrumental in creating a vast body of literature on vortex stability. An isolated vortex supports waves and as already mentioned, is a modally stable object. In chapter 2 we will discuss the existing knowledge about vortex column oscillations, known as Kelvin modes in detail. The popularity of Kelvin modes stems from their frequent observations in experiments and simulations (figure 1.4) and also their role in cooperative instabilities. As it would be seen in chapter 2, these Kelvin modes are by construction incapable of representing linear interaction of an isolated vortex column with an external vortical disturbance field (a linear representation of a turbulent field). Thus scenarios like the one in figure 1.2 cannot be understood purely in terms of the dynamics of Kelvin modes. Recent efforts (Antkowiak & Brancher [2004], Pradeep & Hussain [2006],Antkowiak & Brancher [2007]) have identified non-modal mechanisms to be crucial in the understanding of the linear response of a vortex column. In the current study this is done using the singular eigenfunctions, which serve as a basis for representing the initial vortical disturbance residing outside the vortex core. The singular eigenfunctions are first found for the Rankine vortex and then extended to more realistic vorticity profiles for both 2D and 3D disturbances. While studying the continuous spectra for 3D disturbances in vortices with smooth vorticity profiles, an approximate analogy with stratified shear flow is exploited. It involves drawing the analogy between density stratification and angular momentum stratification (figures 1.5 and 1.6, adapted from Antkowiak [2005]). To complement the modal analysis, an initial-value problem is carried out in chapter 3. After proving completeness of the modal expansion, qualitative comparisons are then made with the optimal-perturbation based transient growth calculations. Vortices/coherent structures being the "the sinews and muscles of fluid motion", a suppression of such structures in presence of additives (e.g. - polymers) serves as a common diagnostic for drag reduction in turbulent flows. Figure 1.7 shows such a scenario where the addition of polymers in few parts per million (ppm) leads to dramatic alteration of the boundary layer vortices. A minimal set for such systems is an isolated vortex evolving in the presence of high inertia and elasticity. In chapter 4, a vortex which is modally stable for a Newtonian fluid exhibits elastic

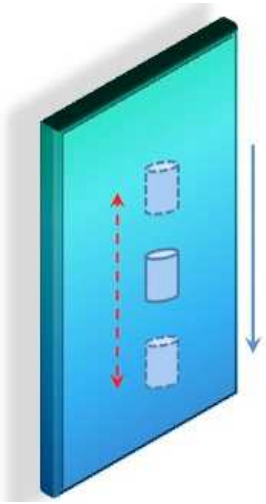

Figure 1.5: Stratified flow.
Consider a fluid parcel being displaced vertically (δz) with velocity u_z in a density stratified fluid ($\rho_0(z)$, with ρ_m being its reference value).

$$\frac{\partial u_z}{\partial t} \sim \delta z \frac{d\rho_0}{dz} g,$$
$$\frac{\partial^2 \delta z}{\partial t^2} + N^2 \delta z = 0,\ N^2 = -\frac{g}{\rho_m}\frac{d\rho_0}{dz}$$

where N is the Brunt-Väisälä frequency.

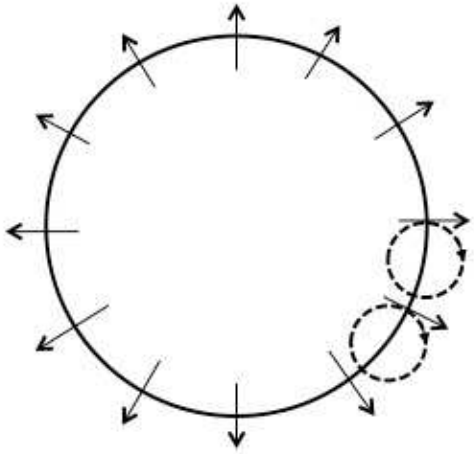

Figure 1.6: Rotating flow.
Consider a fluid parcel being displaced radially (δr) in a rotating fluid in cyclostrophic balance (Ω being its angular velocity). $u_{r,\theta}$ being its radial and azimuthal velocity.

$$\frac{\partial u_r}{\partial t} \sim 2\Omega u_\theta,\ \frac{\partial u_\theta}{\partial t} + \frac{\kappa^2}{2\Omega} u_r = 0,$$
$$\frac{\partial^2 \delta r}{\partial t^2} + \kappa^2 \delta r = 0,\ \kappa^2 = \frac{2\Omega}{r}\frac{d}{dr}\left(r^2\Omega\right)$$

where κ is the epicyclic frequency.

instability due to resonance of shear waves. The knowledge of the singular eigenfunctions helps to understand instability as the unstable mode emerges from the elastic continuous spectra. Finally in chapter 5 optimal perturbation calculations are carried out for stratified shear flows - both linear shear and stratification being chosen as an example.

In the present thesis, chapters 2-4 have been done under the supervision of Prof. Ganesh Subramanian, and chapter 5 has been done under the supervision of Prof. Rama Govindarajan.

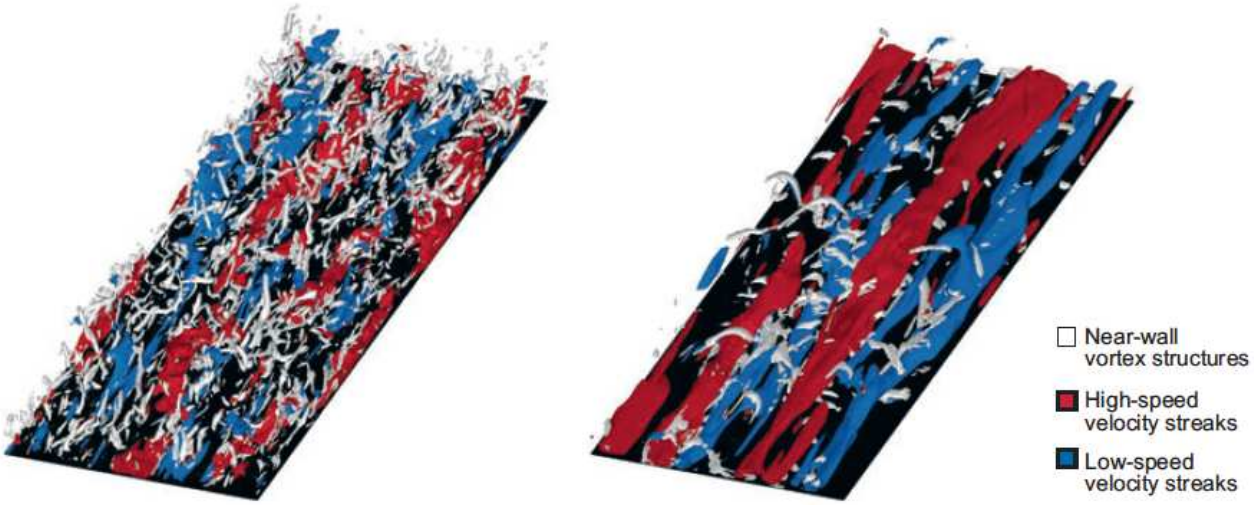

Figure 1.7: Near wall vortex structures of Newtonian flow (left) and polymer drag reduced (60%) flow (right) White & Mungal [2008]

Chapter 2

Linearized oscillations of a vortex column: the singular eigenfunctions

2.1 Introduction

Helmholtz's demonstration of the permanence of vortical structures in an inviscid fluid, and the resulting implications for a theory of vortex atoms, motivated Lord Kelvin to carry out exhaustive investigations on inviscid vortex motion and stability in the late nineteenth century. Of particular importance is his 1880 paper wherein he characterized the spectrum of waves supported on a central core of rigidly rotating liquid surrounded by an irrotational flow (Kelvin [1880]). The top-hat vorticity profile of a column of uniform vorticity surrounded by irrotational fluid, commonly referred to as the Rankine vortex, was shown to support a countable infinity of neutrally stable oscillations now known as the Kelvin modes. The resulting dispersion curves are shown in figure 2.1 where the modal frequency (ω) is plotted as a function of the axial wavenumber (k) for a fixed non-zero azimuthal wavenumber (m). For any non-zero k, one may evidently classify the modes into two groups - the co-grade modes ($\omega > m\Omega$, Ω being the core angular velocity) that travel faster than the fluid in the undisturbed core and the retrograde modes ($\omega < m\Omega$) that travel slower (Saffman [1992]). An underlying feature of the Kelvin modes is that the perturbation vorticity arises due to the oscillating column, and is evidently restricted to the region within the core and its edge; there is no perturbation vorticity outside the core. The analysis here shows that the Kelvin modes constitute the discrete spectrum of the Rankine vortex. There is an additional continuous spectrum consisting of singular non-axisymmetric modes that make up the frequency intervals between the neighboring retrograde dispersion curves in figure 2.1 (see, for instance, figure 2.3 in section 2.2.2), thereby spanning the entire base-state range of frequencies ($\omega \, \epsilon \, (0, m\Omega)$). These singular eigenfunctions have perturbation vorticity (2D - axial vorticity, 3D - 2 families providing all components of vorticity) outside the vortex core. While the Kelvin modes are sufficient to determine the linearized inviscid evolution of an initially deformed vortex column (Arendt *et al.* [1997]), the inclusion of additional singular modes is necessary to similarly characterize the interactions of such a column with external vortical disturbances.

Apart from its fundamental significance, the interaction of a vortex column with ambient turbulence is relevant to the stability of aircraft trailing vortices (Widnall [1975],Spalart [1998]), to the dynamics of coherent structures in quasi-geostrophic turbulence (McWilliams [1984]) and intense geophysical vortices such as tropical cyclones (Montgomery & Kallenbach [1997], McWilliams *et al.* [2003] and Graves *et al.* [2006]). Motivated by such applications, there have been several studies of vortex column dynamics from both modal and non-modal perspectives. Modal analyses include those of Le Dizès and co-workers who have examined, using a

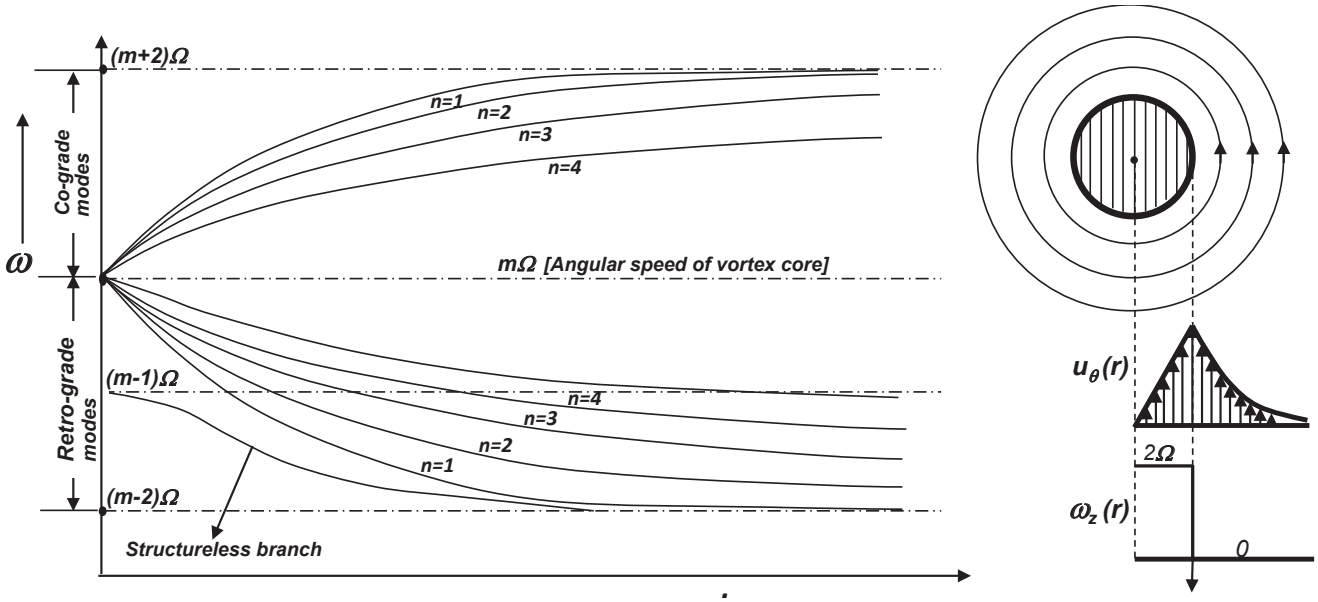

Figure 2.1: The figure is a sketch of the dispersion curves for the non-axisymmetric ($m \neq 0$) modes associated with a Rankine vortex. m is the azimuthal wavenumber, k is the axial wavenumber and n is the modal index.

WKBJ formalism[1], the characteristics of Kelvin modes for a wide class of homogeneous swirling flows with or without an axial flow component in appropriate asymptotic limits (Fabre [2002],Le Dizès & Lacaze [2005],Fabre *et al.* [2006],Heaton [2007a],Le Dizès & Fabre [2007],Fabre & Le Dizès [2008]); recent investigations along these lines have included the effects of a stable stratification along the rotation axis (Le Dizès & Billant [2009]). Fabre and co-workers (Fabre *et al.* [2006]) have conducted a detailed numerical study of the viscous eigenspectrum of a Lamb-Oseen profile. The authors show that, in contrast to the neutral retrograde modes of the Rankine vortex, one obtains instead multiple families of singular (inviscidly) damped modes in the base-state range of frequencies, the damping arising from a viscous critical layer; further, there arises a new family of modes that owes its origin entirely to viscosity. These results, although substantially more complicated, are similar in a sense to the non-trivial differences originally identified between the eigenspectra of the Rayleigh and the Orr-Sommerfeld equations in the context of parallel shearing flows (Lin [1955]). Complementing such modal investigations are the studies of Hussain and co-workers (Melander & Hussain [1993],Pradeep & Hussain [2006],Pradeep & Hussain [2010],Heaton [2007b]; also see Antkowiak & Brancher [2004]) who have examined the transient growth of a vortex column via both linear and non-linear direct numerical simulations. The short-time algebraic growth of column perturbations owes its origin to the non-normal evolution operator and the physics of the transient growth, in the linear regime, has been elucidated in detail (Pradeep & Hussain [2006]). However, quantitative results for the growth amplitude, and

[1]WKBJ (Wentzel-Kramers-Brillouin-Jeffreys; also known as the Liouville-Green method) is a perturbative technique in mathematical physics used for solving linear differential equations via a multiple scale approach (Bender & Orszag [1999], Hinch [1995]). WKBJ is used for problems which suffer a global breakdown, unlike boundary layer techniques (popularly used in fluid mechanics) which suffer a local breakdown, with decreasing small parameter ($\epsilon \to 0$). E.g - $\epsilon^2 y''(x) + Q(x)y(x) = 0$ can be solved via WKBJ method to have solution of the form - $y(x) \sim c_1 Q(x)^{-1/4} \exp[\epsilon^{-1} \int^x dx' \sqrt{Q(x')}] + c_2 Q(x)^{-1/4} \exp[-\epsilon^{-1} \int^x dx' \sqrt{Q(x')}]$. In the context of vortex stability, WKBJ technique has been used to do a large-axial-wavenumber asymptotic analysis of the vortex waves.

the nature of optimal perturbations, are restricted to a Lamb-Oseen profile, and for Reynolds numbers (Re) upto $O(10^4)$.

The formidable difficulty of the eigenvalue problem for a general swirling flow implies that the above modal investigations are typically restricted to a fraction of the full eigenspectrum. The complexity of the latter is evident with the inclusion of an axial flow which leads to an intricate array of instabilities of both invsicid (Lessen *et al.* [1974],Heaton & Peake [2006],Heaton & Peake [2007]) and viscous origins (Mayer & Powell [1992],Fabre & Le Dizès [2008]). The instabilities typically occur as nearly-convected center-modes, in the vicinity of the continuous spectrum, with the eigenfunction concentrated in a region asymptotically close to the critical radius - the spatial location that corresponds to the singularity of the inviscid equations. Such modes have been shown to determine the inviscid stability characteristics of the Batchelor vortex (Heaton [2007b]). However, even for a linearly stable base-state with a purely azimuthal flow and a monotonically decreasing (axial) vorticity profile, a sensible comparison of the results (Fabre [2002],Fabre *et al.* [2006]) with those of a Rankine vortex is impeded by the unavailability of the complete eigenspectrum in the latter case. The Rankine vortex may be regarded as the Couette-flow-equivalent for swirling flows - both correspond to (piecewise) constant vorticity profiles, leading to analytically soluble eigenvalue problems. It was originally shown by Case (1960) that the singular modes comprising the inviscid continuous spectrum of Couette flow are flow-aligned vortex sheets in two-dimensions; for a non-linear base-state, these eigenfunctions possess a principal-value singularity in addition to the vortex-sheet contribution (Balmforth & Morrison [1995a]). While the Rankine vortex eigenfunctions in two dimensions consist of cylindrical vortex sheets, similar to Couette flow, the three-dimensional spectrum exhibits interesting differences. In contrast to Couette flow (a purely continuous inviscid spectrum (Fadeev [1971])) or piecewise variants of the same (discrete neutral modes arise solely due to kinks in the base-state profile (Sazonov [1989])), as already mentioned, the restoring action of Coriolis forces implies that the Rankine vortex supports a denumerable infinity of discrete modes; only one of these, the so-called structureless or isolated mode, (the dispersion curve in figure 2.1 with $\omega \to (m-1)\Omega$ for $k \to 0$), arises from the discontinuity in the top-hat vorticity profile. Even for the CS-modes, the singularity in the vorticity eigenfunctions, in three dimensions, differs from that known for parallel flows (Sazonov [1996]). The analysis here, while similar in spirit to that of Case (1960), accounts for these differences in characterizing the Rankine continuous spectrum. The discrete (Kelvin) modes emerge as exceptional instances when the amplitude of the singular vortical structure goes to zero; indeed, the requirement that this amplitude equal zero yields the Kelvin-mode dispersion relation. The normal-mode analysis here may be regarded as a 'baseline' scenario for more general vorticity profiles - at least as far as the singular modes are concerned. It should also serve as a starting point towards unravelling the more complicated continuous spectra that would emerge with the incorporation of stratification or viscoelasticity. To this end, we present a local analysis, based on Frobenius expansions, that examines the non-trivial effect of a small but finite base-state vorticity (present for a smooth vorticity profile) on the nature of the singularity in the CS-eigenfunctions; the approach to the Rankine CS-modes is elucidated.

The initial value problem (IVP) for a Rankine vortex that extends the analysis of Arendt *et al.* [1997] to include exterior vortical disturbances, and its equivalence to the modal rep-

resentation given here, will be the subject of chapter 3. It is nevertheless worth noting the relation between the modal and non-modal (IVP) perspectives. Studies on parallel shearing flows show that the transient growth phenomenon is intimately related to an underlying inviscid continuous spectrum. While the original IVP analyses for Couette flow were in terms of Fourier modes with time-dependent wave vectors (also known as Kelvin modes, see Farrell [1984]), an equivalent description exists in terms of a convected superposition of flow-aligned vortex sheets (the CS-modes). The work of Farrell and co-workers (Farrell [1984],Farrell [1989],Farrell & Ioannou [1993b]) has shown that one of the mechanisms leading to transient growth, the Orr-mechanism (Orr [1907]), involves the progressive phase-alignment of an initially staggered superposition of singular vortex-sheet eigenfunctions. The lift-up mechanism Landahl [1980], responsible for the growth of spanwise perturbations, may also be interpreted in terms of a gradual de-phasing of a vortex-sheet eigenfunction and the corresponding ensemble of singular Squire-jet modes (chapter 6). In general, for problems where the continuous spectrum governs the temporal evolution, the dynamics may be divided into three regimes: an initial phase characterized by the aforementioned algebraic growth, a terminal phase with an algebraic-decay in integral measures such as the perturbation kinetic energy due to the eventual de-phasing of the CS-modes by differential shear (Bassom & Gilbert [1998]), and an intermediate phase with exponential asymptotics. In this latter regime, appropriate superpositions of the CS-modes behave as decaying discrete (quasi)-modes, a phenomenon known as Landau damping (Briggs *et al.* [1970],Schecter *et al.* [2000],Schecter & Montgomery [2003]). Both Couette flow and the Rankine vortex constitute important and singular limiting scenarios in that although neither exhibits the aforementioned exponential asymptotics, the addition of a small curvature or a small vorticity-gradient/vorticity does lead to quasi-modes (Balmforth *et al.* [2001],Shrira & Sazonov [2001],Shrira & Sazonov [2003]). For instance the solution of the two-dimensional IVP shows that a 'near-Rankine' profile exhibits an exponential decay phase with the damping rate being proportional to the (small) vorticity gradient at the critical radius (Schecter *et al.* [2000],Le Dizès [2000]). The analogous scenario for three dimensions is not known, however; numerical results for a Lamb-Oseen profile indicate a denumerable infinite of quasi-modes (Fabre [2002]). Although we discuss the Rankine vortex and 'near-Rankine' profiles from the normal-mode persective in this thesis, the above discussion highlights the relevance of these limiting scenarios from the IVP perspective.

This chapter is organized as follows. In section 2.2, we examine the inviscid continuous spectrum of a Rankine vortex. Section 2.2.1 analyzes the family of 2D-singular modes (zero axial wavenumber, $k = 0$) for which the perturbation vorticity is confined to a pair of cylindrical vortex sheets - one at the edge of the core and the other at the critical radius, the radial location where the base-state angular velocity equals the modal frequency; a physical interpretation of the twin-vortex-sheet structure is given. A second family of singular eigenfunctions, in two dimensions, takes the form of (infinitely) localized axial jets. The localization of the axial velocity perturbation implies that these jets remain valid eigenfunctions for an arbitrary base-state vorticity profile. It is then shown that an arbitrary distribution of axial vorticity may be evolved as a superposition of the 2D CS-modes. In section 2.2.2, the analysis is extended to three-dimensional modes all of which also possess vorticity in the interior of the core. The CS-

eigenfunctions that arise, in addition to the denumerably infinite number of Kelvin modes, may be conveniently classified based on the nature of the singularity in the perturbation vorticity at the critical radius. The first family (6.3.1) resembles the two-dimensional singular modes in that the singularity is again a cylindrical vortex sheet, one threaded by helical vortex lines, in the otherwise irrotational exterior. For the second family (6.3.2), the singular structure includes radial vorticity and has a dipole-singularity at the critical radius; members of this family asymptote to the aforementioned axial-jet eigenfunctions in the limit of a vanishing axial wavenumber. In section 2.2.2, it is shown that an arbitrary initial distribution of vorticity may be evolved as a superposition of the discrete and continuous spectrum modes, this modal representation being equivalent to the solution of the corresponding IVP for the Rankine vortex (chapter 3). In section 2.3.1, the Rankine modal representation in section 2.2.1, for an initial distribution of axial vorticity, is extended to the case of a smooth vorticity profile. Next, we examine the singular eigenfunctions associated with a smooth vorticity profile in three dimensions. The analysis is, of necessity a local one using Frobenius expansions, and determines the perturbation vorticity field in the vicinity of the critical radius by drawing on an analogy with the eigenfunctions known for the case of a stratified shear flow. The approach of these eigenfunctions towards the singular forms, obtained for the Rankine vortex in earlier sections, is then examined. Section 2.5 summarizes the main results of the analysis, and connects them to other efforts that include viscous and non-linear effects.

2.2 Inviscid normal mode analysis for a Rankine vortex

If a and Ω_0 be the core radius and angular velocity, respectively, the Rankine velocity profile is given by $u_\theta^{(0)} = r\Omega(r)$, with $\Omega(r) = \Omega_0$ for $r < a$ and $\Omega(r) = \Omega_0(a/r)^2$ for $r \geq a$; the base-state (axial) vorticity (Z) and vorticity gradient are $Z(r) = 2\Omega_0\mathcal{H}(a-r)$ and $DZ(r) = -2\Omega_0\delta(r-a)$, $\mathcal{H}(z)$ and $\delta(z)$ being the Heaviside and delta functions, respectively. The Rankine vortex corresponds to a stable stratification of angular momentum, and supports neutrally stable axisymmetric oscillations in the absence of viscosity (Chandrasekhar [1961]). Further, Z being a monotonically decreasing (generalized) function of r, the analog of Rayleigh's inflection point theorem in a cylindrical geometry implies (modal) stability to 2D non-axisymmetric perturbations (Drazin & Reid [1981], Michalke & Timme [1967]). The governing equation for the linearized evolution of inviscid perturbations is, however, singular at the point (the critical radius) where the modal frequency equals the base-state angular velocity, and this leads to an inviscid continuous spectrum. The normal mode analysis in the following subsections is carried out with an emphasis on the CS-modes. Two-dimensional perturbations are examined in section 2.2.1, and the analysis is extended to perturbations with a finite axial wavenumber (k) in section 2.2.2.

2.2.1 The $2D$ continuous spectrum modes

Assuming small amplitude perturbations of the form $(u_r', u_\theta') = (\hat{u}_r(r), \hat{u}_\theta(r))\mathrm{e}^{\mathrm{i}(m\theta-\omega t)}$, where m is the azimuthal wavenumber and ω is the (real) angular frequency, the inviscid stability equation governing the radial velocity eigenfunction, $\hat{u}_r(r)$, may be derived along lines similar to that for

the Rayleigh equation for parallel shear flows (Drazin & Reid [1981]), and is given by:

$$[(\omega - m\Omega)\{r^2D^2 + 3rD - (m^2 - 1)\} + mr\,DZ]\hat{u}_r = 0, \tag{2.1}$$

where $D \equiv d/dr$. Since Z is constant within the core and zero outside it, (2.1) simplifies to:

$$(\omega - m\Omega)\{r^2D^2 + 3rD - (m^2 - 1)\}\hat{u}_r = 0. \tag{2.2}$$

or realizing the axial vorticity $\hat{w}_z = 1/rD(r\hat{u}_r) - im/r\hat{u}_\theta$,

$$(\omega - m\Omega)\{-imr\hat{w}_z\} = 0. \tag{2.3}$$

for $r \neq a$, and thereby allows for two possibilities. The first rather obvious one is the homogeneous solution,

$$\{r^2D^2 + 3rD - (m^2 - 1)\}\hat{u}_r = 0. \tag{2.4}$$

Physically, this corresponds to an irrotational velocity perturbation both within and outside the core. The perturbation vorticity resides in a cylindrical vortex sheet at $r = a$, and is the linearized representation of a small amplitude wavy deformation. The eigenvalue problem involving (2.4), with the required continuity of radial and (total) tangential velocity[2] components at $r = a$, was originally solved by Lord Kelvin (see Kelvin [1880]), and yields a single neutral mode for each m with $\omega_d = (m - 1)\Omega_0$. In the context of stability of hurricanes and tornadoes, this is also known as vortex 'Rossby' edge wave (Smith & Montgomery [1995], Guinn & Schubert [1993]; see 2.2.1 for the discussion). In geophysical flows, Rossby waves arise due to a restoring mechanism produced by planetary vorticity gradient (β-plane). Similarly Rankine vortex has a background vorticity gradient, albeit localized at the edge of the vortex core ($\propto \delta(r - a)$), which is responsible for the Kelvin mode - a vortex 'Rossby' wave. Kelvin mode lags behind the fluid motion in the core since the velocity perturbation acts to deform the core in a retrograde sense. These Kelvin modes make up the $2D$ discrete spectrum (see Saffman [1992]). They are interpreted here as (regular) discrete modes despite the singular vorticity eigenfunction ($\propto \delta(r - a)$), since the singularity arises solely due to the kink in the base-state vorticity profile. If the Rankine profile were to be smoothed such that Z decreases from $2\Omega_0$ to 0 in a small but finite interval ensuring it is a compact vorticity profile, then the vorticity eigenfunction would no longer be singular. On the other hand, the CS-modes, to be discussed below, continue to be singular even with this smoothing, since they owe their origin to the singular point in the governing equation (2.2).

The second possibility, leading to the CS-spectrum, was recognized by Case [1960] (among others; see Dikii [1960]), in the context of Couette flow; that (2.2) also allows for

$$\{r^2D^2 + 3rD - (m^2 - 1)\}\hat{u}_r \propto \delta(\omega - m\Omega), \tag{2.5}$$

since $x\delta(x) = 0$ is an equality in the generalized sense (Lighthill [1958]). Physically, (2.5) implies the existence of a cylindrical vortex sheet, threaded by axial vortex lines, and coincident with

[2]This is equivalent to continuity of pressure perturbations.

the streamsurface at the critical radius, r_f, satisfying $\omega = m\Omega(r_f)$. The sheet is convected with the base-state velocity at $r = r_f$, while its infinitesimal thickness prevents smearing out by the shear. One has therefore a singular normal mode. The Rankine core is degenerate in the sense that an arbitrary distribution of axial vorticity is convected unchanged in this region; thus, it is sufficient to consider the case where the vortex sheet is located outside the core. The equality $\omega = m\Omega(r_f)$ implies $r_f = (\frac{m\Omega_0}{\omega})^{\frac{1}{2}}a$, and for r_f ranging from a^+ to infinity, one obtains the $2D$-continuous spectrum with ω decreasing from $m\Omega_0$ to 0. There remains the one exceptional value of r_f where the vortex sheet amplitude goes to zero, corresponding to the Kelvin mode above. To see this, one may rewrite (2.5) as:

$$\{r^2D^2 + 3rD - (m^2 - 1)\}\hat{u}_r = \mathrm{i}mr_fA(r_f)\delta(r - r_f), \tag{2.6}$$

where $-A(r_f)$ denotes the (unknown) vortex sheet strength (see (2.3)). The solution of (2.6) is readily obtained by separate consideration of the regions: $r < a$, $a < r < r_f$, and $r_f < r < \infty$. The solutions in these regions, consistent with the absence of singularities at the origin and at infinity, are:

$$\hat{u}_r^1 = d\left(\frac{r}{a}\right)^{m-1}, \qquad (0 < r < a), \tag{2.7}$$

$$\hat{u}_r^2 = c_1\left(\frac{r}{a}\right)^{m-1} + c_2\left(\frac{a}{r}\right)^{m+1}, \qquad (a < r < r_f), \tag{2.8}$$

$$\hat{u}_r^3 = \Omega_0\frac{a^2}{r_f}\left(\frac{a}{r}\right)^{m+1}, \qquad (r > r_f), \tag{2.9}$$

where the constant in (2.9) is chosen as $(\Omega_0 a^2/r_f)$ for convenience. The constants c_1 and c_2 may be determined following the standard procedure for the determination of the Green's function of a second order differential equation (Friedman [1990]). Thus, integrating (2.6) over an infinitesimal interval including $r = r_f$, one obtains the following matching conditions:

$$\hat{u}_r^2 = \hat{u}_r^3 \qquad \text{at} \qquad r = r_f, \tag{2.10}$$

$$D\hat{u}_r^3 - D\hat{u}_r^2 = \frac{\mathrm{i}mA(r_f)}{r_f} \qquad \text{at} \qquad r = r_f, \tag{2.11}$$

Since $\hat{u}_\theta = i/mD(r\hat{u}_r)$, (2.11) denotes the jump in the tangential perturbation velocity across the vortex sheet at $r = r_f$. From (2.8), (2.9), (2.10) and (2.11),

$$c_1 = -\frac{\mathrm{i}A(r_f)}{2}\left(\frac{a}{r_f}\right)^{m-1}, \tag{2.12}$$

$$c_2 = \frac{\Omega_0 a^2}{r_f} + \frac{\mathrm{i}A(r_f)}{2}\left(\frac{r_f}{a}\right)^{m+1}. \tag{2.13}$$

The constant d in (2.7) is determined from the continuity of the radial velocity at $r = a$:

$$d = \frac{\Omega_0 a^2}{r_f} + \frac{\mathrm{i}A(r_f)}{2}\left[\left(\frac{r_f}{a}\right)^{m+1} - \left(\frac{a}{r_f}\right)^{m-1}\right]. \tag{2.14}$$

Finally, the vortex sheet amplitude, $A(r_f)$, is determined by the jump in tangential velocity

across $r = a$. The latter is obtained by integrating (2.1), with $DZ = -2\Omega_0\delta(r-a)$ included, over an infinitesimal interval including $r = a$:

$$(\omega - m\Omega_0)\left[D\hat{u}_r^2 - D\hat{u}_r^1\right] = 2m\frac{\Omega_0}{a}\hat{u}_r \qquad \text{at} \qquad r = a. \tag{2.15}$$

Using $\omega = m\Omega_0(a/r_f)^2$, and after some algebra,

$$A = \frac{2\mathrm{i}\Omega_0\left(\dfrac{a^2}{r_f}\right)(\omega_d - \omega)}{\Omega_0\left(\dfrac{a}{r_f}\right)^{m-1} + (\omega_d - \omega)\left(\dfrac{r_f}{a}\right)^{m+1}}. \tag{2.16}$$

where $\omega_d = (m-1)\Omega_0$ is the frequency of the $2D$ Kelvin mode.
The denominator in (2.16) may be written in the form:

$$(m\text{–}1)\left(\frac{r_f}{a}\right)^m - m\left(\frac{r_f}{a}\right)^{m-2} + \left(\frac{a}{r_f}\right)^m = \frac{[(\frac{r_f}{a})^2 - 1]}{(\frac{r_f}{a})^m}\Big[[(\frac{r_f}{a})^{2m-2} - 1] + [(\frac{r_f}{a})^{2m-2} - (\frac{r_f}{a})^2] + \ldots + [(\frac{r_f}{a})^{2m-2} - (\frac{r_f}{a})^{2m-4}]\Big], \tag{2.17}$$

and is therefore can be seen to be always positive when $r_f > a$. The sign of $\mathrm{Re}(A(r_f))$ is therefore determined by the numerator in (2.16); in particular, the vortex sheet disappears when $\omega = \omega_d$; critical radius of Kelvin mode $r_{fk} = \left(\frac{m}{m-1}\right)^{\frac{1}{2}}a$. Thus, the generic eigenmodes comprising the $2D$ CS-spectrum have a twin-vortex-sheet structure, and for the chosen normalization, the vorticity eigenfunction is given by:

$$\hat{w}_z^{CSM}(r; r_f) = \left[\frac{2i\Omega_0 d}{\omega - m\Omega_0}\delta(r-a) - A(r_f)\delta(r-r_f)\right]. \tag{2.18}$$

The jumps in tangential velocity across the two vortex sheets having the same sign for $r > r_{fk}\,(\mathrm{Re}(A) < 0)$, and having opposite signs when $a < r_f < r_{fk}\,(\mathrm{Re}(A) > 0)$; see figure 2.2. The amplitude of the second vortex sheet vanishes for $r_f = r_{fk}$, leading to the Kelvin mode eigenfunction:

$$\hat{w}_z^{\mathrm{Kelvin}}(r) = -\frac{2i\Omega_0 a^2}{r_{fk}}\delta(r-a), \tag{2.19}$$

with a single vortex sheet at $r = a$. In contrast to Case's original analysis of the $2D$ continuous spectrum in Couette flow, wherein the normal component of the velocity perturbation in Couette flow is required to vanish at each boundary (or at infinity for an unbounded domain), the radial velocity field induced by the vortex sheet at $r = r_f$ will not, in general, vanish at $r = a$. Instead, it acts to deform the core, leading to the additional edge vortex sheet. Although the strength, $A(r_f)$, of the vortex sheet at $r = r_f$ is still arbitrary, as in Couette flow, the ratio of the strengths of the two vortex sheets is not, and a discrete mode arises when this ratio is zero. The exact analog of Couette flow would be a point vortex that results for $\Omega_0 \to \infty, a \to 0$ with $\Omega_0 a^2$ fixed. In this limit, $r_{fk} \to 0$, and a purely continuous spectrum remains. On the other hand, the parallel flow analog of the Rankine vortex would be the piecewise linear profile, with a single jump in the velocity gradient, analyzed by Sazonov [1989].

The existence of singular modes, in addition to well-known Kelvin mode, becomes evident

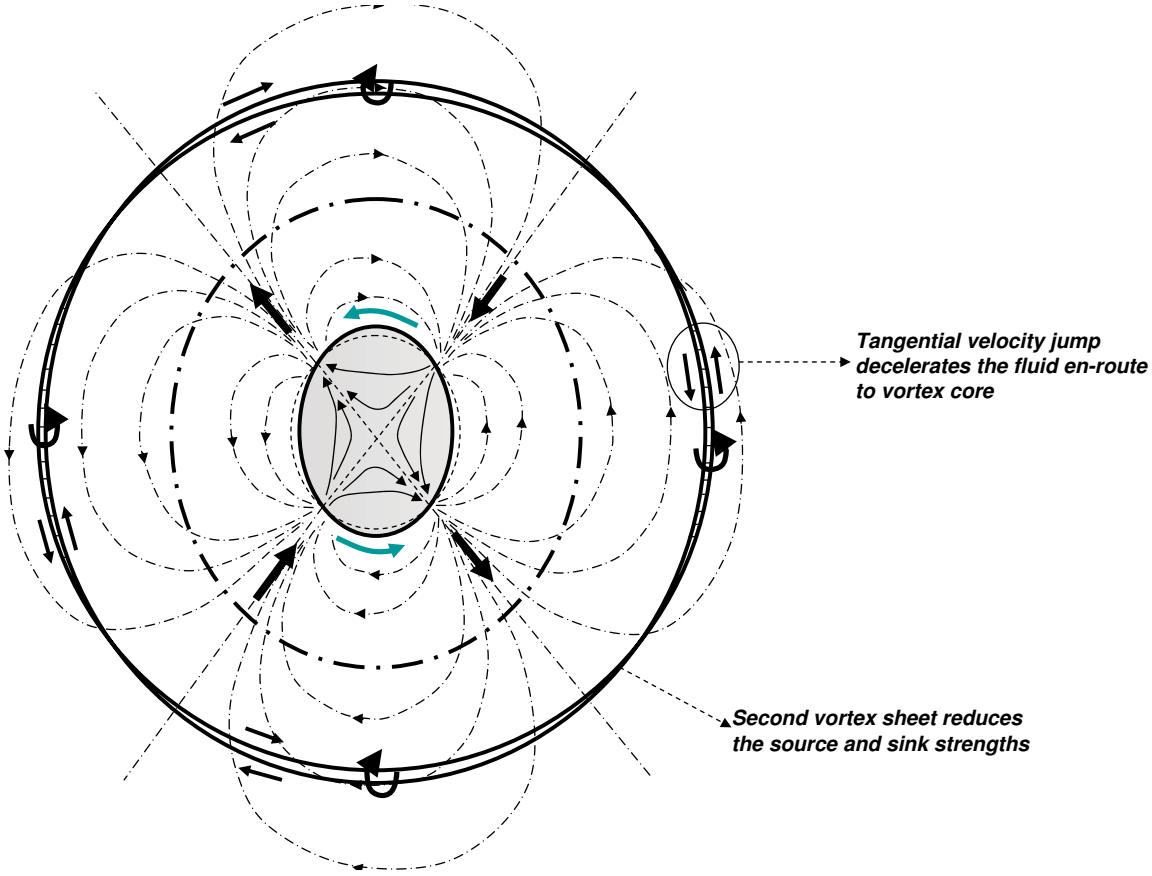

(a)

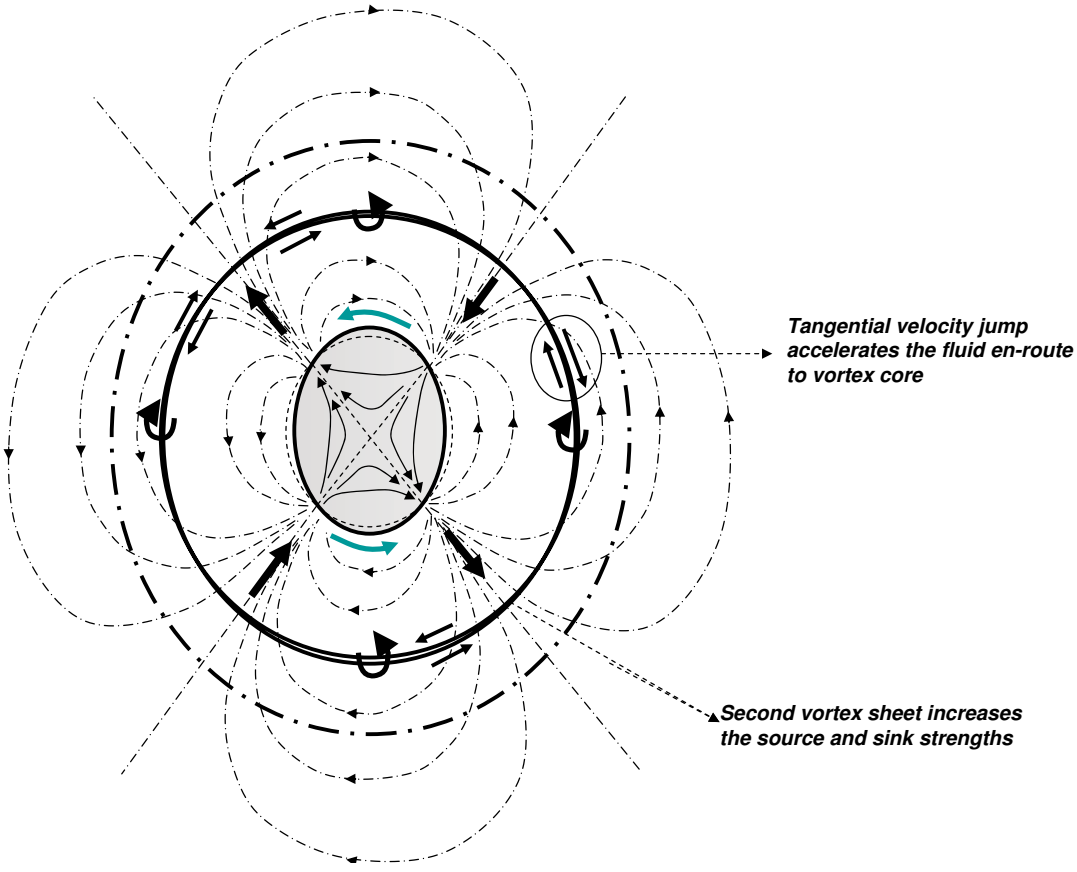

(b)

Figure 2.2: (a) The disturbance velocity field when the vortex sheet at $r = r_f$ co-rotates with the elliptically deformed vortex core at a frequency lower than the $m = 2$ Kelvin mode; (b) the disturbance velocity field when the vortex sheet at $r = r_f$ co-rotates with the elliptically deformed vortex core at a frequency higher than the $m = 2$ Kelvin mode. The dash-dot circle denotes the ring of fluid rotating at the Kelvin mode frequency.

on considering the underlying physical mechanism. Without loss of generality, one may look at $m = 2$, in which case the Kelvin mode is the small amplitude limit of the well-known Kirchoff vortex (Lamb [1932]). The exterior velocity field associated with the Kelvin mode may be regarded as the result of a distribution of sources and sinks along the edge of the unperturbed core, the strength of the source or sink being proportional to the local slope of the wavy core-perturbation. The source and sink strengths are the greatest midway between the principal axes of the elliptical core, and the regions of outflow and inflow are centered around these directions. The core rotation may be slowed down or accelerated, and the modal frequency altered, by an appropriate change of the strength of these radial flows. A co-rotating vortex sheet in the otherwise irrotational region, via tangential velocity jumps, provides for just such a mechanism, and leads to the $2D$ CS-modes. Figure 2.2 shows the velocity field associated with CS-modes with frequencies both lower and higher than the corresponding Kelvin mode. In each case, the perturbation velocity field for $r > r_f$ remains identical to the the Kelvin mode, but the jumps in tangential velocity across $r = r_f$ alter the velocity field in the region $r < r_f$.

The discussion above applies to $m \geq 2$. The case $m = 1$, in two dimensions, corresponds to a mere displacement of the vortex core. Translational invariance for an unbounded domain implies the absence of any restoring force, and the $2D$ Kelvin modes are therefore restricted to $m \geq 2$ ($r_{fk} \to \infty$ for $m = 1$). The CS-modes continue to exist for $m = 1$ since the outer vortex sheet breaks the invariance. However, naively setting $m = 1$ in (2.16) leads to a divergence of the vortex sheet amplitude for any r_f. This is because the analysis above proceeds by normalizing the velocity field for $r > r_f$, while for $m = 1$, the second vortex sheet 'screens' the disturbance velocity field induced by the displaced core, and the velocity perturbation is confined to the region $r < r_f$. Physically, the $m = 1$ CS-modes correspond to the small amplitude orbiting motion of the displaced (but undeformed) vortex core around the center of a cylindrical vessel with radius r_f. The image vorticity needed to satisfy the impenetrability condition is, to linear order, a vortex sheet coincident with the vessel wall. The ratio of the vortex sheet strengths, predicted by the analysis above, is unaffected by the velocity field normalization, and equals $-(a/r_f)$; the trivial translatory (discrete) mode thus corresponds to a vessel with an infinitely large radius ($r_f \to \infty$). In section 2.2.2, we encounter modes of a similar nature for a finite axial wavenumber. Unlike the two-dimensional case, where an $m = 1$ CS-mode may be interpreted as a vessel mode for any $r_f > a$, the analogy, for a non-zero axial wavenumber, remains true only for a denumerably infinite sequence of r_f's (see Appendix A).

The discussion of the CS-modes has thus far been for cases where the perturbation vorticity is restricted to the region $r \geq a$. As pointed out earlier, modes with core axial vorticity are expected to have a degenerate character, since rigid-body rotation allows for an arbitrary axial vorticity distribution to evolve with its structure unchanged. From a normal mode perspective, there is still a mild restriction, however, since an arbitrary core vorticity distribution would deform the core, thereby also exciting a Kelvin mode. This would lead to a pair of frequencies that characterize the evolution for a given azimuthal wavenumber - one being the core angular frequency ($m\Omega_0$) corresponding to the interior vorticity and the second being the Kelvin mode frequency ($(m-1)\Omega_0$) corresponding to the edge vorticity. Thus, any normal mode with core vorticity must have, in addition, a projection at the edge of the core that cancels out the Kelvin

mode contribution. Assuming the core vorticity distribution to be given by $g(r)$ (with $g(r) = 0$ for $r \geq a$), it may be shown that the (axial) vorticity eigenfunction of a core eigenmode is given by

$$\hat{w}_z^{core}(r) = g(r) - \delta(r-a)\int_0^a g(r')\left(\frac{r'}{a}\right)^{m+1} dr', \tag{2.20}$$

where the delta function denotes the additional edge-vorticity component. That $g(r)$ is arbitrary is consistent with the aforementioned degeneracy. The velocity eigenfunction is restricted to $r < a$, so the exterior irrotational region remains quiescent. These $2D$ core eigenmodes find a mention in Kopiev and Chernyshev (1997) in the context of vortex ring oscillations. Note that $g(r)$ may be expanded in terms of any of the standard orthogonal families, and each of these representations will lead to a particular, denumerably infinite, representation of the core eigenmodes. One such representation, in terms of Bessel functions, arises naturally as the limiting form of the $3D$ structured modes in section 2.2.2.

The evolution of an initial axial vorticity distribution of the form $w_{z0}(r)e^{im\theta}$, as an integral superposition of the 2D Kelvin and CS-modes, is given by:

$$w_z(r,\theta,t) = w_z^{\text{core}} e^{im(\theta-\Omega_0 t)} + \int_{a^+}^{\infty} B_1(r_f)\hat{w}_z^{\text{CSM}}(r;r_f)e^{im(\theta-\Omega(r_f)t)}dr_f + \int_0^{\infty} B_2(r_f)\hat{w}_z^{\text{Kelvin}}(r)e^{i(m\theta-\omega_d t)}dr_f, \tag{2.21}$$

where $\hat{w}_z^{\text{CSM}}$ and $\hat{w}_r^{\text{Kelvin}}$ are given by (2.18) and (2.19), and the respective eigenfunction amplitudes are given by $B_1(r_f) = -\dfrac{w_{z0}(r_f)}{A(r_f)}$, $B_2(r_f) = -\dfrac{i}{2}\dfrac{w_{z0}(r_f)r_{fk}}{a^2(\omega_d - m\Omega)}\left(\dfrac{a}{r_f}\right)^{qm-1}$ and $q = \text{sgn}(r_f - a)$. On substituting the expressions for B_1, B_2 and $A(r_f)$, equation 2.21 can be simplified to,

$$\begin{aligned} w_z(r,\theta,t) \;=\; & w_{z0}(r)e^{i[m(\theta-\Omega(r)t)]}\mathcal{H}(r-a) + \hat{w}_z^{core}e^{im[\theta-\Omega_0 t]} + \delta(r-a)\left[e^{-i\omega_d t}\int_0^a w_{z0}(r_f)\left(\frac{r_f}{a}\right)^{m+1}dr_f + \right. \\ & \left. \int_{a^+}^{\infty}\Omega_0\left(\frac{a}{r_f}\right)^{m-1} w_{z0}(r_f)\frac{e^{-im\Omega(r_f)t} - e^{-i\omega_d t}}{(\omega_d - m\Omega(r_f))}dr_f\right] e^{im\theta} \end{aligned} \tag{2.22}$$

In (2.21), the second term accounts for the distribution of CS-modes required to represent a specified axial vorticity distribution outside the core. The edge-vorticity contribution that arises from this superposition is then projected onto the Kelvin mode which appears as the third term in (2.21); the lower limit a^+ instead of a ensures that an initial condition consisting solely of edge-vorticity evolves as a Kelvin mode. The equivalence of (2.21) to a solution of the 2D IVP is readily established (section 3.2.1). The coefficients B_1 and B_2 are singular at $r_f = r_{fk}$, when $A(r_f) = 0$, and this is a signature of the secular growth for an initial condition localized at the Kelvin critical radius. The growth is linear in time for the velocity field, and with reference to the plasma physics literature (Hirota *et al.* [2003]), the secular growth may be interpreted as a resonance between the point and continuous spectra. The 2D linear response of a Rankine vortex to an initial vortical perturbation was obtained by Smith & Montgomery [1995] using a different ansatz than the present analysis. The authors split the vorticity response in terms of a smooth response (one due to the advection of background angular velocity) and a vortex sheet response at the edge of the core (due to the discontinuous base-state vorticity). (2.22) is identical to the vorticity equation corresponding to equation 5.22 in Smith & Montgomery

[1995].

For a point vortex, as pointed out earlier, the inviscid spectrum is purely continuous, and an initial axial vorticity distribution evolves as a superposition of the CS-modes alone. Thus, (2.21) reduces to the much simpler form:

$$w_z(r,\theta,t) = \int_0^\infty w_{z0}(r_f)\hat{w}_z^{\mathrm{CSM}}(r;r_f)e^{im(\theta-\Omega(r_f)t)}dr_f \tag{2.23}$$

with $\hat{w}_z^{\mathrm{CSM}}(r;r_f) = \delta(r-r_f)$.

Interestingly, the degeneracy associated with the core-eigenmodes of a vortex column disappears on considering the analogous modes for a vortex ring. This is because the base-state circumferential vorticity is required to increase in proportion to the distance from the axis of symmetry in order satisfy the Euler equations that now include an additional vortex-stretching term. The resulting differential shear in a meridional plane, even within the vortical ring core, ensures that the CS-modes have a uniquely determined structure. The analog of the $2D$-column disturbances are the axisymmetrical ring-modes that do not depend on the coordinate along the ring perimeter. For the isochronous ring, where the ratio of the azimuthal vorticity to the transverse radial distance is a constant [3], the axisymmetrical CS-modes again exhibit a twin-vortex sheet structure, the vortex sheets being in the form of hollow tori (Kopiev & Chernyshev [1997]). The original analysis of Kopiev and Chernyshev (1997), for rings with a small cross-section ($\mu \ll 1$, where $\mu = a/R$ is the ratio of the cross-sectional radius to the ring radius), was restricted to the CS-modes within the ring cores. In what follows, we digress a little to show that their analysis applies equally to the CS-modes that govern the evolution of vortical disturbances in the much-larger envelope of irrotational fluid that is entrained by the propagating ring.

Finally, there are certain exceptional eigenmodes, those that do not involve a radial velocity perturbation, and are therefore not covered by the above analysis. The simplest among these is the trivial case of an axisymmetric hollow vortex sheet at $r = a$. The resulting perturbation velocity field corresponds to a quiescent core, and is identical to the base-state ($u'_\theta \sim 1/r$) outside it. This mode is, in fact, included in (3.12). In enforcing a quiescent exterior for all m, (3.12), for $m = 0$, requires an axisymmetric vortex sheet at the edge of the core with a strength equal and opposite to the core circulation. A second class of eigenmodes neglected by the analysis are those wherein the axial velocity component itself has a delta-function singularity; physically, this would be a concentrated jet-like profile. Although not relevant to an IVP involving only an axial vorticity component as given by (2.21) above, these modes rise as limiting forms of the $3D$ CS-modes (the Λ_2 family) that include radial vorticity. Sazonov [1996] has identified similar modes for inviscid Couette flow which, together with the $3D$-generalization of the Case vortex sheets, complete the $3D$-continuous spectrum.

Vortex Rossby waves

The importance of vortex waves in geophysical fluid dynamics, specially in the context of hurricanes and tornadoes, deserves a separate mention. Though Kelvin's circulation theorem is extremely useful for inviscid, barotropic (density is a function of pressure) flows, for oceanic and

[3] As shown by Fraenkel (1970), in the limit of small-cored rings, this is only one of an infinite set of vorticity distributions that allow for a steadily propagating distribution of vorticity.

atmospheric applications a more relevant conserved quantity is the potential vorticity (Vallis [2006]). Unlike the circulation theorem, the potential vorticity conservation is a conservation law of a field and is valid for baroclinic flows too - crucial for geophysical flows. If Θ is the potential temperature (the temperature a fluid would have if adiabatically moved to a reference pressure) then the potential vorticity conservation is given as,

$$\frac{D}{Dt}\left(\frac{w_a.\nabla\Theta}{\rho}\right) = 0 \tag{2.24}$$

where $w_a = w + f$ is the absolute vorticity (w is the flow vorticity while f represents the planetary vorticity - the component of earth's rotation at a certain latitude). Since f varies with latitude (maximum at the poles and vanishing at the equator), it can be linearized as $f = f_0 + \beta y$ (known as $\beta-$plane approximation). y is a locally cartesian coordinate in the north-south direction. Thus for a fluid with uniform density we have from (2.24)

$$\frac{\partial w}{\partial t} + \mathbf{u}.\nabla w + \beta u_y = 0 \tag{2.25}$$

On assuming plane-wave solutions, $\propto \exp\{i(kx + ly - \omega t)\}$, the dispersion relation is obtained to be

$$\omega = -\beta\frac{k}{k^2 + l^2}, \tag{2.26}$$

a set of westward propagating waves known as Rossby waves. Thus Rossby wave arises due to gradient of planetary (background) vorticity. From (2.1) the vorticity perturbation equation for a swirling flow is,

$$\left(\frac{\partial}{\partial t} + im\Omega\right) w_z + DZu_r = 0 \tag{2.27}$$

Comparing (2.25) and (2.27) we realise the similarities in the evolution of flow vorticity, w, in the $\beta-$plane and that of perturbation vorticity, w_z, when the base-state vorticity gradient DZ is seen as the equivalent of β, the planetary vorticity gradient. Thus the vortex waves discussed so far can be seen as equivalent vortex analogs of Rossby waves and more importantly the 2D Kelvin mode is an edge vortex Rossby wave (Guinn & Schubert [1993], Smith & Montgomery [1995], Montgomery & Kallenbach [1997]).

2.2.2 The $3D$ continuous spectrum modes

In this section we analyze the CS-modes with a non-zero axial wavenumber. The equations governing the inviscid evolution of $3D$ disturbances have been written down in various forms by different authors. Howard & Gupta [1962] reduce the set of stability equations to a single one governing the radial velocity eigenfunction (the Howard-Gupta equation) as in section 2.2.1. On the other hand, Saffman [1992] derives an equation governing the disturbance pressure field that has since been generalized to a base-state with axial flow (Le Dizès [2004]) . Herein, following Arendt *et al.* [1997], we write down the stability equation in terms of the axial velocity eigen-

function $\hat{u}_z(r)$ which is best suited for the Rankine vortex. For small amplitude perturbations of the form $(u'_r, u'_{theta}, u'_z) = [\hat{u}_r(r), \hat{u}_\theta(r), \hat{u}_z(r)]\mathrm{e}^{\mathrm{i}(kz+m\theta-\omega t)}$, one obtains:

$$[(\omega-m\Omega)^2\{r^2D^2+rD-m^2-k^2r^2\}-r(\omega-m\Omega)\{m(2r\Omega'D+\mathcal{D}Z)+Q'Q^{-1}\{(\omega-m\Omega)rD-mZ\}\}+2k^2r^2\Omega Z]\hat{u}_z = 0, \tag{2.28}$$

for a general vorticity profile where $Q \equiv \{(\omega - m\Omega)^2 - 2\Omega Z\}$; here, $2\Omega Z$ is proportional to the Rayleigh discriminant governing centrifugal stability (see Chandrasekhar [1961]), and equals $4\Omega_0^2 H(a-r)$ for a Rankine vortex. The radial and azimuthal components of the perturbation velocity field are given by:

$$Q\hat{u}_r = -\frac{i}{rk}(\omega - m\Omega)[(\omega - m\Omega)rD - mZ]\hat{u}_z, \tag{2.29}$$

$$Q\hat{u}_\theta = -\frac{1}{rk}[Z(\omega - m\Omega)rD - m\{(\omega - m\Omega)^2 + r\Omega' Z\}]\hat{u}_z. \tag{2.30}$$

For a Rankine vortex, (2.28) may be solved, separately, inside the core ($r \leq a$) and in the irrotational exterior ($r > a$). Note that (2.28) involves the base-state vorticity itself in addition to its radial gradient, and equations inside the core therefore differ in form from those outside. This is a reflection of Coriolis forces coming into play within the core in three dimensions. Inviscid axisymmetric oscillations (the 'sausaging' modes) of a vortex column result from Coriolis forces driving the alternate expansion and contraction of closed material curves, within the core, in a plane transverse to the rotation axis (Batchelor [1967]); there exists an equivalent interpretation in terms of the periodic twisting and untwisting of vortex lines (Melander & Hussain [1994]). Since $\Omega = \Omega_0, Z = 2\Omega_0$ and $Q' = 0$ inside the core, (2.28)-(2.30) reduce to:

$$[(\omega - m\Omega_0)^2\{r^2D^2 + rD - m^2 - k^2r^2\} + 4k^2r^2\Omega_0^2]\hat{u}_z^i = 0, \tag{2.31}$$

$$\{(\omega - m\Omega_0)^2 - 4\Omega_0^2\}\hat{u}_r^i = -\frac{i}{rk}(\omega - m\Omega_0)[(\omega - m\Omega_0)rD - 2m\Omega_0]\hat{u}_z^i, \tag{2.32}$$

$$\{(\omega - m\Omega_0)^2 - 4\Omega_0^2\}\hat{u}_\theta^i = -\frac{1}{rk}(\omega - m\Omega_0)[2\Omega_0 rD - m(\omega - m\Omega_0)]\hat{u}_z^i. \tag{2.33}$$

In the outer irrotational region, $Z = 0$ and (2.28)-(2.30) simplify to:

$$(\omega - m\Omega)^2[r^2D^2 + rD - m^2 - k^2r^2]\hat{u}_z^o = 0, \tag{2.34}$$

$$\hat{u}_r^o = -\frac{i}{k}D\hat{u}_z^o, \tag{2.35}$$

$$\hat{u}_\theta^o = \frac{m}{rk}\hat{u}_z^o, \tag{2.36}$$

where the superscripts i and o denote the core and exterior regions, respectively.

The equation for $\hat{u}_z^i$ may be rewritten as a Bessel equation, and analyticity at the origin implies:

$$\hat{u}_z^i \propto dJ_m(\beta r), \tag{2.37}$$

In (2.37), $\beta^2 \equiv k^2(4\Omega_0^2 - g^2)/g^2$ with $g = (m\Omega_0 - \omega)$ may be regarded as a radial wavenumber. The equation for $\hat{u}_z^o$ is the modified Bessel equation, and similar to the $2D$ scenario, allows for

two possibilities. The first is the homogeneous solution consistent with a decaying far-field:

$$\hat{u}_z^o \propto K_m(kr), \tag{2.38}$$

$K_m(z)$ being the modified bessel function of the second kind, and leads to an irrotational velocity field outside the core. Continuity of u_z at $r = a$ gives

$$\hat{u}_z^i = \frac{J_m(\beta r)}{J_m(\beta a)}, \qquad \hat{u}_z^o = \frac{K_m(kr)}{K_m(ka)}, \tag{2.39}$$

and further, enforcing continuity of u_r at $r = a$ gives the familiar dispersion relation for the $3D$ Kelvin modes (see Saffman [1992]):

$$\frac{g^2}{(4\Omega_0^2 - g^2)}\left[\frac{\beta a J_m'(\beta a)}{J_m(\beta a)} + \frac{2m\Omega_0}{g}\right] = -\frac{kaK_m'(ka)}{K_m(ka)}. \tag{2.40}$$

The relation (2.40) yields a denumerable infinity of modes for a fixed k and m. For a given non-zero m, the dispersion curves (see LHS of figure 2.3) span the interval $\omega \equiv [(m-2)\Omega_0, (m+2)\Omega_0]$. The modes may be classified based on the sign of the Doppler frequency; $g < 0$ corresponds to the co-grade modes and $g > 0$ to the retrograde modes. The co-grade and retrograde families are not symmetric (about $m\Omega_0$) for non-zero m and, apart from numerical differences in the ω values for a given k, the retrograde family includes an additional (structureless) branch that reduces to the $2D$ Kelvin mode, with $\omega = (m-1)\Omega_0$, for $k \to 0$. It is convenient to use a modal index, n, to enumerate the solutions (β_n) of (2.40); thus, $\beta_{n,-1}$ and $\beta_{n,+1}$, with n being a positive integer, correspond to the retrograde and co-grade afamilies, respectively. $\beta_{1,-1}$ corresponds to the structureless mode, while the remainder of the dispersion curves, both co-grade and retrograde, correspond to the 'structured' modes, a measure of this structure being the number of zero-crossings of the axial vorticity $(w_z \propto J_m(\beta_n r))$ which increases with increasing n. Further, $\beta_n \to \infty$, $\omega_n \to m\Omega_0$ for $n \to \infty$, so the structured modes become nearly-convected modes, concentrated in the vicinity of the symmetry axis, for large n. The Kelvin-mode vorticity eigenfunctions are given by:

$$\hat{w}^{\text{Kelvin}}_{z,n,\pm1}(r) = -\frac{2g_n\Omega_0\beta_n^2}{k\{g_n^2 - 4\Omega_0^2\}}\frac{J_m(\beta_n r)}{J_m(\beta_n a)}\mathcal{H}(a-r) + [\hat{u}_\theta]^{r=a^+}_{r=a^-}\,\delta(r-a), \tag{2.41}$$

$$\hat{w}^{\text{Kelvin}}_{r,n,\pm1}(r) = -\frac{2i\Omega_0}{r\{g_n^2 - 4\Omega_0^2\}}\left[g_n\frac{\beta_n r J_m'(\beta_n r)}{J_m(\beta_n a)} + 2m\Omega_0\frac{J_m(\beta_n r)}{J_m(\beta_n a)}\right]\mathcal{H}(a-r), \tag{2.42}$$

$$\hat{w}^{\text{Kelvin}}_{\theta,n,\pm1}(r) = \frac{2\Omega_0}{r\{g_n^2 - 4\Omega_0^2\}}\left[2\Omega_0\frac{\beta_n r J_m'(\beta_n r)}{J_m(\beta_n a)} + mg_n\frac{J_m(\beta_n r)}{J_m(\beta_n a)}\right]\mathcal{H}(a-r), \tag{2.43}$$

where

$$[\hat{u}_\theta]^{r=a^+}_{r=a^-} = -\frac{2\Omega_0}{ka(g_n^2 - 4\Omega_0^2)}\left\{g_n\frac{\beta_n a J_m'(\beta_n a)}{J_m(\beta_n a)} + 2m\Omega_0\right\}, \tag{2.44}$$

with $g_n = (m\Omega_0 - \omega_n)$ and $\beta_n^2 = k^2(4\Omega_0^2 - g_n^2)/g_n^2$; the subscript ±1 in (2.41)-(2.43) discriminates between co-grade and retrograde modes.

As mentioned in the introduction, the $2D$ Kelvin mode transforms into a damped singular mode for a general smooth vorticity profile with $DZ(r_f) \neq 0$ (Le Dizès [2000]). The damping

rate is independent of Re for $Re \gg 1$, arising due to an increasingly fine-scaled structure (the spatial scale being $O(Re^{-\frac{1}{2}})$) inside a viscous critical layer with a thickness of $O(DZ)$ around r_f (Lin [1955]). Both computations for large Re, and estimates based on a contour deformation calculation, for a Lamb-Oseen profile, show that the $3D$ retrograde modes of a Rankine vortex are again replaced by inviscidly damped critical-layer modes (Fabre [2002],Fabre *et al.* [2006]). There appear to exist a countable infinity of such modes with the damping rate possibly dependent on the values of both Z and DZ at r_f. The singular effect of viscosity is especially important for the structured modes; in sharp contrast to the predictions of (2.40), the dispersion curves for the Lamb-Oseen profile do not asymptote to the core angular frequency in the limit $k \to 0$. Bending modes ($m = 1$) are particularly important in this regard, since (2.40) for $m = 1$ allows for modes with a negative ω (counter-grade) that then lie outside the base-state range of frequencies. Every retrograde bending mode invariably becomes counter-grade for large enough k, and correspondingly, the critical radius moves off to infinity and onto the complex plane. Counter-grade modes for a smooth vorticity profile are therefore expected to remain qualitatively unaltered for a general vorticity profile, and with the inclusion of viscosity, as is confirmed by numerical calculations (Fabre *et al.* [2006]).

The dispersion curves for axisymmetric ($m = 0$) column oscillations are symmetric about $\omega = 0$, and denote sausaging modes that travel in opposite directions along the core. The dynamics involves the alternate twisting and un-twisting of the vortex lines on surfaces approximately concentric with the cylindrical core boundary; the associated radial displacements are smaller for larger n, and the weaker (Coriolis) restoring forces imply that $\omega_n \to 0$ for $n \to \infty$. Importantly, (2.28), for $m = 0$, defines a regular Sturm-Liouville problem for an arbitrary axial vorticity profile and the completeness of the denumerably infinite family of axisymmetric modes follows (Chandrasekhar [1961],Ince [1956]). The absence of a critical layer singularity also implies that the dispersion curves for the sausaging modes remain qualitatively unaltered for a smooth vorticity profile and for large but finite Re (Fabre [2002]). Thus, for a general non-compact vorticity profile, an arbitrary small-amplitude axisymmetric disturbance may still be represented as a superposition of evolving axisymmetric Kelvin modes. For a Rankine vortex, however, the complete separation of the regions of strain ($r > a$) and vorticity ($r < a$) implies that one must distinguish between vortical perturbations related to an axisymmetric column deformation and similar disturbances present in the irrotational exterior. The standard Sturm-Liouville arguments allow one to infer the completeness of the axisymmetric Kelvin modes, with frequencies obtained from (2.40), for the former class of disturbances (column deformations). The question regarding the response of the Rankine vortex to exterior vortical perturbations remains. Since any perturbation with $m = 0$ evolves unchanged even in the presence of differential shear, there is evidently a degeneracy as regards a modal decomposition for exterior perturbations. We return to this point, and the related implications for the transient growth observed in recent simulations, even for $m = 0$ (Pradeep & Hussain [2006]), after the analysis for the non-axisymmetric CS-modes in sections 6.3.1 and 6.3.2.

Since the Kelvin modes above arise from the homogeneous solution of (2.34), they have vorticity within the core and an axial vortex sheet at its edge. A natural question is if these modes can therefore represent an arbitrary vortical initial condition restricted to the region

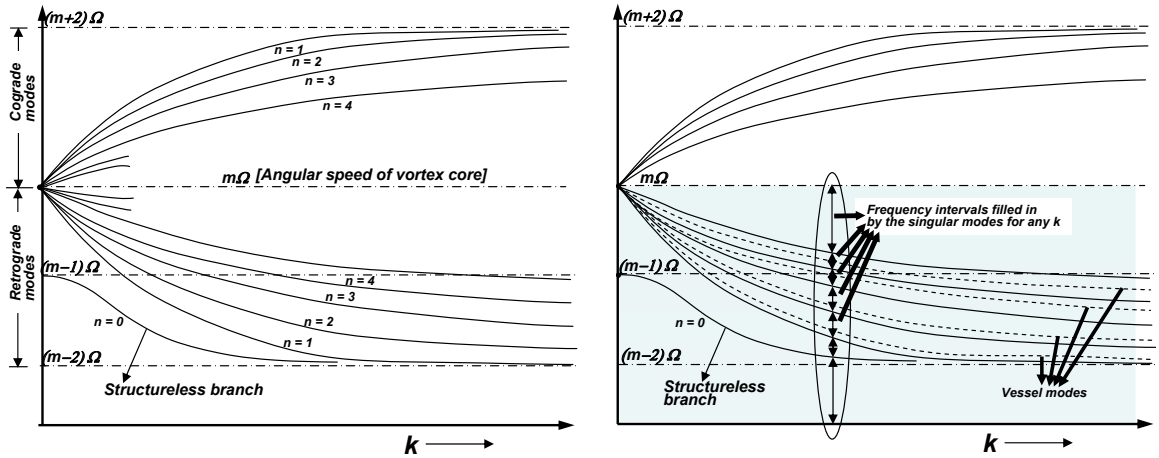

Figure 2.3: The figure on the left is a sketch of the dispersion curves that result from (2.40 for a given m. The figure on the right includes the continuous spectrum depicted by the shaded region; the additional dashed curves in the retrograde frequency range denote the $3D$ vessel modes defined by (A.8). For each k, the singular eigenmodes that make up the continuous spectrum fill up the frequency intervals between the retrograde dispersion curves.

$r \leq a$; in effect, an arbitrary small-amplitude deformation of the vortex column. The discussion in the preceding paragraph shows that this is certainly true for $m = 0$. For non-zero m, however, (2.28) has singular coefficients, and the standard Sturm-Liouville arguments do not apply. Thus, the completeness of the Kelvin modes alone, in the absence of additional singular eigenmodes (constituting the continuous spectrum), is not obvious. This question has been recently answered in the affirmative by Arendt *et al.* [1997], and our primary focus here is on the complementary situation; that is, on the additional modes required for the evolution of an arbitrary vortical initial condition outside the core, a situation of particular relevance to the transient growth recently observed for single vortices (see Antkowiak & Brancher [2004],Pradeep & Hussain [2006]). In what follows, we show that there are two families of singular eigenmodes needed to evolve an arbitrary initial condition (an arbitrary solenoidal distribution of vorticity). With the inclusion of these singular eigenmodes, every retrograde frequency except for those corresponding to the Kelvin modes, is doubly degenerate. There is some leeway as to how the aforementioned partition of the continuous spectrum may be made, and we choose a division based on the presence or absence of radial vorticity in the singular part of the eigenfunction. For the eigenfunctions in the first family, the singular structure is a cylindrical vortex sheet at the critical radius, threaded by helical lines, and thereby devoid of radial vorticity. For the eigenfunctions in the second family, the singular structure is again localized at the critical radius, but possesses radial vorticity; the vortex lines in this case form cells of an infinitesimal thickness in the plane transverse to the rotation axis.

3D continuous spectrum modes - the Λ_1-family (zero radial vorticity)

The Λ_1-eigenmodes are the natural generalization of the $2D$ CS-modes analyzed in section 2.2.1. Equation (2.34) allows for a vortex sheet, threaded by helical lines, in the outer irrotational region. Thus,

$$[r^2D^2 + rD - m^2 - r^2k^2]\hat{u}_z^o = a_1\delta(\omega - m\Omega) + a_2\delta'(\omega - m\Omega), \tag{2.45}$$

so that, as in (2.5), there is again an inhomogeneity proportional to a generalized function; here, we have used the identity $x^2\{a_1\delta(x) + a_2\delta'(x)\} = 0$. One may rewrite (2.45) as:

$$[r^2D^2 + rD - m^2 - r^2k^2]\hat{u}_z^o = A_1(r_f)\delta(r - r_f) + A_2(r_f)\delta'(r - r_f), \tag{2.46}$$

with $r_f = (\frac{m\Omega_0}{\omega})^{\frac{1}{2}}a$ denoting the location of the exterior vortex sheet. For the vortex sheet to lie in the physical domain, r_f must be real, and ω must therefore lie in the base-state range of angular frequencies. The analysis that follows is thus restricted to the retrograde frequency range $(0, m\Omega_0]$. Using $\boldsymbol{w} = \boldsymbol{\nabla} \wedge \boldsymbol{u}$, and in the absence of radial vorticity ($\hat{w}_r = 0$), the following relation between $\hat{u}_z$ and the vorticity field holds for $r \geq a$:

$$[r^2D^2 + rD - m^2 - r^2k^2]\hat{u}_z = -rD(r\hat{w}_\theta). \tag{2.47}$$

Comparing (2.47) and (2.46), and noting that $\hat{w}_\theta$ for the Λ_1-family is proportional to $\delta(r - r_f)$, one obtains $A_2(r_f) = -r_fA_1(r_f)$. The azimuthal and axial components of the (helical) vortex sheet strength (A_{Λ_1}) are $A_{\theta\Lambda_1} = A_1(r_f)/r_f$ and $A_{z\Lambda_1} = -mA_1(r_f)/(kr_f^2)$, respectively, the pitch of a helical vortex line being $|2\pi r_f(A_{z\Lambda_1}/A_{\theta\Lambda_1})| = (2\pi m)/k$.

The solution of (2.46) is obtained by separate consideration of three ($r < a, a < r < r_f$, and $r > r_f$) rather than two regions (as was the case for the regular modes). The solutions in these regions, consistent with regularity both at the origin and at infinity, are:

$$\hat{u}_z^{i1} = dJ_m(\beta r), \qquad (0 < r < a), \tag{2.48}$$

$$\hat{u}_z^{o2} = c_1I_m(kr) + c_2K_m(kr), \qquad (a < r < r_f), \tag{2.49}$$

$$\hat{u}_z^{o3} = f(ka)\frac{\Omega_0a^2}{r_f}K_m(kr), \qquad (r > r_f), \tag{2.50}$$

where the normalization, as in section 2.2.1, is applied to the region outside the vortex sheet at $r = r_f$. The normalizing factor, $f(ka) = -\mathrm{i}/[m\,kaK_m(ka)]$, enforces agreement between the limiting forms of the $3D$-modes, for $k \to 0$, and the $2D$-modes found earlier. The constants c_1 and c_2 are determined from the following matching conditions obtained by integrating (2.46) over an infinitesimal interval including $r = r_f$:

$$A_2(r_f) = -r_fA_1(r_f), \tag{2.51}$$

$$\hat{u}_z^{o2} - \hat{u}_z^{o3} = -\frac{A_2(r_f)}{r_f^2} = \frac{A_1(r_f)}{r_f}, \qquad \text{at} \qquad r = r_f, \tag{2.52}$$

$$D\hat{u}_z^{o2} = D\hat{u}_z^{o3}, \qquad \text{at} \qquad r = r_f. \tag{2.53}$$

The condition (2.51) has already been obtained above, and shows that the jumps in the axial and azimuthal components of the velocity perturbation are not independent, being related by the fact that the pitch of the helical vortex lines at $r = r_f$ is entirely determined by m and k. (2.53) enforces continuity of the radial velocity perturbation, thereby excluding a singular jet-like profile riding on the vortex sheet, while (2.52) characterizes the jump in the axial velocity

across the helical vortex sheet at $r = r_f$. From (2.49), (2.50), and (2.52), (2.53), one obtains:

$$c_1 = -kK'_m(kr_f)A_1(r_f), \tag{2.54}$$

$$c_2 = f(ka)\frac{\Omega_0 a^2}{r_f} + kI'_m(kr_f)A_1(r_f), \tag{2.55}$$

the simplified expressions arising from use of the Wronskian for the modified Bessel equation. The constant d in (2.48) is determined from the continuity of the axial velocity at $r = a$, and given by:

$$d = \frac{(f(ka)\Omega_0 a^2/r_f)K_m(ka) + kA_1(r_f)\{I'_m(kr_f)K_m(ka) - K'_m(kr_f)I_m(ka)\}}{J_m(\beta a)} \tag{2.56}$$

From (2.32) and (2.35) we have the following expressions for radial velocity at $r = a$,

$$\hat{u}_r^{i1}|_{r=a} = -\frac{idg}{ka(g^2 - 4\Omega_0^2)}\{g\beta a J'_m(\beta a) + 2m\Omega_0 J_m(\beta a)\}, \tag{2.57}$$

$$\hat{u}_r^{o2}|_{r=a} = -\frac{i}{I'_m(kr_f)}[c_2\{I'_m(kr_f)K'_m(ka) - K'_m(kr_f)I'_m(ka)\} + K'_m(kr_f)I'_m(ka)]. \tag{2.58}$$

Equating (2.57) and (2.58), to enforce continuity of the radial velocity at $r = a$, one obtains, after some algebra, the following expression for the vortex sheet amplitude:

$$A_1(r_f) = f(ka)\frac{\Omega_0 a^2}{r_f}\frac{M(r_f; ka, \beta a)}{k\{K'_m(kr_f)N(r_f; ka, \beta a) - I'_m(kr_f)M(r_f; ka, \beta a)\}}, \tag{2.59}$$

where

$$M(r_f; ka, \beta a) = g^2\beta a J'_m(\beta a)K_m(ka) + 2m\Omega_0 g J_m(\beta a)K_m(ka) + (4\Omega_0^2 - g^2)J_m(\beta a)kaK'_m(ka), \tag{2.60}$$

$$N(r_f; ka, \beta a) = g^2\beta a J'_m(\beta a)I_m(ka) + 2m\Omega_0 g J_m(\beta a)I_m(ka) + (4\Omega_0^2 - g^2)J_m(\beta a)kaI'_m(ka). \tag{2.61}$$

As in section 2.2.1, the retrograde Kelvin modes naturally emerge as the ones for which $A_1(r_f) = 0$. The functions M and N remain finite for any finite r_f, and so do the modified Bessel functions. Further, since the zeroes of M and N interlace each other, the condition of a vanishing vortex sheet amplitude implies $M = 0$; this is precisely the dispersion relation for the Kelvin modes (see (2.40)). In contrast to the $2D$ case, where a vanishing vortex sheet amplitude led to a single value of r_f (the structureless mode) for a fixed m ($r_{fk} = (\frac{m}{m-1})^{\frac{1}{2}}a$), in $3D$ one has a countable infinity of critical radii for a given m and k. The vorticity field associated with a Λ_1-eigenmode

is given by

$$\hat{w}_z^{\Lambda_1}(r;r_f) = -\frac{2dg\Omega_0\beta^2 J_m(\beta r)}{k\{g^2-4\Omega_0^2\}}\mathcal{H}(a-r) + [\hat{u}_\theta]_{r=a^-}^{r=a^+}\,\delta(r-a) - \frac{mA_1(r_f)}{kr_f^2}\,\delta(r-r_f), \tag{2.62}$$

$$\hat{w}_r^{\Lambda_1}(r;r_f) = -\frac{2id\Omega_0}{r\{g^2-4\Omega_0^2\}}\left[g\beta r J_m'(\beta r) + 2m\Omega_0 J_m(\beta r)\right]\mathcal{H}(a-r), \tag{2.63}$$

$$\hat{w}_\theta^{\Lambda_1}(r;r_f) = \frac{2d\Omega_0}{r\{g^2-4\Omega_0^2\}}\left[2\Omega_0\beta r J_m'(\beta r) + mgJ_m(\beta r)\right]\mathcal{H}(a-r) + \frac{A_1(r_f)}{r_f}\,\delta(r-r_f), \tag{2.64}$$

$$\text{where}\quad [\hat{u}_\theta]_{r=a^-}^{r=a^+} = \frac{m}{ka}\left[c_1 I_m(ka)+c_2 K_m(ka)\right] - \frac{dg}{ka\{g^2-4\Omega_0^2\}}\left[2\Omega_0\beta a J_m'(\beta a)+mgJ_m(\beta a)\right], \tag{2.65}$$

with the radial vorticity field, expectedly, being confined to the core region. Here, c_1, c_2 and d are given by (2.54)-(2.56). The structure of typical Λ_1-eigenmodes is shown in figure **??**.

Figure 2.4 plots $A_1(r_f)$ as a function of r_f for $m = 2$ and $k = 3$; the essential features remain unchanged for other values of m and k. Interestingly, in addition to the values of r_f corresponding to the Kelvin mode frequencies, for which $A_1(r_f) = 0$, there are values at which $A_1(r_f)$ diverges. Since M and N have zeroes interlacing each other as a function of r_f, the zeroes and singularities of $A_1(r_f)$ also interlace each other, and the latter again form a countably infinite set. The divergences are an artifact of the normalization used in (2.48)-(2.50), and physically, at these r_f's, the vortex sheet entirely screens the perturbation velocity field induced by the oscillating column (that is, $\hat{u}_z^{o3} = 0$). In doing so, the sheet acts as an impenetrable wall, and, for the given m and k, the corresponding frequency must therefore be a solution of the dispersion relation for a Rankine vortex in a cylindrical vessel of size r_f. From (2.59), the locations at which $A_1(r_f) \to \infty$ must satisfy $K_m'(kr_f)N - I_m'(kr_f)M = 0$; in appendix A, it is shown that this is indeed the relation governing the normal modes of a Rankine vortex with a core of radius a embedded in a vessel of radius r_f. For a fixed r_f, and thence, a fixed $\omega\,(= m\Omega_0(a/r_f)^2)$ in the range $[(m-2)\Omega_0, m\Omega_0]$, the singular eigenmodes are coincident with vessel modes, in the region $0 < r < r_f$, at a denumerable infinity of axial wavenumbers (the limit point being infinity). Not all vessel modes will be recovered from the present analysis since, although the vessel wall may always be regarded as a vortex sheet, one has here the additional constraint that the vortex sheet convect with the base-state flow velocity at $r = r_f$.

A sketch of the frequency intervals spanned by the CS-modes, including the vessel mode loci, appears on the RHS in figure 2.3. The CS-modes occupy the intervals between the discrete retrograde frequencies, and with their inclusion, the Rankine spectrum, for fixed m and k, consists of the denumerable infinity of co-grade frequencies together with the entire retrograde frequency interval $(0, m\Omega_0)$. The case $m = 1$ is an exception, since the counter-grade mode frequencies remain unaffected, and the spectrum therefore remains discrete in the interval $[-\Omega_0, 0]$. The analysis for the Λ_1-eigenmodes above, although more involved algebraically, is still analogous to the one in two dimensions; in that the difference between the regular (retrograde Kelvin) and singular eigenmodes is the existence, in the latter case, of an additional vortex sheet at the critical radius. This may be seen from comparing the vorticity eigenfunctions for a Λ_1-eigenmode,

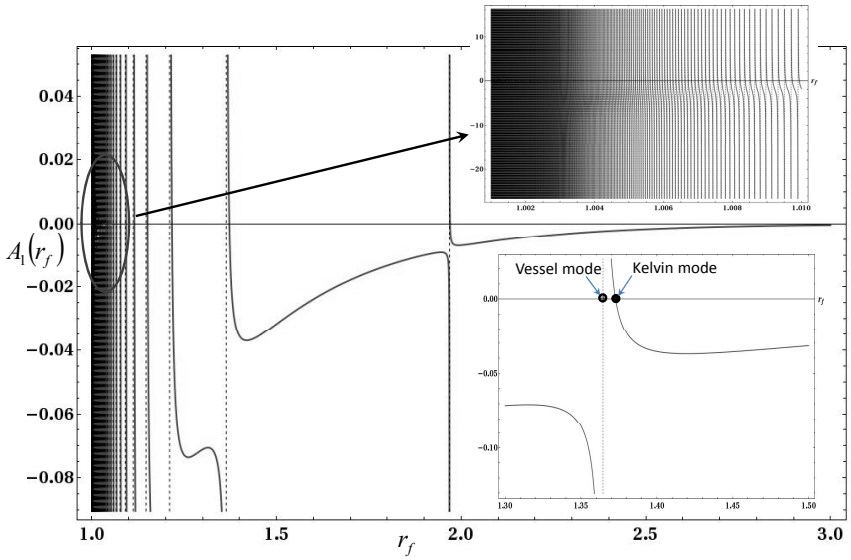

(a)

Figure 2.4: The vortex sheet amplitude, $A_1(r_f)$ for $m = 2$ and $k = 3$. The vertical dashed lines, defined by $1/A_1 = 0$, correspond to the vessel mode loci (that interlace the Kelvin mode frequencies). The amplitude changes sign at an increasingly rapid rate as $r_f \to 1$, and the inset offers a magnified view of the variation near the core.

given by (2.62)-(2.64), to those of a Kelvin mode given by (2.41)-(2.43).

The singularity of the Λ_2-eigenmodes analyzed below, although not a vortex sheet, is again localized at the critical radius. This localization of the vorticity is possible due to the complete spatial separation of the regions of (base-state) vorticity and shear for a Rankine vortex. For a parallel flow, on the other hand, the lack of such a separation makes the three-dimensional singular eigenmodes quite different from the two-dimensional ones. As shown in Sazonov [1996], for unbounded Couette flow, the singular modes with wave vectors inclined to the plane of shear are no longer localized vortex sheets coincident with streamlines of the base-state flow like those originally found by Case [1960] in two dimensions. Instead, the spanwise variation of the perturbation velocity field acts to stretch and tilt the ambient vorticity, leading to additional non-local contributions (with a principal-value singularity) to the perturbation vorticity field. As will be seen in 2.2.2, this makes the solution of the 3D IVP for the Rankine vortex, via a modal superposition, (conceptually) easier than the one for Couette flow.

3D continuous spectrum modes - the Λ_2-family (with radial vorticity)

Unlike the Λ_1 family, the Λ_2-eigenmodes possess radial vorticity localized in the singular vortical structure at the critical radius. It is convenient to analyze this case starting from (2.47) now generalized to a non-zero $\hat{w}_r$:

$$[r^2D^2 + rD - m^2 - r^2k^2]\hat{u}_z = -rD(r\hat{w}_\theta) + imr\hat{w}_r. \tag{2.66}$$

The Λ_2 family, in its simplest form, may be obtained by setting $\hat{w}_z = 0$ for $r > a$, while allowing for the radial vorticity field to include a delta function. The resulting singular structure at $r = r_f$ is characterized by a vorticity field in the plane transverse to the rotation axis,

$(\hat{w}_r, \hat{w}_\theta) \equiv [A_{r\Lambda_2}\delta(r-r_f), r_f A_{\theta\Lambda_2}\delta'(r-r_f)]$, with $r_f \geq a$ and $A_{r\Lambda_2} = -imA_{\theta\Lambda_2}$. Equation (2.66) takes the form:

$$[r^2D^2 + rD - m^2 - r^2k^2]\hat{u}_z^o = A_1(r_f)\delta(r-r_f) + A_2(r_f)\delta'(r-r_f) + A_3(r_f)\delta''(r-r_f), \quad (2.67)$$

where $A_1 = (m^2-1)r_f A_{\theta\Lambda_2}$, $A_2 = 3r_f^2 A_{\theta\Lambda_2}$ and $A_3 = -r_f^3 A_{\theta\Lambda_2}$. For the Λ_2 modes, $\hat{u}_r$ is discontinuous at $r = r_f$, implying a delta-function singularity in $\hat{u}_z$, and thence, a localized axial jet riding on the convected singular structure. With $\hat{u}_z = \hat{u}_z^{\text{reg}} + P_1\delta(r-r_f)$, P_1 being a measure of the jet volumetric flux, the following matching conditions result from integrating (2.67) in an infinitesimal interval around r_f:

$$r_f^2[D\hat{u}_z^{\text{reg}}]_{r_f^-}^{r_f^+} - r_f[\hat{u}_z^{\text{reg}}]_{r_f^-}^{r_f^+} - P_1\{(m^2-1) + (kr_f)^2\} = A_1, \quad (2.68)$$

$$-r_f^2[\hat{u}_z^{\text{reg}}]_{r_f^-}^{r_f^+} + 3r_f P_1 = -A_2, \quad (2.69)$$

$$2r_f^2 P_1 = 2A_3. \quad (2.70)$$

The expressions for the velocity fields and the different regions under consideration remain identical to section 6.3.1. Enforcing the continuity of the radial and axial velocity components at $r = a$, and a little algebra, leads to the following expressions for the constants characterizing the velocity fields in the different regions (see equations (2.48), (2.49) and (2.50)):

$$c_1 = A_{\theta\Lambda_2}K_m(kr_f)(kr_f)^2, \quad (2.71)$$

$$c_2 = f(ka)\frac{\Omega_0 a^2}{r_f} - A_{\theta\Lambda_2}I_m(kr_f)(kr_f)^2 \quad (2.72)$$

$$d = \frac{(f(ka)\Omega_0 a^2/r_f)K_m(ka) + A_{\theta\Lambda_2}(kr_f)^2\{K_m(kr_f)I_m(ka) - I_m(kr_f)K_m(ka)\}}{J_m(\beta a)} \quad (2.73)$$

The amplitude of the singular vortical structure at $r = r_f$ is given by:

$$A_{\theta\Lambda_2}(r_f) = -f(ka)\frac{\Omega_0 a^2}{r_f}\frac{M(r_f; ka, \beta a)}{(kr_f)^2\{K_m(kr_f)N(r_f; ka, \beta a) - I_m(kr_f)M(r_f; ka, \beta a)\}}. \quad (2.74)$$

with $P_1 = r_f A_{\theta\Lambda_2}$; a sketch of a typical Λ_2-eigenmode ($m = 3$) appears in figure **??**(d). From (2.74), and similar to the case of the $\Lambda 1$-modes, the singular structure again disappears for $M = 0$ - the dispersion relation for the Kelvin modes. The amplitude, $A_{\theta\Lambda_2}$, also diverges at the zeros of $K_m(kr_f)N - I_m(kr_f)M$ with the zeroes and divergences of $A_{\theta\Lambda_2}$ interlacing each other as shown in figure 2.5. The singularities again imply a quiescent exterior ($r > r_f$) as the singular structure at these radii screens the perturbation velocity field induced by the column oscillations. An analogy with a bounded domain problem is, however, not evident owing to the axial jet riding on the vessel walls. Finally, the vorticity field associated with a Λ_2-eigenmode is

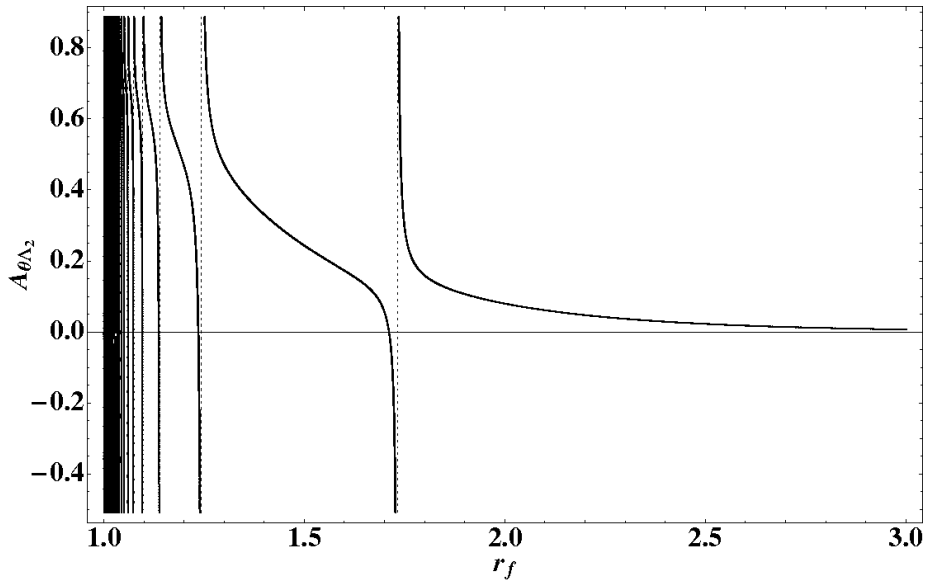

(a)

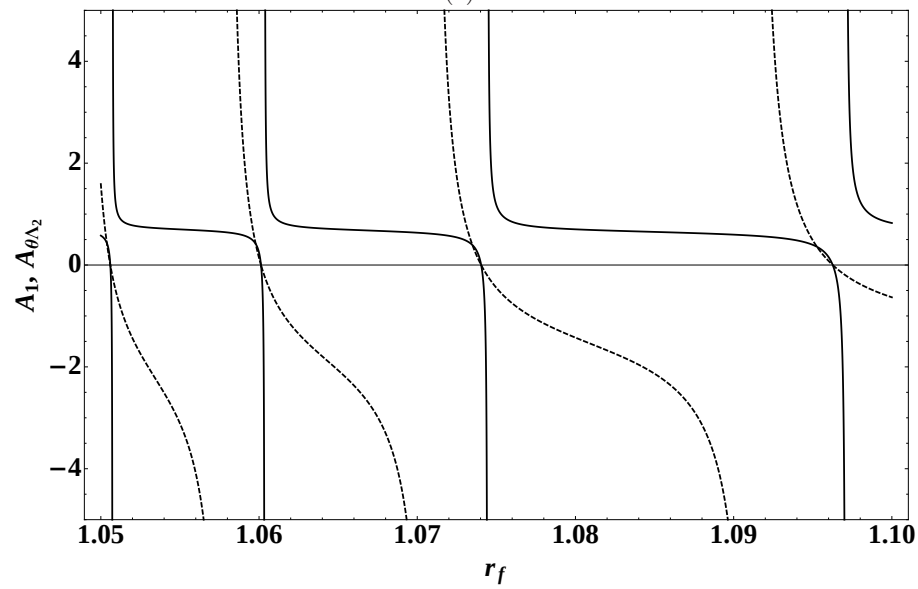

(b)

Figure 2.5: (a)The amplitude of the vortex sheet for Λ_2 family, $A_{\theta\Lambda_2}$, as a function of r_f, for $m = 2$ and $k = 2$; the figure on the right (b) offers a magnified view of the rapid variation near the core of the amplitudes of the singular structures for the Λ_2 (dashed) family and its comparison with its Λ_1 (continuous) counterpart. The amplitudes A_1 and $A_{\theta\Lambda_2}$ evidently have coincident zeros (which correspond to the Kelvin radii) but distinct singularities.

given by

$$\hat{w}_z^{\Lambda_2}(r;r_f) = -\frac{2dg\Omega_0\beta^2 J_m(\beta r)}{k\{g^2-4\Omega_0^2\}}\mathcal{H}(a-r) + [\hat{u}_\theta]_{r=a^-}^{r=a^+}\,\delta(r-a), \tag{2.75}$$

$$\hat{w}_r^{\Lambda_2}(r;r_f) = -\frac{2id\Omega_0}{r\{g^2-4\Omega_0^2\}}\left[g\beta r J_m'(\beta r) + 2m\Omega_0 J_m(\beta r)\right]\mathcal{H}(a-r) - imA_{\theta\Lambda_2}\delta(r-r_f), \tag{2.76}$$

$$\hat{w}_\theta^{\Lambda_2}(r;r_f) = \frac{2d\Omega_0}{r\{g^2-4\Omega_0^2\}}\left[2\Omega_0\beta r J_m'(\beta r) + mgJ_m(\beta r)\right]\mathcal{H}(a-r) + r_f A_{\theta\Lambda_2}\delta'(r-r_f), \tag{2.77}$$

$$\text{where}\quad [\hat{u}_\theta]_{r=a^-}^{r=a^+} = \frac{m}{ka}\left[c_1 I_m(ka)+c_2 K_m(ka)\right] - \frac{dg}{ka\{g^2-4\Omega_0^2\}}\left[2\Omega_0\beta a J_m'(\beta a)+mgJ_m(\beta a)\right], \tag{2.78}$$

and c_1, c_2 and d being given by (2.71)-(2.73).

As shown in figure 2.5(b), in light of the Λ_1 and Λ_2 families, the Kelvin mode frequencies and the corresponding eigenfunctions ((2.41)-(2.43)) may now be regarded as degenerate in that they correspond to the zeroes of both $A_1(r_f)$ and $A_{\theta\Lambda_2}(r_f)$.

The modal decomposition for an arbitrary vortical initial condition

For a fixed $m\,(\neq 0)$ and k, an arbitrary smooth initial distribution of vorticity of the form $\boldsymbol{w}(\boldsymbol{x},0) = [w_{r0}(r), w_{\theta 0}(r), \frac{i}{(kr)}(imw_{\theta 0}(r) + (rw_{r0}(r))')]e^{i(kz+m\theta)}$ now evolves as the following superposition of the Kelvin modes, and the Λ_1 and Λ_2 families:

$$\begin{aligned}\boldsymbol{w}(\boldsymbol{x},t) = &\int_{a^+}^{\infty}\left[X_{\Lambda_1}(r_f)\hat{\boldsymbol{w}}^{\Lambda_1}(r;r_f)+X_{\Lambda_2}(r_f)\hat{\boldsymbol{w}}^{\Lambda_2}(r;r_f)\right]e^{i[kz+m(\theta-\Omega(r_f)t)]}dr_f \\ &+\left\{\sum_{b=\pm 1}\sum_{n=1}^{\infty}(C_{nb}-A_{nb})\hat{\boldsymbol{w}}_{nb}^{\text{Kelvin}}(r)e^{-i\omega_n t}\right\}e^{i(kz+m\theta)},\end{aligned} \tag{2.79}$$

where

$$X_{\Lambda_1}(r_f) = \frac{r_f}{A_1}\left[w_{\theta 0}(r_f)\mathcal{H}(r_f-a) - \frac{i}{m}\left(r_f w_{r0}(r_f)\mathcal{H}(r_f-a)\right)'\right], \tag{2.80}$$

$$X_{\Lambda_2}(r_f) = \frac{i}{m}\frac{w_{r0}(r_f)\mathcal{H}(r_f-a)}{A_{\theta\Lambda_2}}, \tag{2.81}$$

and $\hat{\boldsymbol{w}}_{nb}^{\text{Kelvin}}$, $\hat{\boldsymbol{w}}^{\Lambda_1}$ and $\hat{\boldsymbol{w}}^{\Lambda_2}$ are known from (2.41)-(2.43), (2.62)-(2.64) and (2.75)-(2.77), respectively. The ω_n's in (2.79) are the Kelvin mode frequencies obtained from (2.40), and the C_{nb}'s and A_{nb}'s denote the corresponding modal amplitudes. The expression (2.79) may be arrived at by examining the modal superposition at $t = 0$. The latter is obtained by first determining the superposition of Λ_2-eigenmodes needed to represent the initial radial vorticity in $r > a$; the required amplitude distribution is given by (3.58). The difference between the initial and Λ_2-azimuthal vorticities, for $r > a$, may then be represented by a superposition of Λ_1-eigenmodes (the axial component is automatically determined from the solenoidal constraint) with the amplitude distribution being given by (2.80). This superposition of Λ_1 and Λ_2-eigenmodes now accounts for the entire initial vorticity outside the core. What remains is

the initial vorticity inside the core (and a possible axial vortex sheet at its edge) and the additional core and edge vorticities generated by the Λ_i-superposition. Using the results of Arendt et al (1997), both these contributions may be expressed as a summation over Kelvin modes. The required Kelvin-mode amplitude distributions are

$$C_{nb}\,(A_{nb}) = \left[\frac{g_{C(A)}(a)J'_m(k\xi_n a)}{k\xi_n a J_m(k\xi_n a)} - a\frac{g'_{C(A)}(a)}{(k\xi_n a)^2} + P_{C(A)}\right] B^b_n, \tag{2.82}$$

where

$$B^b_n = \frac{2\xi_n^2 bi\Omega_0}{(\xi_n^2+1)^{3/2}}\left[\frac{2J'_m(k\xi_n a)}{k\xi_n a J_m(k\xi_n a)} + \left\{\frac{J'_m(k\xi_n a)}{J_m(k\xi_n a)}\right\}^2 + 1 - \frac{m^2}{(k\xi_n a)^2} + \frac{bm(\xi_n^2+2)}{\sqrt{\xi_n^2+1}(k\xi_n a)^2}\right]^{-1}, \tag{2.83}$$

$$P_{C(A)} = \frac{1}{k^2 a}\left\{\frac{2\Omega_0 w^{\rm core}_{rC(A)}(a) + i(\omega_n - m\Omega_0)w^{\rm core}_{\theta C(A)}(a)}{(\omega_n - m\Omega_0)^2 - 4\Omega_0^2}\right\}, \tag{2.84}$$

$$g_{C(A)}(a) = \int_0^a \frac{\pi r'}{2}\left[\frac{2\Omega_0 ik}{(\omega_n - m\Omega_0)^2} w^{\rm core}_{zC(A)} - \frac{i}{\omega_n - m\Omega_0}\left\{\frac{d}{dr'}(r' w^{\rm core}_{\theta C(A)}) - imw^{\rm core}_{rC(A)}\right\}\right], \\ \left\{Y_m(k\xi_n a)J_m(k\xi_n r') - J_m(k\xi_n a)Y_m(k\xi_n r')\right\} dr' \tag{2.85}$$

$$\xi_n = \frac{4\Omega_0^2}{g_n^2} - 1, \quad g_n = (m\Omega_0 - \omega_n) \tag{2.86}$$

Equation 2.82 could also be written in the following simplified manner,

$$C_{nb}\,(A_{nb}) = -\frac{B^b_n}{g_n^2(\beta_n a)^2}\left[\int_0^a \left\{2\Omega_0 ikr' w^{\rm core}_{zC(A)} + ig_n\left\{\frac{d}{dr'}(r' w^{\rm core}_{\theta C(A)}) - \right.\right.\right. \\ \left.\left.\left. imw^{\rm core}_{rC(A)}\right\}\right\}\frac{J_m(k\xi_n r')}{J_m(k\xi_n a)}dr' + a\left\{w^{\rm core}_{rC(A)}(a) - ig_n w^{\rm core}_{\theta C(A)}(a)\right\}\right] \tag{2.87}$$

Here, $\boldsymbol{w}^{\rm core}_C(\boldsymbol{x},t)$ is the initial vorticity in the core viz. $(w^{\rm core}_{rC}(r), w^{\rm core}_{\theta C}(r) \equiv (w_{r0}(r), w_{\theta 0}(r))\mathcal{H}(a-r)e^{i(kz+m\theta)}$, and $\boldsymbol{w}^{\rm core}_A(\boldsymbol{x},t)$ is the core projection of the Λ_i-modes given by

$$w^{\rm core}_{rA}(r) = \int_{a^+}^{\infty} X_{\Lambda_2}(r_f)\hat{w}_r^{\Lambda_2}(r;r_f)dr_f\,\mathcal{H}(a-r), \tag{2.88}$$

$$w^{\rm core}_{\theta A}(r) = \int_{a^+}^{\infty}\Big[X_{\Lambda_1}(r_f)w_\theta^{\Lambda_1}(r;r_f) + X_{\Lambda_2}(r_f)w_\theta^{\Lambda_2}(r;r_f)\Big]dr_f\,\mathcal{H}(a-r). \tag{2.89}$$

The expressions (3.60) and (2.86) suggest singularities at the frequency values $\omega = m\Omega_0$ and $\omega = (m \pm 2)\Omega_0$, corresponding to the limits $k \to 0$ and $k \to \infty$, respsectively, of the dispersion curves. It may be shown that $\omega = (m \pm 2)\Omega_0$ are apparent singularities. The core angular frequency $(\omega = m\Omega_0)$, although an essential singularity of the Bessel functions in (2.83), does not contribute for any initial condition that lacks a singular w^θ projection at the edge of the core $(\propto \delta(r-a))$.

The modal superposition, (2.79), may be rewritten as:

$$\begin{aligned}\boldsymbol{w}(\boldsymbol{x},t) &= \int_{a^+}^{\infty}\left[X_{\Lambda_1}(r_f)\hat{\boldsymbol{w}}^{\Lambda_1}(r;r_f)+X_{\Lambda_2}(r_f)\hat{\boldsymbol{w}}^{\Lambda_2}(r;r_f)\right]e^{i[kz+m(\theta-\Omega(r_f)t)]}dr_f\mathcal{H}(r-a)+\\ &\left\{\sum_{b=\pm1}\sum_{n=1}^{\infty}C_{nb}\hat{\boldsymbol{w}}^{\text{Kelvin}}_{nb}(r)e^{-i\omega_n t}\right.\\ &\left.-\int_{a^+}^{\infty}\sum_{b=\pm1}\sum_{n=1}^{\infty}\left[X_{\Lambda_1}(r_f)G^{\Lambda_1}_{nb}+X_{\Lambda_2}(r_f)G^{\Lambda_2}_{nb}\right]\hat{\boldsymbol{w}}^{\text{Kelvin}}_{nb}(r)(e^{-i\omega_n t}-e^{-im\Omega(r_f)t})dr_f\right\}e^{i(kz+m\theta)},\end{aligned} \tag{2.90}$$

with

$$G^{\Lambda_i}_{nb}=\left[\frac{g_i(a)J'_m(k\xi_n a)}{k\xi_n aJ_m(k\xi_n a)}-a\frac{g'_i(a)}{(k\xi_n a)^2}+P_i\right]B^b_n, \tag{2.91}$$

where

$$P_i = \frac{1}{k^2a}\left\{\frac{2\Omega_0 w_r^{\Lambda_i}(a)+i(\omega_n-m\Omega_0)w_\theta^{\Lambda_i}(a)}{(\omega_n-m\Omega_0)^2-4\Omega_0^2}\right\}, \tag{2.92}$$

$$\begin{aligned}g_i(a) &= \int_0^a\frac{\pi r'}{2}\left[\frac{2\Omega_0 ik}{(\omega_n-m\Omega_0)^2}w_z^{\Lambda_i}-\frac{i}{\omega_n-m\Omega_0}\left\{\frac{d}{dr'}(rw_\theta^{\Lambda_i})-imw_r^{\Lambda_i}\right\}\right]\\ &\quad\left\{Y_m(k\xi_n a)J_m(k\xi_n r')-J_m(k\xi_n a)Y_m(k\xi_n r')\right\}dr',\end{aligned} \tag{2.93}$$

and $i=1,2$. Using the expressions for CSMs $(w_r^{\Lambda_i},w_\theta^{\Lambda_i},w_z^{\Lambda_i})$ from equations (2.62)-(2.64) and (2.75)-(2.77) one could simplify $G^{\Lambda_i}_{nb}$ as,

$$G^{\Lambda_i}_{nb}=\frac{d^{\Lambda_i}}{i(\omega_n-m\Omega)}\frac{M}{(ka)^2K_m(ka)}\frac{1}{4\Omega_0^2-g^2}B^b_n \tag{2.94}$$

where, M is defined in equation 2.60 (the Kelvin mode dispersion relation).

For any finite t, each of the Λ_i modes in the initial superposition is convected with the local angular velocity $\Omega(r_f)$ in the irrotational exterior, leading to the first term in (3.58) that denotes exterior vorticity. The evolution of the initial core vorticity is entirely characterized by the Kelvin modes, leading to the second term in (3.58). Finally, the third term accounts for the de-phasing between the core projection of the Λ_i eigenmodes, that is convected with $\Omega(r_f)$, and the Kelvin-mode contributions, characterized by the ω_n's, that cancel out this core projection at the initial instant. The amplitude coefficients in this term, A_{nb}, have a denumerably infinite sequence of singularities of at $\omega=\omega_n$ corresponding to the zeroes of A_1 and $A_{\theta\Lambda 2}$. These singularities are the signatures of the secular growth that would occur for singular initial conditions localized at the Kelvin critical radii, and as in the two-dimensional case, may again be interpreted as resonances between the point and continuous spectra. For helical vortex sheet-type initial conditions, localized at one or more Kelvin radii, resonant interactions between the advected sheet and the corresponding Kelvin mode (s) lead to a quadratic growth in the kinetic energy. In three dimensions, one may also have a localized initial radial vorticity field, in which case there is a further enhancement due to the tilting and stretching of the initial radial vorticity field by the shear in the irrotational exterior. A resonant interaction arises now between a Kelvin mode and a co-rotating exterior azimuthal vorticity field that grows linearly with time, and the resulting

kinetic energy grows quartically with time (chapter 3).

For a point vortex, the spectrum is purely continuous, being made up of the Λ_1 and Λ_2 families, and only the first term in (3.58) remains. Redefining the CS-mode eigenfunctions as $\tilde{\boldsymbol{w}}_{\Lambda_1} \equiv (0, -kr_f\delta(r-r_f), m\delta(r-r_f))$ and $\tilde{\boldsymbol{w}}_{\Lambda_2} \equiv (-imkr_f\delta(r-r_f), kr_f^2\delta'(r-r_f), 0)$, an arbitrary initial condition evolves as the following integral superposition of these convected modes:

$$\boldsymbol{w}(\boldsymbol{x},t) = \int_0^\infty \{X_{\Lambda_1}(r_f)\hat{\boldsymbol{w}}_{\Lambda_1}(r;r_f) + X_{\Lambda_2}(r_f)\hat{\boldsymbol{w}}_{\Lambda_2}(r;r_f)\}\, e^{i[kz+m(\theta-\Omega(r_f)t)]}dr_f, \quad (2.95)$$

where $X_{\Lambda_1}(r_f) = -\dfrac{1}{kr_f}\left(w_{\theta 0}(r_f) - \dfrac{i}{m}\dfrac{d}{dr_f}(rw_{r0}(r_f))\right)$ and $X_{\Lambda_2}(r_f) = \dfrac{i}{m}\dfrac{w_{r0}(r_f)}{kr_f}$. For an initial condition with $w_{r0} = 0$, the evolution is on account of differential convection, and (2.95) reduces to $\boldsymbol{w}(\boldsymbol{x},t) = \boldsymbol{w}(\boldsymbol{x},0)e^{i[kz+m(\theta-\Omega(r)t)]}$; with radial vorticity, an integration by parts of $\delta'(r-r_f)$ naturally accounts for the (non-modal) linear growth in w_θ with t, and one obtains $\boldsymbol{w}(\boldsymbol{x},t) = [w_{r0}(r), w_{\theta 0}(r) - 2\Omega(r)tw_{r0}(r), w_{z0}(r)]e^{i[kz+m(\theta-\Omega(r)t)]}$. The equivalence of (2.95) to the solution of the corresponding IVP is readily established, while that of (3.58) is shown in chapter 3.

The axisymmetric eigenmodes

As already pointed out, axisymmetric Kelvin modes are the eigenfunctions of an ordinary differential equation that conforms to classical Sturm-Liouville theory (Ince [1956]) provided only that the base-state vorticity is non-zero. However, the spatial separation of the regions of strain and vorticity in the Rankine vortex means that the completeness of these oscillatory modes only extends to axisymmetric column deformations. Radial-vorticity in the region $r > a$ leads to a non-modal (secular) response. This is immediate from the governing (linearized) equation for w_θ which, for axisymmetric perturbations outside the core, takes the form $\frac{\partial w_\theta}{\partial t} = (w_r r)\frac{\partial \Omega}{\partial r}$ with $\Omega(r) = \Omega_0\frac{a^2}{r^2}$; so, an arbitrary $w_r(r)$ for $r > a$ leads to $w_\theta(r,t) \propto t$. Although the modal representation in the earlier section, given by (2.79), was developed for a non-zero m, the evolution of an arbitrary axisymmetric vorticity field at the initial instant may nevertheless be obtained by taking the limit $m \to 0$ in (2.79).

For $m = 0$, the dispersion curves for positive and negative ω are symmetric about $\omega = 0$, there no longer being a structureless branch. Thus, we have $\omega_n(b=-1) = -\omega_n(b=1), B_n^{-1} = -B_n^{+1}, \hat{w}^{\text{Kelvin}}_{r,n(-1)}(r) = -\hat{w}^{\text{Kelvin}}_{r,n(+1)}(r)$ and $\hat{w}^{\text{Kelvin}}_{\theta,n(-1)}(r) = \hat{w}^{\text{Kelvin}}_{\theta,n(+1)}(r)$, and the modal superposition may be expressed in terms of either family. We choose the cograde branch with $\hat{w}^{\text{Kelvin}}_{r,n}(r) \equiv \hat{w}^{\text{Kelvin}}_{r,n(+1)}(r), \hat{w}^{\text{Kelvin}}_{\theta,n}(r) \equiv \hat{w}^{\text{Kelvin}}_{\theta,n(+1)}(r)$ and $B_n = B_n^{+1}$. The resulting radial and azimuthal vorticity

components at time t are then given by

$$\begin{aligned}
w_r(\boldsymbol{x},t) &= w_{r0}(r)\mathcal{H}(r-a)\mathrm{e}^{\mathrm{i}kz} + 2\sum_{n=1}^{\infty}\frac{B_n}{\omega_n^2(\beta_n a)^2}\hat{w}_{r,n}^{\mathrm{Kelvin}}(r)\left\{2\Omega_0\cos(\omega_n t)F_{n1} - \omega_n\sin(\omega_n t)F_{n2}\right\}e^{ikz} \\
&+2\sum_{n=1}^{\infty}\frac{B_n}{\omega_n}\hat{w}_{r,n}^{\mathrm{Kelvin}}(r)\mathrm{e}^{\mathrm{i}kz}\Bigg\{\sin(\omega_n t)\int_a^{\infty}\frac{K_0(kr')}{(ka)^2K_0(ka)}\frac{d}{dr'}[r'w_{\theta 0}(r')]dr' + \\
&\frac{\cos(\omega_n t)-1}{\omega_n}\int_a^{\infty}\frac{K_0(kr')}{(ka)^2K_0(ka)}2\Omega w_{r0}(r')dr'\Bigg\}, \\
w_\theta(\boldsymbol{x},t) &= \{w_{\theta 0}(r) - 2\Omega t\, w_{r0}(r)\}\mathcal{H}(r-a)\mathrm{e}^{\mathrm{i}kz} - 2i\sum_{n=1}^{\infty}\frac{B_n}{\omega_n^2(\beta_n a)^2}\hat{w}_{\theta,n}^{\mathrm{Kelvin}}(r)\left\{2\Omega_0\sin(\omega_n t)F_{n1} + \right. \\
&\left.\omega_n\cos(\omega_n t)F_{n2}\right\}e^{ikz} + 2i\sum_{n=1}^{\infty}\frac{B_n}{\omega_n}\hat{w}_{\theta,n}^{\mathrm{Kelvin}}(r)\mathrm{e}^{\mathrm{i}kz}\Bigg\{(\cos(\omega_n t)-1)\int_a^{\infty}\frac{K_0(kr')}{(ka)^2K_0(ka)}\frac{d}{dr'}[r'w_{\theta 0}(r')]dr' + \\
&\left(t-\frac{\sin(\omega_n t)}{\omega_n}\right)\int_a^{\infty}\frac{K_0(kr')}{(ka)^2K_0(ka)}2\Omega w_{r0}(r')dr'\Bigg\},
\end{aligned} \tag{2.96}$$

where

$$F_{n1} = \int_0^a ikr' w_{z0}(r')\frac{J_0(\beta_n r')}{J_0(\beta_n a)}dr' + a w_{r0}(a), \tag{2.97}$$

$$F_{n2} = \int_0^a \frac{d}{dr'}\left(r' w_{\theta 0}(r')\right)\frac{J_0(\beta_n r')}{J_0(\beta_n a)}dr' - a w_{\theta 0}(a), \tag{2.98}$$

and the secular terms arise due to the initial radial vorticity. With $w_{r0}(r) = 0$, $w_\theta(\boldsymbol{x},t)$ reduces to the following simpler form:

$$\begin{aligned}
w_\theta(\boldsymbol{x},t) &= w_{\theta 0}(r)\mathcal{H}(r-a)\mathrm{e}^{\mathrm{i}kz} - 2i\sum_{n=1}^{\infty}\frac{B_n}{\omega_n(\beta_n a)^2}\hat{w}_{\theta,n}^{\mathrm{Kelvin}}(r)\cos(\omega_n t)F_{n2}\,e^{ikz} \\
&+2i\sum_{n=1}^{\infty}\frac{B_n^{-1}}{\omega_n}\hat{w}_{\theta,n}^{\mathrm{Kelvin}}(r)\mathrm{e}^{\mathrm{i}kz}\left(\cos(\omega_n t)-1\right)\int_a^{\infty}\frac{K_0(kr')}{(ka)^2K_0(ka)}\frac{d}{dr'}\left(r' w_{\theta 0}(r')\right)dr',
\end{aligned} \tag{2.99}$$

without algebraically growing terms. The response given by (2.99) may be divided into two components - the term proportional to C_n^b denotes core-vorticity that evolves as a discrete summation of sausaging modes; the term proportional to B_n^b, together with the first term, denote the response to exterior azimuthal vorticity and involve both a superposition of sausaging modes and a steady contribution. The unsteady part arises due to the vortex column deformation induced by the exterior vorticity. Since this deformation is driven by $u_r|_{r=a} = \int_a^{\infty}\frac{d}{dr'}[r'w_{\theta 0}(r')]K_0(kr')dr'$, the restriction $\int_a^{\infty}\frac{d}{dr'}[r'w_{\theta 0}(r')]K_0(kr')dr' = 0$, $C_n^b = 0$, leads to an undeformed vortex column with a quiescent core. The resulting steady vorticity field, $w_{\theta 0}(r)\mathcal{H}(r-a)\mathrm{e}^{\mathrm{i}kz}$, or the associated velocity field given by $u_z = e^{ikz}\left[K_0(kr)\int_a^r I_0(kr')\frac{d}{dr'}[r'w_{\theta 0}(r')]\,dr' + I_0(kr)\int_r^{\infty}K_0(kr')\frac{d}{dr'}[r'w_{\theta 0}(r')]\,dr'\right]\mathcal{H}(r-a)$ may be regarded as the degenerate zero-frequency axisymmetric eigenmode.

There are a couple of points worth emphasizing here. The first is that transient growth has been observed in numerical simulations for axisymmetric perturbations to a smooth (Lamb-Oseen) vorticity profile (Pradeep & Hussain [2006]) which would appear to go against the notion of such growth only being associated with non-normal differential operators with an underlying

continuous spectrum (Trefethen *et al.* [1993],Schmid & Henningson [2001]). There is no contradiction, however. The self-adjointness of the differential operator for the axisymmetric case is not in the energy norm, and the velocity eigenfunctions are by themselves not mutually orthogonal. Except for rigid-body rotation Greenspan [1968], the energy associated with any modal superposition will therefore necessarily vary with time, albeit only in an oscillatory fashion in the inviscid limit (there are quantities such as the pseudo-momentum and the pseudo energy that are indeed time-invariant, and point to additional weighting functions that must be included in an inner product in order to render the eigenfunctions orthogonal (Held [1985])). Physically, the presence of a shear allows for an exchange of energy between the base-state and the perturbation, via a Reynolds stress contribution, but this exchange averages out to zero over a time period of oscillation for $m = 0$. For sufficiently slow oscillations, the short-time dynamics of the energy is indistinguishable from transient growth, and is governed by the same physical mechanisms.

The response of a Rankine vortex to an axisymmetric perturbation is a singular limiting case of a smooth profile. In the latter case, the perturbation vorticity field associated with the eigenfunctions extends throughout the domain, allowing for an arbitrary axisymmetric vorticity field to be expressed as a summation over sausaging modes alone. For a monotonically decaying base-state vorticity profile, the radial length scale of a typical vorticity eigenfunction increases with increasing r with a corresponding decrease in the eigenfunction amplitude. For sufficiently large modal indices, the vorticity eigenfunction for a smooth vortex exhibits a rapid large-amplitude oscillation in the near-field that transitions to a small-amplitude increasingly gentle waviness in the distant nearly irrotational exterior. If one now considers an initial distribution of radial vorticity localized in the irrotational region, the required modal superposition will involve eigenfunctions with a projection in this region having a length-scale of the same order as that characterizing the initial condition. The near-field projection of each of these eigenfunctions has a much larger amplitude, and is also characterized by a much smaller radial length scale. These near-field contributions from the different eigenfunctions involved in the superposition will cancel out at the initial instant, but the gradual de-phasing with time would eventually lead to a large-amplitude fine-scaled oscillatory core response (Pradeep & Hussain [2006]). The approach to this large amplitude oscillation would be via a short-time transient wherein core perturbations are driven by an exterior azimuthal vorticity field that grows linearly with time. The deviation from this behavior due to the eventual decay of the source term (w_r), on account of Coriolis forces, would occur on a much longer time scale of the order of the inverse eigenfrequency. The Rankine limit corresponds to the oscillation time period approaching infinity, leading to a true algebraic growth.

The relation between the $2D$ and $3D$ eigenspectra

It is easily shown that a Λ_1-mode, characterized by (2.62)-(2.64), approaches the corresponding $2D$ singular mode given by (2.18) for $k \to 0$ and for a fixed ω (or r_f). On the other hand, a Λ_2-mode, characterized by (2.75)-(2.77), approaches an axial jet localized at the critical radius ($u_z^{\Lambda_2} \propto \delta(r - r_f); u_r^{\Lambda_2}, u_\theta^{\Lambda_2} \to 0$) in the same limit, and plays no role in the evolution of an axial vorticity distribution. Of most relevance is the $k \to 0$ limit along a fixed dispersion curve (rather than with ω fixed). The approach of the structureless mode, in this limit, to the 2D Kelvin mode given by (2.19), is well documented (see Leibovich & Ma [1983],Saffman [1992]),

and we consider only the structured modes with $\omega_n \to m\Omega_0$ for $k \to 0$. The frequency intervals between the structured modes, corresponding to the CS-spectrum, become vanishingly small for $k \to 0$, and it suffices to examine the dispersion curves alone. Further, consideration of the cograde family is sufficient since the β_n's for the co-grade and retro-grade families (excluding the structureless branch, $n = 1$) equal each other in the limit $k \to 0$, and the corresponding eigenfunctions are no longer independent. The cograde eigenfunctions are given by (2.41)-(2.43). The small k asymptotes for ω_n of cograde modes are given as,

$$\omega_n = \begin{cases} \dfrac{2ka}{j_n^0}\left[1-(1-2\log ka)\dfrac{(ka)^2}{2j_n^{0\,2}}\right]+\ldots & \text{for } m=0, \\ \\ m\Omega_0+\Omega_0\dfrac{2ka}{j_n^m}\left[1-\dfrac{(m-2)}{m}\dfrac{(ka)^2}{2j_n^{m\,2}}\right]+\ldots & \text{for } m\neq 0 \end{cases}, \tag{2.100}$$

and the β_n's are readily obtained from (2.40) as:

$$\lim_{k\to 0}(\beta_n a) = j_n^m - \frac{(ka)^2}{mj_n^m}, \tag{2.101}$$

for $m \neq 0$, where j_n^m is the n^{th} zero of J_m. The use of (2.101) in (2.41)-(2.43) leads to the following limiting expressions for the vorticity components associated with the cograde modes:

$$\lim_{k\to 0}\hat{w}_{z,n(-1)}^{Kelvin} = \frac{mj_n^m}{a(ka)^2}\left[\frac{j_n^m J_m(j_n^m\frac{r}{a})}{J'_m(j_n^m)}+a\,\delta(r-a)\right], \tag{2.102}$$

$$\lim_{k\to 0}\hat{w}_{r,n(-1)}^{Kelvin} = -\frac{\mathrm{i}m^2 j_n^m}{(ka)^2}\left[\frac{J_m(j_n^m\frac{r}{a})}{rJ'_m(j_n^m)}\right], \tag{2.103}$$

$$\lim_{k\to 0}\hat{w}_{\theta,n(-1)}^{Kelvin} = \frac{mj_n^m}{a(ka)^2}\left[\frac{j_n^m J'_m(j_n^m\frac{r}{a})}{J'_m(j_n^m)}\right]. \tag{2.104}$$

The above vorticity field drives an $O(1/k^2)$ flow within the core. The normalization used in the analysis is based on the exterior axial velocity field which therefore remains $O(1)$ with the exterior radial component being $O(1/k)$. Thus, the exterior becomes increasingly quiescent relative to the core for $k \to 0$, suggesting a relation between the long-wavelength structured modes and the 2D core-eigenmodes in section 2.2.1. Considering the general expression, (3.12), for the latter, and expanding $g(\frac{r}{a})$ as a Fourier-Bessel series, one obtains

$$\hat{w}_z^{core} = \sum_{n=1}^{\infty} a_n\left[J_m(j_n^m\frac{r}{a})-\delta(r-a)\int_0^a\left(\frac{r'}{a}\right)^{m+1}J_m(j_n^m\frac{r'}{a})dr'\right], \tag{2.105}$$

where the a_n's are the coefficients in the Fourier-Bessel expansion of $g(\frac{r}{a})$, being defined as

$$a_n = \frac{2}{J_{m+1}^2(j_n^m)}\int_0^1 xg(x)J_m(j_n^m x)dx. \tag{2.106}$$

Using the relation $x^m = \sum_{p=1}^{\infty} \frac{2J_m(j_p^m x)}{j_p^m J_{m+1}(j_p^m)}$ (see Watson [1927]),

$$\hat{w}_z^{core} = \sum_{n=1}^{\infty} a_n \left[J_m(j_n^m \frac{r}{a}) - \delta(r-a) \sum_{p=1}^{\infty} \frac{2}{j_p^m J_{m+1}(j_p^m)} \int_0^a \frac{r'}{a} J_m(j_n^m \frac{r'}{a}) J_m(j_p^m \frac{r'}{a}) dr' \right]. \quad (2.107)$$

Using the orthogonality of the Bessel functions, and that $J_{m+1}(j_n^m) = -J'_m(j_n^m)$, the above expression simplifies to

$$\hat{w}_z^{core} = \sum_{n=1}^{\infty} a_n \left[J_m\left(j_n^m \frac{r}{a}\right) + \frac{a J'_m(j_n^m)}{j_n^m} \delta(r-a) \right], \quad (2.108)$$

which may be rewritten as

$$\hat{w}_z^{core} = \sum_{n=1}^{\infty} a'_n \lim_{k \to 0} \hat{w}_{z,n(-1)}^{Kelvin}, \quad (2.109)$$

with $a'_n = a_n \frac{J'_m(j_n^m)}{m} (\frac{ka}{j_n^m})^2$. Thus, a linear superposition of the axial vorticity components of the structured Kelvin modes, in the limit of vanishing axial wavenumber, maps onto the Fourier-Bessel representation of the general core eigenmode given by (3.12). Note that the radial and azimuthal vorticity components of the structured modes are of the same order as the axial vorticity for $k \to 0$ (see (2.102) and (2.103)), but drive a purely axial flow. Thus, the original 3D velocity field splits into independent axial ($[\hat{w}_z; \hat{u}_r, \hat{u}_\theta]$ and transverse ($[\hat{w}_r, \hat{w}_\theta; \hat{u}_z]$) components. For an initial condition of the form $\hat{\boldsymbol{w}}(\boldsymbol{x}, t) = \hat{w}_{z0}(r)\delta(k)e^{im\theta}\mathbf{1}_z$, the use of the limiting forms of the discrete and CS-modes discussed above in (2.79) leads to (2.21) as must be the case.

The main result obtained thus far is a modal interpretation of the initial value problem involving a Rankine vortex. Such an interpretation leads to the expressions (2.21) and (2.79)-(3.58) for vortical initial conditions in two and three dimensions, respectively. Herein, we show the manner in which (2.79) reduces to (2.21) in the limit of a vanishing axial wavenumber.

Consider an initial vorticity field devoid of radial vorticity, $\boldsymbol{w}(\boldsymbol{x}, 0) = [0, -\frac{kr}{m} w_{z0}(r), w_{z0}(r)] e^{i(kz+m\theta)}$. Thus we have $X_{\Lambda_1} = -\frac{kr_f^2}{mA_1} w_{z0}(r_f)\mathcal{H}(r_f - a), X_{\Lambda_2} = 0$. Now we would need to consider the $k \to 0$ of the arbitrary time expression for axial vorticity,

$$\begin{aligned} w_z(\boldsymbol{x}, t) \;=\; & \int_{a^+}^{\infty} X_{\Lambda_1}(r_f) \hat{w}_z^{\Lambda_1}(r; r_f) e^{i[kz+m(\theta-\Omega(r_f)t)]} dr_f \mathcal{H}(r-a) + \Bigg\{ \sum_{b=\pm 1} \sum_{n=1}^{\infty} C_{nb} \hat{w}_{z,nb}^{\text{Kelvin}}(r) e^{-i\omega_n t} \\ & - \int_{a^+}^{\infty} \sum_{b=\pm 1} \sum_{n=1}^{\infty} X_{\Lambda_1}(r_f) G_{nb}^{\Lambda_1} \hat{w}_{z,nb}^{\text{Kelvin}}(r) (e^{-i\omega_n t} - e^{-im\Omega(r_f)t}) dr_f \Bigg\} e^{i(kz+m\theta)}, \end{aligned} \quad (2.110)$$

Further simplification could be obtained by using the expression for $G_{nb}^{\Lambda_1}$ from (3.62) and C_{nb}

from (2.87),

$$
\begin{aligned}
w_z(\boldsymbol{x},t) &= w_{z0}(r)e^{i[kz+m(\theta-\Omega(r)t)]}\mathcal{H}(r-a)+ \\
&\left[-ika\sum_{b=\pm1}\sum_{n=1}^{\infty}\frac{B_n^b}{g_n^2(\beta_n a)^2}\hat{w}_{z,nb}^{\text{Kelvin}}(r)\int_0^a w_{z0}(r_f)\left(\frac{r_f}{a}\right)\left\{2\Omega_0\frac{J_m(\beta_n r_f)}{J_m(\beta_n a)}+\frac{g_n}{m}\frac{\beta_n r_f J_m'(\beta_n r_f)}{J_m(\beta_n a)}\right\}\right. \\
&\left. dr_f e^{-i\omega_n t}+\sum_{b=\pm1}\sum_{n=1}^{\infty}B_n^b\hat{w}_{z,nb}^{\text{Kelvin}}(r)\int_{a^+}^{\infty}\left(\frac{r_f}{a}\right)^2\frac{K_m'(kr_f)}{K_m(ka)}\frac{w_{z0}(r_f)}{m}\frac{e^{-i\omega_n t}-e^{-im\Omega(r_f)t}}{i(\omega_n-m\Omega(r_f))}dr_f\right]e^{i(kz+m\theta)},
\end{aligned}
\tag{2.111}
$$

The summations in the above expression can be split into two contributions - arising from structureless branch ($\omega_n \to (m-1)\Omega_0$) or structured branch ($\omega_n \to m\Omega_0$) as $k \to 0$. To draw analogies the 2d limit of the structureless branch will be labelled ω_d. Table 2.1 highlights the various $k \to 0$ asymptotic forms for both the structureless and structured branches. Glossing through the expressions in table 2.1 and the revisiting equation 2.111 reveals that in the second summation only the structureless branch survives as $k \to 0$ (the structured branches are $)(k^2)$ weaker). On the contrary the first summation will have contributions from both structured and structureless branches. The double summation for the structureless branches can be reduced to a single summation by realizing that $B_n^{-1} = -B_n^{+1}$ and $\hat{w}_{z,n(-1)}^{\text{Kelvin}}(r) = -\hat{w}_{z,n(+1)}^{\text{Kelvin}}(r) \equiv \hat{w}_{z,n}^{\text{Kelvin}}(r)$. On substituting expressions from table 2.1 in (2.111) and considering $k \to 0$ limit,

$$
\begin{aligned}
w_z(\boldsymbol{x},t) &= w_{z0}(r)e^{i[m(\theta-\Omega(r)t)]}\mathcal{H}(r-a)+ \\
&\left[\delta(r-a)e^{-i\omega_d t}\int_0^a w_{z0}(r_f)\left(\frac{r_f}{a}\right)^{m+1}dr_f+\right. \\
&2\sum_{n=1}^{\infty}\frac{1}{m}\left(\frac{ka}{j_n^m}\right)^2\int_0^a w_{z0}(r_f)\frac{r_f}{a}\frac{J_m\left(j_n^m\frac{r_f}{a}\right)}{J_m'(j_n^m)}dr_f\frac{mj_n^m}{a(ka)^2}\left\{\frac{j_n^m J_m(j_n^m\frac{r}{a})}{J_m'(j_n^m)}+a\,\delta(r-a)\right\}e^{-im\Omega_0 t} \\
&\left.+\,\delta(r-a)\int_{a^+}^{\infty}\Omega_0\left(\frac{a}{r_f}\right)^{m-1}w_{z0}(r_f)\frac{e^{-im\Omega(r_f)t}-e^{-i\omega_n t}}{(\omega_d-m\Omega(r_f))}dr_f\right]e^{im\theta}, \\
&= w_{z0}(r)e^{i[m(\theta-\Omega(r)t)]}\mathcal{H}(r-a)+\hat{w}_z^{core}e^{im[\theta-\Omega_0 t]}+\delta(r-a)\left[e^{-i\omega_d t}\int_0^a w_{z0}(r_f)\left(\frac{r_f}{a}\right)^{m+1}dr_f+\right. \\
&\left.\int_{a^+}^{\infty}\Omega_0\left(\frac{a}{r_f}\right)^{m-1}w_{z0}(r_f)\frac{e^{-im\Omega(r_f)t}-e^{-i\omega_d t}}{(\omega_d-m\Omega(r_f))}dr_f\right]e^{im\theta}
\end{aligned}
\tag{2.112}
$$

The reduction of the summation to $\hat{w}_z^{core}$ has been done using equation (2.108). Thus we have obtained the 2d modal superposition result as given in (2.21).

The absence of a contribution from $\omega = m\Omega_0$ in the spectrum associated with the evolving core vorticity (see (2.79)), but its relevance to the evolution of a 2D axial vorticity distribution (the core-eigenmode contribution in (2.21)), highlights the non-trivial relation between the $2D$ and $3D$ eigenspectra.

2.3 The singular eigenspectrum of a smooth vortex

The analysis for the non-axisymmetric modes has so far been restricted to the Rankine vortex. The natural question is as to how the results, including the modal representations (2.21) and

	Structureless (ω_d)	Structured (Cograde)
ω_n	$(m-1)\Omega_0$	$m\Omega_0 + \Omega_0 \dfrac{2ka}{j_n^m}$
g_n	Ω_0	$-\Omega_0 \dfrac{2ka}{j_n^m}$
ξ_n	$\sqrt{3}$	$\dfrac{j_n^m}{ka}$
$\beta_n a$	$\sqrt{3}ka$	$j_n^m - \dfrac{(ka)^2}{m j_n^m}$
B_n^b	$\dfrac{i\Omega_0}{2}\dfrac{(ka)^2}{m}$	$\dfrac{-2i\Omega_0}{m^2}\dfrac{(ka)^5}{(j_n^m)^3}$
$\hat{w}_{z,n}^{\text{Kelvin}}(r)$	$\dfrac{2m}{ka}\delta(r-a)$	$\dfrac{m j_n^m}{a(ka)^2}\left\{\dfrac{j_n^m J_m(j_n^m \frac{r}{a})}{J'_m(j_n^m)} + a\,\delta(r-a)\right\}$

Table 2.1: $k \to 0$ asymptotic forms of quantities related to Kelvin modes

(2.79), generalize to a smooth vorticity profile. For 2D perturbations, this is answered in section 2.3.1 below by adapting the analysis of Balmforth and Morrison (1995), developed originally for homogeneous non-linear parallel flows, to the case of a vortex. The nature of the regular singular point in the governing linearized equations for 2D perturbations remains the same in both cases, with DZ for the vortex column playing the role of U'' in a parallel flow. The Frobenius indices are integers (0 and 1), and one of the radial velocity eigenfunctions must, for non-zero DZ, have a logarithmic branch point at the critical radius (r_f). As a result, the vorticity eigenfunctions of the 2D CS-modes associated with a smooth vortex include both a delta-function singularity and a non-local principal-value (PV) singularity, proportional to DZ, arising from the aforementioned logarithmic term. This latter contribution is absent for a Rankine vortex since DZ is zero for $r > a$.

The 3D spectrum of a smooth vortex bears an analogy to stratified parallel flows, and one may indeed define a Richardson number associated with a perturbation of a given axial wavenumber involving the local vorticity and vorticity gradient [Le Dizès [2004]; also, see section 2.4]. Physically, the Coriolis forces in the case of a smooth vortex play the same role as buoyancy forces in the stratified context. This analogy is exploited in section 2.4 where we develop stratified flow configurations whose eigenspectra bear a direct analogy to those of Rankine and smooth vortices. Here, in section 2.3.3, we focus on the structure of the smooth vortex 3D CS-modes in the vicinity of r_f. The differences in the nature of the singularity in the 3D vorticity eigenfunctions relative to those of a Rankine vortex (where both 2D and 3D vorticity eigenfunctions have only localized generalized function singularities), and those for 2D perturbations (where the vorticity eigenfunctions have an additional non-local PV-singular term), that arise due to the singular point of the Howard-Gupta equation now having fractional Frobenius exponents, are highlighted. In particular, it is shown, based on the known solution for stratified Couette flow [Engevik [1971]], that the singular terms in the vorticity eigenfunctions of the 3D CS-modes must be interpreted in the sense of a principal finite part [Gel'fand & Shilov [1964], Lighthill [1958]]. This in turn implies that the forcing terms, localized at the critical radius,

that must appear in the governing equation for the 3D CS-modes (that is identical in form to the Taylor-Goldstein equation in the vicinity of r_f), are not the delta function and its derivative - as for the Rankine vortex (see equations (2.46) and (2.67) for the Λ_1 and Λ_2 families). The forcing terms must, in fact, correspond to genuinely non-summable singularities, and are therefore, not even generalized functions [Gel'fand & Shilov [1964]]; they may, symbolically, be likened to the product of a delta function and an inverse algebraic power that depends on the Frobenius exponent.

2.3.1 2D singular eigenspectrum

With (2.5) governing the evolution of 2D perturbations, the axial vorticity eigenfunction for the CS-mode associated with a smooth vortex may be written as [Van Kampen [1955]]:

$$\hat{w}_z^{\mathrm{CSM}}(r;r_f) = A_1(r_f)\delta(r-r_f) - \mathcal{P}\frac{1}{r}\frac{DZ(r)\hat{\psi}^{\mathrm{CSM}}(r;r_f)}{\Omega(r)-\Omega(r_f)}, \tag{2.113}$$

where the symbol $\mathcal{P}$ implies that the second term in (2.113), integrated over an interval that includes r_f, must be interpreted in the sense of a Cauchy principal value. Thus, the 2D CS-modes associated with a smooth vortex have, in addition to a delta-function singularity, a non-local PV-singular contribution proportional to DZ. This latter singularity arises because, for any DZ however small, the azimuthal convection of $\hat{w}_z$ becomes asymptotically weak, close to r_f, compared to the radial convection of the base-state vorticity by $\hat{u}_r\,(\propto \hat{\psi})$. The PV-singular contribution depends on the radial inhomogeneity of the base-state vorticity, and is therefore absent for a Rankine vortex. Note that the perturbation streamfunction, $\hat{\psi}^{CSM}$, in (2.113) satisfies

$$\left(rD^2 + D - \frac{m^2}{r}\right)\hat{\psi}^{\mathrm{CSM}}(r;r_f) = -r\hat{w}_z^{\mathrm{CSM}}(r;r_f). \tag{2.114}$$

A normalization that is particularly convenient is one based on the total (axial) vorticity in a CS-mode. As shown by Balmforth and Morrison (1995), with $\int_0^\infty \hat{w}_z^{\mathrm{CSM}}(r';r_f)dr' = 1$, (2.113) takes the form

$$\hat{w}_z^{\mathrm{CSM}}(r;r_f) = \left\{1 + \mathcal{P}\int_0^\infty \frac{1}{r'}\frac{DZ(r')\hat{\psi}^{\mathrm{CSM}}(r';r_f)}{\Omega(r')-\Omega(r_f)}dr'\right\}\delta(r-r_f) - \mathcal{P}\frac{1}{r}\frac{DZ(r)\hat{\psi}^{\mathrm{CSM}}(r;r_f)}{\Omega(r)-\Omega(r_f)}. \tag{2.115}$$

The streamfunction $\hat{\psi}^{\mathrm{CSM}}$ then satisfies an inhomogeneous Fredholm integral equation of the second kind (rather than a Cauchy integral equation with a PV-singular kernel), and is readily obtained numerically. Using (**??**) and (2.115), it is easily shown that

$$\hat{\psi}^{\mathrm{CSM}}(r;r_f) - \int_0^\infty \mathcal{M}(r,r';r_f)\hat{\psi}^{\mathrm{CSM}}(r';r_f)dr' = -r_f\mathcal{G}(r;r_f), \tag{2.116}$$

where $\mathcal{G}(r;r_f) = -\frac{1}{2m}\left(\frac{r_<}{r_>}\right)^m$, with $r_<(r_>)$ denoting the smaller (larger) of r and r_f, is the Green's function of (2.114), and the regularized kernel, $\mathcal{M}(r,r';r_f)$, is given by

$$\mathcal{M}(r,r';r_f) = \frac{DZ(r')}{r'}\left\{\frac{r'\mathcal{G}(r;r') - r_f\mathcal{G}(r;r_f)}{\Omega(r') - \Omega(r_f)}\right\} \tag{2.117}$$

An artifact of the above normalization is that the CS-modes that are homogeneous solutions of (2.116) must be handled separately (see Balmforth & Morrison [1995a] for details). Such solutions are expected for smooth vortices, at least those that closely approximate the Rankine profile, and correspond to the CS-mode having zero net axial vorticity in $r\,\epsilon\,[0,\infty)$ for any θ. For the Rankine vortex, this would be equivalent to the sum of the vortex sheet amplitudes at $r = a$ and $r = r_f$ being zero; using (2.16) and (2.18), this implies $m(a/r_f)^2 + (a/r_f)^{(m-1)} = (m-1)$, which has a unique solution in (a,∞) for any $m > 1$. It must be emphasized that the homogeneous solutions of the Fredholm equation are generic CS-modes and do not have any particular physical significance. However, the homogeneous solutions of the original Cauchy integral equation (that is, those with $A_1 = 0$) correspond to singular free oscillations; this is in contrast to the 2D Kelvin mode of the Rankine vortex. Such singular oscillations (one for each $m \geq 2$) are consistent with a non-linear critical layer at the particular r_f, of a vanishingly small thickness that supports a zero phase-jump across it, and are therefore the vortex-analogs of the Benney-Bergeron-Davis modes for parallel flows [Benney & Bergeron [1969]].

2.3.2 The modal decomposition for an arbitrary distribution of axial vorticity

The evolution of an initial axial vorticity distribution of the form $w_{z0}(r)e^{im\theta}$, as an integral superposition of the 2D CS-modes (and the singular discrete mode), is given by:

$$w_z(r,\theta,t) \;=\; \int_0^\infty \Pi(r_f)\hat{w}_z^{\rm CSM}(r;r_f)e^{im(\theta-\Omega(r_f)t)}dr_f, \tag{2.118}$$

where the amplitude distribution of the CS-modes is given by

$$\Pi(r_f) \;=\; \frac{1}{(\epsilon_{\rm R}^2+\epsilon_{\rm L}^2)}\left\{\epsilon_{\rm R}w_{z0}(r_f) - \frac{\epsilon_{\rm L}}{\pi}\frac{\Omega'(r_f)}{\hat{\psi}^{\rm CSM}(r_f;r_f)}\mathcal{P}\int_0^\infty \frac{w_{z0}(r')\hat{\psi}^{\rm CSM}(r_f;r')}{\Omega(r')-\Omega(r_f)}dr'\right\} \tag{2.119}$$

$$\epsilon_{\rm R} \;=\; 1 + \mathcal{P}\int_0^\infty \frac{1}{r'}\frac{DZ(r')\hat{\psi}^{\rm CSM}(r';r_f)}{\Omega(r')-\Omega(r_f)}dr'; \qquad \epsilon_{\rm L} = \pi\frac{DZ(r_f)\hat{\psi}^{\rm CSM}(r_f;r_f)}{r_f\Omega'(r_f)}. \tag{2.120}$$

The above modal representation is obtained from the solution of a Riemann-Hilbert problem in the complex plane [Gakhov [1990]], and is the required extension of (2.21) to a smooth vorticity profile. Note that the representation is only known in terms of the singular eigenfunctions, and for a general smooth vorticity profile, the latter must be obtained from the numerical solution of (2.116). The analysis leading to (2.118) closely follows that of Balmforth and Morrison (1995) for parallel shearing flows, and is therefore relegated to appendix C.

As pointed out in the introduction, unlike the Rankine vortex, the large-t analysis of (2.118) reveals an intermediate asymptotic regime, with an exponential decaying velocity perturbation

associated with a quasi-mode, that precedes the eventual (and expected) algebraic decay for still longer times arising from the de-phasing of the CS-mode superposition. For smooth vortices approaching the Rankine profile, the decay rate (Landau damping) in this exponential regime is well known (see, for instance, Briggs *et al.* [1970]; Schecter *et al.* [2000]) and may be obtained from (2.118) by identifying the zeroes of $\epsilon_{\mathrm{R}}^2 + \epsilon_{\mathrm{L}}^2$ in the complex plane. The integration contour (over $r\,\epsilon\,[0,\infty)$) in the PV-singular integral in (2.120) is now interpreted as passing below the critical radius of the quasi-mode in the complex plane; regarding the contour as the real axis would lead to no zeros for a monotonically decaying vorticity profile, consistent with the Rayleigh criterion. Writing $\epsilon_{\mathrm{R}}^2 + \epsilon_{\mathrm{L}}^2 = \epsilon^+\epsilon^-$ (see appendix C), with

$$\epsilon^{\pm} = 1 + \mathcal{P}\int_0^{\infty} \frac{1}{r'}\frac{DZ(r')\hat{\psi}^{\mathrm{CSM}}(r';r)}{\Omega(r')-\Omega(r)}dr' \pm \pi i \frac{DZ(r)\hat{\psi}^{\mathrm{CSM}}(r;r)}{r\Omega'(r)}, \tag{2.121}$$

and anticipating a decaying mode, the zeroes must correspond to those of ϵ^-. Further, assuming the critical radius of the quasi-mode (r_Q) to be close to the real axis with the real part being r_{Qr} ($r_{Qr} \to r_{fk}$ for $DZ \to -2\Omega_0\delta(r-a)$), one may write $\Omega(r_Q) \approx \Omega_{r_{Qr}} - i\Omega_i$ with $\Omega_i \ll \Omega_{r_{Qr}}$ and $r_{Qi} \approx \frac{\Omega_i}{\Omega'(r_{fk})}$. The relation $\epsilon^-(r_Q) = 0$ takes the approximate form:

$$1 + \int_0^{\infty} \frac{1}{r'}\frac{DZ(r')\hat{\psi}^{\mathrm{CSM}}(r';r_{Qr})}{\Omega(r')-\Omega(r_{Qr})+i\Omega_i}dr' - \pi i \frac{DZ(r)\hat{\psi}^{\mathrm{CSM}}(r_{Qr};r_{Qr})}{r_{Qr}\Omega'(r_{Qr})} = 0, \tag{2.122}$$

where, for non-zero Ω_i, the integral does not need a PV-interpretation. Expanding for small Ω_i, one obtains

$$1 + \mathcal{P}\int_0^{\infty} \frac{1}{r'}\frac{DZ(r')\hat{\psi}^{\mathrm{CSM}}(r';r_{Qr})}{\Omega(r')-\Omega(r_{Qr})}dr' \approx 0, \tag{2.123}$$

from the real part with the resulting r_{Qr} determining the angular frequency of the quasi-mode. Using the approximate form, $DZ \approx -2\Omega_0\delta(r-a)$, for a Rankine vortex, one obtains $r_{Qr} = r_{fk}$ and $\Omega_{r_{Qr}} \approx \left(\frac{m-1}{m}\right)\Omega_0$. The imaginary part of (2.122) leads to

$$\Omega_i \approx \frac{-\pi\dfrac{DZ(r_{Qr})\hat{\psi}^{\mathrm{CSM}}(r_{Qr};r_{Qr})}{r_{Qr}\Omega'(r_{Qr})}}{\left[\mathcal{P}\displaystyle\int_0^{\infty}\frac{DZ(r')D\hat{\psi}^{\mathrm{CSM}}(r';r_{Qr})}{r'\Omega'(r_{Qr})}\frac{1}{(\Omega(r')-\Omega(r_{Qr}))^2}dr' + \mathrm{Pf.}\int_0^{\infty}\frac{1}{r'}\frac{DZ(r')\hat{\psi}^{\mathrm{CSM}}(r';r_{Qr})}{(\Omega(r')-\Omega(r_{Qr}))^2}dr'\right]}, \tag{2.124}$$

which characterizes the decay rate of the quasi-mode; here, Pf. denotes the principal finite part of the singular integral. Again, using the expressions for DZ, $\hat{\psi}^{\mathrm{CSM}}$ and $D\hat{\psi}^{\mathrm{CSM}}$ for a Rankine-profile, one obtains

$$\Omega_i \approx -\frac{\pi a}{4m^2}DZ(r_{Qr})\left(\frac{m-1}{m}\right)^{m-\frac{3}{2}}. \tag{2.125}$$

Although the expression for the damping rate originally given by Briggs et al (1970) is correct, there appears to be an error in the expressions given in Balmforth and Morrison (1995) (the analog of (2.125) for parallel flows), and in Le Dizès (2000) which has the exponent in (2.125) as $(m-1)$ rather than $(m-\frac{3}{2})$.

2.3.3 3D singular eigenspectrum

The 3D eigenvalue problem for a smooth vorticity profile is, of course, analytically intractable, and we therefore analyze the 3D smooth vortex CS-modes only in the vicinity of r_f. This is the region of interest since the Rankine vortex is a singular limit, and the approach of the vorticity eigenfunctions of a smooth (Rankine-like) profile to the corresponding Rankine eigenfunctions is therefore non-uniform; there always being an arbitrarily large difference between the two sufficiently close to r_c. The Howard-Gupta (HG) equation for $\hat{u}_r$, rather than (2.28) for $\hat{u}_z$, is suited to such a local analysis, and is given by [Howard & Gupta [1962]]:

$$\left(\frac{S}{r}(r\hat{u}_r)'\right)' - \hat{u}_r + \left(\frac{SZ}{r^2}\right)' \frac{mr\hat{u}_r}{\Sigma} + \frac{2k^2SZ\Omega}{\Sigma^2}\hat{u}_r = 0, \tag{2.126}$$

with $S = \dfrac{r^2}{m^2 + (kr)^2}$. For r close to r_f, (2.126) reduces to

$$\hat{u}_r'' + \frac{2k^2Z(r_f)\Omega(r_f)}{[m\Omega'(r_f)]^2}\frac{\hat{u}_r}{(r-r_f)^2} = 0. \tag{2.127}$$

which is similar to the well-known Taylor-Goldstein (TG) equation that governs the inviscid evolution of infinitesimal disturbances in stratified shear flows [Turner [1973]]. The TG equation for stratified Couette flow, with $U(y) \propto y\mathbf{1}_x$, is given by

$$\left(\frac{d^2}{dy^2} - k^2\right)\hat{u}_y + Ri\frac{\hat{u}_y}{(y-y_c)^2} = 0, \tag{2.128}$$

for the normal velocity component of a single Fourier mode of the form $u_y = \hat{u}_y(y)e^{ik(x-ct)}$, with y_c being the critical level at which the wave speed (c) equals that of the shear flow. Here, Ri is the Richardson number, a dimensionless measure of competing buoyancy and inertial forces (see section 2.4). Notwithstanding the additional term proportional to k^2u_y which does not affect the nature of the singular point (as characterized by the Frobenius exponents; see (2.129) below), the similarity between (2.127) and (2.128) is evident. One may therefore define $\mathrm{Ri}_v = \frac{2k^2Z(r_f)\Omega(r_f)}{[m\Omega'(r_f)]^2}$ as a local Richardson number for a smooth vortex [Le Dizès [2004]], and the singularity of the 3D CS-modes must be analogous to those of the CS-modes in stratified shear flows. The solution of (2.127) in the vicinity of r_f may then be written in the general form:

$$\hat{u}_r = A_0|r-r_f|^{\frac{1}{2}-\nu}\{1 + \alpha_1(r-r_f) + O(r-r_f)^2\} + B_0|r-r_f|^{\frac{1}{2}+\nu}\{1 + \beta_1(r-r_f) + O(r-r_f)^2\}, \tag{2.129}$$

where

$$A_0 = A_0^- H(r_f - r) + A_0^+ H(r - r_f),\ B_0 = B_0^- H(r_f - r) + B_0^+ H(r - r_f), \tag{2.130}$$

and $\nu = \sqrt{\frac{1}{4} - \mathrm{Ri}_v}$; the series coefficients α_i and β_i in (2.129) may be determined in the usual manner. From (2.129), we see that, for any finite $\mathrm{Ri}_v(r_f)$ however small, the constraining effects of Coriolis forces cause the radial velocity associated with any 3D singular mode to approach

zero at the critical radius. An appropriate choice of the constants $A_0^{\pm}$ and $B_0^{\pm}$ in (2.130) should lead to the analog of the Λ_1 and Λ_2 CS-mode families. Since the Frobenius exponents $(\frac{1}{2}+\nu)$ and $(\frac{1}{2}-\nu)$ approach 1 and 0 in the Rankine limit ($Ri_v \to 0$ due to $Z \to 0$ with k and r_f fixed), the radial velocity eigenfunctions corresponding to the Λ_1 and Λ_2 families, for r close to r_f, are given by:

$$\begin{aligned}\hat{u}_r^{\Lambda_1}(r;r_f) &= A_0|r-r_f|^{\frac{1}{2}-\nu} + B_0^-|r-r_f|^{\frac{1}{2}+\nu} && r<r_f, \qquad (2.131)\\ &= A_0|r-r_f|^{\frac{1}{2}-\nu} + B_0^+|r-r_f|^{\frac{1}{2}+\nu} && r>r_f,\\ \hat{u}_r^{\Lambda_2}(r;r_f) &= A_0^-|r-r_f|^{\frac{1}{2}-\nu} + B_0|r-r_f|^{\frac{1}{2}+\nu} && r<r_f, \qquad (2.132)\\ &= A_0^+|r-r_f|^{\frac{1}{2}-\nu} - B_0|r-r_f|^{\frac{1}{2}+\nu} && r>r_f.\end{aligned}$$

The connection with the Λ_i-families of the Rankine vortex may be seen by expanding the Frobenius forms above for small Ri_v [Maslowe & Nigam [2008]], whence one obtains the corresponding forms for the homogeneous case except in a region of $O(e^{-\frac{1}{Ri_v}})$ around r_f wherein the expansion breaks down. Consistent with the Rankine analysis in section 2.2.2, this outer solution has an apparent kink at $r = r_f$ for the choice of constants $(A_0^- = A_0^+ = A_0)$ in (2.131) and an apparent step-discontinuity for the choice $(B_0^- = -B_0^+ = B_0)$ in (2.132). Using $\hat{u}_\theta = ik^2S\left(-\frac{Z}{\Sigma}u_r + \frac{m}{(kr)^2}(ru_r)'\right)$, and the continuity equation, one obtains the remaining velocity components as:

$$\hat{u}_\theta^{\Lambda_i}(r;r_f) = R_1^{\Lambda_i}|r-r_f|^{-\frac{1}{2}-\nu} + R_2^{\Lambda_i}|r-r_f|^{-\frac{1}{2}+\nu} + R_3^{\Lambda_i}|r-r_f|^{\frac{1}{2}-\nu} + R_4^{\Lambda_i}|r-r_f|^{\frac{1}{2}+\nu} + R_5^{\Lambda_i}|r-r_f|^{\frac{3}{2}-\nu} + O(|r-r_f|^{\frac{3}{2}+\nu}), \qquad (2.133)$$

$$\hat{u}_z^{\Lambda_i}(r;r_f) = Q_1^{\Lambda_i}|r-r_f|^{-\frac{1}{2}-\nu} + Q_2^{\Lambda_i}|r-r_f|^{-\frac{1}{2}+\nu} + Q_3^{\Lambda_i}|r-r_f|^{\frac{1}{2}-\nu} + Q_4^{\Lambda_i}|r-r_f|^{\frac{1}{2}+\nu} + Q_5^{\Lambda_i}|r-r_f|^{\frac{3}{2}-\nu} + O(|r-r_f|^{\frac{3}{2}+\nu}), \qquad (2.134)$$

where the coefficients $R_1^{\Lambda_i} - R_5^{\Lambda_i}$, $Q_1^{\Lambda_i} - Q_5^{\Lambda_i}$ are listed in appendix B. In obtaining (2.133) and (2.134), we have used that $|x|^\alpha\delta(x) = 0$ for any $\alpha > 0$. Strictly speaking, the product of the two generalized functions $|x|^\alpha$ and $\delta(x)$ is not a generalized function, and thus, $x^\alpha\delta(x)$, for fractional α cannot be regarded as a generalized zero; the interpretation needed is discussed below after the expressions for the vorticity eigenfunctions.

Given the local forms (2.131)-(2.134) for the Λ_1 and Λ_2 families, it is now of interest to determine the singular forcing that must appear in the HG equation in each case. Note that, in doing so, we are proceeding for the smooth vortex in a manner opposite to that for the Rankine vortex. This is because the nature of the singular structures in the the latter case, a vortex-sheet for the Λ_1 family (see (2.46) in section 6.3.1) and a localized axial jet for the Λ_2 family (see (2.67) in section 6.3.2), was clear from physical considerations associated with a shape-preserving inviscid normal mode; from the mathematical standpoint, the required singular forcings were the usual generalized functions. In contrast, a vortex-sheet (or any derivative singular structures thereof) cannot constitute the singular forcing for a smooth vortex since such a structure leads to a non-zero radial velocity at r_f, and is thereby inconsistent with the aforementioned Frobenius forms. To arrive at the singular forcing for a smooth vortex CS-mode, we first note that the dominant contribution to the axial vorticity eigenfunction, for r close to r_f,

is proportional to $\frac{d^2\hat{u}_r}{dr^2}$, implying that the vorticity eigenfunctions associated with the Λ_1 or Λ_2-analogs of a smooth vortex are, on one hand, non-local due to the distributed 'baroclinic' source of vorticity, and on the other hand, have a non-integrable singularity at r_f. A non-integrable singularity at the critical radius is, however, inconsistent with the requirements of a modal superposition which involves an integration over the CS-spectrum, with appropriately weighted amplitudes, over the entire domain. It was first shown by Engevik (1971), in the context of Couette flow with a uniform (stable) stratification, that a sensible modal superposition emerges only when the divergent integrals involving the vorticity eigenfunctions are interpreted in the sense of a principal-finite-part (Pf.)[Gel'fand & Shilov [1964]]. Based on the local analogy with the stratified flow CS-modes, the CS-modes, given by (2.131) and (2.132), must therefore be regarded as generalized functions requiring a Pf. interpretation; the Pf. interpretation also implies that the singular forcing cannot be a generalized function. The vorticity eigenfunctions corresponding to (2.131) and (2.132) may now be written as:

$$\hat{w}_z^{\Lambda_1}(r;r_f) = \text{Pf.}\,\frac{iS_f m}{r_f}\left(\frac{B_0^- + B_0^+}{2}\right)(\nu-\frac{1}{2})|r-r_f|^{-(\frac{3}{2}-\nu)} + \ldots, \tag{2.135}$$

$$\hat{w}_r^{\Lambda_1}(r;r_f) = -\text{Pf.}\,\frac{mA_0}{kr_f}(\nu-\frac{1}{2})\,\text{sgn}(r-r_f)|r-r_f|^{(\frac{1}{2}+\nu)} + \ldots, \tag{2.136}$$

$$\hat{w}_\theta^{\Lambda_1}(r;r_f) = \text{Pf.}\,ikS_f\left(\frac{B_0^- + B_0^+}{2}\right)(\frac{1}{2}-\nu)|r-r_f|^{-(\frac{3}{2}-\nu)} + \ldots, \tag{2.137}$$

and

$$\hat{w}_z^{\Lambda_2}(r;r_f) = \text{Pf.}\,\frac{imS_f}{2r_f}\left(\frac{A_0^- - A_0^+}{2}\right)\left(\alpha_1+\frac{1}{r_f}\right)(\nu-\frac{1}{2})\left\{|r-r_f|^{-(\frac{3}{2}-\nu)} + |r-r_f|^{-(\frac{1}{2}+\nu)}\right\}, \tag{2.138}$$

$$\hat{w}_r^{\Lambda_2}(r;r_f) = \text{Pf.}\,\frac{m}{kr_f}\left(\frac{A_0^- - A_0^+}{2}\right)(\frac{1}{2}-\nu)|r-r_f|^{-(\frac{1}{2}+\nu)} + \ldots, \tag{2.139}$$

$$\hat{w}_\theta^{\Lambda_2}(r;r_f) = -\text{Pf.}\,\frac{i}{k}\left(\frac{A_0^- - A_0^+}{2}\right)(\frac{1}{2}-\nu)\,\text{sgn}(r-r_f)|r-r_f|^{-(\frac{3}{2}+\nu)} + \ldots, \tag{2.140}$$

where we have only included the most singular contributions. From generalized function theory [Lighthill [1958], Gel'fand & Shilov [1964]], it is known that,

$$\lim_{\lambda\to-2k-1}\frac{|x|^\lambda}{\Gamma\left(\frac{\lambda+1}{2}\right)} = \frac{(-1)^k k!}{(2k)!}\delta^{(2k)}(x), \tag{2.141}$$

$$\lim_{\lambda\to-2k}\frac{|x|^\lambda \text{sgn}(x)}{\Gamma\left(\frac{\lambda+2}{2}\right)} = \frac{(-1)^k (k-1)!}{(2k-1)!}\delta^{(2k-1)}(x), \tag{2.142}$$

and zero otherwise. Using this, one obtains from (2.135)-(2.137), $\lim_{\nu\to\frac{1}{2}}\hat{w}_z^{\Lambda_1} = iS_c m(B_0^- + B_0^+)/r_f\,\delta(r-r_f)$, $\lim_{\nu\to\frac{1}{2}}\hat{w}_\theta^{\Lambda_1} = -ikS_c(B_0^- + B_0^+)\delta(r-r_f)$, $\lim_{\nu\to\frac{1}{2}}\hat{w}_r^{\Lambda_1} = 0$; and from (2.138)-(2.140), $\lim_{\nu\to\frac{1}{2}}\hat{w}_z^{\Lambda_2} = 0$,$\lim_{\nu\to\frac{1}{2}}\hat{w}_r^{\Lambda_2} = m/(kr_f)(A_0^- - A_0^+)\delta(r-r_f)$, $\lim_{\nu\to\frac{1}{2}}\hat{w}_\theta^{\Lambda_2} = i/k(A_0^- - A_0^+)\delta'(r-r_f)$; all regular contributions, not explicitly included in (2.135)-(2.140), vanish in this limit. This then ensures consistency with the singular form of the Rankine CS-modes in the irrotational exterior.

The nature of the singular forcing leading to the 3D smooth vortex CS-modes is an issue

that needs clarification. For shearing flows, the discrete spectrum is almost always finite [Drazin & Reid [1981]], and it is thus routinely mentioned (for instance, see Maslowe [1986]) that the additional CS-modes, needed for purposes of completeness, arise from including generalized function forcings in the governing equation for linearized perturbations. This is true only for homogeneous shearing flows, and for the 2D modes in the vortex case as seen in section 2.2.1; here, the forcings are indeed proportional to the delta function and/or its derivatives. The Pf. interpretation needed for the stratified flow and the 3D smooth vortex CS-modes implies that the underlying singular forcing is no longer a generalized function. This may be seen from (2.127) wherein such a forcing is the residue that needs to be subtracted from the baroclinic source term to remove the non-integrable singularity in the vorticity field. Loosely speaking, the Pf. interpretation implies that the source term in (2.127) not be $Ri_v \frac{u_r}{(r-r_f)^2}$, but instead be $Ri_v[\frac{u_r}{(r-r_f)^2} - F_1\frac{\delta(r-r_f)}{(r-r_f)^{\frac{1}{2}+\nu}} - F_2\frac{\delta(r-r_f)}{(r-r_f)^{\frac{1}{2}+\nu}}]$, with the F_i's being related to the coefficients of the Frobenius forms in u_r. In turn, this points to a forced HG equation that, for r close to r_f, takes the form

$$\hat{u}_r'' + \frac{2k^2 Z(r_f)\Omega(r_f)}{[m\Omega'(r_f)]^2}\frac{\hat{u}_r}{(r-r_f)^2} = Ri_v\left[F_1\frac{\delta(r-r_f)}{(r-r_f)^{\frac{1}{2}-\nu}} + F_2\frac{\delta(r-r_f)}{(r-r_f)^{\frac{1}{2}+\nu}}\right]. \tag{2.143}$$

Now, the mathematical theory constructs a linear space of generalized functions, and within this framework, the product of an infinitely differentiable function with a generalized function is allowed, but the product of two generalized functions does not in general have an unambiguous interpretation [Gel'fand & Shilov [1964]]; in other words, the terms proportional to $\delta(r-r_f)$ on the RHS in (2.143) are not generalized functions for non-integral $\frac{1}{2} \pm \nu$. In the Rankine limit ($Ri_v \to 0, \nu \to \frac{1}{2}$), however, the non-generalized function forcings become vanishingly small while the baroclinic source term on the LHS reduces to the generalized function forcing that led to the Λ_1 and Λ_2 families in sections 6.3.1 and 6.3.2. The crucial difference in the nature of the singular forcing terms between the Rankine and smooth vortex CS-modes, at least as far as their mathematical interpretation is concerned, is often not recognized. It does not find explicit mention in the early work on the CS-spectrum of stratified Couette flow (see Eliassen *et al.* [1953]; Engevik [1971]), and there have been cases where the forcings have been erroneously taken to be similar to those for the homogeneous case - Case (1960b), in extending his analysis from the homogeneous case to the stratified scenario, writes down the TG equation forced with a delta function and its derivative.

The nature of the singular forcing is also relevant from the standpoint of an initial value problem. The singular forcing in the governing equation for linearized perturbations is the initial impulsive forcing that recovers an isolated CS-mode for long times. A weaker forcing will lead to a long-time algebraic decay, while a stronger forcing will lead to secular growth (even in the absence of a resonant interaction). Physically, the presence of the singular forcing implies that a CS-mode is associated with perturbation vorticity generated by an 'extraneous' force distribution; here, extraneous refers to mechanisms outside of the physics already included in the governing equations. For instance, in homogeneous flows, the (regular) discrete modes arise from a rearrangement of the base-state vorticity while the CS-modes require the generation of a vortex sheet via a baroclinic force distribution proportional to a delta function. For Couette flow,

an initial gradient-directed impulsive forcing of the form $\delta(y-y_c)e^{ikx}$ generates precisely a single CS-mode with $\omega = ky_c$. For a non-linear flow profile, such a forcing leads to an isolated CS-mode but only for long times; since the forcing only generates the vortex-sheet contribution and not the PV-singular contribution of a single CS-mode, the finite-time response is a polychromatic one involving the entire CS-spectrum [Kelbert & Sazonov [1996]]. For the Rankine vortex, a localized forcing of the form $\delta(r - r_f)e^{i(m\theta+kz)}$ must similarly lead to the corresponding (2D or 3D) CS-mode, together with a superposition of Kelvin modes, when r_f does not coincide with any of the Kelvin-mode critical radii. For stratified shear flows, however, a delta-function extraneous forcing is weaker than the non-generalized function forcings, associated with the Pf. interpretation, and that appear in (2.143). Thus, one expects a non-modal response for long times characterized by an algebraic decay ($\propto t^{-(\frac{1}{2}\pm\nu)}$), the associated exponents being precisely those appearing in the denominators of the RHS terms in (2.143). This has been shown for the case of Couette flow with a uniform stratification (Brown & Stewartson [1980], Booker & Bretherton [1967]), and a similar scenario must hold for a smooth vortex in three dimensions. Finally, regarding the singular forcings in the Rayleigh and TG equations (and their vortex analogs) as resulting in the limit of a vanishing viscosity for the homogeneous case, and in the limit of both vanishing viscosity and (mass or thermal) diffusivity for the stratified case, it also follows that the homogeneous critical layer solution (Stewartson 1981) must approach a generalized function forcing in the limit $Re \to \infty$, but that the analogous critical layer solution in the stratified case must not exhibit this property in the limit $Re, Pr^{-1} \to \infty$ (Pr is the Prandtl number and denotes the ratio of the relevant diffusivities).

2.3.4 The modal decomposition for an arbitrary vortical initial condition

Having examined the local structure of the 3D CS-modes, we clarify the manner in which the modal superposition for a smooth vorticity profile, corresponding to an evolving (arbitrary) three-dimensional distribution of perturbation vorticity, would approach that obtained in section 2.2.2 for the Rankine vortex. The clarification must necessarily be an indirect one since analytical forms for the eigenmodes associated with a smooth vorticity profile do not exist. The non-trivial aspect in the comparison between the Rankine vortex and smooth Rankine-like profiles concerns the crucial difference in the singularities of the 3D CS-modes, and the relation betwen the two modal superpositions may therefore be illustrated by considering the respective parallel flow analogies with the CS-modes having the same singularities as in the vortex case. The Rankine vortex would then correspond to homogeneous Couette flow, the analytically tractable analog of a smooth vortex with vorticity that monotonically decays with radial distance would be a Couette flow with a uniform stable stratification, and the approach to the Rankine limit involves making the stratification vanishingly small.

The modal superpositions in the parallel flow analogies evolve an arbitrary initial distribution of vorticity and density perturbations. The azimuthal vorticity (w_θ) in the vortex case corresponds to the vorticity in stratified flow (w_z being the only non-zero component for the two-dimensional perturbations considered), and the radial vorticity (w_r) in the vortex case cor-

responds to the density perturbation (ρ') in the stratified flow problem; the remaining perturbation fields being determined from solenoidal constraints. Assuming $U(y) \propto y$ and $\rho_0(y)$ to characterize the unperturbed stratified flow, the correspondence, $(w_\theta, w_r) \leftrightarrow (w_z, \rho')$, may be seen from the governing equations in the respective cases, which in the inviscid non-diffusive limit, are given by:

$$\left(\frac{\partial}{\partial t} + \Omega(r)\frac{\partial}{\partial \theta}\right) w_\theta = Z\frac{\partial u_\theta}{\partial z} + [r\Omega'(r)]w_r, \tag{2.144}$$

$$\left(\frac{\partial}{\partial t} + \Omega(r)\frac{\partial}{\partial \theta}\right) w_r = Z\frac{\partial u_r}{\partial z}, \tag{2.145}$$

$$\left(\frac{\partial}{\partial t} + U(y)\frac{\partial}{\partial x}\right) w_z = -g\frac{\partial \rho'}{\partial x}, \tag{2.146}$$

$$\left(\frac{\partial}{\partial t} + U(y)\frac{\partial}{\partial x}\right) \rho' = -\frac{d\rho_0}{dy}u_y. \tag{2.147}$$

The w_r and ρ' perturbations are seen to arise from a balance between the convection and induction terms (the latter being proportional to the base-state vorticity in (2.145) and to the density gradient in (2.147)). These perturbations then act as source terms for w_θ and w_z, respectively, via (2.144) and (2.146). The changes in w_θ and w_z couple back to (2.145) and (2.147) via u_r and u_y, and the overall effect is that of buoyancy forces resisting the deformation of the iso-pycnic lines in the same manner that the Coriolis forces resist the generation of radial vorticity by endowing the (axial) vortex lines in the base-state with a certain stiffness. For homogeneous Couette flow, ρ_0 is a constant, and for the Rankine vortex, $Z = 0$ (the irrotational exterior being the region of interest for CS-modes), so ρ' and w_r are merely advected by the base-flow. The correspondence is not an exact one since there exists an additional source term for w_θ in the vortex case. But, the contribution form this term becomes asymptotically small in the Rankine limit ($Z \to 0$); if one were to neglect this contribution in (2.144), then the resulting equation for u_r would involve a Richardson number that differs from Ri_v in (2.128) only by $O(Z^2)$.

We now examine the manner in which the modal superposition for stratified Couette flow involving singular Pf. eigenfunctions, originally obtained by Engevik (1971), reduces to the simpler more familiar form, involving delta functions, for homogeneous Couette flow in the limit of a vanishingly small stratification. The equations (2.146) and (2.147), rewritten in terms of the streamfunction ψ and ρ', are given by

$$(\partial_t + y\partial_x)\,\nabla^2\psi = -\frac{1}{\mathrm{Fr}^2}\,\partial_x\rho', \tag{2.148}$$

$$(\partial_t + y\partial_x)\,\rho' = \left(\frac{N}{N_0}\right)^2 \partial_x\psi, \tag{2.149}$$

in dimensionless form with $\nabla^2 \equiv \frac{\partial^2}{\partial x^2} + \frac{\partial^2}{\partial y^2}$. The parameter $\mathrm{Fr} = U_0/(N_0 L)^{\frac{1}{2}}$ in (2.148) is a reference Froude number with (U_0/L) being a characteristic scale for the base-state velocity gradient. The ratio N/N_0 in (2.149) is a dimensionless measure of the base-state stratification with $N^2 = -\frac{g}{\rho_m}\frac{d\rho_0}{dy}$ being the square of the (constant) Brunt-Väisälä frequency, $N_0 = (\frac{g}{L})^{\frac{1}{2}}$ being

a reference frequency scale, and ρ_m being an appropriate mean density within the Boussinesq approximation. The separation of the single parameter, the Richardson number ($Ri = (\frac{N}{N_0})^2 \mathrm{Fr}^{-2}$) in the TG equation that results from combining (2.148) and (2.149), into two parameters, one in each of (2.148) and (2.149), allows for one to discriminate between the cases where Ri vanishes due to the absence of gravity (N/N_0 finite, $\mathrm{Fr}^{-1} \to 0$, leading to a de-coupling of the velocity and density fields), and where Ri vanishes because of a homogeneous base-state ($N/N_0 \to 0$ with Fr finite). We are interested in the latter case since this allows for density perturbations to persist and drive a flow even in a homogeneous base-state.

For homogeneous Couette flow ($N/N_0 = 0$), assuming a normal mode form proportional to $e^{ik(x-y_c t)}$, one obtains from (2.148) and (2.149):

$$(y - y_c)\, w_z = -\frac{1}{\mathrm{Fr}^2}\rho', \tag{2.150}$$

$$(y - y_c)\, \rho' = 0, \tag{2.151}$$

where $w_z = (D^2 - k^2)\psi$. The above system of equations supports two families of CS-modes. The Case vortex-sheet modes with $w_z \propto \delta(y - y_c)$ were discussed in section 2.2.1, and arise from the homogeneous solution of (2.150); they are the analog of the Λ_1 family for the Rankine vortex. The analog of the Λ_2 family are density sheets with a dipole singularity ($w_z \propto \delta'(y - y_c)$) corresponding to a tangential jet riding at the critical level. Thus,

$$(w_z^{\Lambda_1}, \rho'^{\Lambda_1}) = (\delta(y - y_c), 0), \tag{2.152}$$

$$(w_z^{\Lambda_2}, \rho'^{\Lambda_2}) = (\frac{1}{Fr^2}\,\delta'(y - y_c), \delta(y - y_c)). \tag{2.153}$$

For a bounded domain, the arbitrary-time vorticity field may then be written as the following modal superposition:

$$w_z(y,t) = \int_{-1}^{1} X_{\Lambda_1}(y_c) w_z^{\Lambda_1} e^{-iky_c t} dy_c + \int_{-1}^{1} X_{\Lambda_2}(y_c) w_z^{\Lambda_2} e^{-iky_c t} dy_c, \tag{2.154}$$

with $X_{\Lambda_1}(y_c) = w_{z0}(y_c) - \frac{1}{Fr^2}\,\rho_0'(y_c)$ and $X_{\Lambda_2}(y_c) = \rho_0'(y_c)$. The superposition is easily found by first finding the Λ_2-superposition needed to represent the initial perturbation density field (ρ_0'), and then finding the necessary Λ_1-superposition to account for the residual vorticity field.

For stratified Couette flow, the equations in normal-mode form are

$$(y - y_c)\, w_z = -\frac{1}{\mathrm{Fr}^2}\rho', \tag{2.155}$$

$$(y - y_c)\, \rho' = \frac{N^2}{N_0^2}\psi. \tag{2.156}$$

The TG equation obtained from combining the above pair of equations has linearly independent solutions given by $f(y) = \sqrt{ik(y - y_c)}J_{-\nu}[ik(y - y_c)]$ and $g(y) = \sqrt{ik(y - y_c)}J_{\nu}[ik(y - y_c)]$ with $\nu = \sqrt{1/4 - \mathrm{Ri}}$ as before. For $y \to y_c$, these Bessel solutions reduce to the local Frobenius forms, obtained from (2.128), and that are valid for a general Ri-profile. For a constant-Ri Couette flow, the spectrum is purely continuous when $0 <\mathrm{Ri}< 1/4$ [Taylor [1931],Eliassen *et al.* [1953]] and from the results of Engevik (1971), the arbitrary-time streamfunction may be written as the

following integral superposition over Pf. singular eigenfunctions:

$$\psi(y,t) = \text{Pf.}\int_{-1}^{y} A_1(y_c)\Psi(1-y_c, y-y_c)e^{-iky_ct}dy_c + \text{Pf.}\int_{y}^{1} A_2(y_c)\Psi(1+y_c, y_c-y)e^{-iky_ct}dy_c, \tag{2.157}$$

where $A_1(y_c)$ and $A_2(y_c)$ are given by

$$-4ikA_1(y_c)f(1-y_c)g(1-y_c)\sin\pi\nu - 2ikA_2(y_c)\Delta(y_c) = B_1(y_c)\cot\pi\nu, \tag{2.158}$$

$$2ikA_1(y_c)\Delta(y_c) - 4ikA_2(y_c)f(1+y_c)g(1+y_c)\sin\pi\nu = B_2(y_c)\cot\pi\nu, \tag{2.159}$$

with

$$B_1(y_c) = \text{Pf.}\int_{y_c}^{1}\left\{\frac{w_{z0}}{y-y_c} - \frac{Fr^{-1}\rho_0'}{(y-y_c)^2}\right\}\Psi(1-y_c, y-y_c)dy, \tag{2.160}$$

$$B_2(y_c) = \text{Pf.}\int_{-1}^{y_c}\left\{\frac{w_{z0}}{y_c-y} + \frac{Fr^{-1}\rho_0'}{(y_c-y)^2}\right\}\Psi(1+y_c, y_c-y)dy, \tag{2.161}$$

$$\Delta(y_c) = f(1+y_c)g(1-y_c) - f(1-y_c)g(1+y_c). \tag{2.162}$$

In (2.157), the singular CS-modes are the one-sided eigenfunctions originally defined by Eliassen et al. (1953), and given by

$$\text{Pf.}\Psi(1-y_c, y-y_c) = \text{Pf.}\left\{g(1-y_c)f(y-y_c) - f(1-y_c)g(y-y_c)\right\} \text{ if } y_c < y, \tag{2.163}$$

$$\text{Pf.}\Psi(1+y_c, y_c-y) = \text{Pf.}\left\{g(1+y_c)f(y_c-y) - f(1+y_c)g(y_c-y)\right\} \text{ if } y_c > y. \tag{2.164}$$

From (2.165), the modal superposition for w_z may be written in the form

$$w_z(y,t) = \text{Pf.}\int_{-1}^{y} A_1(y_c)\frac{\Psi(1-y_c, y-y_c)}{(y-y_c)^2}e^{-iky_ct}dy_c + \text{Pf.}\int_{y}^{1} A_2(y_c)\frac{\Psi(1+y_c, y_c-y)}{(y-y_c)^2}e^{-iky_ct}dy_c. \tag{2.165}$$

In order to show that (2.154) arises as the limiting form of (2.165) for $(N/N_0) \to 0$, it is convenient to first consider the following linear combinations of the one-sided eigenfunctions defined above:

$$\Psi^{\Lambda_1} = g(1+y_c)\Psi(1-y_c, y-y_c)\mathcal{H}(y-y_c) + g(1-y_c)\Psi(y_c+1, y_c-y)\mathcal{H}(y_c-y) \tag{2.166}$$

$$= c_1^{\Lambda_1}f(|y-y_c|) - \left(\frac{c_2^{\Lambda_1}+c_3^{\Lambda_1}}{2}\right)g(|y-y_c|) - \left(\frac{c_2^{\Lambda_1}-c_3^{\Lambda_1}}{2}\right)g(|y-y_c|)\text{sgn}(y-y_c) \tag{2.167}$$

$$\Psi^{\Lambda_2} = f(1+y_c)\Psi(1-y_c, y-y_c)\mathcal{H}(y-y_c) - f(1-y_c)\Psi(y_c+1, y_c-y)\mathcal{H}(y_c-y) \tag{2.168}$$

$$= -c_1^{\Lambda_2}g(|y-y_c|)\text{sgn}(y-y_c) + \left(\frac{c_2^{\Lambda_2}-c_3^{\Lambda_2}}{2}\right)f(|y-y_c|) + \left(\frac{c_2^{\Lambda_2}+c_3^{\Lambda_2}}{2}\right)f(|y-y_c|)\text{sgn}(y-y_c) \tag{2.169}$$

where $c_1^{\Lambda_1} = g(1+y_c)g(1-y_c)$, $c_1^{\Lambda_2} = f(1+y_c)f(1-y_c)$, $c_2^{\Lambda_1} = c_3^{\Lambda_2} = f(1-y_c)g(1+y_c)$ and $c_3^{\Lambda_1} = c_2^{\Lambda_2} = f(1+y_c)g(1-y_c)$. As evident from the notation, the linear combinations in (2.167)

and (2.169) may be identified with the Λ_1 and Λ_2 analogs of a smooth vorticity profile; the Frobenius forms in the vicinity of y_c reduce to those defined in (2.131) and (2.132) for a smooth vortex. As will be seen below, (2.167) and (2.169) reduce to the vortex-sheets and density-sheets defined in (2.152) and (2.153) for $N/N_0 \to 0$. Using (2.167) and (2.169), (2.165) may be rewritten as

$$\begin{aligned} w_z(y,t) &= -\text{Pf.}\int_{-1}^{1}\{A_1(y_c)f(1-y_c)+A_2(y_c)f(1+y_c)\}\frac{\text{Ri}\,\Psi^{\Lambda_1}}{(y-y_c)^2W(y_c)}e^{-iky_ct}dy_c \\ &\quad -\text{Pf.}\int_{-1}^{1}\{A_1(y_c)g(1-y_c)-A_2(y_c)g(1+y_c)\}\frac{\text{Ri}\,\Psi^{\Lambda_2}}{(y-y_c)^2W(y_c)}e^{-iky_ct}dy_c \end{aligned} \tag{2.170}$$

where $W(y_c) = f(1+y_c)g(1-y_c)+f(1-y_c)g(1+y_c)$ with (2.160) and (2.161) now being given by:

$$\begin{aligned} \text{Ri}\,B_1(y_c) &= \text{Pf.}\int_{-1}^{1}\left[\frac{f(1-y_c)}{W(y_c)}\left\{w_{y0}\frac{\text{Ri}\,\Psi^{\Lambda_1}}{|y-y_c|}-Fr^{-1}\rho_0\frac{\text{Ri}\,\Psi^{\Lambda_1}}{(y-y_c)^2}\right\}+\right. \\ &\quad \left.\frac{g(1-y_c)}{W(y_c)}\left\{w_{y0}\frac{\text{Ri}\,\Psi^{\Lambda_2}}{|y-y_c|}-Fr^{-1}\rho_0\frac{\text{Ri}\,\Psi^{\Lambda_2}}{(y-y_c)^2}\right\}\right]dy, \end{aligned} \tag{2.171}$$

$$\begin{aligned} \text{Ri}\,B_2(y_c) &= \text{Pf.}\int_{-1}^{1}\left[\frac{f(1+y_c)}{W(y_c)}\left\{w_{y0}\frac{\text{Ri}\,\Psi^{\Lambda_1}}{|y-y_c|}+Fr^{-1}\rho_0\frac{\text{Ri}\,\Psi^{\Lambda_1}}{(y-y_c)^2}\right\}+\right. \\ &\quad \left.\frac{g(1+y_c)}{W(y_c)}\left\{w_{y0}\frac{\text{Ri}\,\Psi^{\Lambda_2}}{|y-y_c|}+Fr^{-1}\rho_0\frac{\text{Ri}\,\Psi^{\Lambda_2}}{(y-y_c)^2}\right\}\right]dy, \end{aligned} \tag{2.172}$$

in terms of Ψ^{Λ_1} and Ψ^{Λ_2}.

In the limit $(N/N_0) \to 0$, $\Delta(y_c) \sim -\dfrac{2i\sinh 2ky_c}{\pi}$, $W(y_c) \sim \dfrac{2i\sinh 2k}{\pi}$, and (2.158) and (2.159) reduce to:

$$B_1(y_c)\pi\text{Ri} \sim \frac{4k}{\pi}\left\{A_1(y_c)\sinh 2k(1-y_c)-A_2(y_c)\sinh 2ky_c\right\}, \tag{2.173}$$

$$B_2(y_c)\pi\text{Ri} \sim \frac{4k}{\pi}\left\{A_1(y_c)\sinh 2ky_c+A_2(y_c)\sinh 2k(1+y_c)\right\}. \tag{2.174}$$

Further, only the limiting forms of f and g for y close to y_c, given by $f(z) \sim \frac{2^{\frac{1}{2}-\epsilon}(ikz)^{\epsilon}}{\Gamma(\frac{1}{2}+\epsilon)}$ and $g(z) \sim \frac{2^{-\frac{1}{2}+\epsilon}(ikz)^{1-\epsilon}}{\Gamma(\frac{3}{2}-\epsilon)}$, are needed in this limit, and from the theory of generalized functions, we have

$$\lim_{\frac{N}{N_0}\to 0}\begin{Bmatrix} \text{Ri}\dfrac{f(|y-y_c|)}{|y-y_c|}(1,\text{sgn}(y-y_c)) \\ \text{Ri}\dfrac{f(|y-y_c|)}{|y-y_c|^2}(1,\text{sgn}(y-y_c)) \\ \text{Ri}\dfrac{g(|y-y_c|)}{|y-y_c|}(1,\text{sgn}(y-y_c)) \\ \text{Ri}\dfrac{g(|y-y_c|)}{|y-y_c|^2}(1,\text{sgn}(y-y_c)) \end{Bmatrix} = \begin{Bmatrix} 2\sqrt{\dfrac{2}{\pi}}(\delta(y-y_c),0) \\ -2\sqrt{\dfrac{2}{\pi}}(0,\delta'(y-y_c)) \\ 0 \\ -2ik\sqrt{\dfrac{2}{\pi}}(\delta(y-y_c),0) \end{Bmatrix} \tag{2.175}$$

This leads to the corrected expressions for the vorticity eigenfunctions in the unstratified limit:

$$\lim_{\frac{N}{N_0}\to 0} -\frac{\mathrm{Ri}\,\Psi^{\Lambda_1}}{(y-y_c)^2} = k\sinh 2k\left(\frac{2}{\pi}\right)^{3/2}\delta(y-y_c), \tag{2.176}$$

$$\lim_{\frac{N}{N_0}\to 0} -\frac{\mathrm{Ri}\,\Psi^{\Lambda_2}}{(y-y_c)^2} = i\sinh 2k\left(\frac{2}{\pi}\right)^{3/2}\delta'(y-y_c). \tag{2.177}$$

Substituting (2.175) in (2.171) and (2.172) leads to the following simplified expressions:

$$\begin{aligned}\mathrm{Ri}\,B_1(y_c) &= \frac{i}{\pi}\left[\mathrm{cosech}\,2k\left\{\cosh k(3-y_c)-\cosh k(1+y_c)\right\}(w_{y0}(y_c)-Fr^{-1}\rho'(y_c))-\right.\\ &\quad \left.2k\cosh k(1-y_c)Fr^{-1}\rho_0(y_c)\right],\\ \mathrm{Ri}\,B_2(y_c) &= \frac{2i}{\pi}\left[\sinh k(1+y_c)(w_{y0}(y_c)-Fr^{-1}\rho_0'(y_c))+k\cosh k(1+y_c)Fr^{-1}\rho_0(y_c)\right],\end{aligned} \tag{2.178}$$

Finally, on susbtituting the above expressions in (2.173) and (2.174), one finds

$$A_1(y_c)f(1-y_c)+A_2(y_c)f(1+y_c) = \frac{i}{k}\sqrt{\frac{\pi}{2}}(w_{y0}(y_c)-Fr^{-1}\rho'(y_c)), \tag{2.179}$$

$$A_1(y_c)g(1-y_c)-A_2(y_c)g(1+y_c) = \sqrt{\frac{\pi}{2}}Fr^{-1}\rho(y_c), \tag{2.180}$$

which, on substitution in (2.170) and use of (2.176) and (2.177) leads to (2.154).

Although the analysis shows the essential manner in which modal superposition for a smooth vorticity profile approaches that of a Rankine vortex, the appeal to the stratified flow analogies ends up ignoring the discrete spectra. Both Rankine and smooth vortices support a denumerable infinity of Kelvin modes (only co-grade ones in the latter case); in contrast, the spectrum of homogeneous Couette flow is purely continuous [Case [1960]; Fadeev [1971]] and stratified Couette flow again exhibits only a continuous spectrum when $Ri < \frac{1}{4}$ [Taylor [1931]]. This is not a fundamental constraint, however, and in section 2.4, we develop more elaborate stratified flow analogies that mirror both the discrete and continuous spectra of vortical flows. The analysis above may readily be extended to these cases where the modal superpositions will include additional summation terms over the discrete modes. Finally, in drawing the analogy between a smooth vorticity profile and stratified Couette flow, we have neglected the effect of the curvature of the velocity profile on the CS-spectrum. The additional induction term in the governing equation does not alter the local Frobenius forms, and thence, the nature of the singular forcing needed at the critical level.

2.4 A stratified flow analogy and the inviscid center-modes

There exists an analogy between parallel flows with stratification and rotational flows because buoyancy forces in the former case arrest vertical motion in the same manner as Coriolis forces arrest radial motion in the latter case. This analogy between the stiffening of the vortex lines and isopycnic lines is a qualitative one [Yih [1980]] - as seen in section 2.3.3, the governing equations for the relevant velocity components reduce to a common form only in the vicinity of the respective critical levels; an exact mathematical correspondence exists in two dimensions with

the rotation and stratification axes being at right angles to each other [Broadbent [1967]]. The physical analogy is nevertheless exploited here to construct stratified flow configurations with dispersion curves resembling those characterizing vortex column oscillations. The stratified flow analogs of the Rankine and smooth vorticity profiles highlight the manner in which the so-called inviscid center-modes, present in the latter case, disappear in the Rankine limit. Center-modes are nearly-convected modes (that is, with a vanishingly small Doppler frequency) with their structure concentrated in the vicinity of the rotation axis, and are known to play an important role in determining the inviscid stability characteristics of the Batchelor vortex [Heaton [2007a];Fabre & Le Dizès [2008]]. In the absence of an axial flow component in the base-state, as is the case for the vorticity profiles examined here, center-mode behavior is observed in the limit of small axial wavenumbers. Each of the structured modes becomes a center-mode for $k \to 0$, the corresponding eigenfunction being characterized by a vanishingly small radial length scale (the focus here is on the co-grade modes; the retrograde modes transform to inviscidly damped singular oscillations best interpreted in terms of a superposition of decaying quasi-modes) [Leibovich *et al.* [1986]].

The center-mode behavior may be seen by considering the one-parameter family of smooth vorticity profiles given by $\Omega(r) = \Omega_0 - \frac{r^{2p}}{2p!}\Omega_{2p}$ for small r with $\Omega_{2p} > 0$; $p = 1$ corresponds to a Lamb-Oseen profile and the limit $p \to \infty$ to the Rankine vortex. Substitution in the HG equation gives:

$$r\frac{d}{dr}\left[\frac{m^2 r}{m^2+k^2r^2}\frac{d}{dr}(ru_r)\right] - \left[m^2 - \frac{4m\left\{\frac{k^2r^2\Omega_0}{m^2} + \left(p - \frac{k^2r^2}{m^2}\right)\frac{(p+1)\Omega_{2p}r^{2p}}{(2p)!}\right\}}{(m\Omega-\omega)} - \frac{4k^2r^2\Omega_0^2\left\{1 - \frac{r^{2p}(p+2)}{(2p)!}\frac{\Omega_{2p}}{\Omega_0} + \frac{r^{4p}(p+1)}{(2p)!}\left(\frac{\Omega_{2p}}{\Omega_0}\right)^2\right\}}{(m\Omega-\omega)^2}\right] ru_r = 0, \tag{2.181}$$

for $r \to 0$. For the Rankine (co-grade) Kelvin modes, $\omega - m\Omega_0 \sim O(k)$ for $k \to 0$, implying a finite group velocity in the longwave limit. On use of this limiting form in (2.181), the terms proportional to inverse powers of the Doppler frequency are found to remain finite as $k \to 0$ with r fixed. This is no longer true for the flatter dispersion curves ($\omega - m\Omega_0 \propto k^x$ for $k \to 0$ with $x > 1$; see Fabre [2002]) characterizing smooth vorticity profiles (with p finite). The said terms now diverge with decreasing k, and this has the effect of concentrating the (oscillatory) eigenfunction in the vicinity of $r = 0$. This may be seen by using re-scaled boundary layer variables defined by $r^{2p} = \epsilon(k)s$, $ru_r(r) = U(s)$, whence one obtains, at leading order,

$$s^2U'' + sU' + \left[-\frac{m^2}{4p^2} + \frac{p+1}{p}\frac{s}{s+1} + \mu(\mu+1)\frac{s^{\frac{1}{p}}}{(s+1)^2}\right]U = 0, \tag{2.182}$$

with $\mu(\mu+1) = 4[(2p-1)!\Omega_0]^2$. The radial extent of the boundary layer is $\epsilon(k) = (\frac{k}{m\Omega_{2p}})^{\frac{1}{2p-1}}$ and determines the radial scale of the eigenmode. The case $p = 1$, for which $\epsilon(k) \sim O(k)$ and (2.182) reduces to the hypergeometric equation, was analyzed by Leibovich Brown & Patel (1983). For

large p, the reduction in the radial length scale ($\propto k^{\frac{1}{2p}}$) of the eigenfunction with decreasing k becomes increasingly gradual, and correspondingly, the transition to a center-mode behavior occurs at an increasingly small value of k; until, in the limit $p \to \infty$, there is no boundary layer, and consequently no center-mode behavior. The latter implies that the radial length scale (β_n^{-1}), characterizing a given structured mode eigenfunction ($\propto J_m(\beta_n r)$) of a Rankine vortex, remains fixed even as k goes to zero. This is seen from the analysis in section 2.2.2 which shows that $\beta_n^{-1} \approx \frac{a}{j_n^m}$, for $k \to 0$, where $J_m(j_n^m) = 0$; for $k \to \infty$, it is readily shown using (2.40) that $\omega_n \sim (m+2)\Omega_0 - \frac{\Omega_0 (j_n^{m+1})^2}{(ka)^2}$, so $\beta_n^{-1} \approx \frac{a}{j_n^{m+1}}$. Thus, unlike a smooth Rankine-like profile (p large but finite) the radial length scale, β_n^{-1}, varies only by $O(1)$ for n fixed. A physical interpretation of the above difference between a Rankine vortex and smooth Rankine-like profiles is given below after developing the appropriate stratified flow analogs.

The stratified flow analog of a Rankine vortex is shown in figure 2.6. A region of plug flow of height $(h_2 - h_1)$ overlies a region of uniform shear of height h_1, the uniform (stable) stratification in each region being characterized by a Brunt-Väisälä frequency: N_1 and N_2 for the shear and plug flow regions, respectively. In the absence of any stratification ($N_1 = N_2 = 0$), one has a homogeneous flow with a vorticity jump at $y = h_1$ - the interface between the plug and shear flow regions. This jump in vorticity leads to a single discrete mode, the so-called edge-wave with the vorticity eigenfunction being a vortex sheet at $y = h_1$; this corresponds to the 2D Kelvin mode for the Rankine vortex. The shear region gives rise to a CS-spectrum with the CS-mode vorticity eigenfunctions having a twin-vortex-sheet structure (one at the interface as for the discrete mode and the other at the critical level) similar to the 2D Rankine CS-modes. Thus, the unstratified piecewise linear flow reproduces the 2D Rankine spectrum. This is already known, and as pointed out in section 2.2.1, such flows have been analyzed before (Sazonov [1989]). Further, smoothing the kink in the base-state profile, into a region involving a rapid variation in the velocity gradient, reproduces the 2D spectrum of a smooth Rankine-like vorticity profile. An understanding of the center-modes, however, requires mimicking the corresponding 3D spectra. The analog of the 3D Rankine spectrum results from introducing a stratification in the plug region alone ($N_1 = 0, N_2 \neq 0$). As a result, the plug region now supports a denumerable infinity of internal gravity (IG) waves modified by the adjoining sheared region [Turner [1973]]. The waves that travel faster than the fluid in the plug region correspond to the co-grade Kelvin modes while those that travel slower correspond to the retrograde Kelvin modes some or all of which have critical levels in the shear zone depending on U_0 and the height of the shear flow region. The additional baroclinic source implies that the vorticity associated with the sheared IG waves is spread throughout the plug flow region and not localized in an interfacial vortex sheet as in the absence of stratification. This is similar to the 3D Kelvin modes which, unlike the 2D Kelvin mode, have interior vorticity in addition to the (axial) vortex sheet at the edge of the core (the term proportional to $\mathcal{H}(a-r)$) in (2.41)-(2.43)). A generic wave speed within the range of velocities spanned by the shear zone, but not equalling those of the retrograde IG waves, corresponds to the 3D CS-spectrum and one obtains the analogs of the Λ_1 and Λ_2 families depending on the conditions imposed at the critical level; the tangential velocity eigenfunction associated with the Λ_1 CS-mode analog and the normal velocity eigenfunction associated with the Λ_2-analog undergo jumps across the critical level.

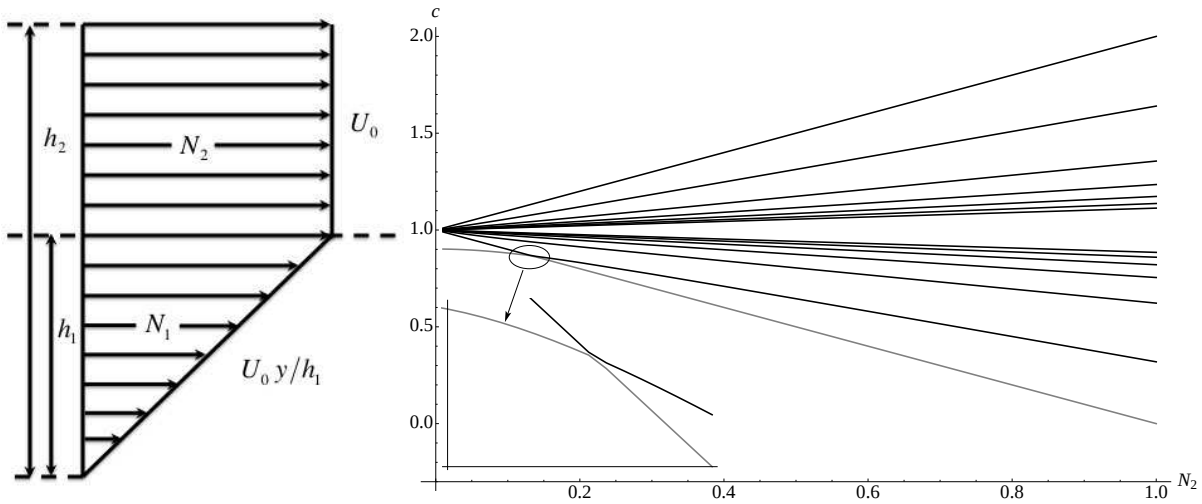

(a) (b)

Figure 2.6: (a)A piece-wise stratified shear flow that serves as an analog of the Rankine vortex, (b)Dispersion curves for the stratified analog of the Rankine vortex. ($k_x = 1, h_1 = 5, h_2 = 7, U_0 = 1, y_c = 4, N_1 = 0$)

The underlying rationale for the above 3D analogy is that the variation of the Richardson number, $Ri = N(y)^2/(\frac{dU}{dy})^2$, with y for varying $\bar{N}$, $\bar{N}$ being a scale for the Brunt-Väisälä frequency profile characterizing the stratified flow configuration, must mimic the variation in the vortex Richardson number, $Ri_v = \frac{2k^2 Z(r_f)\Omega(r_f)}{[m\Omega'(r_f)]^2}$, with r (see (2.127)) for varying k. For the Rankine vortex, $Ri_v = \infty\,(0)$ for $r < a\,(> a)$, and the absence of a shear in the plug flow region implies that the choice $(N_1, N_2) = (0, N_2)$ above achieves the same $Ri-$profile for the stratified flow model: $Ri = \infty\,(0)$ for $y > h_1\,(< h_1)$; see figure 2.6. The unstratified limit, $Ri = 0\,\forall\, r$, corresponds to 2D perturbations. Finally, the streamwise wavenumber (k_x) in the stratified flow model is the continuous analog of the azimuthal wavenumber (m) of the vortex, and determines the range of wave speeds corresponding to the CS-spectrum.

A straightforward calculation for the flow configuration in figure 2.6(a) shows that, with $N_1 = N_2 = 0$, the edge-wave satisfies the following dispersion relation:

$$\mathscr{D}(c_d) = \coth(k_x(h_2 - h_1)) + \coth k_x h_1 - \frac{1}{(h_1 - y_d)k_x} = 0, \tag{2.183}$$

where k_x is the stream-wise wavenumber, c_d the speed of the edge-wave and $y_d = \dfrac{h_1 c_d}{U_0}$ the critical level. The corresponding axial vorticity eigenfunction is proportional to $\delta(y - h_1)$, and is the analog of (2.19). The generic CS-mode axial vorticity eigenfunctions, in the absence of stratification, are given by

$$ik_x\hat{w}_z = [D\hat{u}_y]_{y=y_c^-}^{y=y_c^+}\delta(y - y_c) + [D\hat{u}_y]_{y=h_1^-}^{y=h_1^+}\delta(y - h_1) \tag{2.184}$$

where y_c is the critical level, and

$$[D\hat{u}_y]_{y=y_c^-}^{y=y_c^+} = \frac{k_x \sinh k_x h_1 \sinh(k_x(h_2-h_1))}{\sinh k_x y_c}\mathscr{D}(c), \tag{2.185}$$

$$[D\hat{u}_y]_{y=h_1^-}^{y=h_1^+} = k_x\left[\cosh(k_x(h_1-h_2)) - \sinh(k_x(h_1-h_2))\left\{\coth k_x h_1 - \mathscr{D}(c)\right\}\right]. \tag{2.186}$$

Equation (2.184) is to be compared with (2.18). The amplitude of the vortex sheet at $y = y_c$, expectedly, vanishes when $c = c_d$ since $\mathscr{D}(c_d) = 0$ and (2.184) is then proportional to the edge-wave vorticity eigenfunction.

With $N_2 \neq 0$, the dispersion relation for the sheared IG waves, the analog of (2.40), is given by

$$\mathscr{D}(c_d, N_2) = \frac{p}{k_x}\cot(p(h_2-h_1)) + \coth k_x h_1 - \frac{1}{(h_1-y_d)k_x} = 0, \tag{2.187}$$

where $p = \sqrt{\dfrac{N_2^2}{(c-U_0)^2} - k_x^2}$ is the vertical 'wavenumber'. The dispersion curves arising from (2.187) are plotted as a function of N_2 in figure 2.6(b), and bear an obvious resemblance to the Kelvin-mode dispersion curves in figure 2.1; note that $c - U_0 \propto N_2$ for $N_2 \to 0$, so p^{-1} remains finite in this limit, and similar to the Rankine vortex, there is no center-mode behavior. A difference, a detail as far as the center-mode-argument goes, is that the dispersion curves in figure 2.6(b) asymptote to $\omega = \pm\infty$ for $N_2 \to \infty$, while it is well known that the Doppler frequency in the vortex case must lie in the interval $[-2\Omega_0, 2\Omega_0]$ for any k. For a generic wave speed $(c \neq c_d)$, with y_c again being the critical level, one obtains the analog of the Rankine 3D CS-spectrum. The analogs of the Λ_1 CS-modes, with a tangential velocity discontinuity, are given by

$$ik_x\hat{w}_z = [D\hat{u}_y]_{y=y_c^-}^{y=y_c^+}\delta(y-y_c) + [D\hat{u}_y]_{y=h_1^-}^{y=h_1^+}\delta(y-h_1) - (p^2+k_x^2)\sin(p(y-h_2))\mathcal{H}(y-h_2), \tag{2.188}$$

where

$$[D\hat{u}_y]_{y=y_c^-}^{y=y_c^+} = \frac{k_x \sinh k_x h_1 \sin(p(h_2-h_1))}{\sinh k_x y_c}\mathscr{D}(c, N_2,$$

$$[D\hat{u}_y]_{y=h_1^-}^{y=h_1^+} = \left[p\cos(p(h_1-h_2)) - k_x\sin(p(h_1-h_2))\left\{\coth k_x h_1 - \mathscr{D}(c,N_2)\right\}\right],$$

while the Λ_2-analogs, with a normal velocity discontinuity, are given by

$$ik_x\hat{w}_z = [u_y]_{y=y_c^-}^{y=y_c^+}\delta'(y-y_c) + [Du_y]_{y=h_1^-}^{y=h_1^+}\delta(y-h_1) - (p^2+k_x^2)\sin(p(y-h_2))\mathcal{H}(y-h_2), \tag{2.189}$$

where

$$[\hat{u}_y]_{y=y_c^-}^{y=y_c^+} = \frac{\sinh k_x h_1 \sin(p(h_1-h_2))}{\cosh k_x y_c}\mathscr{D}(c, N_2),$$

with $[D\hat{u}_y]_{y=h_1^-}^{y=h_1^+}$ being the same as above. The amplitudes of the critical level singularities for both the Λ_1 and Λ_2 analogs are proportional to $\mathcal{D}(c, N_2)$, and one obtains the regular IG waves

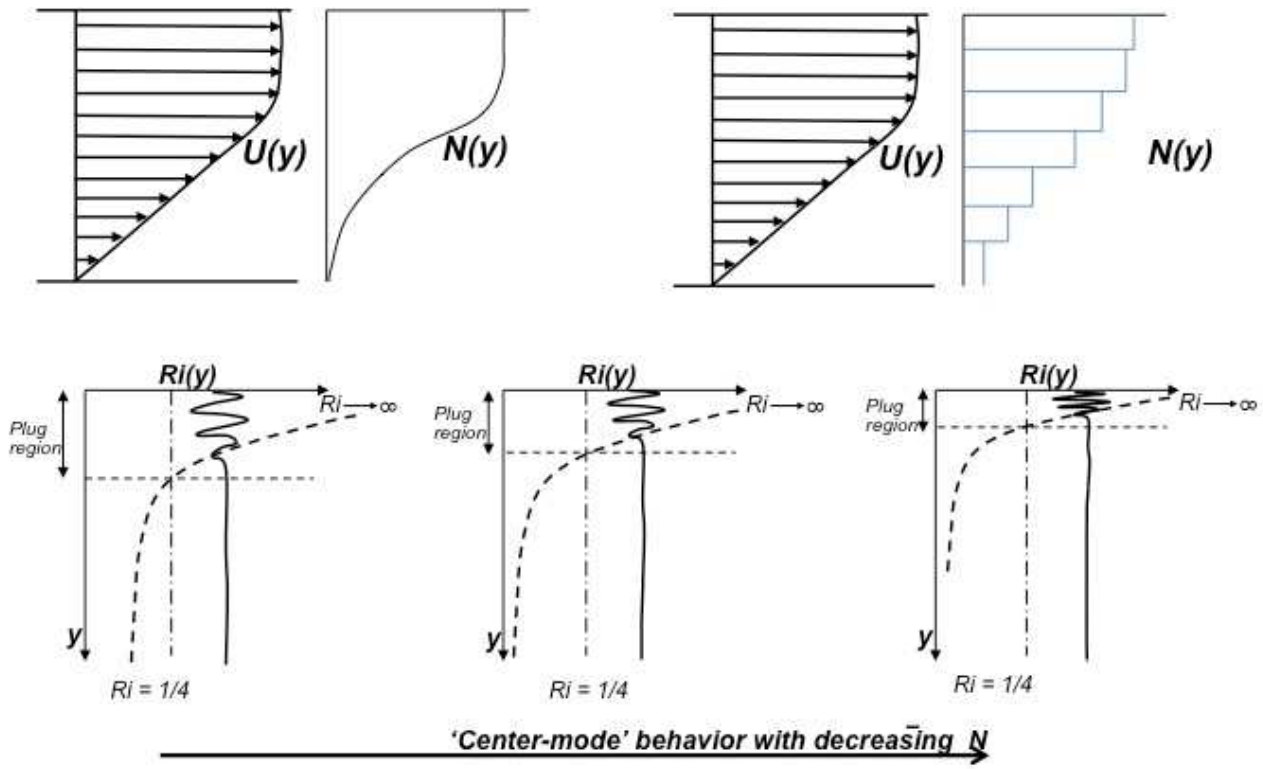

Figure 2.7: A smooth vortex analog

for $c = c_d$ when $\mathcal{D}(c_d, N_2) = 0$. As mentioned earlier, the $Ri - y$ profile of the stratified flow model, as a function of $\bar{N}$, must correspond to the $Ri_v - r$ profile of the vortex as a function of k; the wavenumbers k_x and m remaining fixed in the respective cases. For the Rankine vortex (its stratified flow analog), the associated Ri_v (Ri)-profile is invariant to k ($\bar{N}$) with the core (plug) always corresponding to $Ri = \infty$ and the shear flow region (irrotational exterior) corresponding to $Ri = 0$. On the other hand, for a smooth vortex, $Ri_v = \infty$ only on the rotation axis ($r = 0$), and for any other r, Ri_v is finite, and will decrease with decreasing k. The finiteness of Ri_v for any non-zero r implies that the stratified flow analog of a smooth vortex must also have the shear regions being stably stratified as in figure 2.7. Now, it is known from the analytically soluble case of stratified Couette flow, with a constant Brunt-Väisälä frequency, and in a bounded domain (Taylor [1931],Eliassen *et al.* [1953]), that there exists a regular IG-wave spectrum only for $Ri > \frac{1}{4}$ (only shearing flows where the velocity extrema are approached with a vanishing gradient, as for instance in a shear layer, can sustain a finite number of IG waves even as $Ri \to 0$; see Banks *et al.* [1976], Drazin *et al.* [1979]. We neglect these exceptional modes). Thus, for the stratified flow configuration in figure 2.7, the 'plug' region that sustains vorticity oscillations may be identified as the region where $Ri > \frac{1}{4}$; even within this plug, the constraint of a normal mode, that is, an invariant transverse structure propagating with a fixed speed implies, that the length scale of the oscillation must decrease continuously with increasing $Ri(y)$. With decreasing $\bar{N}$, the plug region becomes progressively thinner in extent. The central 'core' of a smooth vortex, capable of sustaining vorticity oscillations resembling the IG waves, may, in a similar manner, be identified with $Ri_v > Ri_v^*$; although, Ri_v^* will not be $\frac{1}{4}$ since, as already indicated, the analogy is not a precise mathematical one. As shown in figure 2.7, this core region must recede towards

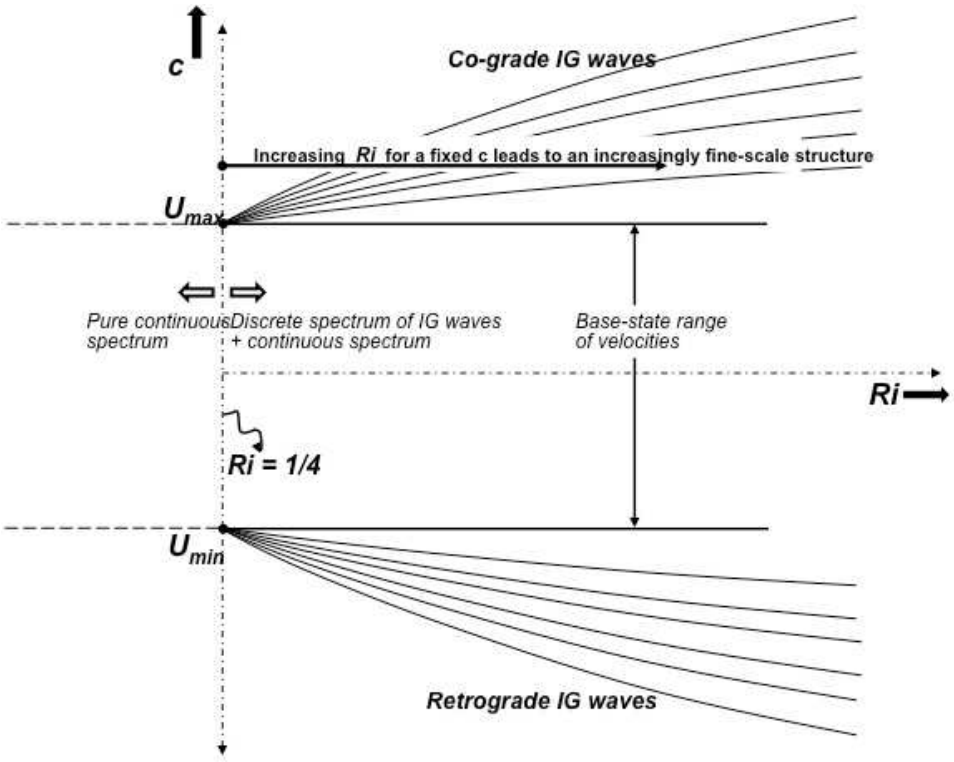

Figure 2.8: Schematic of dispersion curves for the stratified shear flow problem shown in figure 2.7

the axis with decreasing k. There must then be a corresponding reduction in the radial length scale of the oscillations along a given dispersion curve, and therefore, a transition to center-mode behavior for $k \to 0$. From the known (local) dispersion relation for inertial waves in rotational flows [Greenspan [1968]], the resulting fine-scaled radial structure also implies that the group velocity must vanish for any smooth vorticity profile for $k \to 0$ (figure 2.8). The boundary-layer scaling obtained above is physically equivalent to keeping Ri_v fixed even for $k \to 0$, and thereby precludes the structureless branch along which $\lim_{k\to 0} Ri_v \to 0$. For smooth profiles approaching the Rankine vortex, the rate of recession of the oscillatory core region towards the rotation axis becomes increasingly insensitive to a decrease in k, until in the Rankine limit, the size of the core region (which now corresponds to $Ri_v = \infty$) becomes independent of k. From the point of view of solvability, one may imagine replacing the actual stratified flow analog by a layered approximation of the same. Such an approximation would seem to suffer from the familiar disadvantage of every such kink leading to a eigenmode only one of which would correspond to the structureless branch of the original smooth vorticity profile [Shrira & Sazonov [2001];Shrira & Sazonov [2003]]. However, the center-modes arise due to the imposed stratification rather than the jumps in vorticity in the piecewise linear approximation, and the eigenmodes associated with the kinks in the base-state may easily be excluded because, in having non-trivial 2D limits, they correspond to the dispersion curves that lack a center-mode behavior. From the known solution for Couette flow with a uniform stratification, one expects that the eigenfunctions for the simplified model would now involve Bessel functions The principal-finite-part interpretation required for the CS-modes should also be clear from the discussion in section 2.3.3, and we

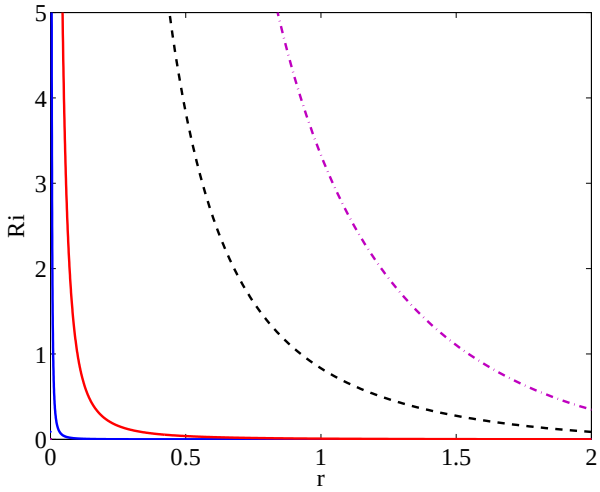

(a) Lamb Oseen vortex, $Z = e^{-r^2}$

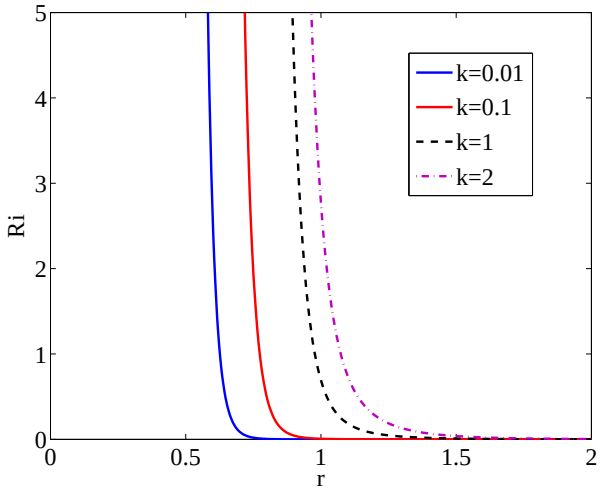

(b) $Z = \dfrac{1}{1+r^{2p}}, p = 6$

Figure 2.9: Spatial variation of vortex 'Ri' for various k for relatively flat vortex (Lamb Oseen) and an intense vortex

therefore avoid a detailed solution.

2.5 Conclusions

In this chapter we have obtained the complete inviscid spectrum for a Rankine vortex (sections 2.2.1 and 2.2.2). The well-known Kelvin modes do not form a complete set by themselves. The inclusion of the singular eigenfunctions completes the spectrum, and these eigenfunctions allow one to represent the evolution of exterior vortical disturbances. A modal superposition, involving both the discrete and the continuous spectra, is arrived at for describing evolution of an arbitrary initial vorticity field (equations (2.21) and (2.79)). The completeness of the modal approach, and thereby its equivalence to the solution of the initial value problem, is shown later in chapter 3 where we also examine the inviscid resonances arising due to initial conditions localized at the critical radii of the discrete modes. The analysis for the Rankine vortex is also extended to the continuous spectrum modes of smooth vorticity profiles (sections 2.3.1 and 2.3.3). While in 2D, one may again obtain the required modal representation by solving a Riemann-Hilbert problem, even in the absence of closed-form expressions for the eigenfunctions, in 3D the analysis is approximate, being based on approximate forms of the eigenfunctions close to the critical radius. An analogy with the known solution for stratified shear flows is used to clarify the nature of the modal representation. The analogy with stratified shear flows also allows for a physical interpretation of the inviscid center-modes (section 2.4).

In what follows, we obtain spectral representations of the Green's function for the fluid dynamical problems considered here. Such representations, when used in the solution of the initial value problem, immediately yield the required modal decompositions, and are therefore an equivalent way of characterizing the spectrum of the linear operator. To the extent that the Green's function denotes the response to a general impulsive forcing, the expressions below should be of use beyond the context of hydrodynamic stability. An example in this regard is the dynamics of an active suspension of tumbling bacteria where the probability density of bacterial orientations behaves in a manner analogous to the vorticity field in a non-linear shear flow, and the eigenfunctions in orientation space (the unit sphere) again consist of a delta function and a non-local PV-integral term (Subramaniam & Nott [2011]); another example arises in the kinetic theory of gases where Ferziger [1965] has shown that similar eigenfunctions make up the CS-spectrum of the linearized spatially homogeneous Boltzmann operator. The spectral representation for a self-adjoint operator ($\mathcal{L}(y)$) is well-known (Friedman [1990]). When $\mathcal{L}(y)$ is compact, the Green's function for $(\mathcal{L}(y)-\lambda)$ may be written as $\mathrm{G}(y,y';\lambda)=\sum_{n=0}^{\infty}\dfrac{\chi_n(y)\chi_n(y')}{(\lambda_n-\lambda)}$ with $[\lambda_n,\chi_n(y)]$ characterizing the discrete spectrum; for an unbounded domain, the summation above is replaced by an integral, so $\mathrm{G}(y,y';\lambda)=\displaystyle\int_0^{\infty}\dfrac{\chi(y;\lambda')\chi(y';\lambda')}{(\lambda'-\lambda)}d\lambda'$ (the eigenfunctions now satisfy the less restrictive conditions of boundedness at infinity.). The Green's functions obtained below also involve an integral over the (finite) interval corresponding to the CS-spectrum, but the eigenfunctions are now singular, needing a Cauchy-principal-value or a principal-finite-part interpretation. Given this interpretation, the derivation proceeds along lines similar to the textbook examples, with appropriately modified eigenfunction expansions and orthgonality

relations, and we only present the final expressions below for three canonical cases with different CS-spectra; discrete modes are not accounted for in these expressions since the additional summation term, that must appear in the spectral representation, is of a standard form.

The simplest problem is homogeneous Couette flow. With $U(y) \propto y$, 2D vorticity perturbations obey:

$$(y - y_c)\hat{w}_z(y; y_c) = 0, \tag{2.190}$$

where y_c, as before, denotes the critical level and plays the role of the eigenvalue. The multiplication operator, $\mathcal{L}(y; y_c) = (y - y_c)$, in (2.190) is trivially self-adjoint, the direct and adjoint eigenfunctions being given by:

$$\hat{w}_z(y; y_c) = \hat{w}_z^\dagger(y; y_c) = \delta(y - y_c) \tag{2.191}$$

The self-adjoint nature of the perturbation vorticity equation for Couette flow implies that enstrophy is a conserved quantity for 2D infinitesimal disturbances. Note, however, that the Rayleigh equation isn't self-adjoint, and is responsible for the non-modal behaviour of the perturbation energy even in Couette flow (Schmid & Henningson [2001]). The Green's function, for two-dimensional vortical perturbations in Couette flow, defined by

$$(y - \lambda)\tilde{\mathrm{G}}(y, y'; \lambda) = \delta(y - y'), \tag{2.192}$$

may be written as:

$$\tilde{\mathrm{G}}(y, y'; \lambda) = \int_{-1}^{1} \frac{\delta(y - y_c)\delta(y' - y_c)}{(y_c - \lambda)} dy_c. \tag{2.193}$$

The tilde over G denotes the frequency domain.

The self-adjointness in the vorticity formulation is lost for a mean flow with nonlinear shear. The governing equation for vorticity perturbations may now be written as:

$$[(U(y) - U(y_c)) - U''(y)\nabla^{-2}]\hat{w}_z(y; y_c) = 0. \tag{2.194}$$

with the adjoint operator being given by $\mathcal{L}(y; y_c)^\dagger = (U(y) - U(y_c)) - \nabla^{-2}U''(y)$. Here, ∇^{-2} denotes the inverse Laplacian that relates the perturbation streamfunction to $\hat{w}_z(y; y_c)$, being defined by $\nabla^{-2}f(y) \equiv \int_{-1}^{1} \mathcal{G}(y; y')f(y')dy'$, where $\mathcal{G}(y; y') = -\dfrac{\sinh k(1 - y_>)\sinh k(1 + y_<)}{k \sinh 2k}$ for the bounded domain considered here, and $y_<(y_>)$ denotes the smaller (larger) of y and y'. The direct and adjoint eigenfunctions are no longer the same, and are given by:

$$\hat{w}_z(y; y_c) = U''(y)\hat{w}_z^\dagger(y; y_c) = \epsilon_{\mathrm{R}}(y_c)\delta(y - y_c) + \mathcal{P}\frac{U''(y)\hat{\psi}(y; y_c)}{U(y) - U(y_c)}, \tag{2.195}$$

where

$$\epsilon_{\mathrm{R}}(y) = 1 - \mathcal{P}\int_{-1}^{1} \frac{U''(y)\hat{\psi}(y';y)}{U(y')-U(y)}dy', \tag{2.196}$$

$$\hat{\psi}(y;y_c) = -\mathcal{G}(y;y_c) + \int_{-1}^{1} U''(y')\hat{\psi}(y';y_c)\frac{\mathcal{G}(y;y')-\mathcal{G}(y;y_c)}{U(y')-U(y_c)}dz'. \tag{2.197}$$

with the normalization $\int_{-1}^{1} \hat{w}_z(y;y_c)dy = 1$. The orthogonality relation between the direct and adjoint eigenfunctions is

$$\int_{-1}^{1} \hat{w}_z(y;y_c)\hat{w}_z^{\dagger}(y;y_c)dy = C(y_c)\delta(y-y_c) \tag{2.198}$$

where

$$C(y) = \frac{\epsilon_{\mathrm{R}}^2(y)+\epsilon_{\mathrm{L}}^2(y)}{U''(y)}, \tag{2.199}$$

$$\epsilon_{\mathrm{L}}(y) = -\pi\hat{\psi}(y;y)\frac{U''(y)}{U'(y)}.$$

The above relation uses the Poincare-Bertrand transposition formula (Gakhov [1990]).
The vorticity eigenfunctions are now orthogonal to each other under an inner product weighted by the inverse of the curvature, and perturbation enstrophy is no longer a conserved quantity. This orthogonality leads to a standard result in wave-mean flow interaction theory - the conservation of pseudomomentum of two-dimensional disturbances for parallel shear flows (Held [1985]). The Green's function for 2D vortical perturbations in a non-linear parallel shearing flow is defined by

$$[(U(y)-\lambda) - U''(y)\nabla^{-2}]\tilde{\mathrm{G}}(y,y';\lambda) = \delta(y-y'), \tag{2.200}$$

the solution for which may be written as:

$$\tilde{\mathrm{G}}(y,y';\lambda) = \int_{-1}^{1} \frac{\left\{\epsilon_{\mathrm{R}}(y_c)\delta(y-y_c) + \mathcal{P}\frac{U''(y)\hat{\psi}(y;y_c)}{U(y)-U(y_c)}\right\}\left\{\epsilon_{\mathrm{R}}(y_c)\delta(y'-y_c) + \mathcal{P}\frac{U''(y')\hat{\psi}(y';y_c)}{U(y')-U(y_c)}\right\}}{U''(y')C(y_c)(U(y_c)-\lambda)}dy_c, \tag{2.201}$$

Finally, we consider a stratified shear flow under the Bousinessq approximation. As is evident from the Taylor-Goldstein equation in section 2.3.3, the governing equation is in this case a nonlinear eigenvalue problem if expressed in terms of a single variable - either the normal velocity or the density field. The standard method leading to the spectral reprsentations above works only for a linear eigenvalue problem, and the Taylor-Goldstein equation is therefore transformed to a two-dimensional linear eigenvalue problem in terms of a vector flow variable consisting of both the vorticity ($\hat{w}_z$) and the density ($\hat{\rho}$) fields. Further, one must now have a matrix Green's function since an impulsive forcing in the density field can induce a velocity field and vice versa. Towards this end, (2.155) and (2.156) are now written as the following matrix eigenvalue

problem:

$$\mathbf{L}(y)\mathbf{\Phi}(y;y_c) = y_c\mathbf{\Phi}(y;y_c), \tag{2.202}$$

where

$$\mathbf{L}(y) = \begin{bmatrix} y & 1/\mathrm{Fr}^2 \\ N^2/N_0^2\nabla^{-2} & y \end{bmatrix}, \tag{2.203}$$

and $\mathbf{\Phi}(y;y_c)$ is an eigenfunction matrix whose individual columns denote $[\hat{w}_z(y;y_c)\ \hat{\rho}(y;y_c)]^{\mathrm{T}}$, and correspond to vector eigenfunctions of the Λ_1 and Λ_2 families. The dimensionless parameters in (2.202) and (2.203) have been defined earlier in section 2.3.4. The matrix Green's function, $\tilde{\mathbf{G}}(y,y';\lambda)$, satisfies:

$$[\mathbf{L}(y) - \lambda\mathbf{I}]\tilde{\mathbf{G}}(y,y';\lambda) = \delta(y-y')\mathbf{I}. \tag{2.204}$$

We first consider the simpler case of a homogeneous base state with $N = 0$. In this case, the governing stability operator reduces to

$$\mathbf{L}(y) = \begin{bmatrix} y & 1/\mathrm{Fr}^2 \\ 0 & y \end{bmatrix}, \tag{2.205}$$

The corresponding adjoint operator is $\mathbf{L}(y)^\dagger = \mathbf{L}(y)^{\mathrm{T}}$, and thus, the direct ($\mathbf{\Phi}(y;y_c)$) and adjoint ($\mathbf{\Psi}(y;y_c)$) eigenmatrices are:

$$\mathbf{\Phi}(y;y_c) = \mathbf{\Psi}^{\mathrm{T}}(y;y_c) = \begin{bmatrix} \delta(y-y_c) & 1/\mathrm{Fr}^2\delta'(y-y_c) \\ 0 & \delta(y-y_c) \end{bmatrix}, \tag{2.206}$$

with the Green's function, $\tilde{\mathbf{G}}(y,y';y_c)$ being

$$\tilde{\mathbf{G}}(y,y';\lambda) = \int_{-1}^{1} \frac{\mathbf{\Phi}(y;y_c)\mathbf{\Psi}^T(y';y_c)}{(y_c-\lambda)}dy_c. \tag{2.207}$$

Stratification with a constant N introduces the additional self-adjoint term, $N^2/N_0^2\nabla^{-2}$, so that the relation $\mathbf{L}(y)^\dagger = \mathbf{L}(y)^{\mathrm{T}}$ continues to hold but with $\mathbf{L}(y)$ now given by (2.203). Thus, even for heterogeneous Couette flow the Green's function is given by (2.207). However, the direct and adjoint eigenfunction matrices are no longer transposes of each other. The former is given by

$$\mathbf{\Phi}(y;y_c) = \begin{bmatrix} \hat{w}_z^{\Lambda_1}(y;y_c) & \hat{w}_z^{\Lambda_2}(y;y_c) \\ \hat{\rho}^{\Lambda_1}(y;y_c) & \hat{\rho}^{\Lambda_2}(y;y_c) \end{bmatrix} \tag{2.208}$$

with $\mathbf{\Psi}(y,y_c)$ defined by orthogonality relations where the integrals involved require a Pf. interpretation. Invoking the relations $\hat{w}_z(y;y_c) = \dfrac{\mathrm{Ri}}{(y-y_c)^2}\hat{\psi}(y;y_c)$ and $\hat{\rho}(y;y_c) = \dfrac{N^2}{N_0^2(y-y_c)}\hat{\psi}(y;y_c)$, it is sufficient to know the expressions for the streamfunction for the Λ_1 and Λ_2 families, and the latter are given by (2.167)-(2.169).

The spectral representations correspond to the form of the operator in the frequency domain.

On noting that the initial value of the Green's function in the time domain, $\mathrm{G}(y, y', t = 0)$, given by $\lim_{\lambda\to\infty}[\lambda\tilde{\mathrm{G}}(y, y'; \lambda)]$, is either a scalar delta function or a delta function times an identity matrix for stratified shear flow, (2.193), leads to an identity, while (2.201) and (2.207) (for finite N) lead to interesting non-trivial representations for the delta function in terms of PV-singular and Pf-singular eigenfunctions.

Chapter 3

Initial value problem and the inviscid resonances

3.1 Introduction

The initial value problem (IVP) for a Rankine vortex, with an emphasis on exterior vortical disturbances, and its equivalence to the modal representation discussed in chapter 2, will be addressed in the present chapter. Before jumping to the formulation, it is worth noting the relation between the modal and non-modal (IVP) perspectives within the framework of linear hydrodynamic stability. The non-modal perspective typically focuses on the transient dynamics characterized by an algebraic growth in the various dynamical quantities for short times. This behavior, referred to as transient growth in the literature, is typical for shearing flows where the governing differential operators are non-normal (in the relevant norm - energy, enstrophy, etc.), and estimates based on the operator eigenvalues only apply in the limit of long times. This implies that, even for 'stable' flows, there can be significant algebraic growth before eventual decay (Schmid & Henningson [2001], Trefethen *et al.* [1993]). Herein, it is important to note that the physics underlying transient growth, regardless of the particular mechanism (Orr, lift-up, etc.) is entirely inviscid; this is in contrast to the well-known viscous instability for non-inflectional profiles in the classical literature. In fact, despite the 'non-modal' terminology used, studies on parallel shearing flows show that the transient growth phenomenon is intimately related to the dynamics of the underlying inviscid continuous spectra. For the simplest case, inviscid Couette flow, the original IVP analyses were in terms of Fourier modes with time-dependent wave vectors (also known as Kelvin modes, see Farrell [1984]). The work of Farrell and co-workers (Farrell [1984],Farrell [1989],Farrell & Ioannou [1993b]) has analyzed one of the mechanisms leading to transient growth, the Orr-mechanism (Orr [1907]), in terms of the aforementioned Fourier mode. But, an equivalent description exists in terms of a convected superposition of flow-aligned vortex sheets (the CS-modes of Couette flow): the Orr mechanism involves the progressive phase-alignment of an initially staggered superposition of singular vortex-sheet eigenfunctions. The celebrated lift-up mechanism (Arnol'd [1972], Landahl [1980]) which is absent in two dimensions, and is responsible for the growth of spanwise perturbations, may also be interpreted in terms of CS-mode dynamics. As shown in chapter (6) for a general paralel flow, the lift-up effect arises in the limit of an infinitely gradual de-phasing of a vortex-sheet eigenfunction and the corresponding ensemble of singular Squire-jet modes (Sazonov [1996]).

In general, for problems where only the continuous spectrum governs the temporal evolution, the dynamics may be divided into three regimes: an initial phase characterized by the aforementioned algebraic growth, a terminal phase with an algebraic-decay in integral measures such as the perturbation kinetic energy due to the eventual de-phasing of the CS-modes by

differential shear (Bassom & Gilbert [1998], Farrell [1984]), and an intermediate phase with exponential asymptotics. In this latter regime, appropriate superpositions of the CS-modes behave as decaying discrete (quasi)-modes, a phenomenon known as Landau damping (Briggs *et al.* [1970],Schecter *et al.* [2000],Schecter & Montgomery [2003]). Both Couette flow and the Rankine vortex constitute important and singular limiting scenarios in that although neither exhibits the aforementioned exponential asymptotics, the addition of a small curvature or a small vorticity-gradient/vorticity does lead to quasi-modes (Balmforth *et al.* [2001],Shrira & Sazonov [2001],Shrira & Sazonov [2003]). For instance the solution of the two-dimensional IVP shows that a 'near-Rankine' profile exhibits an exponential decay phase with the damping rate being proportional to the (small) vorticity gradient at the critical radius (Schecter *et al.* [2000],Le Dizès [2000]). The analogous scenario for three dimensions is not known, however; numerical results, for the particular case of a Lamb-Oseen profile, indicate a denumerable infinity of quasi-modes (Fabre [2002]). It is worth noting that for the above singular cases (Rankine vortex in Couette flow), the existence of a neutral discrete ('free') mode implies that the terminal algebraic decay only applies to the CS-spectrum, and the response for long times always approaches the discrete mode(s) (also see Smith & Montgomery [1995]).

Motivated by the presence of vortex-waves in numerical simulation of gravity wave breaking Arendt *et al.* [1997] performed an analysis of the initial-value problem for core perturbations for a Rankine vortex. The authors showed that any core perturbation can be represented as a summation of Kelvin modes and hence, proved their completeness for vortical perturbations inside and at the edge of the core. Physically, the restriction to such core perturbations implies the consideration of suitably deformed vortex columns as initial conditions.The effect of the external straining field on vortical disturbances was neglected as core dynamics was the primary concern. Later, Criminale *et al.* [2001] considered the initial-value problem for a mean flow given by a strained point vortex, but the analysis evidently excluded any vortex oscillations arising due to a finite core. They demonstrated that an initial radial vorticity configuration will lead to a linear growth in azimuthal vorticity due to stretching and tilting by the ambient shear. In this chapter, we will solve the IVP for a Rankine vortex for an arbitrary initial (vortical) condition, thereby combining the above efforts. More recently a detailed study of transient growth in a columnar vortex subjected to three-dimensional disturbances was done independently by Antkowiak & Brancher [2004] and Pradeep & Hussain [2006]. The two-dimensional disturbances exhibited the usual algebraic growth arising from the Orr mechanism mentioned above. Further, the tilting and stretching of radial vorticity in three dimensions, to form azimuthal vorticity by the background shear (also seen in Criminale *et al.* [2001]) above led to a stronger growth which was eventually arrested by vorticity waves arising doe to the non-zero base-state vorticity. Antkowiak & Brancher [2007] termed this latter mechanism the *anti-lift-up effect*, since azimuthal streaks (radial vorticity) give birth to azimuthal rolls (azimuthal vorticity) in contrast to the well-known *lift-up effect* present in rectilinear flows where rectilinear rolls give way to streaks (Landahl [1980], Schmid & Henningson [2001]). The authors identified vortex rings wrapped around the vortex column as an optimal perturbation for transient growth thus revisiting DNS results of Melander & Hussain [1993] which highlighted an arrangement of alternate signed vortex rings wrapped around a vortex column as a prevalent secondary struc-

ture arising in a vortex column's interaction with a fine-scale homogeneous, isotropic turbulent field. A novel mechanism which was highlighted in the study of Pradeep & Hussain [2006] is the stronger transient growth arising for initial conditions localized at the critical radii of one or more of Kelvin modes. This resonance-aided stronger algebraic growth was identified in the context of a full viscous (linearized) DNS. In this chapter we will explain, by way of the inviscid Rankine initial value problem calculations, as to how these resonances and the manner in which they couple with the *anti lift-up effect* mentioned above. Miyazaki & Hunt [2000], in an effort to understand the (linearized) interaction of a columnar vortex with external (weak) turbulence through the framework of rapid distortion theory (RDT) (Townsend [1956]) identified an initial random velocity field that, again, wraps around the vortex column and forms vortex ring like structures. This is consistent with the aforementioned stretch-tilt mechanism, that leads to azimuthal vorticity linearly from an initial field with radial vorticity. The vortex response as determined from the framework of an initial value problem, is identical to computing the linear response in the spirit of RDT. Recently, Heaton & Peake [2007] have investigated the transient growth for a vortex with axial flow, the Batchelor vortex, in a regime where the vortex exhibits no exponential instability.

In this chapter we will begin by addressing the 2D initial value problem for a Rankine vortex in section 3.2 and then discuss the evolution for localized initial conditions (narrow Gaussian profiles) located both at and way from the Kelvin critical radius. The modal decomposition found in the previous chapter is shown to be equivalent to IVP. An identical sequence is followed for the 3D problem in section 3.3.

3.2 2D Initial value problem

The inviscid evolution in 2D is governed by the following PDE for the radial velocity, $\tilde{u}_r$;

$$\left(\frac{\partial}{\partial t} + im\Omega\right)\left(r^2D^2\tilde{u}_r + 3rD\tilde{u}_r - (m^2-1)\tilde{u}_r\right) - imrDZ\tilde{u}_r = 0, \tag{3.1}$$

for a fixed m. Here, $\tilde{u}_r \equiv \tilde{u}_r(r,t)$.

To obtain a representation in terms of the initial conditions we Laplace transform the above equation. Using the following definitions:

$$\begin{aligned}\hat{f}(s) &= \int_0^\infty \tilde{f}(t)e^{-st}dt,\\ \tilde{f}(t) &= \frac{1}{2\pi i}\int_{\gamma-i\infty}^{\gamma+i\infty}\hat{f}(s)e^{st}ds,\end{aligned}$$

where a hat denotes the transformed quantities, one obtains:

$$D^2\hat{u}_r + \frac{3}{r}D\hat{u}_r - \frac{(m^2-1)}{r^2}\hat{u}_r + \frac{2im\Omega_0\delta(r-a)}{r(s+im\Omega)}\hat{u}_r = -\frac{im}{r}\frac{\tilde{w}_{z0}(r)}{s+im\Omega}. \tag{3.2}$$

where $\tilde{w}_{z0}(r) = \tilde{w}_z(r,0)$ is the initial perturbation vorticity (axial) and we have used that $DZ = -2\Omega_0\delta(r-a)$. From (3.2), we solve for $\hat{u_r}(r,s)$ both inside and outside the core:

$$\underline{r<a}$$
$$\hat{u}_r(r,s) = Ar^{m-1} + \frac{i}{2}\left\{r^{-(m+1)}\int_0^r r'^{m+1}\frac{\tilde{w}_{z0}(r')}{s+im\Omega(r')}dr' - r^{m-1}\int_0^r r'^{-(m-1)}\frac{\tilde{w}_{z0}(r')}{s+im\Omega(r')}dr'\right\}, \quad (3.3)$$
$$\underline{r>a}$$
$$\hat{u}_r(r,s) = Br^{-(m+1)} + \frac{i}{2}\left\{r^{m-1}\int_r^\infty r'^{-(m-1)}\frac{\tilde{w}_{z0}(r')}{s+im\Omega(r')}dr' - r^{-(m+1)}\int_r^\infty r'^{m+1}\frac{\tilde{w}_{z0}(r')}{s+im\Omega(r')}dr'\right\}. \quad (3.4)$$

As boundary conditions we have the continuity of radial velocity perturbation, $\hat{u}_r$, across the vortex core and, from (3.2), the following jump in $D\hat{u}_r$:

$$[D\hat{u}_r]_{r=a^-}^{r=a^+} \equiv D\hat{u}_r(r=a^+) - D\hat{u}_r(r=a^-) = -\frac{2im\Omega_0\hat{u}_r(r=a)}{a(s+im\Omega_0)}. \quad (3.5)$$

Enforcing the above conditions we have:

$$A = \frac{i}{2a^{m-1}}\left[\int_0^\infty\left(\frac{a}{r'}\right)^{m-1}\frac{\tilde{w}_{z0}(r')}{s+im\Omega(r')}dr' + \frac{i\Omega_0}{(s+i\omega_d)}\left\{\int_0^a\left(\frac{r'}{a}\right)^{m+1}\frac{\tilde{w}_{z0}(r')}{s+im\Omega(r')}dr' + \int_a^\infty\left(\frac{a}{r'}\right)^{m-1}\frac{\tilde{w}_{z0}(r')}{s+im\Omega(r')}dr'\right\}\right], \quad (3.6)$$

$$B = \frac{ia^{m+1}}{2}\left[\int_a^\infty\left(\frac{r'}{a}\right)^{m+1}\frac{\tilde{w}_{z0}(r')}{s+im\Omega(r')}dr' + \frac{1}{(s+i\omega_d)}\left\{(s+im\Omega_0)\int_0^a\left(\frac{r'}{a}\right)^{m+1}\frac{\tilde{w}_{z0}(r')}{s+im\Omega(r')}dr' + i\Omega_0\int_a^\infty\left(\frac{a}{r'}\right)^{m-1}\frac{\tilde{w}_{z0}(r')}{s+im\Omega(r')}dr'\right\}\right], \quad (3.7)$$

where $\omega_d = (m-1)\Omega_0$. Thus, one observes how the 2D Kelvin mode (the pole at $s=-i\omega_d$) naturally arises in the solution of the initial-value problem. Using the Cauchy residue theorem, we obtain the following expression for the velocity field in the time domain:

$$\tilde{u}_r(r,t) = \frac{i}{2}\int_0^\infty\tilde{w}_{z0}(r')\left[\left(\frac{r'}{r}\right)^{p(r')m+1}e^{-im\Omega(r')t} - \Omega_0\left(\frac{a}{r}\right)^{p(a)m+1}\left(\frac{a}{r'}\right)^{q_1(r')m-1}\frac{e^{-im\Omega(r')t}-e^{-i\omega_d t}}{m\Omega(r')-\omega_d}\right]dr' \quad (3.8)$$

where $p(x) = \mathrm{sgn}(r-x)$ and $q_1(x) = \mathrm{sgn}(x-a)$. The above expression represent the evolution of the radial velocity perturbation when a Rankine vortex is subjected to an arbitrary initial axial vorticity field. As was previously mentioned, (3.8) is identical the response obtained by Smith & Montgomery [1995].

In this general form, one can clearly see contributions from both the discrete and continuous spectra. As must be the case, introducing an initial condition with a twin vortex-sheet structure in (3.8), a single continuous spectrum eigenmode is obtained.

3.2.1 Equivalence to modal superposition

Obtaining the equivalence of the IVP with the modal superposition obtained in chapter 2 is essential for proving the completeness of the latter. From equation (2.21) we have the following modal representation for the time-dependent axial vorticity field:

$$\tilde{w}_z(r,t) = w_z^{\text{core}} e^{-im\Omega_0 t} + \int_{a^+}^{\infty} B_1(r')\hat{w}_z^{\text{CSM}}(r;r')e^{-im\Omega(r')t}dr' + \int_0^{\infty} B_2(r')\hat{w}_z^{\text{Kelvin}}(r)e^{-im\omega_d t}dr', \quad (3.9)$$

where,

$$\hat{w}_z^{CSM}(r;r') = \left[\frac{2i\Omega_0 d}{\omega - m\Omega_0}\delta(r-a) - A(r')\delta(r-r')\right]. \quad (3.10)$$

$$\hat{w}_z^{\text{Kelvin}}(r) = -\frac{2i\Omega_0 a^2}{r_c}\delta(r-a), \quad (3.11)$$

$$\hat{w}_z^{core}(r) = \tilde{w}_{z0}(r)\mathcal{H}(a-r) - \delta(r-a)\int_0^a \tilde{w}_{z0}(r')\left(\frac{r'}{a}\right)^{m+1}dr', \quad (3.12)$$

$$A(r') = \frac{2\mathrm{i}\Omega_0\left(\frac{a^2}{r'}\right)(\omega_d-\omega)}{\Omega_0\left(\frac{a}{r'}\right)^{m-1} + (\omega_d-\omega)\left(\frac{r'}{a}\right)^{m+1}}. \quad (3.13)$$

and, r_c is the critical radius of a 2D Kelvin mode - $r_c = a\sqrt{m/(m-1)}$. The discrete and continuous spectrum eigenfunction amplitudes are given by,
$B_1(r') = -\dfrac{\tilde{w}_{z0}(r')}{A(r')}$, $B_2(r') = -\dfrac{i}{2}\dfrac{\tilde{w}_{z0}(r')r_c}{a^2(\omega_d - m\Omega)}\left(\dfrac{a}{r'}\right)^{q_1(r')m-1}$.
On substituting the expressions for B_1, B_2 and $A(r')$, (3.9) can be simplified to,

$$\tilde{w}_z(r,t) = \tilde{w}_{z0}(r)e^{-im\Omega(r)t} + \delta(r-a)\int_0^{\infty}\tilde{w}_{z0}(r')\left(\frac{a}{r'}\right)^{q_1(r')m-1}\Omega_0\frac{e^{-im\Omega(r')t} - e^{-i\omega_d t}}{(\omega_d - m\Omega(r'))}dr' \quad (3.14)$$

We know from combining $(\nabla \wedge \mathbf{u})_z = w_z$ and $\nabla.\mathbf{u} = 0$, that

$$\tilde{w}_z(r,t) = \frac{i}{m}\mathscr{L}\left(r\tilde{u}_r(r,t)\right) = \frac{i}{m}\left(rD^2 + 3D - \frac{(m^2-1)}{r}\right)\tilde{u}_r(r,t) \quad (3.15)$$

where $\mathscr{L} = DD^* - (m^2-1)/r^2$ is the Laplacian operator in cylindrical coordinates ($D^* = D + 1/r$). On inverting the above relation in terms of the Greens function of the Laplacian, we have,

$$\tilde{u}_r(r,t) = \frac{i}{2}\int_0^{\infty}\left(\frac{r'}{r}\right)^{p(r')m+1}\tilde{w}_z(r',t)dr' \quad (3.16)$$

Substituting the (3.14) for the axial vorticity field gives (3.8), thus proving the equivalence of the 2D modal superposition to the initial value problem.

3.2.2 Excitation by a cylindrical vortex sheet and 2D inviscid resonance

In two dimensions, (3.9) reveals two possible growth mechanisms - the Orr mechanism and the resonant excitation of the Kelvin mode. In section 3.1 we have already discussed the Orr mechanism for plane parallel flows. In the context of swirling flows, the physics remain identical. The Orr mechanism requires the initial condition to have a finite spatial extent and, further that it be azimuthally staggered in the (local) upstream direction. The equivalent of an upstream tilt here would an outward propagating spiral initial condition. Figure 3.1 depicts the evolution of such an initial condition via the Orr mechanism. Although the Orr mechanism is already contained in the general expression (3.9), here onwards we will only be focussing on transversely coherent (no tilt either upstream or downstream) initial condition in the context of resonant excitation of the Kelvin mode.

To begin with, we choose a cylindrical vortex sheet stationed at $r = r_1$, as an initial condition. Thus, $\tilde{w}_{z0} = V_0\delta(r - r_1),\ r_1 > a$. The velocity field in (3.8) then simplifies to,

$$\tilde{u}_r(r,t) = \frac{i}{2}V_0\left[\left(\frac{r_1}{r}\right)^{p(r_1)m+1} e^{-im\Omega_1 t} - \Omega_0\left(\frac{a}{r}\right)^{p(a)m+1}\left(\frac{a}{r_1}\right)^{m-1}\frac{e^{-im\Omega(r_1)t} - e^{-i\omega_d t}}{m\Omega(r_1) - \omega_d}\right] \tag{3.17}$$

where $\Omega_1 = \Omega(r_1) = \frac{\Omega_0 a^2}{r_1^2}$. The above expression highlights the existence of a secular limit when $m\Omega_1 \to \omega_d$, the corresponding value of r_1 being, of course, the critical radius of the 2D Kelvin mode. We can write the resonant solution as:

$$\tilde{u}_r(r,t) = \frac{i}{2}V_0 e^{-i\omega_d t}\left[\left(\frac{r_c}{r}\right)^{p(r_c)m+1} + i\,\Omega_0\,t\left(\frac{a}{r}\right)^{p(a)m+1}\left(\frac{a}{r_c}\right)^{m-1}\right], \tag{3.18}$$

where we have used that $\lim_{r_1\to r_c}\left(\frac{e^{-im\Omega(r_1)t} - e^{-i\omega_d t}}{m\Omega(r_1) - \omega_d}\right) = -ite^{-i\omega_d t}$.

Thus, the 2D IVP captures the resonant interaction between the discrete (the Kelvin mode) and the continuous spectra. The resonance arises because of the absence of a normal mode with a finite projection at $r = r_c$ which precludes a harmonic time dependence. A similar study of the interaction between the discrete and continuous spectra has been carried out for a piece-wise continuous plane shear flow profile by Sazonov [1989] and analogs of this behavior are known in the context of plasma physics (Hirota *et al.* [2003]). The normalised energy spectrum, as a function of m, due to the resonant vortex sheet initial condition is;

$$\frac{E(m,t_{\max})}{E(m,0)} = \Omega_0^2\left(\frac{m-1}{m}\right)^m t_{max}^2 \tag{3.19}$$

where,

$$E(m,t) = \frac{1}{2}\int_0^\infty \{u_r u_r^* + u_\theta u_\theta^*\}\, r dr \tag{3.20}$$

In (3.19) we have included only the secularly growing contribution. Increasing azimuthal wavenumber leads to an increas in the amplitude of the energy. For $m \to \infty$ it attains a

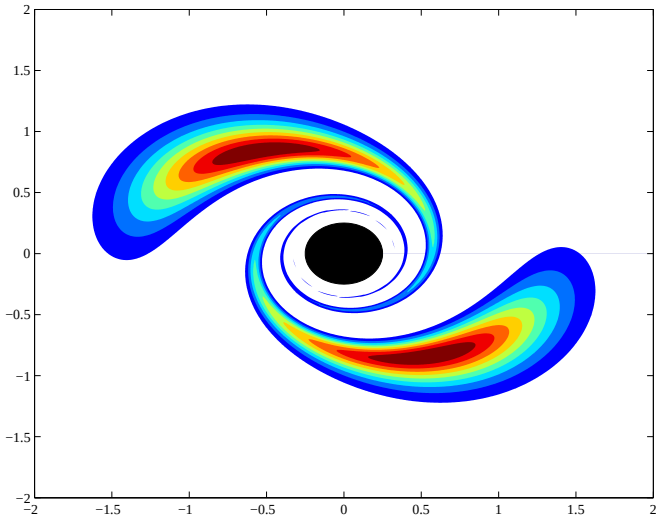

(a) $t = t_0$

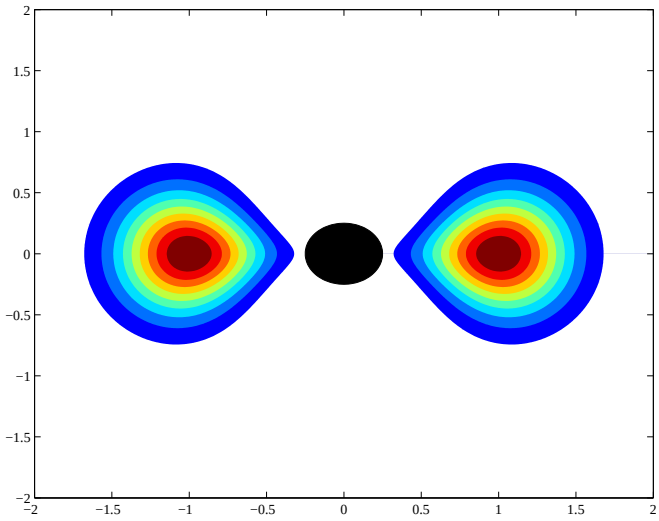

(b) $t = t_1$

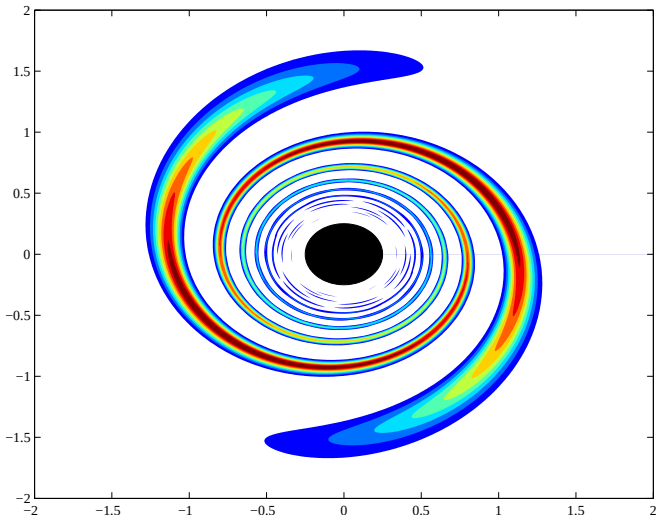

(c) $t = t_2$

Figure 3.1: Orr mechanism for evolution of disturbances in swirling flow (the black patch represents a 'roller' setting up an irrotational base-state - $\Omega \propto 1/r^2$, anti-clockwise sense). $t_0 < t_1 < t_2$. An initial upstream tilted vorticity perturbation attains a transversely coherent state ($t_0 < t < t_1$. Energy amplifies in this stage. For $t > t_1$, the disturbance vorticity becomes more 'down-shear' tilted, leading to a fine-scaled structure of vorticity field and hence resulting in decay in energy.)

limiting form $(\Omega_0 t_{\max})^2/e$. Note that it does not make sense to talk about resonant interaction for $m = 1$ in 2D in the absence of a non-trivial core structure (as is the case for the Rankine vortex), since this is just a translational mode with its critical radius at infinity.

3.2.3 Excitation by a smooth initial condition

In section 3.2.2 we discussed the response of the Rankine vortex to a cylindrical vortex sheet in the irrotational exterior and the response arising from it. A vortex sheet is the only structure that will not be smeared by the (shearing) irrotational flow and this leads to an unbounded secular growth as evident in (3.18) and (3.19). When excited by a smooth initial condition, a resonant growth can only be observed until the shearing action of the mean flow starts to dominate. For long times, this differential shear destroys the transverse coherence of the initial condition. The long-time response in all cases is the Kelvin mode, and the amplitude of that free mode varies with the location of the initial condition, peaking when this location coincides with the Kelvin mode critical radius. To see this, we choose the following initial condition,

$$\tilde{\omega}_z(0) = V_0 \frac{e^{-(r'-r_1)^2/(4\epsilon)}}{2\sqrt{\pi\epsilon}}, \tag{3.21}$$

corresponds to a narrow Gaussian distribution centered around r_1, and that approaches the delta function initial condition in the section 3.2.2 in the limit $\epsilon \to 0$.

Asymptotic evaluation

First, we analyze the time-dependent solution asymptotically for $\epsilon \ll 1$. This could be done both for a resonant initial condition ($r_1 = r_c$) or a non-resonant one ($r_1 \neq r_c$).

1. Resonant Gaussian initial condition -
   For the resonant case, we choose r_1 in (3.21) to be the critical radius for the Kelvin mode, so that $m\Omega(r_1) = \omega_d$. The asymptotic expression for the radial velocity for $\epsilon \ll 1$ is,

$$\begin{aligned} \tilde{u}_r \quad \sim \quad & \frac{i}{2} V_0 e^{-i\omega_d t} \left[\left(\frac{r_c}{r}\right)^{p(r_c)m+1} \left\{ 1 + \epsilon \frac{p(r_c)m+1}{r_c^2} (4i\omega_d t + p(r_c)m) \right\} e^{-b^2} + \right. \\ & \left. \frac{a^{m(p(a)+1)}\Omega_0}{2r^{p(a)m+1} r_c^{m-1}\omega_d} \left\{ \frac{ir_c}{2} \sqrt{\frac{\pi}{\epsilon}} \mathrm{Erf}\,(b) - (m-1)\left(e^{-b^2} - 1\right) \right\} \right], \end{aligned} \tag{3.22}$$

   where $\quad b = \dfrac{2\omega_d}{r_c}\sqrt{\epsilon} t.$

   Here $\mathrm{Erf}(z)$ is the error function ($\mathrm{Erf}(z) = \frac{2}{\sqrt{\pi}} \int_0^z e^{-x^2} dx$ Abramowitz & Stegun [1965]) and $\mathrm{sgn}(z)$ is the signum function. Amongst the terms obtained above by asymptotic evaluation, the most important one is the modification of the linear resonant term, $\Omega_0 t e^{-i\omega_d t}$, in case of cylindrical vortex sheet to the error function term,

$$\Upsilon = \frac{\Omega_0}{\omega_d} \frac{r_c}{2} \sqrt{\frac{\pi}{\epsilon}}\, \mathrm{Erf}\left(\frac{2\omega_d t}{r_1} \sqrt{\epsilon} \right) e^{-i\omega_d t}.$$

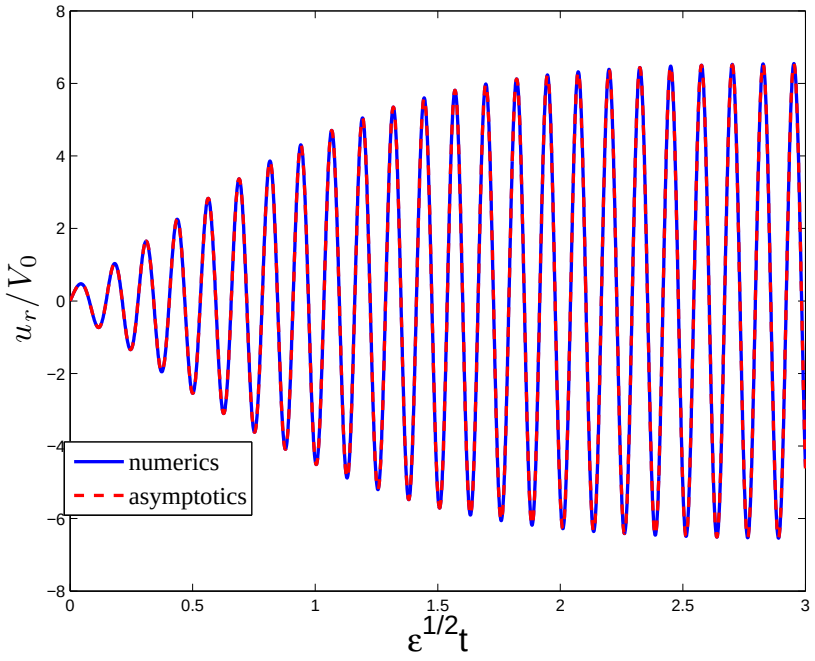

(a) $\epsilon = 10^{-4}$

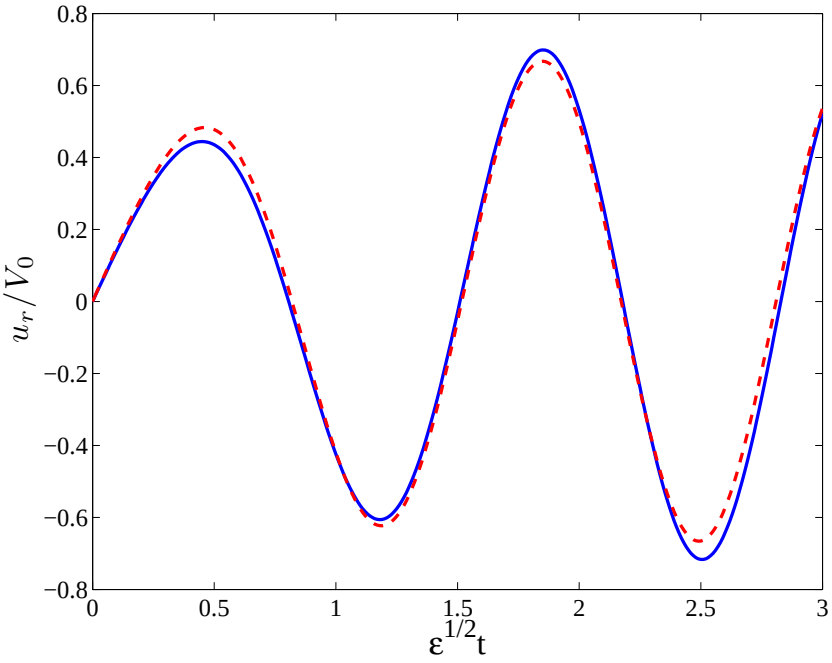

(b) $\epsilon = 0.01$

Figure 3.2: Comparison of u_r evolution computed using numerical integration of (3.8) and the asymptotic expression (3.22), valid for $\epsilon \ll 1$, for a resonant Gaussian forcing ($V_0 = 1, \epsilon = 10^{-4}(a), 10^{-2}(b), m = 2, a = 1, \Omega_0 = 0.5, r = 1.5$)

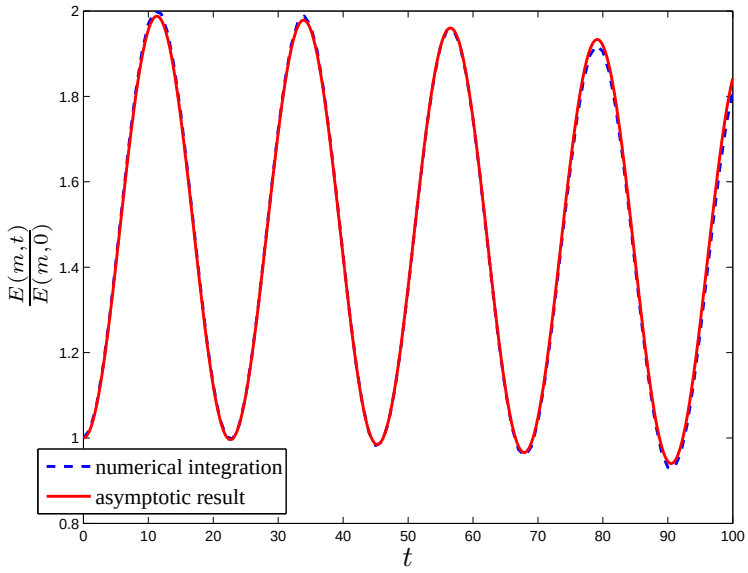

Figure 3.3: Comparison of $E(m,t)$ (3.81) evolution computed using numerical integration of (3.8) and asymptotic evaluation (3.25) for non-resonant Gaussian forcing ($V_0 = 1, \epsilon = 10^{-4}, m = 2, a = 1, \Omega_0 = 0.5$)

The error function for small values of argument, $t < O\left(\epsilon^{-1/2}\right)$, would behave like a linear term, consistent with the secular growth obtained for the singular initial condition considered previously, and for large t, would saturate to 1, again consistent with the eventual de-phasing of any initial condition with a finite radial extent. Thus for

$$t \ll O\left(\epsilon^{-1/2}\right), \qquad \Upsilon \approx \Omega_0 t e^{-i\omega_d t} \tag{3.23}$$

$$t \gg O\left(\epsilon^{-1/2}\right), \qquad \Upsilon \approx \frac{\Omega_0}{\omega_d}\frac{r_c}{2}\sqrt{\frac{\pi}{\epsilon}}e^{-i\omega_d t} \tag{3.24}$$

Thus, for an initial Gaussian axial vorticity distribution of width $\epsilon^{1/2}$, the radial velocity field must linearly amplify to $O(\epsilon^{-1/2})$ in a time of $O\left(\epsilon^{-1/2}\right)$. For later times the response would be an oscillatory. The $O\left(\epsilon^{-1/2}\right)$ time-scale for resonant growth for smooth initial conditions can be explained as a destructive intereference mechanism due to the background shear. From figure 3.2 one observes good agreement between the asymptotic expansions and the numerical integration results for $\epsilon \ll 1$. The expansion starts to deteriorate as the initial Gaussian distribution starts to widen ($\epsilon \sim O(10^{-2})$).

2. Non-resonant Gaussian initial condition -

For the non-resonant case, $m\Omega(r_1) \neq \omega_d$, the asymptotic expression for the radial velocity evolution for $\epsilon \ll 1$ and $t < \epsilon^{-1/2}$ is,

$$\begin{aligned}\tilde{u}_r \quad \sim \quad & \frac{i}{2}V_0\left[e^{-im\Omega_1 t}\left(\frac{r_1}{r}\right)^{p(r_1)m+1}\left\{1+\epsilon\,\frac{p(r_1)m+1}{r_1^2}(4im\Omega_1 t + p(r_1)m)\right\}e^{-b_1^2} - \right. \\ & \left.\Omega_0\left(\frac{a}{r}\right)^{p(a)m+1}\left(\frac{a}{r_1}\right)^{m-1}\frac{e^{-im\Omega(r_1)t}-e^{-i\omega_d t}}{m\Omega(r_1)-\omega_d}\right],\end{aligned} \tag{3.25}$$

where $\qquad b_1 = \dfrac{2m\Omega_1}{r_c}\sqrt{\epsilon}t.$

The non-resonant Gaussian forcing case indicates the possibility of 'beats' - an interaction of the excited continuous spectrum mode (frequency - $m\Omega_1$) and the Kelvin mode (frequency - ω_d).

Numerical evaluation

On numerically integrating (3.8) for the initial condition (3.21) several interesting aspects get highlighted (see figure 3.4), confirming predictions from asymptotic calculations. On choosing the centre of the Gaussian axial vorticity distribution (r_1) to coincide with r_c, we note that for $\epsilon \ll 1$, the signature of resonance is evidently present for short times. For later times, after the decay of the continuous spectrum contribution, the growth saturates and the oscillatory Kelvin mode persists. Figure 3.4 (b)-(c) confirms that when the excitation location r_1 is slightly offset from the critical radius r_c ($r_1 = r_c + 0.1$), the distant, but closely spaced, frequencies of the Kelvin mode and the sharply localized CS-spectrum response lead to the 'beats' phenomenon in the temporal response. For $\epsilon \ll 1$ figure 3.4 (f) shows that the maximum amplitude attained by radial velocity is $O(\epsilon^{-1/2})$ and is attained in a time $O(\epsilon^{-1/2})$. This scaling arises from the width of the initial condition - $O(\sqrt{\epsilon})$. Consider two circular waves of azimuthal wavenumber, m, aligned initially in a radially coherent fashion separated by a distance $O(\sqrt{\epsilon})$. Due to the differentially rotating ambient flow, the outer wave-speed lags the inner one by $O(\sqrt{\epsilon})$. Thus the perfectly aligned crests and troughs of the two waves will undergo destructive interference in time $O(\epsilon^{-1/2})$.

Figure 3.5 depicts the evolution of the perturbation energy (3.81), within a linear and inviscid framework, for an initial Gaussian axial vorticity disturbance centered around r_c, the critical radius of a Kelvin mode for an equivalent Rankine vortex. Here, a comparison is made between the response of a Rankine vortex (3.8), the asymptotic approximation for a Rankine vortex (3.22) and the response of a smooth Rankine-like vorticity profile given by,

$$Z(r) = \frac{1}{2}\left[1 - \tanh\left(\frac{r-a}{d}\right)\right] \tag{3.26}$$

Here, $a = 1$ and d is the (small) length scale of the transition region between the core and the irrotational exterior. d may thus be considered an estimate of the 'steepness' of the vortex, and is varied from 0.01 to 0.1 in the figure. The response for the smooth vorticity profile above is obtained from the numerical solution of (3.1). For the numerical calculation, the spatial discretization in the radial domain is done using the Chebyshev spectral collocation method (Trefethen [2000]) and the time integration is carried out using the MATLAB software command ODE45, based on an explicit Runge-Kutta formula with adaptive step-sizes. Though beyond the scope of the present study, for 'intense' Rankine-like vortices there exists an intermediate exponentially damped regime and the decay rate of such regime can be obtained from the Riemann-Hilbert problem approach for smooth vortices (section 2.3.1). We consider a one parameter 'intense' vortex (Le Dizès [2000]),

$$Z(r) = \mathcal{H}(a-r) + \exp\left(-\frac{(r-a)^2}{(1-a)^2}\right)\mathcal{H}(r-a) \tag{3.27}$$

where $0 \leqslant a \leqslant 1$. $a = 0$ describes a Gaussian vortex and $a = 1$ corresponds to the Rankine

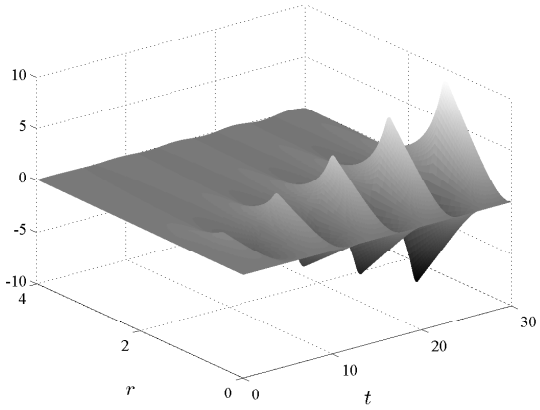

(a) Excitation by a cylindrical vortex sheet. $\mathrm{Re}u_r/V_0$

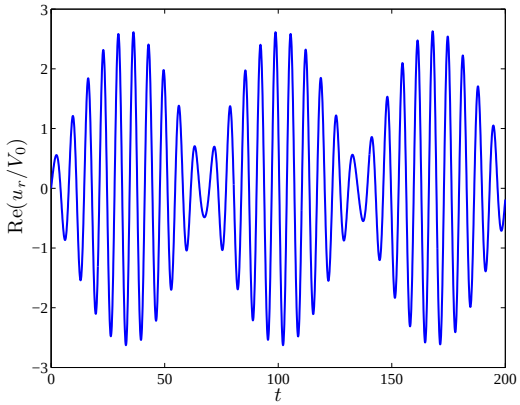

(b)

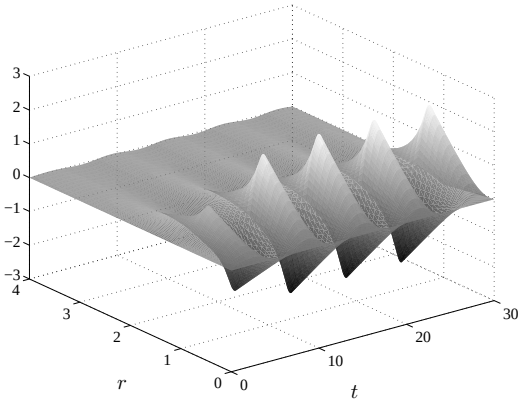

(c) Excitation by a resonant Gaussian axial vorticity, $\epsilon = 10^{-2}$

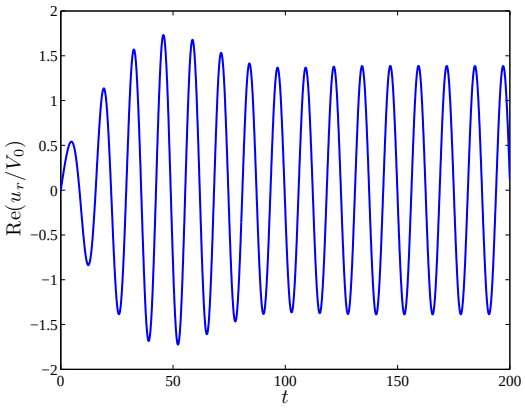

(d)

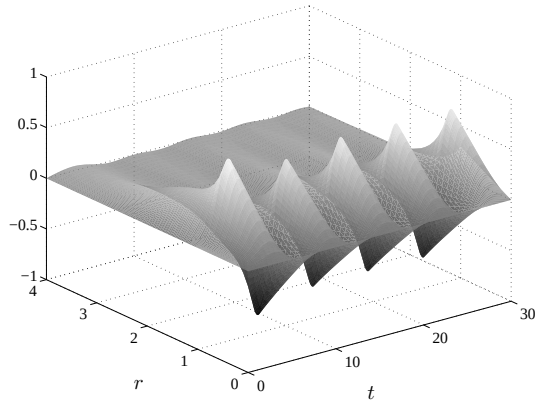

(e) Excitation by a non-resonant Gaussian axial vorticity distribution, $\epsilon = 0.1$

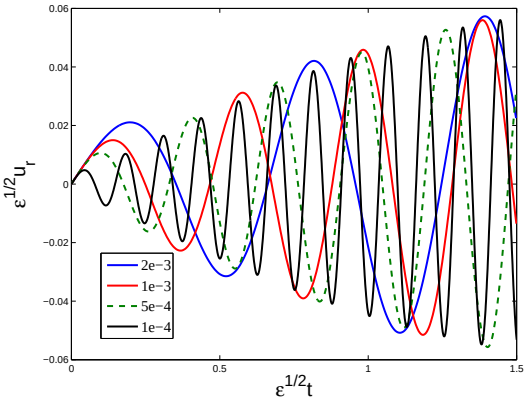

(f)

Figure 3.4: Space-time plots for the 2D initial value problem for a Rankine vortex. The results are computed for $m = 2$, core radius $a = 1$ and core angular velocity $\Omega_0 = 1$. Figures (a),(c) and (e) depict the time evolution of radial velocity ($\mathrm{Re}u_r/V_0$) for excitation by a cylindrical vortex sheet stationed at $r_1 = r_c$ and Gaussian axial vorticity distributions (equation 3.21, $\epsilon = 10^{-2}, 0.1$) centered at r_c and $1.05r_c$ (r_c is the critical radius of the 2D Kelvin mode) respectively. Figure (b) and (d) show the time response of u_r at $r = 1.5$ when excited by a cylindrical vortex sheet and Gaussian axial vorticity ($\epsilon = 10^{-3}$) positioned at $r_1 = 1.05r_c$ respectively. (f) shows u_r temporal history during resonant excitation by Gaussian distributions of various width (ϵ). The tilde's have been dropped from the perturbation quantities in the above plots.

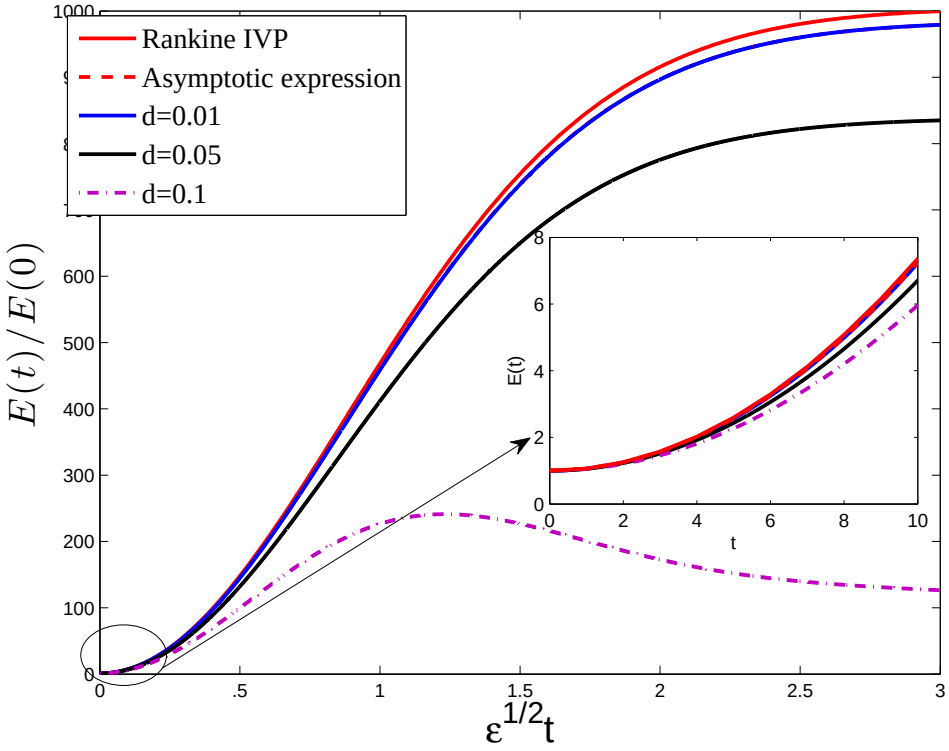

(a) $\epsilon = 10^{-4}$

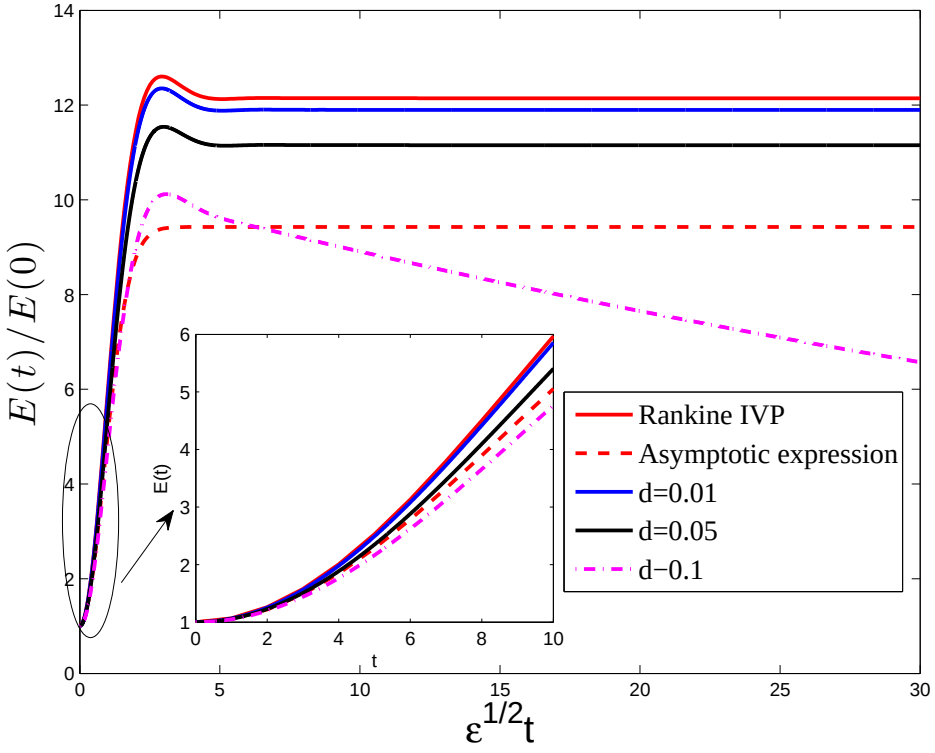

(b) $\epsilon = 0.01$

Figure 3.5: Evolution of perturbation energy for smooth vortices ($d = 0.01, 0.05$ and 0.1) and Rankine vortex to Gaussian vorticity excitation (equation 3.21, $m = 2, r_1 = a\sqrt{\frac{m}{m-1}}$)

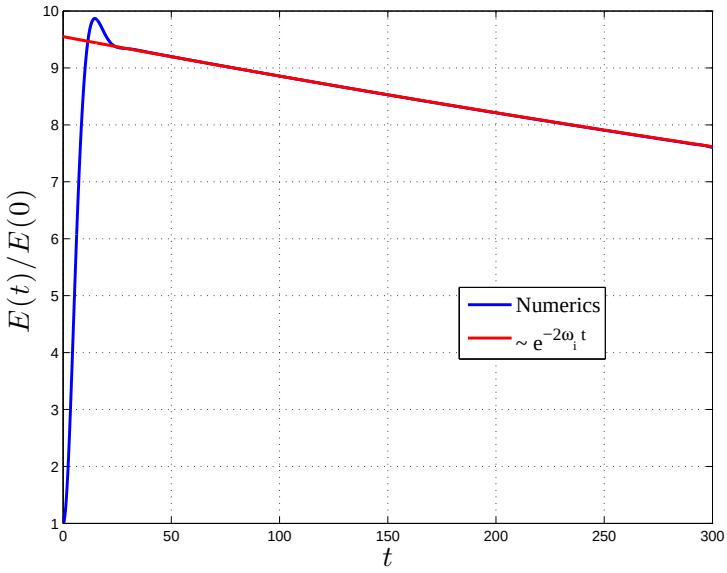

Figure 3.6: Evolution of energy for a smooth vortex (3.27) and its comparison with decay as predicted by Riemann-Hilbert theory (2.125)

vortex. Figure 3.6 depicts the comparison for a vortex given by $a = 0.82$ with decay rate predicted by (2.125).

In this section we have focused on the 2D IVP for a Rankine vortex, and have highlighted the resonant interaction of the Kelvin mode and the continuous spectrum. Such interactions between the discrete and continuous spectra isn't uncommon in problems of hydrodynamic stability. For a piecewise linear shear flow Sazonov [1989] has studied the resonant interaction between the continuous spectrum and the discrete edge wave arising from the discontinuity in shear. Even earlier Pedlosky [1964] examined the response of a canonical model for baroclinic instability; the Eady model, to external disturbances through an initial value problem. The quasi-geostrophic vorticity in this case obeys an equation identical to the axial vorticity in our problem, and the temporal response was again governed by the discrete Eady waves and the continuous spectrum. Although not explicitly mentioned, one can immediately deduce the possibility of resonance between the Eady and continuous spectrum modes from the expression given in Pedlosky [1964]. Indeed Farrell [1984] when studying the initial value problem of Pedlosky [1964] showed this from a treatment involving the modal and non-modal solutions. Though neutral modes are incapable of extracting energy from the mean flow, the presence of non-modal solutions leads to the projection of the energy extracted from the mean onto the neutral mode, and thus, leads to an initial algebraic growth. Gorshkov *et al.* [2000] discussed the possibility of resonance for discrete and continuous spectra and suggested that the secular growth would lead to destruction of the vortex. Finally Lansky *et al.* [1997] investigated a model for vortex merger, between dissimilar vortices by considering, a weak point vortex revolving around a strong vortex patch. As the point vortex rotate at the critical radius of a Kelvin mode, it resonated with the corresponding surface wave on the vortex. The point vortex is convected by both the purely azimuthal flow and the disturbance velocity field due to the Kelvin mode. For large enough amplitudes, the critical layers of the different Kelvin modes overlap and in the limit, the point vortex collapses into the vortex patch. Note that the finite extent of a critical layer (with an associated cat's

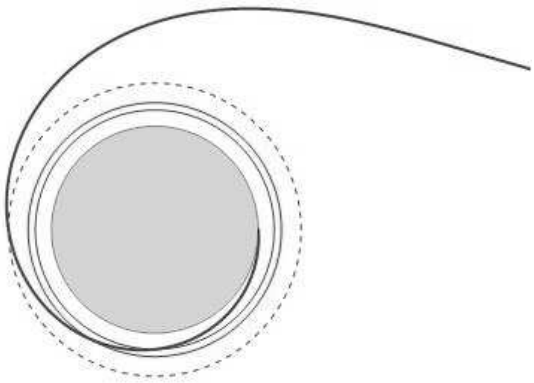

Figure 3.7: Schematic of a vortex filament from a neighbouring vortex exciting a spectrum of Kelvin modes of a vortex during merger (the critical radius of modes $m = 2, 3$ and 4 are shown in the figure)

eye structure in this region) arises from non-linear effects and in the linearized limit, the critical layer has a zero thickness, and one may then speak of a critical radius (as in the present case).

It was noted above, in the context of a Rankine vortex, that the algebraic growth, either resonant or non-resonant, is eventually arrested for any initial axial vorticity distribution with a finite radial extent. The saturation of growth arises due to differential shearing of the vorticity perturbation by the exterior irrotational flow which leads to a loss of transverse (radial) coherence in the perturbation vorticity field. The duration of the growth phase, due to the combination of the Orr mechanism (relevant to an initial condition in the form of a leading spiral) and resonant interaction, scales inversely with the width of the initial vorticity distribution. In this section, we briefly describe a novel vorticity-screening mechanism first reported by Sheshadri [2010], and present only for a smooth vorticity profile, that leads to a saturation of growth even for an initial condition with a vanishingly small spatial extent (including a delta function initial condition corresponding to a cylindrical vortex-sheet). This is in sharp contrast to the temporal response of a Rankine vortex where, as already seen, a cylindrical vortex at the critical radius leads to unbounded secular growth. The saturation arises because, for a smooth vorticity profile, the duration of the growth phase for sufficiently localized initial conditions is controlled by the base-state vorticity gradient at the critical radius rather than the (slow) differential shear arising from the small but finite spread of the perturbation vorticity distribution. The non-zero base-state vorticity gradient in the vicinity of the critical radius leads to the induction of perturbation vorticity of assign opposite to the vorticity in the initial condition, and for long times, the induced perturbation vorticity ÔscreensÕ the imposed forcing. Thus, for a smooth Rankine-like profile, it is the mechanism operating on a shorter timescale (differential shear versus critical layer vorticity-induction) that controls the duration of the algebraic growth, and thence, the final amplitude of the deformed vortex column. The study of Sheshadri [2010] was restricted to two dimensions, although one expects the vorticity-screening mechanism to be relevant also for the three-dimensional perturbations. For a smooth Rankine-like profile, figure (see figure 11 in Sheshadri [2010]) shows the variation of the perturbation energy with the width of initial condition for the base-state vorticity profiles with differing values of the critical layer vorticity gradient ($DZ(r_c)$). In each case, the initial condition is a Gaussian vorticity

distribution with a finite width (denoted by δ in the figure) and centered at the critical radius. The amplitude of the perturbation energy, at saturation, continues to increase with decreasing δ owing to a corresponding increase in the differential shear time scale. For sufficiently small δ, however the growth characteristics start to become independent of δ owing to a transition in the mechanism of saturation from one driven by the differential shear to the aforementioned screening mechanism associated with the critical layer vorticity gradient. This may also be seen from figure (figure 9 in Sheshadri [2010]) where the perturbation energy is plotted against DZ(rc) rather than δ; the collapse of the curves, in the limit of small δ, suggests a maximum growth envelope corresponding to a vortex-sheet initial condition. The threshold width of the initial vorticity distribution below which there is a crossover from the differential-shear mechanism to the one driven by critical layer vorticity gradient, scales with DZ. The width of the initial condition, for any finite Re, cannot be smaller than $O(\mathrm{Re}^{-1/3})$, a scaling that arises from a balance of (shearing) Re, cannot be smaller than $O(\mathrm{Re}^{-1/3})$, a scaling that arises from a balance of (shearing) convection and viscous diffusion. Thus, the cross-over from the Ôδ-controlled regimeÕ to the ÔDZ-controlled regimeÕ must depend on the relative magnitudes of $\mathrm{Re}^{-1/3}$ and DZ.

3.3 3D Initial value problem

To arrive at the 3D stability equations, we start from the Fourier transformed linearized Euler equations, and the equation of continuity, given by:

$$L\tilde{u}_z = -ik\tilde{p}, \tag{3.28}$$

$$L\tilde{u}_r - 2\Omega\tilde{u}_\theta = -\frac{\partial\tilde{p}}{\partial r}, \tag{3.29}$$

$$L\tilde{u}_\theta + Z\tilde{u}_r = -\frac{im}{r}\tilde{p}, \tag{3.30}$$

$$\frac{\partial\tilde{u}_r}{\partial r} + \frac{\tilde{u}_r}{r} + \frac{im\tilde{u}_\theta}{r} + ik\tilde{u}_z = 0, \tag{3.31}$$

where $L = \dfrac{\partial}{\partial t} + im\Omega$, m being the azimuthal wave number as in the earlier section, and k being the axial wave number. On Laplace transforming, and after some manipulation, one can derive the following equations in terms of the axial velocity perturbation, $\hat{u}_z(r,s)$ with the corresponding $\hat{u}_r(r,s)$ expression:

$\underline{r < a}$

$$\left(D^2 + \frac{1}{r}D - \frac{m^2}{r^2} - k^2 - \frac{4k^2\Omega_0^2}{(s+im\Omega_0)^2}\right)\hat{u}_z = F_1(0) \tag{3.32}$$

$$\hat{u}_r = \frac{2m\Omega_0}{rk}\frac{s+im\Omega_0}{(s+im\Omega_0)^2+4\Omega_0^2}\hat{u}_z - \frac{i}{k}\frac{(s+im\Omega_0)^2}{(s+im\Omega_0)^2+4\Omega_0^2}\frac{d\hat{u}_z}{dr} + F_2(0) \tag{3.33}$$

$\underline{r > a}$

$$\left(D^2 + \frac{1}{r}D - \frac{m^2}{r^2} - k^2\right)\hat{u}_z = F_3(0) \tag{3.34}$$

$$\hat{u}_r = -\frac{i}{k}\frac{d\hat{u}_z}{dr} + F_4(0) \tag{3.35}$$

where

$$F_1(0) = -\frac{2\Omega_0 ik}{(s+im\Omega_0)^2}\tilde{w}_{z0} - \frac{1}{(s+im\Omega_0)}\left\{\frac{1}{r}\frac{d}{dr}(r\tilde{w}_{\theta 0} - \frac{im}{r}\tilde{w}_{r0}\right\}, \tag{3.36}$$

$$F_2(0) = \frac{i}{k}\frac{1}{(s+im\Omega_0)^2+4\Omega_0^2}\left\{2\Omega_0\tilde{w}_{r0} - (s+im\Omega_0)\tilde{w}_{\theta 0}\right\}, \tag{3.37}$$

$$F_3(0) = \frac{1}{r}\frac{d}{dr}\left\{\frac{2r\Omega\tilde{w}_{r0}}{(s+im\Omega)^2} - \frac{r\tilde{w}_{\theta 0}}{(s+im\Omega)}\right\} + \frac{im\tilde{w}_{r0}}{r(s+im\Omega)}, \tag{3.38}$$

$$F_4(0) = -\frac{i}{k}\frac{\tilde{w}_{\theta 0}}{(s+im\Omega)} + \frac{2i\Omega\tilde{w}_{r0}}{k(s+im\Omega)^2}, \tag{3.39}$$

are the functions dependent on the initial vorticity field with $\boldsymbol{w}(r, t=0) = (\tilde{w}_{r0}, \tilde{w}_{\theta 0}.\tilde{w}_{z0})$ being the initial vorticity field.

The initial value problem for a Rankine vortex has been examined earlier by Arendt *et al.* [1997], but for an initial vorticity field restricted to the region $r < a$; such an initial condition can be interpreted as a suitably deformed vortex column at the initial instant. Comparing (3.32)-(3.35) with Arendt *et al.* [1997], we find that (3.32) and (3.33) are the same, but (3.34) and (3.35) differ owing to the presence of $F_3(0)$ and $F_4(0)$. As seen from (3.38) and (3.39) $F_3(0)$ and $F_4(0)$ represent vortical disturbances outside the vortex core. Thus, with the present set of equations, we will be able to investigate the effect of an arbitrary initial vorticity field, and in particular, the effect of an external disturbance field on the Rankine vortex. Solving (3.32) and (3.34) we have the following expressions for $\hat{u}_z$:

$\underline{r < a}$

$$\hat{u}_z = AJ_m(k\xi r) + g(r) \tag{3.40}$$

where $$g(r) = Y_m(k\xi r)\int_0^r \frac{\pi r'}{2}F_1(0)J_m(k\xi r')dr' - J_m(k\xi r)\int_0^r \frac{\pi r'}{2}F_1(0)Y_m(k\xi r')dr',$$

$$\xi^2 = -\frac{4\Omega_0^2}{(s+im\Omega_0)^2} - 1,$$

$\underline{r > a}$

$$\hat{u}_z = BK_m(kr) + h(r), \tag{3.41}$$

where $$h(r) = K_m(kr)\int_r^\infty r'F_3(0)I_m(kr')dr' - I_m(kr)\int_r^\infty r'F_3(0)K_m(kr')dr'.$$

In the absence of any volume sources or sinks, the radial and axial components of the disturbance velocity field (and their transforms) should be continuous across the vortex core boundary ($r = a$). From (3.40) and (3.41), the continuity of the axial velocity field gives:

$$AJ_m(k\xi a) + g(a) = BK_m(ka) + h(a). \tag{3.42}$$

Further from (3.33), (3.35), (3.40) and (3.41) the continuity of radial velocity yields:

$$\frac{2m\Omega_0}{ak}\frac{s+im\Omega_0}{(s+im\Omega_0)^2+4\Omega_0^2}[AJ_m(k\xi a) + g(a)] - \frac{i}{k}\frac{(s+im\Omega_0)^2}{(s+im\Omega_0)^2+4\Omega_0^2}[Ak\xi J_m'(k\xi a) + g'(a)]$$
$$+F_2(0)|_{r=a} = -\frac{i}{k}[BkK_m'(ka) + h'(a)] + F_4(0)|_{r=a}. \tag{3.43}$$

Solving (3.42) and (3.43), one obtains:

$$A = \frac{\{h(a)-g(a)\}\dfrac{K_m'(ka)}{kaK_m(ka)} - \dfrac{1}{k\xi^2 a}\left\{\xi^2 a h'(a) + \dfrac{2im\Omega_0 g(a)}{s+im\Omega_0} + ag'(a)\right\} + \dfrac{i}{ka}\left\{F_2(0)|_{r=a} - F_4(0)|_{r=a}\right\}}{\dfrac{K_m'(ka)}{kaK_m(ka)} + \dfrac{J_m'(k\xi a)}{k\xi aJ_m(k\xi a)} + \dfrac{2im\Omega_0}{(k\xi a)^2(s+im\Omega_0)}}, \tag{3.44}$$

$$B = \frac{\{g(a)-h(a)\}\dfrac{J_m'(k\xi a)}{k\xi aJ_m(k\xi a)} - \dfrac{1}{k\xi^2 a}\left\{\xi^2 a h'(a) + \dfrac{2im\Omega_0 g(a)}{s+im\Omega_0} + ag'(a)\right\} + \dfrac{i}{ka}\left\{F_2(0)|_{r=a} - F_4(0)|_{r=a}\right\}}{\dfrac{K_m'(ka)}{kaK_m(ka)} + \dfrac{J_m'(k\xi a)}{k\xi aJ_m(k\xi a)} + \dfrac{2im\Omega_0}{(k\xi a)^2(s+im\Omega_0)}}. \tag{3.45}$$

Thus, the expression for axial velocity can be written as;

$\underline{r<a}$

$$\hat{u}_z(r,s) = \frac{\dfrac{\displaystyle\int_a^\infty r'K_m(kr')F_3(0)dr'}{(ka)^2K_m(ka)}}{\Delta}\frac{J_m(k\xi r)}{J_m(k\xi a)} + \left\{\frac{-g(a)\dfrac{K_m'(ka)}{kaK_m(ka)} - \dfrac{1}{(k\xi a)^2}\left(ag'(a) + \dfrac{2im\Omega_0}{s+im\Omega_0}g(a)\right) + P}{\Delta}\frac{J_m(k\xi r)}{J_m(k\xi a)} + g(r)\right\}, \tag{3.46}$$

$\underline{r>a}$

$$\hat{u}_z = \frac{\dfrac{\displaystyle\int_a^\infty r'K_m(kr')F_3(0)dr'}{(ka)^2K_m(ka)}}{\Delta}\frac{K_m(kr)}{K_m(ka)} + \left[h(r) - h(a)\frac{K_m(kr)}{K_m(ka)}\right] + \left\{\frac{g(a)\dfrac{J_m'(ka)}{k\xi aJ_m(k\xi a)} - a\dfrac{g'(a)}{(k\xi a)^2} + P}{\Delta}\frac{K_m(kr)}{K_m(ka)}\right\}, \tag{3.47}$$

where

$$P = \frac{i}{ka}\left\{F_2(0)\Big|_{r=a} - F_4(0)\Big|_{r=a}\right\}, \tag{3.48}$$

$$\Delta = \frac{K_m'(ka)}{kaK_m(ka)} + \frac{J_m'(k\xi a)}{k\xi aJ_m(k\xi a)} + \frac{2im\Omega_0}{(k\xi a)^2(s+im\Omega_0)}. \tag{3.49}$$

Having obtained the expressions for the velocity components in transform space, we need to invert the above expressions to obtain the form of velocity perturbations in temporal domain. The terms within braces in the above equations are identical to those obtained by Arendt *et al.* [1997] (with the slight modification that P as seen in (3.48), now includes $F_4(0)$ too). Thus $F_4(0) = 0$, they represent the evolution of a disturbance field when the vortex core alone is perturbed. The remaining terms in (3.46) and (3.47) are new and contain information regarding vortical perturbations outside the vortex core. To obtain the inverse, we need to understand the number and nature of singularities in (3.46) and (3.47). The singularities, both true and

apparent, appear as poles at $s = -im\Omega$ (poles of $F_{3,4}(0)$), $s = -i(m \pm 2)\Omega_0$ (poles of $F_2(0)$) and $s = s_n$ (zeros of Δ) and as a non-isolated essential singularity $s = -im\Omega_0$ - the accumulation point of the discrete spectrum. The results obtained in appendix D show that the contributions to the linear response of a perturbed vortex column arise from the simple poles $s = s_n$, corresponding to the discrete spectrum, the simple pole $s = -im\Omega$ corresponding to the continuous spectrum and $s = -im\Omega_0$ corresponding to the accumulation point of the discrete spectrum $\left(\text{coming from the singularity of } F_4(0)\Big|_{r=a}\right)$.
To obtain the Laplace inverse, we first define the following functions:

$$q_1(s) = \frac{1}{\Delta}\frac{J_m(k\xi r)}{J_m(k\xi a)}, \tag{3.50}$$

$$q_2(s) = \frac{1}{\Delta}\frac{K_m(kr)}{K_m(ka)}. \tag{3.51}$$

The inverse Laplace transform of the above functions are given as:

$$Q_1(t) = \mathcal{L}^{-1}(q_1(s)) = \sum_{b=\pm1}\sum_{n=1}^{\infty} B_n^b e^{-i\omega_n t}\frac{J_m(k\xi_n r)}{J_m(k\xi_n a)} - (ka)^2 K_m(ka) I_m(kr)\delta(t), \tag{3.52}$$

$$Q_2(t) = \mathcal{L}^{-1}(q_2(s)) = \sum_{b=\pm1}\sum_{n=1}^{\infty} B_n^b e^{-i\omega_n t}\frac{K_m(kr)}{K_m(ka)} - (ka)^2 K_m(kr) I_m(ka)\delta(t), \tag{3.53}$$

where

$$\frac{1}{B_n^b} = \frac{\partial\Delta}{\partial s}\Big|_{s=-i\omega_n} = \frac{(\xi_n^2+1)^{3/2}}{2\xi_n^2 bi\Omega_0}\left[\frac{2J_m'(k\xi_n a)}{k\xi_n a J_m(k\xi_n a)} + \left\{\frac{J_m'(k\xi_n a)}{J_m(k\xi_n a)}\right\}^2 + 1 - \frac{m^2}{(k\xi_n a)^2} + \frac{bm(\xi_n^2+2)}{\sqrt{\xi_n^2+1}(k\xi_n a)^2}\right],$$

with $-i\omega_n = s_n$ and $\mathcal{L}^{-1}(.) = \dfrac{1}{2\pi i}\displaystyle\int_{\gamma-i\infty}^{\gamma+i\infty}(.)e^{st}ds$ being the inverse Laplace transform. In (3.52) and (3.53), $b = +1$ corresponds to the retrograde waves and $b = -1$ corresponds to the cograde waves. In the inverse Laplace transforms, apart from the obvious contribution from zeroes of Δ, the term proportional to $\delta(t)$ term arises as neither $q_1(s)$ and $q_2(s)$ do not satisfy Jordan's lemma (Ablowitz & Fokas [2003]).
Applying the convolution theorem to (3.46) and (3.47), and using (3.52) and (3.53) together with the inverse Laplace transform results obtained by Arendt *et al.* [1997] for core perturbations, the disturbance velocity field in temporal domain is given by:

$$\underline{r < a}$$

$$\tilde{u}_z(r,t) = \int_0^t \left[L_1(t-\tau) + L_2(t-\tau)\right] Q_1(\tau)d\tau +$$

$$\mathcal{L}^{-1}\left\{\frac{-g(a)\dfrac{K_m'(ka)}{kaK_m(ka)} - \dfrac{1}{(k\xi a)^2}\left(ag'(a) + \dfrac{2im\Omega_0}{s+im\Omega_0}g(a)\right) + \dfrac{i}{ka}F_2(0)\Big|_{r=a}}{\Delta}\frac{J_m(k\xi r)}{J_m(k\xi a)} + g(r)\right\}$$

$$= \int_0^t \left[L_1(t-\tau) + L_2(t-\tau)\right] Q_1(\tau)d\tau + \sum_{b=\pm1}\sum_{n=1}^{\infty} bC_n^b e^{-i\omega_n t}\frac{J_m(k\xi_n r)}{J_m(k\xi_n a)}, \tag{3.54}$$

$\underline{r > a}$

$$\tilde{u}_z(r,t) = \int_0^t \left[L_1(t-\tau) + L_2(t-\tau)\right] Q_2(\tau) d\tau + \mathcal{L}^{-1}\left[h(r) - h(a)\frac{K_m(kr)}{K_m(ka)}\right] +$$
$$\mathcal{L}^{-1}\left\{\frac{g(a)\dfrac{J_m'(ka)}{k\xi a J_m(k\xi a)} - a\dfrac{g'(a)}{(k\xi a)^2} + \dfrac{i}{ka}F_2(0)\Big|_{r=a}}{\Delta}\,\frac{K_m(kr)}{K_m(ka)}\right\}$$
$$= \int_0^t \left[L_1(t-\tau) + L_2(t-\tau)\right] Q_2(\tau) d\tau + \mathcal{L}^{-1}\left[h(r) - h(a)\frac{K_m(kr)}{K_m(ka)}\right] + \sum_{b=\pm 1}\sum_{n=1}^{\infty} bC_n^b e^{-i\omega_n t}\frac{K_m(kr)}{K_m(ka)}, \tag{3.55}$$

where,

$$C_n^b = b\left[\frac{g(a)J_m'(k\xi_n a)}{k\xi_n a J_m(k\xi_n a)} - a\frac{g'(a)}{(k\xi_n a)^2} + \frac{i}{ka}F_2(0)\Big|_{r=a,s=s_n}\right] B_n^b\,,$$
$$L_1(t) = -\frac{i}{ka}\mathcal{L}^{-1}\left\{F_4(0)\Big|_{r=a}\right\} = -\frac{1}{k^2 a}\left[\,\tilde{w}_{\theta 0}(a) - 2\Omega_0 t\,\tilde{w}_{r0}(a)\right] e^{-im\Omega_0 t},$$
$$L_2(t) = \mathcal{L}^{-1}\left\{\frac{\displaystyle\int_a^\infty r' K_m(kr') F_3(0) dr'}{(ka)^2 K_m(ka)}\right\}$$
$$= \int_a^\infty \frac{K_m(kr')}{(ka)^2 K_m(ka)}\left[im\tilde{w}_{r0}e^{-im\Omega(r')t} + \frac{d}{dr'}\left\{\left(2\Omega(r')t\;\tilde{w}_{r0} - \tilde{w}_{\theta 0}\right) r' e^{-im\Omega(r')t}\right\}\right] dr'.$$

Incorporating all the results obtained above, performing the inverse Fourier transform and accounting for the azimuthal dependence, we can write the following closed-form expression for disturbance velocity field,

$\underline{r < a}$

$$u_z(\boldsymbol{x},t) = \sum_{m=-\infty}^{\infty}\frac{1}{2\pi}\int_{-\infty}^{\infty} e^{i(kz+m\theta)}\left[-I_m(kr)\int_a^\infty K_m(kr')\mathcal{A}\,dr' + \sum_{b=\pm 1}\sum_{n=1}^{\infty} bC_n^b e^{-i\omega_n t}\frac{J_m(k\xi_n r)}{J_m(k\xi_n a)}\right.$$
$$-\frac{1}{k^2 a}\sum_{b=\pm 1}\sum_{n=1}^{\infty} B_n^b\frac{J_m(k\xi_n r)}{J_m(k\xi_n a)}\left\{\tilde{w}_{\theta 0}\mathcal{Z}(a) + \frac{ia}{m}\tilde{w}_{r0}\frac{d\mathcal{Z}}{dr}\Big|_{r=a}\right\} - (ka)^2 K_m(ka) I_m(kr) L_1(t)$$
$$\left. + \sum_{b=\pm 1}\sum_{n=1}^{\infty} B_n^b\frac{J_m(k\xi_n r)}{J_m(k\xi_n a)}\int_a^\infty \frac{K_m(kr')}{(ka)^2 K_m(ka)}\left[im\tilde{w}_{r0}\mathcal{Z} - \frac{d}{dr'}\left\{\left(\tilde{w}_{\theta 0}\mathcal{Z} + \frac{ir'}{m}\,\tilde{w}_{r0}\frac{d\mathcal{Z}}{dr'}\right) r'\right\}\right] dr'\right] dk, \tag{3.56}$$

$\underline{r > a}$

$$u_z(\boldsymbol{x},t) = \sum_{m=-\infty}^{\infty} \frac{1}{2\pi}\int_{-\infty}^{\infty} e^{i(kz+m\theta)}\left[-K_m(kr)\int_a^r I_m(kr')\mathcal{A}\,dr' - \right.$$
$$I_m(kr)\int_r^{\infty} K_m(kr')\mathcal{A}\,dr' + \sum_{b=\pm1}\sum_{n=1}^{\infty} bC_n^b e^{-i\omega_n t}\frac{K_m(kr)}{K_m(ka)}$$
$$-\frac{1}{k^2 a}\sum_{b=\pm1}\sum_{n=1}^{\infty} B_n^b \frac{K_m(kr)}{K_m(ka)}\left\{\tilde{w}_{\theta 0}\mathcal{Z}(a) + \frac{ia}{m}\tilde{w}_{r0}\frac{d\mathcal{Z}}{dr}\Big|_{r=a}\right\} - (ka)^2 I_m(ka)K_m(kr)L_1(t)$$
$$\left. + \sum_{b=\pm1}\sum_{n=1}^{\infty} B_n^b \frac{K_m(kr)}{K_m(ka)}\int_a^{\infty}\frac{K_m(kr')}{(ka)^2 K_m(ka)}\left[im\tilde{w}_{r0}\mathcal{Z} - \frac{d}{dr'}\left\{\left(\tilde{w}_{\theta 0}\mathcal{Z} + \frac{ir'}{m}\,\tilde{w}_{r0}\frac{d\mathcal{Z}}{dr'}\right)r'\right\}\right]dr'\right] dk, \tag{3.57}$$

$$\text{where } \mathcal{Z} = \frac{e^{-i\omega_n t} - e^{-im\Omega(r')t}}{-i(\omega_n - m\Omega(r'))},$$
$$\mathcal{A} = \left[im\tilde{w}_{r0}e^{-im\Omega(r')t} + \frac{d}{dr'}\left\{\left(2\Omega(r')t\;\tilde{w}_{r0} - \tilde{w}_{\theta 0}\right)r' e^{-im\Omega(r')t}\right\}\right].$$

Equations (3.56) and (3.57) are the exact analytical expressions for the linear response of a vortex column to any arbitrary vortical disturbances both inside and outside the vortex core. The above expressions would also be the Greens function within the RDT framework (Townsend [1956], Miyazaki & Hunt [2000]), describing the linear interaction of a turbulent field with a Rankine vortex. As a consistency check, the vorticity field corresponding to the continuous spectrum, given by (2.62)-(2.64), when provided as an initial condition in equations (3.56) and (3.57), leads to the velocity field for the corresponding continuous spectrum eigenmode (2.48)-(2.50). An analogous scenario holds for the Kelvin modes.
The solution in the above form has the following salient features:

1. There exists separate contributions corresponding to the denumerable infinity of discrete modes (the 3D Kelvin modes) and the continuous spectrum (the Λ_1 and Λ_2 families).

2. There exists terms terms of the form $e^{-i\omega_n t} - e^{-im\Omega(r')t}$, which represent the interaction between the discrete and continuous spectra. Thus, similar to the 2D case, there exists limits, $m\Omega \to \omega_n$, when the vortex column must exhibit a secular growth.

3. A novel feature in three dimensions is the algebraic growth (terms involving $\mathcal{A}$ in (3.56) and (3.57) proportional to t) possible due to the non-normality of the advection operator. In (3.56) and (3.57) there exists an $O(t)$ growth associated with an initial radial vorticity perturbation. It arises due to a non-zero $\tilde{w}_{r0}$ producing an algebraically growing $\tilde{w}_\theta$ via vortex stretching-tilting. A detailed discussion in this regard will be presented in section 3.3.3.

There are three possible mechanisms of algebraic growth in 3D - the Orr mechanism, a resonant interaction between the discrete and continuous spectrum, and the algebraic growth via vortex stretching-tilting. The latter two mechanisms have been identified above and, as already indicated the stretching-tilting mechanism is unique to 3D. The severity of algebraic growth in 3D depends on the presence or absence of a coupling between the resonant interaction and

stretch-tilt induced algebraic growth. This too will be elaborated in section 3.3.3. The physics of the Orr mechanism in 3D remains identical to that in 2D (section 3.2.2). We will be therefore only consider (infinitely) localized initial conditions, representable in terms of delta functions and their derivatives. Such initial conditions will not be subject to the differential shear action that leads to the Orr mechanism of growth for an initial condition with an upstream tilt.

3.3.1 Equivalence to modal superposition

From the modal analysis in chapter 2, we have the following expression for the evolution of an arbitrary initial vorticity in terms of the Kelvin modes and the Λ_1 and Λ_2 families of continuous spectrum modes.

$$\begin{aligned}\boldsymbol{w}(\boldsymbol{x},t) &= \int_{a^+}^{\infty}\left[X_{\Lambda_1}(r_f)\hat{\boldsymbol{w}}^{\Lambda_1}(r;r_f)+X_{\Lambda_2}(r_f)\hat{\boldsymbol{w}}^{\Lambda_2}(r;r_f)\right]e^{i[kz+m(\theta-\Omega(r_f)t)]}dr_f\mathcal{H}(r-a)+\\ &\left\{\sum_{b=\pm1}\sum_{n=1}^{\infty}C_{nb}\hat{\boldsymbol{w}}^{\text{Kelvin}}_{nb}(r)e^{-i\omega_n t}-\int_{a^+}^{\infty}\sum_{b=\pm1}\sum_{n=1}^{\infty}\left[X_{\Lambda_1}(r_f)G^{\Lambda_1}_{nb}+X_{\Lambda_2}(r_f)G^{\Lambda_2}_{nb}\right]\right.\\ &\left.\hat{\boldsymbol{w}}^{\text{Kelvin}}_{nb}(r)(e^{-i\omega_n t}-e^{-im\Omega(r_f)t})dr_f\right\}e^{i(kz+m\theta)},\end{aligned} \tag{3.58}$$

with

$$G^{\Lambda_i}_{nb}=\left[\frac{g_i(a)J'_m(k\xi_n a)}{k\xi_n aJ_m(k\xi_n a)}-a\frac{g'_i(a)}{(k\xi_n a)^2}+P_i\right]B^b_n, \tag{3.59}$$

where

$$P_i = \frac{1}{k^2a}\left\{\frac{2\Omega_0 w_r^{\Lambda_i}(a)+i(\omega_n-m\Omega_0)w_\theta^{\Lambda_i}(a)}{(\omega_n-m\Omega_0)^2-4\Omega_0^2}\right\}, \tag{3.60}$$

$$\begin{aligned}g_i(a) &= \int_0^a\frac{\pi r'}{2}\left[\frac{2\Omega_0 ik}{(\omega_n-m\Omega_0)^2}w_z^{\Lambda_i}-\frac{i}{\omega_n-m\Omega_0}\left\{\frac{d}{dr'}(rw_\theta^{\Lambda_i})-imw_r^{\Lambda_i}\right\}\right]\\ &\quad\left\{Y_m(k\xi_n a)J_m(k\xi_n r')-J_m(k\xi_n a)Y_m(k\xi_n r')\right\}dr',\end{aligned} \tag{3.61}$$

and $i=1,2$. $\hat{\boldsymbol{w}}^{\text{Kelvin}}_{nb}(r)$ gives the vorticity eigenfunction of the Kelvin modes, and $\hat{\boldsymbol{w}}^{\Lambda_i}(r;r_f)$ the (singular) vorticity eigenfunctions of the Λ_i family.
Using the expressions for CSM vorticity components, $(w_r^{\Lambda_i}, w_\theta^{\Lambda_i}, w_z^{\Lambda_i})$, from equations (2.62)-(2.64) and (2.75)-(2.77) one could simplify $G^{\Lambda_i}_{nb}$ as:

$$G^{\Lambda_i}_{nb}=\frac{d^{\Lambda_i}}{i(\omega_n-m\Omega)}\frac{M}{(ka)^2K_m(ka)}\frac{1}{4\Omega_0^2-g^2}B^b_n. \tag{3.62}$$

Further from the expressions for X_{Λ_i} and $G^{\Lambda_i}_{nb}$ we have,

$$\begin{aligned}&X_{\Lambda_1}(r_f)G^{\Lambda_1}_{nb}+X_{\Lambda_2}(r_f)G^{\Lambda_2}_{nb}=\frac{1}{i(\omega_n-m\Omega)(ka)^2k_m(ka)}\\ &\left[\left\{kr_fK'_m(kr_f)\left(w_{\theta0}(r_f)-\frac{i}{m}\frac{d}{dr_f}(r_fw_{r0}(r_f))\right)-\frac{i}{m}(kr_f)^2K_m(kr_f)w_{r0}(r_f)\right\}\mathcal{H}(r_f-a)-\right.\\ &\left.\frac{i}{m}ka^2K'_m(ka)w_{r0}(a)\delta(r_f-a)\right]\end{aligned} \tag{3.63}$$

which gives us the following expression for $w_r(r,t)$

$$w_r(r,t) = w_{r0}(r)e^{-im\Omega(r)t}\mathcal{H}(r-a) + \sum_{b=\pm1}\sum_{n=1}^{\infty} C_{nb}\hat{w}^{\text{Kelvin}}_{r,nb}(r)e^{-i\omega_n t} -$$
$$\frac{i}{m}\sum_{b=\pm1}\sum_{n=1}^{\infty} B_{nb}\hat{w}^{\text{Kelvin}}_{r,nb}(r)\int_{a^+}^{\infty}\frac{1}{(ka)^2 k_m(ka)}\left[\left\{kr_f K_m'(kr_f)\left(imw_{\theta 0}(r_f) + \frac{d}{dr_f}(r_f w_{r0}(r_f))\right) + \right.\right.$$
$$\left.\left.(kr_f)^2 K_m(kr_f)w_{r0}(r_f)\right\} + ka^2 K_m'(ka)w_{r0}(a)\delta(r_f-a)\right] Z\, dr_f \tag{3.64}$$
$$\text{where, } Z = \frac{e^{-i\omega_n t} - e^{-im\Omega t}}{-i(\omega_n - m\Omega)}$$

$$\Rightarrow \quad w_r(r,t) = w_{r0}(r)e^{-im\Omega(r)t}\mathcal{H}(r-a) + \sum_{b=\pm1}\sum_{n=1}^{\infty} C_{nb}\hat{w}^{\text{Kelvin}}_{r,nb}(r)e^{-i\omega_n t} -$$
$$\frac{1}{k^2 a}\sum_{b=\pm1}\sum_{n=1}^{\infty} B^b_n\hat{w}^{\text{Kelvin}}_{r,nb}(r)\left\{\tilde{w}_{\theta 0}\mathcal{Z}(a) + \frac{ia}{m}\tilde{w}_{r0}\frac{d\mathcal{Z}}{dr}\Big|_{r=a}\right\} + \sum_{b=\pm1}\sum_{n=1}^{\infty} B^b_n\hat{w}^{\text{Kelvin}}_{r,nb}(r)\int_{a^+}^{\infty}\frac{K_m(kr_f)}{(ka^2)K_m(ka)}$$
$$\left[imw_{r0}(r_f)Z - \frac{d}{dr_f}\left\{r_f\left(w_{\theta 0}(r_f)Z + \frac{ir_f}{m}w_{r0}(r_f)\frac{dZ}{dr_f}\right)\right\}\right] dr_f \tag{3.65}$$

Similarly,

$$w_\theta(r,t) = (w_{\theta 0}(r) - 2\Omega t w_{r0}(r))e^{-im\Omega(r)t}\mathcal{H}(r-a) + \sum_{b=\pm1}\sum_{n=1}^{\infty} C_{nb}\hat{w}^{\text{Kelvin}}_{\theta,nb}(r)e^{-i\omega_n t} -$$
$$\frac{1}{k^2 a}\sum_{b=\pm1}\sum_{n=1}^{\infty} B^b_n\hat{w}^{\text{Kelvin}}_{\theta,nb}(r)\left\{\tilde{w}_{\theta 0}\mathcal{Z}(a) + \frac{ia}{m}\tilde{w}_{\theta 0}\frac{d\mathcal{Z}}{dr}\Big|_{r=a}\right\} + \sum_{b=\pm1}\sum_{n=1}^{\infty} B^b_n\hat{w}^{\text{Kelvin}}_{\theta,nb}(r)\int_{a^+}^{\infty}\frac{K_m(kr_f)}{(ka^2)K_m(ka)}$$
$$\left[imw_{r0}(r_f)Z - \frac{d}{dr_f}\left\{r_f\left(w_{\theta 0}(r_f)Z + \frac{ir_f}{m}w_{r0}(r_f)\frac{dZ}{dr_f}\right)\right\}\right] dr_f \tag{3.66}$$

Recalling the kinematic relation,

$$\mathscr{M}u_z(r,t) = \frac{1}{r}\left[imw_r(r,t) - D(rw_\theta(r,t))\right], \tag{3.67}$$

where $\mathscr{M} = \left(D^2 + 1/rD - m^2/r^2 - k^2\right)$, one obtains:

$$\mathscr{M}u_z(r,t) = \frac{\mathcal{A}}{r}\mathcal{H}(r-a) - (w_{\theta 0}(a) - 2\Omega_0 t w_{r0}(a))e^{-im\Omega_0 t}\delta(r-a) + \sum_{b=\pm1}\sum_{n=1}^{\infty} C_{nb}\mathscr{M}\hat{u}^{\text{Kelvin}}_{z,nb}(r)e^{-i\omega_n t} -$$
$$\frac{1}{k^2 a}\sum_{b=\pm1}\sum_{n=1}^{\infty} B^b_n\mathscr{M}\hat{u}^{\text{Kelvin}}_{z,nb}\left\{\tilde{w}_{\theta 0}\mathcal{Z}(a) + \frac{ia}{m}\tilde{w}_{\theta 0}\frac{d\mathcal{Z}}{dr}\Big|_{r=a}\right\} + \sum_{b=\pm1}\sum_{n=1}^{\infty} B^b_n\ \mathscr{M}\hat{u}^{\text{Kelvin}}_{z,nb}(r)\int_{a^+}^{\infty}\frac{K_m(kr_f)}{(ka^2)K_m(ka)}$$
$$\left[imw_{r0}(r_f)Z - \frac{d}{dr_f}\left\{r_f\left(w_{\theta 0}(r_f)Z + \frac{ir_f}{m}w_{r0}(r_f)\frac{dZ}{dr_f}\right)\right\}\right] dr_f \tag{3.68}$$
$$\hat{u}^{\text{Kelvin}}_{z,nb}(r) = \frac{J_m(k\xi_n r)}{J_m(k\xi_n a)}\mathcal{H}(a-r) + \frac{K_m(kr)}{K_m(ka)}\mathcal{H}(r-a).$$

On inverting the above relation we obtain the expression obtained from IVP, equation (3.56) and (3.57), thus proving the completeness of the modal expansion.

3.3.2 Excitation by a cylindrical vortex sheet : the 3d inviscid resonances

To begin with, we introduce a cylindrical vortex sheet stationed at $r = r_1$ as an initial condition, the associated vorticity field being given by, $w_{r0} = 0$, $w_{\theta 0} = -kr_1V_0/m\ \delta(r-r_1)e^{i(kz+m\theta)}$, $w_{z0} = V_0\delta(r-r_1)e^{i(kz+m\theta)}$ $(r_1 > a)$. The axial component of the velocity field given by (3.56)-(3.57) simplifies to:

$$\tilde{u}_z = \frac{kr_1V_0}{m}e^{i(kz+m\theta)}\Big[kr_1\left\{K'_m(kr_1)I_m(kr)\mathcal{H}(r_1-r) + I'_m(kr_1)K_m(kr)\mathcal{H}(r-r_1)\right\}e^{-im\Omega_1 t} + \sum_{b=\pm1}\sum_{n=1}^{\infty} B_n^b\hat{u}^{\text{Kelvin}}_{z,nb}(r)\frac{kr_1K'_m(kr_1)}{(ka)^2K_m(ka)}\frac{e^{-i\omega_n t}-e^{-im\Omega_1 t}}{i(\omega_n - m\Omega_1)}\Big], \tag{3.69}$$

where $\Omega_1 = \Omega(r_1) = \dfrac{\Omega_0 a^2}{r_1^2}$ and $\hat{u}^{\text{Kelvin}}_{z,nb}(r) = \dfrac{J_m(k\xi_n r)}{J_m(k\xi_n a)}\mathcal{H}(a-r) + \dfrac{K_m(kr)}{K_m(ka)}\mathcal{H}(r-a)$.

Using equations (3.33),(3.35),(3.46) and (3.47) and performing the necessary inverse Laplace transform we can also obtain the radial component of the velocity disturbance field given by,

$$\tilde{u}_r = \frac{r_1V_0}{mr}e^{i(kz+m\theta)}\Big[-ikr_1\left\{K'_m(kr_1)I'_m(kr)\mathcal{H}(r_1-r) + I'_m(kr_1)K'_m(kr)\mathcal{H}(r-r_1)\right\}e^{-im\Omega_1 t} + \sum_{b=\pm1}\sum_{n=1}^{\infty} B_n^b\hat{u}^{\text{Kelvin}}_{r,nb}(r)\frac{kr_1K'_m(kr_1)}{(ka)^2K_m(ka)}\frac{e^{-i\omega_n t}-e^{-im\Omega_1 t}}{i(\omega_n - m\Omega_1)}\Big], \tag{3.70}$$

where

$$\hat{u}^{\text{Kelvin}}_{r,nb}(r) = \frac{1}{\xi_n^2}\left\{\frac{2im\Omega_0}{(\omega_n - m\Omega_0)}\frac{J_m(k\xi_n r)}{J_m(k\xi_n a)} - i\frac{k\xi_n rJ'_m(k\xi_n r)}{J_m(k\xi_n a)}\right\}\mathcal{H}(a-r) - \frac{iK'_m(kr)}{K_m(ka)}\mathcal{H}(r-a).$$

The velocity field at $t = 0$, obtained from (3.69)-(3.70), represents the velocity field induced by a vortex sheet, threaded by helical vortex lines. This may also be deduced from Biot-Savart law. Incidentally, since a helical vortex filament is a Fourier summation of helical vortex sheets over all m for a fixed pitch, one can sum (3.69) and (3.70) over all m keeping m/k fixed to obtain the Kapteyn series representation of velocity field induced by a helical vortex filament (Hardin [1982]).

Now we examine the secular limits, $m\Omega_1 \to \omega_j$, $j \in (1, n)$ (and $b = +1$) in (3.69), which lead to resonant interactions of the continuous spectrum and the 3D discrete spectrum. Unlike the 2D case, herein we have a denumerable infinity of discrete modes interacting with the continuous spectrum, and therefore from the perspective of identifying the most dangerous disturbance, one needs to identify the strongest resonant excitation and its variation with both m and k. From

(3.69),the resonant solution can be written as,

$$\tilde{u}_z = \frac{kr_1 V_0}{m} e^{i(kz+m\theta)} \Big[kr_1 \left\{ K'_m(kr_1) I_m(kr) \mathcal{H}(r_1 - r) + I'_m(kr_1) K_m(kr) \mathcal{H}(r - r_1) \right\} e^{-i\omega_j t} + \sum_{b=\pm 1} \sum_{\substack{n=1 \\ n \neq j \cup b \neq 1}}^{\infty} B_n^b \hat{u}_{z,nb}^{\text{Kelvin}}(r) \frac{kr_1 K'_m(kr_1)}{(ka)^2 K_m(ka)} \frac{e^{-i\omega_n t} - e^{-i\omega_j t}}{i(\omega_n - \omega_j)} - t B_j^1 \hat{u}_{z,j1}^{\text{Kelvin}}(r) \frac{kr_1 K'_m(kr_1)}{(ka)^2 K_m(ka)} e^{-i\omega_j t} \Big] \tag{3.71}$$

$$\tilde{u}_r = \frac{kr_1 V_0}{m} e^{i(kz+m\theta)} \Big[-ikr_1 \left\{ K'_m(kr_1) I'_m(kr) \mathcal{H}(r_1 - r) + I'_m(kr_1) K'_m(kr) \mathcal{H}(r - r_1) \right\} e^{-i\omega_j t} + \sum_{b=\pm 1} \sum_{\substack{n=1 \\ n \neq j \cup b \neq 1}}^{\infty} B_n^b \hat{u}_{r,nb}^{\text{Kelvin}}(r) \frac{kr_1 K'_m(kr_1)}{(ka)^2 K_m(ka)} \frac{e^{-i\omega_n t} - e^{-i\omega_j t}}{i(\omega_n - \omega_j)} - t B_j^1 \hat{u}_{r,j1}^{\text{Kelvin}}(r) \frac{kr_1 K'_m(kr_1)}{(ka)^2 K_m(ka)} e^{-i\omega_j t} \Big] \tag{3.72}$$

where ω_j is the frequency of the resonant Kelvin mode, and the term in the original summation, with $n = j$, now appears as the $O(t)$ secular contribution in 3.71 and 3.72. Since resonance occurs by way of a cylindrical vortex sheet located at one of the Kelvin critical radii, one can resonate only the retrograde Kelvin modes. Further by finding the energy as a function of time for each of these resonant modes, one may quantify the wave-number dependence of the 3D resonant growth rates; this is done in section 3.3.4. It is also worth noting that, due to the absence of critical radii, there cannot be a resonant growth for axisymmetric Kelvin modes in the linear regime.

In section 3.2.3, there was a discussion on studies related to the resonant interaction of the continuous and discrete spectra in various plane parallel flow problems. A problem that is relevant to the 3D inviscid resonances analyzed here is the short wavelength instability of a vortex column in the presence of a straining flow that is popularly known as the elliptic instability. The ambient flow allows for parametric resonances between Kelvin modes of different azimuthal wavenumbers, and the discrete spectrum is fundamentally altered that there are now unstable modes. But, the inviscid resonances and the resulting algebraic growth rates resulting from the resonances between the discrete and continuous spectra would seem to only be marginally altered by the imposed strain, and thus our analysis would continue to hold (over the time scales short compared to that of the (weak) instability). A relevant issue then is the relative importances of the exponential and algebraic growth responses. Fukumoto [2003] mentions that the possibility of resonance between continuous and discrete spectrum needs to be explored. The linearized scenario discussed here may also be modified in a non-trivial manner by non-linear effects. For instance, although there is no resonance possible for axisymmetric modes at linear order, with the inclusion of non-linear effects, one may have a resonance arising from a vortex ring wrapped around a vortex column that propagates at a speed close to the group velocity of a axisymmetric vortex wave resonance occurs. In the linear theory the ring is considered stationary, excluding possibility of resonance.

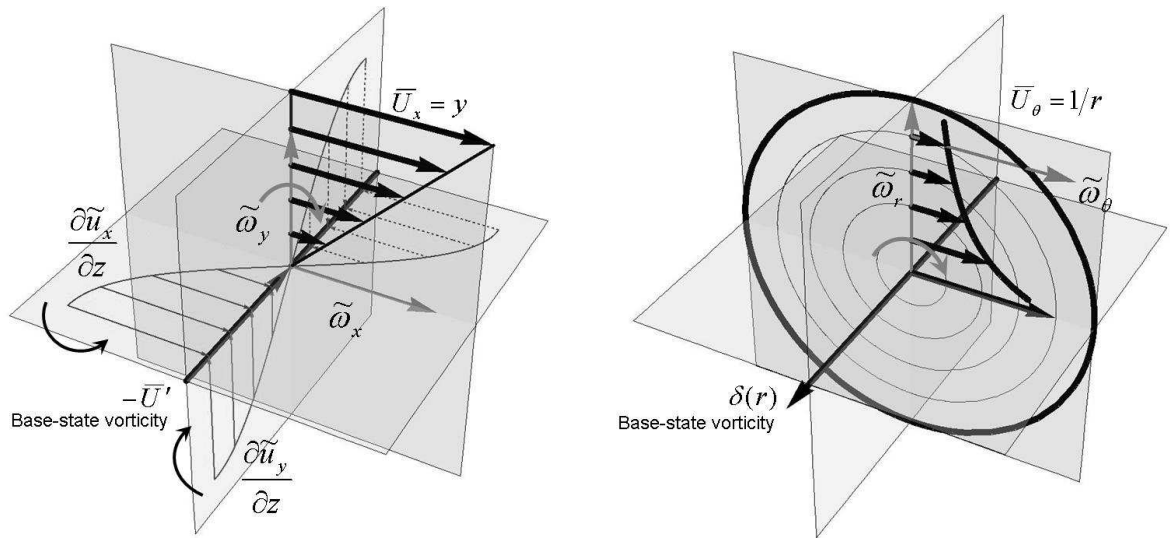

(a) Parallel shear flow - plane couette

(b) Curvilinear shear flow - point vortex

Figure 3.8: Algebraic growth in shear flow due to stretching/tilting of vortex lines.

3.3.3 Excitation by a vortex 'ribbon' (with radial vorticity) : the 3D inviscid (enhanced) resonances

In the context of the transient growth mechanisms in 3D, a reference was made to the algebraic growth (linear in t) associated with an initial radial vorticity perturbation arising from a vortex tilting and stretching mechanism (Pradeep & Hussain [2006]). This may be seen simply by considering the evolution of a perturbation vorticity field in a pure straining flow (due to a point vortex). The governing equations may be written as,

$$\begin{aligned} L\tilde{w}_r &= 0, \\ L\tilde{w}_z &= 0 \\ L\tilde{w}_\theta &= \tilde{w}_r r\Omega', \\ \text{where } L &= \frac{\partial}{\partial t} + im\Omega. \end{aligned} \tag{3.73}$$

The perturbation vorticity field at time t is given by,

$$\tilde{w}_r(r,t) = \tilde{w}_r(r,0)e^{-im\Omega(r)t}, \tag{3.74}$$

$$\tilde{w}_z(r,t) = \tilde{w}_z(r,0)e^{-im\Omega(r)t}, \tag{3.75}$$

$$\tilde{w}_\theta(r,t) = \tilde{w}_\theta(r,0)e^{-im\Omega(r)t} + \tilde{w}_r(r,0)r\Omega' t\, e^{-im\Omega(r)t}. \tag{3.76}$$

Thus, although both radial and axial vorticity components get convected by the flow, an initial ω_r will produce an ω_θ contribution proportional to t in the presence of background strain. The evolution can be visualized as one leading from azimuthal streaks to azimuthal rolls, and therefore been termed as the *anti-lift-up* effect (Antkowiak & Brancher [2007]). The reason is, of course, that the well-known *lift-up* effect, a transient growth mechanism relevant to parallel flows, may be visualized as producing stream-wise *streaks* from stream-wise *rolls*. The popular explanation is one in terms of momentum transport: Schmid & Henningson [2001]. This dy-

namics is consistent with observations, in simulations, of (Melander & Hussain [1993]) vortex turbulence interactions being characterized by vortex-ring structures wrapped around the vortex column.

Despite the aforementioned terminology, both *anti-lift-up* and *lift-up* effects may be explained in a consistent way based on (inviscid) vorticity dynamics. Figure 6.1 depicts the algebraic growth resulting from vortex stretching/tilting in both parallel and curvilinear shear flows. In the parallel shear flow case, the *lift-up* effect arises because the vertical shear in the mean vorticity direction, due to a spanwise variation in the vertical perturbation velocity ($\partial\tilde{u}_y/\partial z$: a 'roll' initial condition) can tilt the mean vorticity ($-\overline{U}'$), producing wall-normal perturbation vorticity ($\tilde{\omega}_y$: streak). One might be led to also conclude that a stretching-tilting of $\tilde{\omega}_y$ by the mean shear ($\overline{U}'$) to produce $\tilde{\omega}_x$, the parallel-flow analog of the *anti-lift-up*, is another possible mechanism of algebraic growth. But such a contribution exactly cancelled by the tilting of the base-state vorticity ($-\overline{U}'$) by a spanwise variation of horizontal perturbation velocity ($\partial\tilde{u}_x/\partial z$: this is responsible for $\tilde{\omega}_y$ in the first place). Thus, only the 'lift-up' mechanism survives. For the curvilinear shear flow induced by a point vortex, the base-state vorticity is zero everywhere in the flow except at the origin (where perturbation shear-rates vanish), and the *lift-up* mechanism is therefore absent in this case. On the other hand, the second mechanism which was absent in parallel flow due to a precise cancellation, persists in the curvilinear case and the radial perturbation vorticity, $\tilde{\omega}_r$ gets stretched-tilted by mean shear to produce $\tilde{\omega}_\theta$.

Now, we illustrate the stronger growth possible when the above growth mechanism for a point vortex is coupled with the resonant interaction possible for the Rankine vortex. To see this, we consider a localized initial condition with radial vorticity, a so-called localized vortex 'ribbon', of the form:

$$w_{r0} = -ikr_1V_0\,\delta(r-r_1)e^{i(kz+m\theta)}, \tag{3.77}$$

$$w_{z0} = V_0r_1^2/r\,\delta'(r-r_1)e^{i(kz+m\theta)}\ \ (r_1>a). \tag{3.78}$$

The above initial conditions are generalized function limits of the smooth initial conditions used by Pradeep & Hussain [2006] for studying the transient growth (see figure 3.9), and the associated optimal perturbations, of a top-hat vortex. For resonance, r_1 is chosen to be the

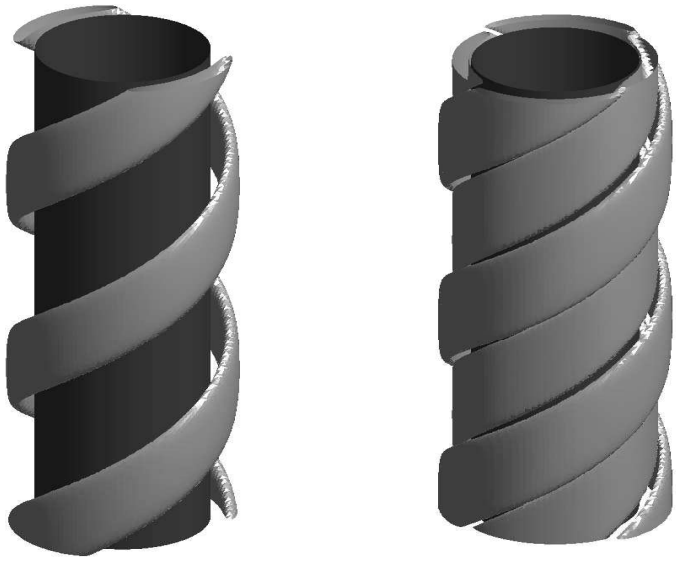

Figure 3.9: Isosurfaces of initial perturbation vorticity wrapped around the vortex column. Smooth versions of generalized function initial condition used (Pradeep & Hussain [2006]). (a) w_r (3.77), (b) w_z (3.78)

critical radius of a Kelvin mode, ω_j, and from (3.56)-(3.57) one obtains:

$$\tilde{u}_z = ikr_1V_0e^{i(kz+m\theta)}\Big[\{(imK_m(kr_1) - 2\Omega_1 t\ kr_1K'_m(kr_1))I_m(kr)\mathcal{H}(r_1-r) + (imI_m(kr_1) - 2\Omega_1 t\ kr_1I'_m(kr_1))K_m(kr)\mathcal{H}(r_1-r)\}e^{-i\omega_j t} + \sum_{b=\pm1}\sum_{\substack{n=1\\ n\neq j\cup b\neq 1}}^{\infty} B_n^b\hat{u}_{z,nb}\left\{\frac{mK_m(kr_1)}{(ka)^2K_m(ka)}\frac{e^{-i\omega_n t}-e^{-i\omega_j t}}{(\omega_n-\omega_j)} - 2\Omega_1\frac{kr_1K'_m(kr_1)}{(ka)^2K_m(ka)}\ \frac{e^{-i\omega_n t}-(1-i(\omega_n-\omega_j)t)e^{-i\omega_j t}}{(\omega_n-\omega_j)^2}\right\} - B_j^1\hat{u}_{z,j1}\frac{\{imK_m(kr_1)-\Omega_1 tkr_1K'_m(kr_1)\}}{(ka)^2K_m(ka)}te^{-i\omega_j t}\Big] \tag{3.79}$$

$$\tilde{u}_r = ikr_1V_0e^{i(kz+m\theta)}\Big[-i\{(imK_m(kr_1) - 2\Omega_1 t\ kr_1K'_m(kr_1))I'_m(kr)\mathcal{H}(r_1-r) + (imI_m(kr_1) - 2\Omega_1 t\ kr_1I'_m(kr_1))K'_m(kr)\mathcal{H}(r_1-r)\}e^{-i\omega_j t} + \sum_{b=\pm1}\sum_{\substack{n=1\\ n\neq j\cup b\neq 1}}^{\infty} B_n^b\hat{u}_{r,nb}\left\{\frac{mK_m(kr_1)}{(ka)^2K_m(ka)}\frac{e^{-i\omega_n t}-e^{-i\omega_j t}}{(\omega_n-\omega_j)} - 2\Omega_1\frac{kr_1K'_m(kr_1)}{(ka)^2K_m(ka)}\ \frac{e^{-i\omega_n t}-(1-i(\omega_n-\omega_j)t)e^{-i\omega_j t}}{(\omega_n-\omega_j)^2}\right\} - B_j^1\hat{u}_{r,j1}\frac{\{imK_m(kr_1)-\Omega_1 tkr_1K'_m(kr_1)\}}{(ka)^2K_m(ka)}te^{-i\omega_j t}\Big] \tag{3.80}$$

where we note that, in contrast to (3.71) and (3.72), the dominant term in (3.80) and (3.80) is $O(t^2)$. Thus, as expected, the presence of radial vorticity transforms the linear resonant growth in section 3.3.2 to a quadratic one. If one instead proceeds with a smooth initial conditions with a finite spatial extent (the ones described in Pradeep & Hussain [2006]) then, akin to 2D calculations, the resonant behavior would eventually be quenched by long time phase-mixing of the continuous spectrum modes, and the long time response would be large amplitude discrete mode superposition. For any finite Re, the phase-mixing leading to progressive fine-scaling of the perturbation vorticity will be arrested at a time $O(\mathrm{Re}^{1/3})$ when transverse viscous diffusion

becomes comparable to differential shear, and a steady spiral structure with a downstream tilt results; this is confirmed by simulations (Pradeep & Hussain [2006]).

3.3.4 Energetics

We define,

$$E(m,k,t) = \frac{1}{2}\int_0^\infty \{u_r u_r^* + u_\theta u_\theta^* + u_z u_z^*\}\, r dr, \tag{3.81}$$

the leading order behavior of energy for large time, for both vortex-sheet and vortex-ribbon initial conditions, can be found from (3.71) and (3.80). For this purpose, we use the following integrals:

$$\int_0^{r_1} x\left\{(I_m'(kx))^2 + \left(1+\frac{m^2}{(kx)^2}\right)(I_m(kx))^2\right\} dx = \frac{r_1 I_m(kr_1) I_m'(kr_1)}{k} \tag{3.82}$$

$$\int_{r_1}^\infty x\left\{(K_m'(kx))^2 + \left(1+\frac{m^2}{(kx)^2}\right)(K_m(kx))^2\right\} dx = -\frac{r_1 K_m(kr_1) K_m'(kr_1)}{k} \tag{3.83}$$

a) Resonance (Cylindrical vortex sheet) -
$w_r(\boldsymbol{x},0) = 0;\;\; w_\theta(\boldsymbol{x},0) = -kr_1 V_0/m\;\delta(r-r_1)e^{i(kz+m\theta)};\;\; w_z(\boldsymbol{x},0) = V_0\delta(r-r_1)e^{i(kz+m\theta)}$

$$\frac{E(m,k,t_{max})}{E(m,k,0)} = -\frac{\mathcal{H}}{r_1^2 I_m'(kr_1)K_m'(kr_1)}\, t_{max}^2 + O(t_{max}) \tag{3.84}$$

b) Vortex stretch-tilt enhanced resonance (Vortex 'ribbon') -
$w_r(\boldsymbol{x},0) = -ikr_1 V_0\;\delta(r-r_1)e^{i(kz+m\theta)};\;\; w_\theta(\boldsymbol{x},0) = 0;\;\; w_z(\boldsymbol{x},0) = V_0 r_1^2/r\;\delta'(r-r_1)e^{i(kz+m\theta)}$

$$\frac{E(m,k,t_{max})}{E(m,k,0)} = \left(\frac{k}{m}\right)^2 \frac{\mathcal{H}}{I_m(kr_1)K_m(kr_1)}\,\Omega_1^2\, t_{max}^4 + O(t_{max}^3) \tag{3.85}$$

where

$$\mathcal{H} = \left(\frac{a|\chi|}{2\xi_j J_m(\beta_j a)(\omega_j - m\Omega_0)}\right)^2 \left[\mathcal{C}_+^2\{J_{m-1}^2(\beta_j a) - J_{m-2}(\beta_j a)J_m(\beta_j a)\} + \right.$$
$$\left. \mathcal{C}_-^2\{J_{m+1}^2(\beta_j a) - J_{m+2}(\beta_j a)J_m(\beta_j a)\} - 2\mathcal{C}_+\mathcal{C}_-\{J_m^2(\beta_j a) - J_{m-1}(\beta_j a)J_{m+1}(\beta_j a)\}\right] - \frac{a|\chi|^2 K_m'(ka)}{kK_m(ka)} \tag{3.86}$$

$$\chi = -B_j^1 \frac{kr_1 K_m'(kr_1)}{(ka)^2 K_m(ka)} \quad \text{and} \quad \mathcal{C}_\pm = \omega_j - (m\pm 2)\Omega_0 \tag{3.87}$$

and, within the inviscid framework as applied to a Rankine vortex, t_{max} is an arbitrarily chosen time instant large enough for the strongest algebraic growth to become prominent. Figure 3.10 shows a comparison between the energy computed due to the singular forcings (including the sub-dominant secular contributions and the non-secular contribution of the Kelvin-mode superposition), and the corresponding leading order secular behaviors. This then gives an idea of the t_{max} beyond which (3.84) and (3.85) closely approximated the growth in perturbation energy. A finite duration of growth, and therefore growth rather than a growth-rate spectrum,

can result from the finite spatial extent of the initial condition, a finite Re or from considering a smooth Rankine-like profile instead (wherein the neutrally stable discrete modes are replaced by decaying quasi-modes).

The above secular growth will be arrested via shear-induced dispersion for a smooth initial condition (section 3.2.3) and for finite Re, viscosity. t_{max} would then assume the role of a cut-off time, beyond which growth is no longer possible. For non-axisymmetric modes, shear-enhanced diffusion is possibly the dominant mechanism - predicting a $O((Re/m^2)^{1/3})$ viscous cut-off time-scale (where Re has been defined based on the local shear-rate). Figure 3.11 illustrates the k-dependence of the normalized energy growth-rate spectrum (3.84) and (3.85) for various m. For pure resonance (cylindrical vortex sheet initial condition) the $k = 0$ case, figure 3.11(a), experiences the largest growth ($\Omega_0^2((m-1)/m)^m$ being the limiting value). With the additional coupling to a stretch-tilt mechanism (figure 3.11(b)), the surprising persistence of quartic growth for $k \to 0$ is on account of the limiting dipole initial condition for ω_z which is equivalent to a source localized at the resonant radius.

That inviscid dynamics associated with a Rankine vortex captures the essential physics of the transient growth observed for vortex columns, may be seen from a qualitative comparison of the growth-rate spectrum in figure 3.12(a) with the results of recent simulations (linearized viscous DNS) for finite Re. Figure 3.12(a) shows that the peak growth-rate, for $m = 1$, occurs at $k \approx 1.2$ while the predicted by the numerical simulations (Pradeep & Hussain [2010], see figure 3.12(b)) at $k \approx 1.35$; a confirmation of earlier claims based on finite Re numerics that the peak owes its orgin due to resonance of Kelvin modes. Of course, the comparison is by no means complete since a growth-rate spectrum in figure 3.12(a) for a transversely coherent initial condition is being compared to the maximum growth rate envelope for a simulation that includes the growth due to the Orr mechanism for an initial condition in the form of a leading spiral. Thus, ideally, one must include the effects of the Orr mechanism in the former case over a time period of $O(\mathrm{Re}^{1/3})$; but, we expect this to leave the k-dependence unaltered. Although the secondary peaks in figure 3.12(a) are not observed in Pradeep & Hussain [2010], the calculation of Antkowiak & Brancher [2004] clearly identifies them. Figure 3.13 shows this interesting mode-hopping behavior in detail for $m = 2$ (present for all m); wherein with increasing k, the largest growth-rate is attained by modes with increasing structure (termed the Bessel modes). This mode-hopping behavior has been observed in linearized viscous calculations (Antkowiak [2005]). It is worth noting that one expects that any resemblance between the inviscid predictions, and actual finite Re numerics, to deteriorate with increasing k on the one hand due to the increasing importance of viscosity for a fixed m, and one other hand because the behavior at large k is governed by increasingly structured Bessel modes in which case the importance of viscosity is even more important.

3.3.5 Excitation by an axisymmetric vortex sheet

Departing from the asymmetric initial conditions focussed so far, in this section, we briefly consider an axisymmetric initial condition in the form of a cylindrical vortex sheet with only azimuthal vorticity, $\omega_\theta = V_0\ \delta(r - r_1)e^{ikz}$, r_1 again being a radial location in the irrotational

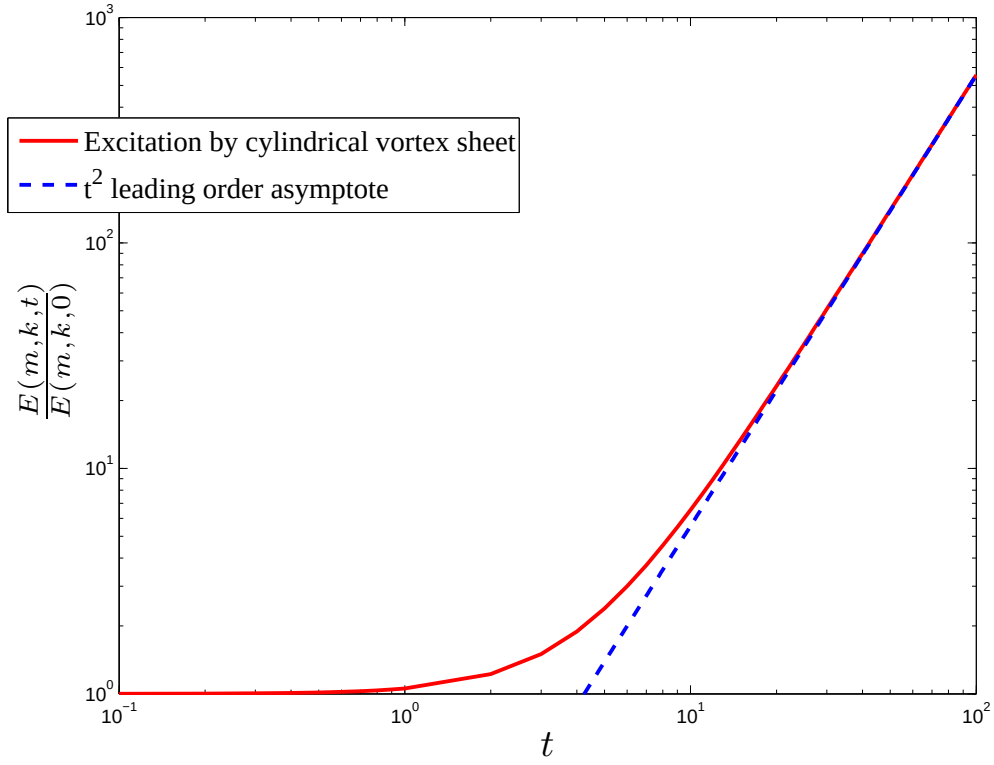

(a) Pure resonance ($\omega_r = 0$)

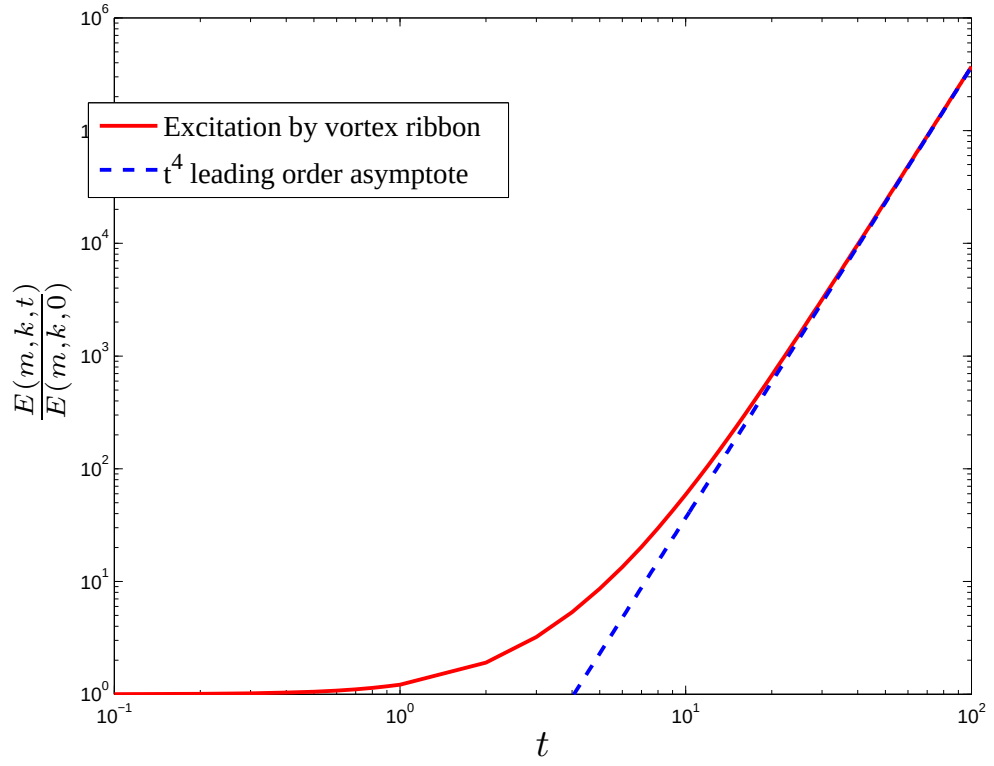

(b) Vortex stretch-tilt enhanced resonance ($\omega_r \neq 0$)

Figure 3.10: Temporal evolution of $E(m,k,t)/E(m,k,0)$ computed for (a) a cylindrical vortex sheet forcing (3.71-3.72) and comparison with the predicted leading order behavior (3.84); (b) a vortex 'ribbon' forcing (3.80-3.80) and comparison with the predicted leading order behavior (3.85)

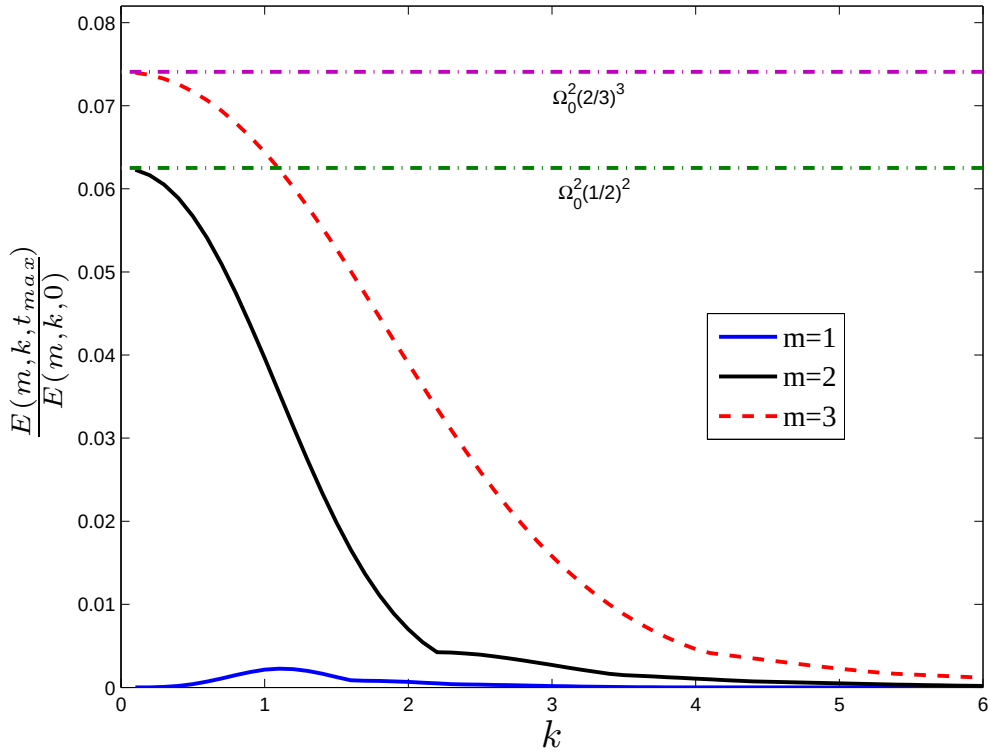

(a) Pure resonance ($\omega_r = 0$)

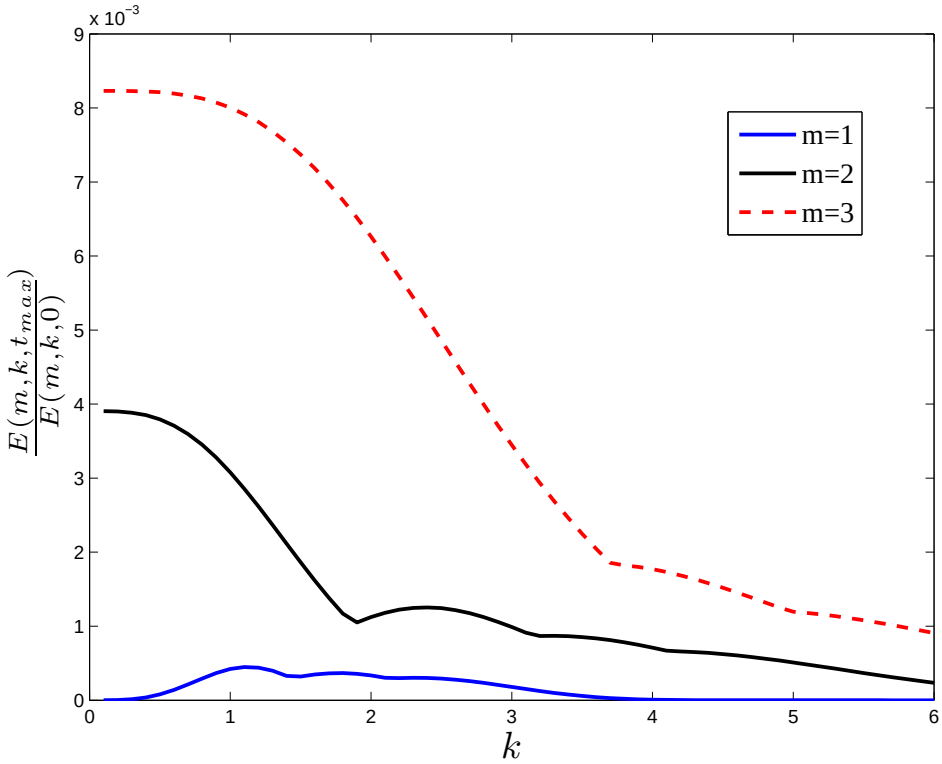

(b) Vortex stretch-tilt enhanced resonance ($\omega_r \neq 0$)

Figure 3.11: The normalized energy growth-rate spectrum ($a = 1, \Omega_0 = 0.5, t_{max} = 1$ in both cases) for vortex-sheet resonance initial condition (a) and vortex stretch-tilt enhanced resonance condition (b).

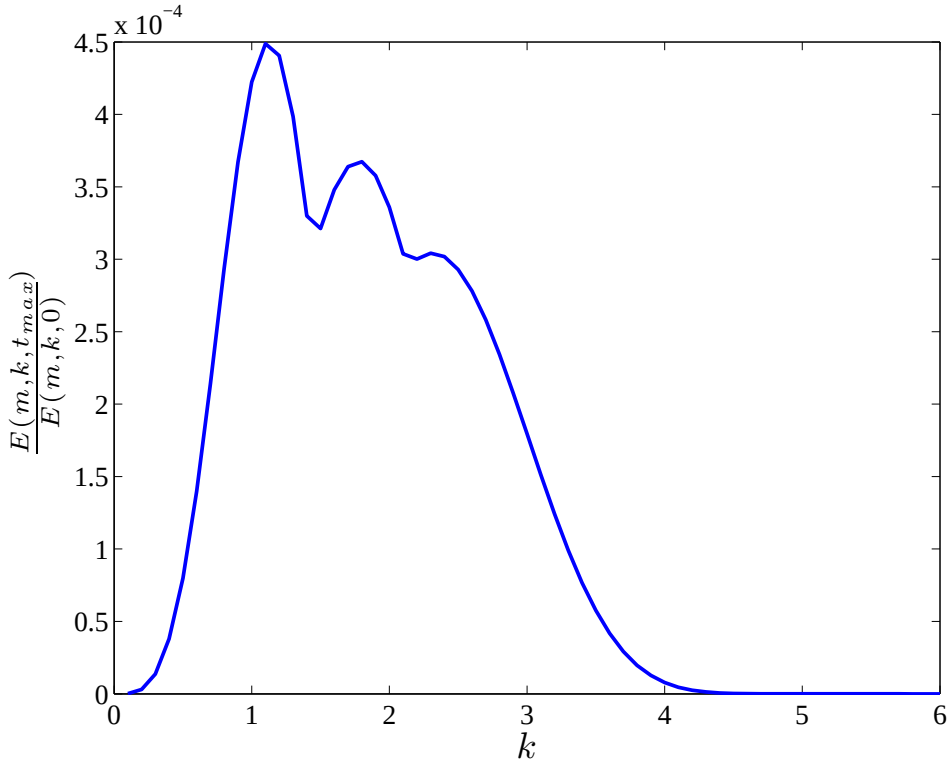

(a) $m = 1$ (present calculations)

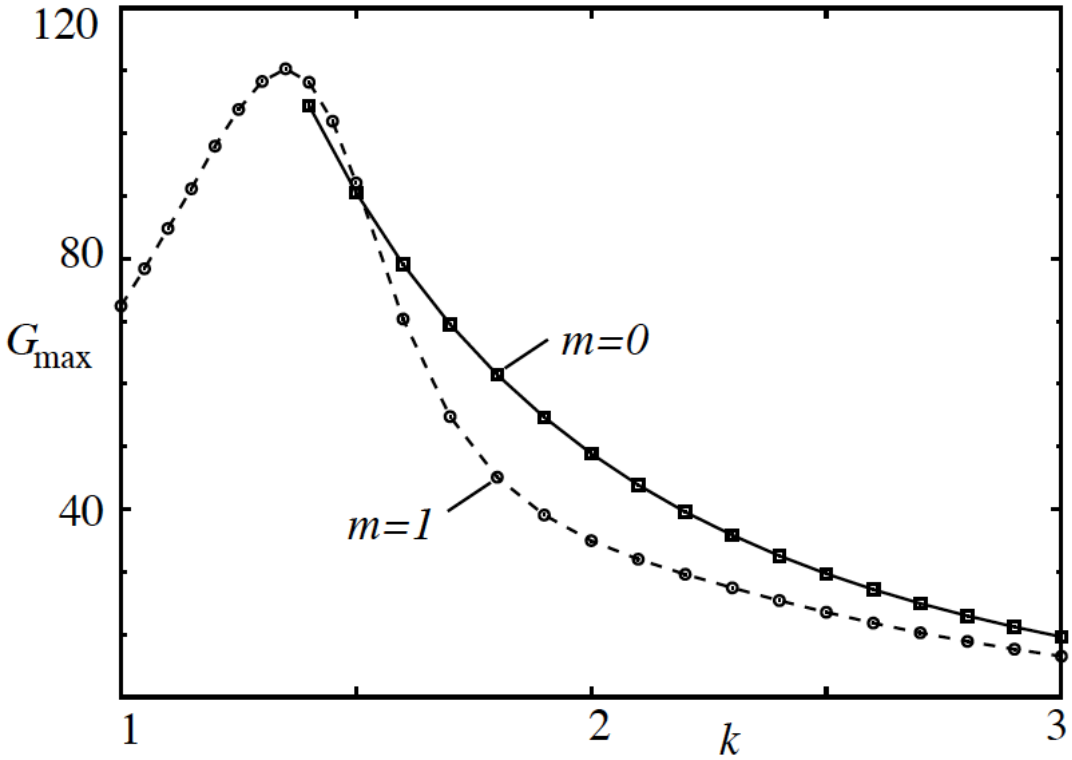

(b) $m = 0, 1$ (optimal perturbation calculations from Pradeep & Hussain [2010])

Figure 3.12: The non-zero k peak for the growth-rate spectrum for $m = 1$ from a) present calculations (initial condition is vortex stretch-tilt enhanced resonance) and its comparison to b) the 'Gain' curve obtained via optimal perturbation calculations (Pradeep & Hussain [2010])

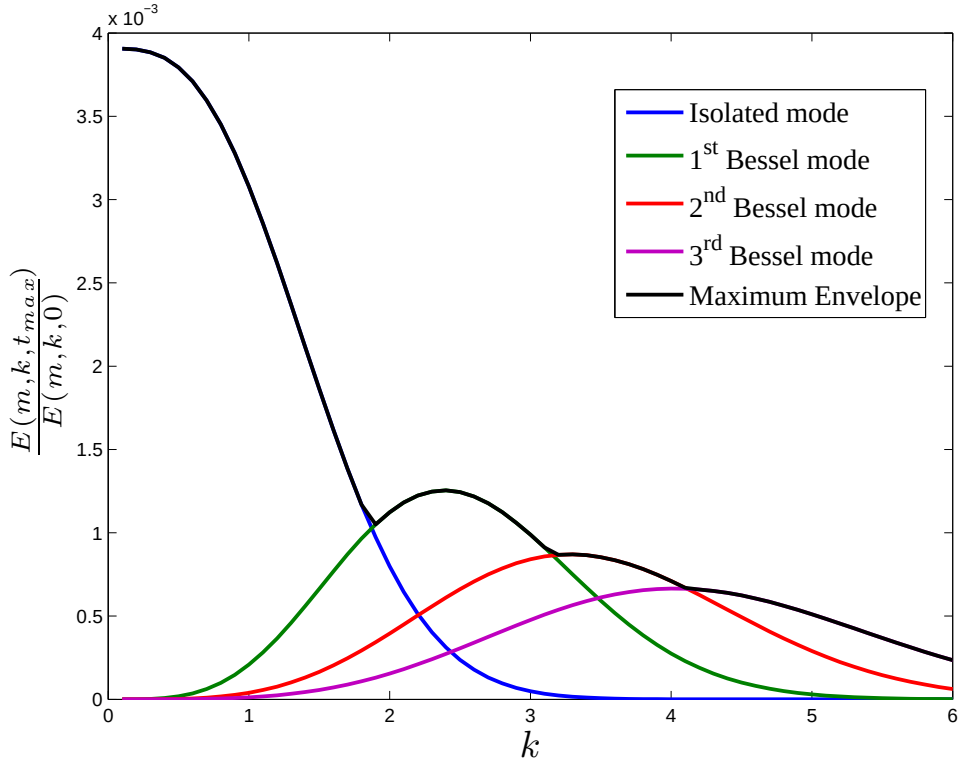

Figure 3.13: Evidence of mode-hopping in the normalized energy growth-rate spectrum for $m = 2$ (initial condition is vortex stretch-tilt enhanced resonance).

exterior. The velocity field can be shown to be,

$$\tilde{u}_z = -V_0 e^{ikz}\Big[kr_1\left\{K_0'(kr_1)I_0(kr)\mathcal{H}(r_1-r) + I_0'(kr_1)K_0(kr)\mathcal{H}(r-r_1)\right\} + \sum_{b=\pm 1}\sum_{n=1}^{\infty} B_n^b \hat{u}_{z,nb}^{\text{Kelvin}}(r)\frac{kr_1K_0'(kr_1)}{(ka)^2K_0(ka)}\frac{e^{-i\omega_n t}-1}{i\omega_n}\Big]. \tag{3.88}$$

Inside the core the velocity field considerably simplifies to:

$$\tilde{u}_z = -V_0 e^{ikz}\sum_{b=\pm 1}\sum_{n=1}^{\infty} B_n^b \frac{J_0(k\xi_n r)}{J_0(k\xi_n a)}\frac{kr_1K_0'(kr_1)}{(ka)^2K_0(ka)}\frac{e^{-i\omega_n t}}{i\omega_n} \tag{3.89}$$

The cancelling of the summation term independent of t with the first term in 3.88 is a result of the Dini series form of the summation term given by,

$$I_0(kr) = \sum_{b=\pm 1}\sum_{n=1}^{\infty} B_n^b \frac{J_0(\beta_n r)}{J_0(\beta_n a)}\frac{1}{(ka)^2K_0(ka)}\frac{1}{i\omega_n} \tag{3.90}$$

(This result is proved in Appendix G). Thus, rather surprinsingly, a steady axisymmetric vortex sheet excites only a purely oscillatory (zero mean) Kelvin mode response inside the vortex core. Recall from chapter 2 that for the axisymmetric case, the continuous spectrum consists of those steady modes for which the velocity field vanishes inside the core. The constraint of a quiescent core takes the form:

$$\int_1^{\infty} \Psi(r')kr'K_0'(kr')dr' = 0 \tag{3.91}$$

A canonical member of the axisymmetric continuous spectrum mode consists of two vortex sheets located outside the core at $r = a$ and $r = b$ such that the ratio of their amplitudes is $-bK_0'(kb)/(aK_0'(ka))$. Although the mechanism of resonance is absent in the axisymmetric case, it serves as a nice basis for studying response of a vortex column to an arbitrary axisymmetric structure, the most important of them being a vortex ring. As discussed before, since the simulations of Melander & Hussain [1993] - vortex rings wrapped around vortex column has been considered a persistent feature of vortex column - external turbulence interaction (Miyazaki & Hunt [2000], Antkowiak & Brancher [2007]). Marshall [1997] peformed a numerical study of periodic vortex ring wrapped around a vortex column. Rings of weak strength induced standing waves in the core and as they became stronger they led to vorticity being ejected radially outward from the column in form thin sheets which wrapped around the rings.
In appendix E it is shown that the velocity field due to a vortex ring is the integral of velocity field of a helical vortex sheet over the entire $k-$space.

$$\tilde{\boldsymbol{u}}_{ring} = \frac{\Gamma}{2\pi}\int_{-\infty}^{\infty} \tilde{\boldsymbol{u}}_{sheet}\, dk \tag{3.92}$$

Thus we the perturbation velocity field obtained for an axisymmetric vortex sheet would provide the response of a vortex column to a vortex ring of infinitesimal thickness and of finite thickness correspondingly.

3.4 Conclusion

In this chapter we have analyzed the Cauchy initial value problem for a Rankine vortex, both in 2D and 3D, and have shown its equivalence to the modal superposition derived in the chapter 2, involving both the discrete and continuous spectrum modes. The equivalence proved the completeness of the modal description. The IVP approach further iterates the importance of the continuous spectrum modes in acting as a mediator between external vortical disturbances and the vortex column, a fact crucial in early stages of vortex - turbulent field interactions. Qualitative comparisons between the growth-rate spectra for vortex 'ribbons obtained here, with the growth-rate spectra obtained in numerical studies on more realistic vorticity profiles (e.g., the Lamb Oseen profile) and for finite Re ($\sim 10^4$), are encouraging.

For $m = 0$, in absence of resonance, the algebraic growth arising from vortex stretch-tilt gets terminated on a viscous time-scale, $O(\mathrm{Re})$. To adopt a more detailed quantitative comparison one needs to account for the variation of optimal time (viscous cut-off time) with k as observed in numerics unlike the constant t_{max} assumption made here.

Chapter 4

Elastic instability of a vortex column

4.1 Introduction

Non-Newtonian/complex fluids are ubiquitous in our everyday life, challenging the classical distinction of fluids from solids. They cover a wide genre of materials, ranging from volcanic lava to the comparatively mundane toothpaste. Although complex fluids include, a whole range of materials with differing microstructural constituents, for instance, polymeric liquids and melts, colloidal suspensions, micellar solutions, foams and liquid crystals, we will be restricting our attention in this chapter to dilute polymeric solutions. The distinguishing trait of such fluids is the presence of a microstructure, consisting of non-interacting macromolecules, that relaxes on macroscopic time scales (ranging from milliseconds to seconds, and even longer depending primarily on the solvent viscosity). The elasticity endowed by such relaxation has several striking consequences (many of which are well documented in textbooks; e.g. rod climbing, die swell and tubeless siphon; Bird *et al.* [1987]). The aforementioned textbook examples show that the elasticity present is often responsible for completely altering the flow from that observed for Newtonian fluids. The the role of elasticity to either suppress or trigger instabilities (see examples below) in various flows have been of immense interest to researchers in fluid dynamics for a long time. A primary reason for such an interest has been the implications of such instabilities in the polymer and food processing industry. A little over two decades back, the seminal efforts of Phan-Thein [1985] led to the rather surprising discovery of purely elastic instabilities prevalent in the canonical viscometric flow geometries (e.g. - cone and plate flow that are typically used for purposes of rheological characterization). Viscoelastic instabilities next received an impetus with the discovery of elastic instabilities in inertia-less swirling flows beyond cone and plate geometries (Larson *et al.* [1990],Larson. [1992]). It has been argued that (Shaqfeh [1996]) such elastic instabilities are driven by base-state hoop stresses, and instability sets in above a threshold value of a dimensionless parameter known as the Deborah number (De) (De is a dimensionless parameter that denotes the ratio of the elastic to flow time scales[1]). For instance, Taylor-Couette flow of a dilute polymer solution is unstable, even at zero Re, above a certain De_c. In contrast, viscoelastic Couette flow is known to be linearly stable (exponentially) for all De (Renardy [1992]); instability due to hoop stresses, associated with curved streamlines, only sets in at a non-linear order (Morozov & van Saarloos [2005]). It has been experimentally demonstrated that the primary linear instability, followed by the sequences of secondary instabilities leads to a statistically stationary disorderly flow that, on account of its resemblance to Newtonian turbulence, has been elastic turbulence (Groisman & V.Steinberg [2000]).

[1]For a constitutive model with a single relaxation time, De is the only parameter once effects of shear thinning are neglected. Actual polymer molecules, of course, possess a spectra of relaxation times, and the relevant time scale, from the point of view of defining an instability threshold, is the longest one.

Elasticity also plays an important role in flows where inertia is significant. A canonical example is the phenomenon of turbulent drag reduction. The phenomenon which was first reported way back in 1949, entails a reduction in the turbulent drag of up to 80% upon introduction of polymers in a few parts per million by weight (ppm). Lumley (Lumley [1969],Lumley [1973]) established that the basic physics was that the familiar spectrum of length scales in Newtonian turbulence was dramatically altered below a certain length scale, and this happens because the time scale associated with a turbulent eddy decreases with size until at a critical eddy size, the associated De becomes of order unity, and elastic effects (normal stresses) become important (Tabor & de Gennes [1986] too proposed an arrest of the familiar energy cascade but they do so based on a length rather than a time scale). Modification of the shear viscosity by the polymers (shear-thinning) plays a secondary role in such cases. Although the above fundamental scenario is correct, and applicable to the case of homogeneous, isotropic turbulence, in the specific context of turbulent channel flow, an underlying feature which emerges both from numerical simulations and experimental observations is the alteration of vortical structures in the boundary layer with the introduction of polymers (White & Mungal [2008]). Parametrically speaking, turbulent drag reduction, unlike the purely elastic instabilities discussed in the earlier paragraph, corresponds to the high De, high Re regime. The problem examined in this chapter combines the aspects of both groups of studies discussed above in that it involves the linear stability of an elastic vortex column at large De and Re but with the ratio De/Re (known as the elasticity number) being finite. Such an elastic vortex column may for instance, be likened to a turbulent eddy in the aforementioned cascade scenario where the time scale is short enough for elasticity forces to become comparable to inertial forces, while at the same time being much more important than viscosity. As a first step, we only examine the instability of the vortex column to two-dimensional disturbances (zero axial wavenumber). Regarding our study as belonging to the general class of stability investigations of fast viscoelastic flows (high De, high Re), there have been other related investigations in the past. Yarin [1997] studied the effect of polymer additives on the dynamics of a vortex filament in an ambient shear flow. The author considered the bending ($m = 1$) mode, and using a localized-induction approximation (LIA), showed that the vortex stretching gets arrested by high longitudinal elastic stresses generated due to stretching of the deformed filament. Azaiez & Homsy [1994] analysed the instability of a shear layer, modeled by a hyperbolic tangent velocity profile, and found that elasticity led to stabilization; as argued by Hinch (appendix of Azaiez & Homsy [1994]), the stabilizing action of elasticity for the long wavelength perturbations is akin to surface tension. Haj-Hariri & Homsy [1997] studied the role of elasticity on the stability of an unbounded linear flow with elliptical streamlines. The study was motivated by earlier investigations of the well-known elliptical instability (Kerswell [2002]), a short wavelength instability that occurs in flows with elliptical streamlines. The elliptical instability is responsible for destabilizing a vortex column in an ambient straining field by inducing a resonant interaction between pairs of Kelvin modes (the pair correspond to points of intersection of the Kelvin dispersion curves for different m). Rather surprisingly, the authors observed that the instability continued to exist even in 2D, something absent for Newtonian fluids where a parametric resonance is only possible in three dimensions. Rallison & Hinch [1995] identified a novel elastic instability of a submerged jet (both planar and axisymmetric).

The hoop stresses due to elasticity plays a crucial role in that they allow for the propagation of transverse shear waves along the otherwise unperturbed streamlines, and the instability arises due to the resonant interaction of a wave pair. The current study is closely related to that of Rallison & Hinch [1995], in that the vortex column instability may again be related to an underlying resonance between fore- and aft- elastic (transverse) shear waves riding on streamlines just outside the vortex core for small E. An advantage of the vortex column configuration is that it is inertially stable, and hence, unlike the case of Rallison & Hinch [1995] where the jet configuration is susceptible to inertial instabilities, the elastic instability in the vortex case exists in isolation. Recently, Stokes *et al.* [2001] have carried out experiments of confined swirling flows on Boger fluids with inertia being dominant. The experiments were motivated towards understanding the variation, in presence of elasticity, of the vortex-breakdown states known to exist for swirling flows in the Newtonian context. Our findings would be of some relevance to these experiments, though with the caveat that we are presently restricted to two dimensional disturbances and the base-state consists of a purely azimuthal flow (vortex breakdown at least in the inviscid context, requires an axial flow component).
We model the effects of elasticity using an Oldroyd-B constitutive equation, the implicit assumption being that elastic effects are much more important when compared to changes in the shear viscosity, and that the finite extensibility of real polymer molecules does not qualitatively alter the shear-wave resonance mechanism. A related application of this study is in the astrophysical context (Ogilvie & Potter [2008]). This is because the flow of polymeric fluids in the limit Re, De $\to \infty$ with E fixed, bears an exact analogy to magnetohydrodynamic flow in the limit of zero magnetic diffusion. Both the polymeric orientation field $\mathbf{R}$ and magnetic field $\mathbf{B}$ obey identical equations in the absence of relaxation processes (which are not identical: the relaxation being diffusive for $\mathbf{B}$, while being local and non-diffusive for the polymeric case). The corresponding feedback to the flow, via the equations of motion, occurs via the polymeric stress of the form $\boldsymbol{\sigma} \propto \mathbf{RR}$ and the Maxwell stress $\propto \mathbf{BB}$ (Ogilvie & Proctor [2003]), in the respective cases.

4.2 Problem formulation

Let us begin by considering the governing equations for an Oldroyd-B fluid, one of the simplest models that describes dilute polymer solutions as Boger fluids. From a microscopic point of view, the Oldroyd-B constitutive equation results from modelling the dilute polymer solution as a non-interacting suspension of infinitely extensible Hookean dumbbells (Larson [1988]). From the conservation of momentum, a fluid of density ρ obeys the equation,

$$\rho \frac{D\mathbf{v}}{Dt} = -\nabla p + \nabla.\boldsymbol{\sigma}_d \tag{4.1}$$

$$\nabla.\mathbf{v} = 0 \tag{4.2}$$

where $\boldsymbol{\sigma}_d$, the deviatoric stress, satisfies the Oldroyd-B constitutive given by:

$$\boldsymbol{\sigma}_d + \lambda_1 \overset{\triangledown}{\boldsymbol{\sigma}}_d = 2\mu(\mathbf{E} + \lambda_2 \overset{\triangledown}{\mathbf{E}}), \tag{4.3}$$

where μ is the total viscosity, λ_1 the relaxation time and λ_2 the retardation time. $\lambda_2 = 0$ corresponds to the upper-convected Maxwell (UCM) fluid, an appropriate model for a polymer melt, while $\lambda_2 \to \lambda_1$ denotes the Newtonian limit. '$\triangledown$' in (4.3) denotes the upper-convected derivative which is expressed as:

$$\overset{\triangledown}{\mathbf{X}} \equiv \frac{D\mathbf{X}}{Dt} - (\nabla\mathbf{v})^{\dagger}.\mathbf{X} - \mathbf{X}.(\nabla\mathbf{v}). \tag{4.4}$$

The upper-convected derivative is frame-invariant derivative which describes the 'frozen' state of a second order tensor field ($\mathbf{X}$) in a velocity field $\mathbf{v}$ which is a form of the general evolution equation,

$$\frac{\partial\mathbf{X}}{\partial t} + \mathcal{L}_{\mathbf{v}}\mathbf{X} = 0, \tag{4.5}$$

where $\mathcal{L}_{\mathbf{v}}$ is the Lie derivative (Ogilvie & Proctor [2003]). When $\mathbf{X}$ is a tensor field it gives us the upper-convected, lower-convected or Jaumann (co-rotational) derivative (any linear combination of the upper- and lower-convected derivatives continues to be a frame-invariant derivative; although, the coefficient of the Jaumann term is fixed by frame invariance). A physical way to arrive at the form of the upper-convected derivative is by defining $A_{ij} \propto \delta l_i \delta l_j$ where δl_i is a differential line-element which satisfies an equation analogous to that governing the vorticity field in the inviscid limit (Batchelor [1967]):

$$\frac{D\delta l_i}{Dt} = \delta l_k \frac{\partial v_i}{\partial x_k}. \tag{4.6}$$

Thus we have (Subramanian [2011]),

$$\begin{aligned}
\frac{DA_{ij}}{Dt} &\propto \frac{D\delta l_i \delta l_j}{Dt}, \\
&= \frac{D\delta l_i}{Dt}\delta l_j + \frac{D\delta l_j}{Dt}\delta l_i, \\
&= \delta l_k \frac{\partial v_i}{\partial x_k} + \delta l_i \delta l_k \frac{\partial v_j}{\partial x_k}, \\
&= A_{kj}\frac{\partial v_i}{\partial x_k} + A_{ik}\frac{\partial v_j}{\partial x_k}, \\
\frac{D\mathbf{A}}{Dt} &= (\nabla\mathbf{v})^{\dagger}.\mathbf{A} + \mathbf{A}.(\nabla\mathbf{v}),
\end{aligned}$$

The assumption of $\delta\mathbf{l}$ being a material line element reflects the assumed affine dynamics of the Hookean dumbbells at the microscopic level. Assuming $\delta\mathbf{l}$ to be oriented along the unit normal to a material surface, or to rotate at a rate commensurate with the local vorticity vector would lead to the lower-convected and Jaumann derivatives respectively.

Returning to the Oldroyd-B fluid, we assume a decomposition of the total stress into a solvent and polymer contribution of the form $\boldsymbol{\sigma}_d = 2\mu^*\mathbf{E} + G(\mathbf{A} - \mathbf{I})$ with $\mathbf{A}$ being the non-dimensional conformation tensor ($\mathbf{A} \propto \mathbf{RR}$), $\mu^* = \mu\lambda_2/\lambda_1$ (the solvent viscosity), $\mu_p = \mu - \mu^*$ (the polymer

viscosity) and $G = \mu_p/\lambda_1$ (the shear modulus). We can then rewrite (4.1)-(4.3) as,

$$\rho\frac{D\mathbf{v}}{Dt} = -\nabla p^* + \mu^*\nabla^2\mathbf{v} + G\nabla.\mathbf{A}, \tag{4.7}$$

$$\overset{\triangledown}{\mathbf{A}} = -\frac{1}{\tau}(\mathbf{A} - \mathbf{I}), \tag{4.8}$$

$$\nabla.\mathbf{v} = 0, \tag{4.9}$$

where $p^* = p + 2(1-\lambda_2/\lambda_1)\mu/\lambda_1$ and $\tau = \lambda_1$. Here onwards we will be dropping the superscript $*$ and make a distinction based on context.

We wish to now study the evolution of two-dimensional disturbances in a swirling flow of an Oldroyd-B fluid, and therefore write - $\mathbf{v} = \overline{\mathbf{u}} + \mathbf{u}, \mathbf{A} = \overline{\mathbf{A}} + \mathbf{a}$, where the overbar quantities represent the unperturbed base state. Let us consider an axisymmetric swirling flow, $\overline{\mathbf{u}} = (0, \Omega r, 0)$, with $\Omega \equiv \Omega(r)$, and the base-state stresses being given as:

$$\overline{\mathbf{A}} = \begin{bmatrix} 1 & r\Omega'\tau \\ r\Omega'\tau & 1 + 2(r\Omega'\tau)^2 \end{bmatrix} \tag{4.10}$$

in a cylindrical coordinate system where $'$ denotes a derivative w.r.t r. The governing equation for the perturbation velocity is,

$$\frac{\partial\mathbf{u}}{\partial t} + \Omega\frac{\partial\mathbf{u}}{\partial\theta} + \mathbf{u}.\nabla\overline{\mathbf{u}} = -\nabla\left(\frac{p}{\rho}\right) + \nu\nabla^2\mathbf{u} + \frac{G}{\rho}\nabla.\mathbf{a}. \tag{4.11}$$

If $\mathbf{u} \equiv (u_r, u_\theta)$, the governing equation for the evolution of axial vorticity, $w_z = (\nabla \wedge \mathbf{u})_z$, can be written as,

$$\begin{aligned}\left(\frac{\partial}{\partial t} + \Omega\frac{\partial}{\partial\theta}\right)w_z + u_r DZ &= \nu\nabla^2 w_z + \frac{G}{\rho}\left\{\nabla \wedge (\nabla.\mathbf{a})\right\}_z \\ &= \nu\nabla^2 w_z + \frac{G}{r\rho}\left[-\frac{1}{r}\frac{\partial^2}{\partial r\partial\theta}(rN_1) + \frac{\partial}{\partial r}\left(\frac{1}{r}\frac{\partial}{\partial r}(r^2 a_{r\theta})\right) - \frac{1}{r}\frac{\partial^2}{\partial\theta^2}a_{r\theta}\right],\end{aligned} \tag{4.12}$$

where $DZ = r\Omega'' + 3\Omega'$ is the vorticity gradient and $N_1 = a_{rr} - a_{\theta\theta}$ is the first normal stress difference. The perturbation elastic stress components obey the following equations:

$$\left(\frac{\partial}{\partial t} + \Omega\frac{\partial}{\partial\theta} + \frac{1}{\tau}\right)a_{rr} - 2\left\{\overline{A}_{rr}\frac{\partial u_r}{\partial r} + \frac{\overline{A}_{r\theta}}{r}\frac{\partial u_r}{\partial\theta}\right\} = 0, \tag{4.13}$$

$$\begin{aligned}&\left(\frac{\partial}{\partial t} + \Omega\frac{\partial}{\partial\theta} + \frac{1}{\tau}\right)a_{r\theta} + \left\{\overline{A}'_{r\theta}u_r - \overline{A}_{r\theta}\left(\frac{\partial u_r}{\partial r} + \frac{u_r}{r}\right) - \frac{\overline{A}_{\theta\theta}}{r}\frac{\partial u_r}{\partial\theta}\right\} + \\ &\left\{\overline{A}_{rr}\left(\frac{u_\theta}{r} - \frac{\partial u_\theta}{\partial r}\right) - \frac{\overline{A}_{r\theta}}{r}\frac{\partial u_\theta}{\partial\theta}\right\} - r\Omega' a_{rr} = 0,\end{aligned} \tag{4.14}$$

$$\begin{aligned}&\left(\frac{\partial}{\partial t} + \Omega\frac{\partial}{\partial\theta} + \frac{1}{\tau}\right)a_{\theta\theta} - 2\left\{\overline{A}_{r\theta}\left(\frac{\partial u_\theta}{\partial r} - \frac{u_\theta}{r}\right) + \frac{\overline{A}_{\theta\theta}}{r}\frac{\partial u_\theta}{\partial\theta}\right\} + \\ &\left(\overline{A}'_{\theta\theta} - \frac{2\overline{A}_{\theta\theta}}{r}\right)u_r - 2r\Omega' a_{r\theta} = 0.\end{aligned} \tag{4.15}$$

On non-dimensionalising with a length scale a (the vortex core radius), time-scale Ω_0^{-1} (the turnover time), and assuming a normal mode form, $h = \hat{h}(r)e^{i(m\theta-\omega t)}$, for the various perturbation quantities, we have,

$$\Sigma r\mathscr{L}(r\hat{u}_r) + mrDz\hat{u}_r = \frac{i}{\mathrm{Re}}r\mathscr{L}^2(r\hat{u}_r) - \frac{im}{\mathrm{Ma}_e^2}\left[mD^*\hat{N}_1 + iDD^*(r\hat{a}_{r\theta}) + \frac{im^2}{r}\hat{a}_{r\theta}\right] \quad (4.16)$$

$$\Sigma_2\hat{a}_{rr} = 2i\left\{\overline{A}_{rr}D + \frac{im\overline{A}_{r\theta}}{r}\right\}\hat{u}_r, \quad (4.17)$$

$$\Sigma_2\hat{a}_{r\theta} = -\frac{r\overline{A}_{rr}}{m}DD^*\hat{u}_r - \left\{\frac{m}{r}\overline{A}_{\theta\theta} + i\overline{A}'_{r\theta}\right\}\hat{u}_r + i\hat{a}_{rr}r\Omega', \quad (4.18)$$

$$\Sigma_2\hat{a}_{\theta\theta} = -\frac{2r\overline{A}_{r\theta}}{m}DD^*\hat{u}_r - i\left\{\overline{A}'_{\theta\theta} + 2\overline{A}_{\theta\theta}D\right\}\hat{u}_r + 2i\hat{a}_{r\theta}r\Omega', \quad (4.19)$$

where $D = \dfrac{d}{dr}$, $D^* = \dfrac{d}{dr} + \dfrac{1}{r}$, $\Sigma = \omega - m\Omega$ and $\Sigma_2 = \omega - m\Omega + \dfrac{i}{\mathrm{De}}$ and

$$\overline{\mathbf{A}} = \begin{bmatrix} 1 & \mathrm{De}\, r\Omega' \\ \mathrm{De}\, r\Omega' & 1 + 2\mathrm{De}^2(r\Omega')^2 \end{bmatrix}. \quad (4.20)$$

Here, we have used the relation $\hat{w}_z = (i/m)\mathscr{L}(r\hat{u}_r)$ where $\mathscr{L} = DD^* - (m^2-1)/r^2$. Henceforth, we will be dropping $\hat{}$ to denote perturbation quantities. The non-dimensional numbers that appear in (4.16)-(4.19) are the Deborah number - De=$\Omega_0\tau$ (the ratio of the elastic to the flow time scale, the flow time scale also characterizes the time scale on which purely inertial perturbations evolve), the Reynolds number - Re=$\Omega_0 a^2/\nu$ (the ratio of the viscous to the inertial time scale) and the elastic 'Mach' number - $\mathrm{Ma}_e = \Omega_0 a/c_{\mathrm{elas}}$ ($c_{\mathrm{elas}} = \sqrt{G/\rho}$). Similar to its counterpart in compressible flows, Ma_e gives the ratio of the speed with which disturbances are convected by the flow to the shear wave speed (the speed of propagation of infinitesimal amplitude shear stress fluctuations in an otherwise quiescent incompressible medium).

The above system of equations has a pair of continuous spectra which may be identified by studying the resultant fourth-order system, the cylindrical analog of the viscoelastic Orr-Sommerfeld equation for plane parallel flows.

1. Gorodtsov-Leonov Continuous Spectrum (Gorodtsov & Leonov [1967])
   The first continuous spectrum is the so-called Gorodtsov-Leonov (GL) continuous spectrum, named after the authors who originally discovered it in the context of viscoelastic plane Couette flow of a UCM fluid. It is defined by $\Sigma_2(r_c) = 0$ with Σ_2 being as defined as above. Although usually studied in the inertia-less limit for plane Couette flow for an UCM fluid ($\mu^* = 0$), because of its analytical tractability leading to closed-form expressions for the eigenfunctions (Gorodtsov & Leonov [1967], Graham [1998]), the GL continuous spectrum arises essentially due to the 'frozen' character of the polymeric stress field along streamline. This arises because almost all constitutive equations in polymer rheology neglect the centre-of-mass degrees of freedom of the polymer molecules (the basic assumption underlying the continuum mechanics concept of 'simple fluid'; Coleman & Noll [1961]). This neglect of the spatial diffusion of the polymer molecules implies that the polymeric stress (neglecting for the moment the perturbation flow driven by the gradient of this stress) along one streamline develops in a manner independent of the neighboring

ones. Note that this remains true for any De, since the latter parameter only measures the relaxation of the configurational degrees of freedom (for Hookean dumbbells, this refer to the end-to-end vector). This neglect is usually a good approximation on most length scales, $\sqrt{\mathrm{D_{CM}}\tau}$ ($\mathrm{D_{CM}}$ being the center-of-mass diffusivity and τ being the relaxation time),since the "diffusion length" is usually exceedingly small (of the order of μm; Bhave *et al.* [1991]). In this regard the polymeric stress field is similar to the vorticity field in the inviscid limit, and both in principle, allow for arbitrarily large gradients across streamlines. Similar to the vorticity field, there then exist CS-modes with singularities in the polymeric stress fields. Similar to plane parallel flows, the Frobenius exponents characterizing the singular point $r = r_c$ are 0, 1, 3 and 4.

2. Viscous Singular Continuous Spectrum (Wilson *et al.* [1999])
   The second continuous spectrum arises due to the inclusion of solvent viscosity, and is given by $\Sigma_2(r_c) + i\mathrm{Re}/\mathrm{Ma}_e^2 = 0$; this is therefore specific to a polymer solution. Dimensionally, $\omega - m\Omega(r_c) + i/\lambda_2 = 0$ and the spectrum gets pushed to infinity as one approaches the UCM limit ($\lambda_2 \to 0$). Again, similar to the parallel flow case the viscous singular continuous spectrum has Frobenius exponents - 0, 1, 2 and $3 - 2\lambda_1/\lambda_2$. As noted by Kupferman [2005], the last (in general fractional) Frobenius exponent indicates the existence of an algebraic branch point and associated branch cut. The singular eigenfunctions in this case require therefore a Pf. interpretation, akin to the ones for the 3D CSMs for a smooth vortex.

We see from the above that the viscoelastic continuous spectra persists even in the presence of viscosity. As already mentioned, this is possible due to the 'frozen' stress states along streamlines allowing for arbitrarily large cross-stream gradients. One way to remove the associated singular stress fields, and thereby regularize the CS-eigenfunctions, would be to replace the Hookean spring, underlying the Oldroyd-B model, with a nonlinear spring model (a FENE-P model - finitely extensible nonlinear elastic with closure proposed by Peterlin; Larson [1999]) and account for the nonlinearity of the relaxation in the vicinity of the critical radius, which should ensure the finiteness of the polymer extension. Studies thus far have only examined dilute solutions of FENE-P springs in the linearized approximations (Arora & Khomami [2005]). The second alternative which is often used to remove the continuous spectrum is the inclusion of stress diffusion - using either an additional diffusive term in the original Oldroyd-B equation[2] of the form $\nabla^2\boldsymbol{\sigma}$, or an explicit mechanism of mass conservation with the spatial diffusion of polymers included. This again removes the continuous spectrum, and instead one has a diffusive critical layer of a finite spatial extent around the critical point of $O(\mathrm{Pe}^{-1/3})$ (Pe being the Peclet number defined based on the translational diffusivity, $\mathrm{D_{tr}}$, of the polymer chain). For the diffusive Oldroyd B model, the spatial extent of this critical layer is $O(\mathrm{Pe}^{-1/3})$, for strong flows. For weak flows, the leading-order balance in the critical layer is expected to occur between the relaxation and the diffusive terms, leading to a critical layer of thickness $O((\mathrm{De}/\mathrm{Pe})^{1/2})$ which is the non-dimensional equivalent of the $O(\mathrm{De}^{1/2})$ diffusion length given earlier. Note that stress diffusion is routinely used for numerical purposes as a regularizing term, although the diffusion

[2] A similar situation occurs for stratified shear flows. With the inclusion of only viscosity the modified Orr-Sommerfeld equation continues to be singular and necessitates inclusion of mass diffusion to regularize the critical layer (Koppel [1964], Engevik [1974])

coefficient necessary for regularizing is much larger than that of a real macromolecule.

4.3 Elastic Rayleigh Equation (Re$\to\infty$ and De$\to\infty$)

We now proceed to the regime of interest, Re$\to\infty$ and De$\to\infty$, but one not often explored in problems involving laminar viscoelastic flows. As already mentioned in the introduction earlier linear stability investigations exist in the above regime. Azaiez & Homsy [1994] studied the role of elasticity on the linear stability of a mixing layer. Elasticity has a stabilizing effect, and in the limit of long wavelengths, as shown by Hinch in an analysis that appears in an appendix in the same paper, the inclusion of elasticity leads to the shear layer acting like an elastic membrane, and thereby suppressing the inertial instability in a manner similar to surface tension; the surface tension owes its origin to the longitudinal stress in the base-state and the coefficient of surface tension is given as $8G\tau^2u_0^2/3\delta$, where G and τ are the shear modulus and relaxation time respectively and U_0 and δ the shear layer's mean velocity and width. Rallison & Hinch [1995] analyzed the stability of a submerged jet (both planar and axisymmetric), another flow configuration susceptible to inertial instabilities. Once again, elasticity for the most part, acts to stabilize the unstable modes, but the authors also covered a novel instability that owed its origins to elasticity. This was particularly clear for an axisymmetric jet which does not exhibit a varicose inertial instability, but it develops an instability on the inclusion of elasticity. The elastic instability arises because a balance between inertia and elasticity supports the propagation of shear waves. If one defines an elasticity parameter, E=De^2/Ma$_e^2$ $=\mu_p\tau/(\rho a^2)$, then the non-dimensional speed of propagation of a shear wave is $O(\sqrt{\mathrm{E}})$. The ambient shear allows for a forward traveling shear wave at the interface to resonate with a backward travelling shear wave located at an $O(\sqrt{\mathrm{E}})$ distance in the interior, and this resonance leads to the instability. Note that since the jet is submerged in a quiescent fluid; the shear rate is discontinuous across the jet interface, leading to a jump in the elastic stress across the interface. Such a configuration, involving a sharp transition from a quiescent stress-free region to a region that supports large elastic stresses, occurs naturally for an intense vortex. Before going on to examine the instability, we first consider the governing system of equations for linearized perturbations, in the more detail, in the limit Re, De$\to\infty$. Considering the system (4.16)-(4.19) in the limit Re$\to\infty$, De$\to\infty$, which is equivalent to neglecting microstructural relaxation, the result is the following single equation for u_r:

$$\Sigma\left(r^2D^2u_r+3rDu_r-(m^2-1)u_r\right)+mrDZu_r=$$
$$2m^2\mathrm{E}\Bigg[2D^*\left\{\frac{r\Omega'}{\Sigma}\left(\frac{mr\Omega'^2}{\Sigma}+r\Omega'D^*+r\Omega''\right)u_r\right\}-\left(rD^2+3D+\frac{m^2}{r}\right)\left(\frac{r\Omega'^2}{\Sigma}\right)u_r\Bigg] \quad (4.21)$$

or equivalently,

$$\Sigma^3\left[\Sigma r\left(r^2D^2u_r+3rDu_r-(m^2-1)u_r\right)+mrDZu_r\right]=2m^2\mathrm{E}\Omega'\Big[\Sigma^2\Big\{r^2\Omega'D^2u_r+r(r\Omega''+DZ)Du_r$$
$$-(m^2-1)\Omega'u_r\Big\}+mr\Omega'\Sigma\Big\{2r\Omega'Du_r+3(DZ-2\Omega')u_r\Big\}+2m^2r^2\Omega'^3u_r\Big]. \quad (4.22)$$

We again focus on the CS-spectrum of (4.22), the elastic equivalent of the Rayleigh equation for swirling flows. Since the Rayleigh equation is singular at the Doppler frequency, $\Sigma(r_c)=0$, and the earlier discussion of the viscoelastic continuous spectra shows that the GL spectrum coincides with the Doppler frequency ($\Sigma_2\to\Sigma$) in the limit of interest, one expects the elastic Rayleigh equation to be singular when $\Sigma(r_c)=0$. However, and rather surprisingly, a closer inspection reveals otherwise. The local form of (4.22), in the vicinity of $r_c\equiv\Sigma^{-1}(\omega)$, is given by,

$$D^2u_r-\frac{2}{r-r_c}\left\{1+(r-r_c)\left(\frac{1}{2r_c}+\frac{5\Omega_c''}{2\Omega_c'}\right)\right\}Du_r+\frac{2}{(r-r_c)^2}\left\{1+(r-r_c)\left(\frac{1}{2r_c}+\frac{5\Omega_c''}{2\Omega_c'}\right)\right\}u_r\approx 0 \tag{4.23}$$

The indicial equation obtained from (4.23) shows that elastic Rayleigh equation (ERE) has Frobenius exponents of 1 and 2 at $\Sigma(r_c)=0$; the corresponding exponents for the radial displacement field are 0 and 1. Although this isn't a sufficient condition for r_c to be an ordinary point, and for the associated solutions to be regular, this turns out to be the case (the Rayleigh equation serves as a counter-example). To verify this in a more transparent manner, and to analyze the possible existence of additional spectra, let us investigate the equation for the radial displacement, $\xi\equiv iu_r/\Sigma$, which may be written in the following much more compact form:

$$\begin{aligned} &D\left[r^3PD\xi\right]=r(m^2-1)P\xi \qquad (4.24)\\ \text{where,}\quad &P=\Sigma^2-2m^2\mathrm{E}\Omega'^2 \end{aligned}$$

and E=De^2/Ma$_e^2$, as before, measures the relative importance of elasticity and inertia; E$\to$ 0 recovers the familiar inviscid limit. It is evident from the form of (4.24) that $\Sigma(r_c)=0$ corresponds to an ordinary point. But, (4.24) now has a pair of singular points, and hence continuous spectra, given by $P(r_c)=0$. In terms of ω, the singularities correspond to $\omega=m\Omega\pm m\Omega'\sqrt{2\mathrm{E}}$. Physically the singularities correspond to fore- and aft- traveling elastic shear waves. This may be seen by first noting that the (pre-stressed) shear wave speed in dimensional terms is given by $\sqrt{GA_{\theta\theta}/\rho}$. We have already seen that, $A_{\theta\theta}\sim 2\mathrm{De}^2r\Omega'^2$ and $\sqrt{G/\rho}\sim\mathrm{Ma}_e^{-1}$. Thus the shear wave speed in non-dimensional terms in $O(\sqrt{\mathrm{E}})$ which explains the association of $\omega=m\Omega\pm m\Omega'\sqrt{2\mathrm{E}}$ with fore- and aft- traveling elastic shear waves.

Let us now examine the series solutions of the above equation in the vicinity of r_c (either of the two shear waves) that satisfies $P(r_c)=0$. For $E\neq 0$, P has a simple pole and (4.24) may be written in the following approximate form,

$$D^2\xi+\left[\frac{1}{r-r_c}+\left\{\frac{3}{r_c}+\frac{P_c''}{2P_c'}\right\}\right]D\xi-\frac{(m^2-1)}{r_c^2}\xi=0 \tag{4.25}$$

The indicial equation obtained from (4.25) by assuming $\xi\sim(r-r_c)^\alpha$ gives a repeated Frobenius index, $\alpha=0$. Thus one solution must be a constant at leading order, while the other solution

would be logarithmically singular. The two solutions may be shown to be given by,

$$\xi_1 = 1 + \frac{m^2-1}{4r_c^2}(r-r_c)^2 + \ldots \tag{4.26}$$

$$\xi_2 = \left\{1 + \frac{m^2-1}{4r_c^2}(r-r_c)^2\right\}\log(r-r_c) - \left\{\frac{3}{r_c} + \frac{P_c''}{2P_c'}\right\}(r-r_c) + \ldots \tag{4.27}$$

Since $\omega - m\Omega(r_c) \neq 0$ for the viscoelastic case, the singularities of u_r are the same as those of ξ. One can easily construct a modified version of Howard's semi-circle theorem (Howard [1962]) for swirling flows from (4.24), and this leads to the following inequality:

$$\left(\omega_r - \frac{m(\Omega_{\max}+\Omega_{\min})}{2}\right)^2 + \omega_i^2 \leq m^2\left(\frac{\Omega_{\max}-\Omega_{\min}}{2}\right)^2 - 2m^2\mathrm{E}\left(\Omega'^2\right)_{\min} \tag{4.28}$$

Thus, the role of elasticity is to shrink the Newtonian (inviscid) semi-circle of instability, implying a relative stabilization. It is, of course, possible to construct elastic equivalents of the Rayleigh and Fjortoft theorems for the elastic case, but such results are not particularly useful due to the presence of the eigenvalue in the resulting expressions. The analog of (4.24) has been used by Rallison & Hinch [1995] in their study of the effects of elasticity on inertial instabilities in jets. Before proceeding any further, we would like to draw attention to an interesting analogy of viscoelastic flows studied in the above limit ($\mathrm{Re}\to\infty$, $\mathrm{De}\to\infty$) to magnetohydrodyamic (MHD) flows in the limit of $\mathrm{Re}_m \to \infty$ (Ogilvie & Proctor [2003]); here, Re_m is the magnetic Reynolds number and is defined as $\mathrm{Re}_m = \mu^*/(\rho\lambda_m)\mathrm{Re}$. The governing equations for a magnetofluid of density ρ, viscosity μ^*, magnetic diffusivity λ_m and free-space permeability μ_0 (Ogilvie & Proctor [2003]), are given by:

$$\rho\frac{D\mathbf{v}}{Dt} = -\nabla p_m^* + \mu^*\nabla^2\mathbf{v} + \nabla.\mathbf{M} \tag{4.29}$$

$$\overset{\triangledown}{\mathbf{M}} = \frac{\lambda_m}{\mu_0}(\mathbf{B}\nabla^2\mathbf{B} + (\nabla^2\mathbf{B})\mathbf{B}) \tag{4.30}$$

$$\nabla.\mathbf{v} = 0 \tag{4.31}$$

$$\nabla.\mathbf{B} = 0 \tag{4.32}$$

where, $p_m^* = p + B^2/(2\mu_0)$ and $\mathbf{M} = \frac{\mathbf{BB}}{\mu_0}$, the Maxwell stress tensor without the isotropic part (which has been absorbed in the modified pressure, p_m^*). Comparing the above set of equations for vanishing magnetic diffusion, $\mathrm{Re}_m \to \infty$, (which corresponds to $\lambda_m \to 0$ in 4.30), with the infinitely slow relaxation limit, $\mathrm{De}\to\infty$, of (4.7-4.9) highlights the analogy between the two systems. Note that the analogy is an exact one only in the absence of relaxation processes. The relaxation mechanisms are different in the two cases, being diffusive in the MHD case, and being local but non-diffusive in the polymeric case.

In a perfectly conducting fluid, the magnetic field is in a 'frozen' state (Alfvén's theorem; Davidson [2001])) and the corresponding Maxwell stress tensor behaves identically to the polymeric stress tensor in the limit of the molecular relaxation becoming infinitely slow. The system of equations, (4.29)-(4.32), governing the motion of a perfectly conducting fluid supports waves. For instance, if one, imagines a disturbance acting to 'bend' the magnetic field lines (see figure

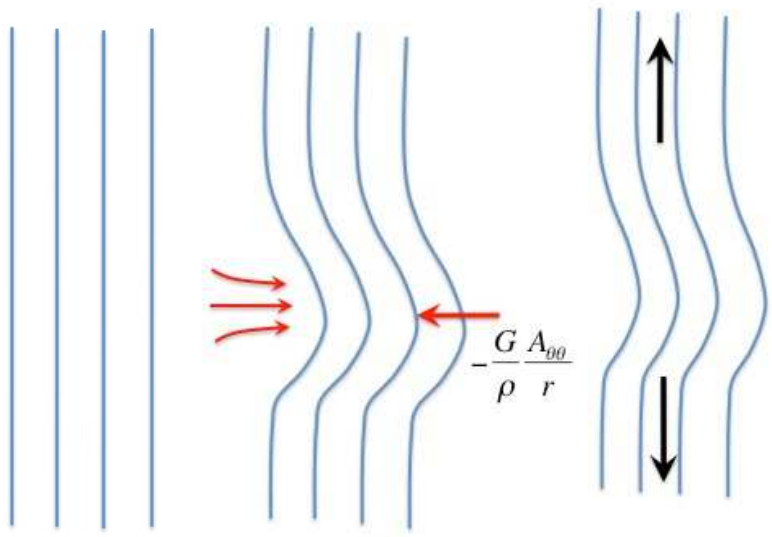

Figure 4.1: Shear waves in a viscoelastic fluid. (a) streamlines in an unperturbed fluid, (b) perturbed streamlines experience restoring mechanism of polymeric stress and (c) propagating shear waves (adapted from generation of Alfvén waves in magnetofluid via Lorentz force (Davidson [2001])

4.1), the curvature leads to a Lorentz force acting to straighten out the field lines; this restoring action coupled with inertia leads to waves known as Alfvén waves. The viscoelastic analog of the Alfvén waves are the transverse shear waves discussed earlier. In both cases, one could visualise the deformation of streamlines, and the subsequent propagation of waves, as being similar to 'plucking' a tensioned string. To illustrate this analogy mathematically, we consider the linear evolution of disturbances both in quiescent and shearing flows. First, we will concentrate on the plane parallel flow geometry.

In the quiescent case, the disturbance vorticity field, $\mathbf{w}$, obeys the following linearized equations in the respective cases:

$$\text{MHD, } (\text{Re}_m \to \infty) \qquad \frac{\partial^2 \mathbf{w}}{\partial t^2} = \frac{1}{\rho\mu_0}(\mathbf{B}.\nabla)^2\mathbf{w} + \nu\nabla^2\left(\frac{\partial \mathbf{w}}{\partial t}\right) \tag{4.33}$$

$$\text{Viscoelastic, } (\text{De} \to \infty) \qquad \frac{\partial^2 \mathbf{w}}{\partial t^2} = \frac{G}{\rho}\nabla^2\mathbf{w} + \nu\nabla^2\left(\frac{\partial \mathbf{w}}{\partial t}\right) \tag{4.34}$$

where $\mathbf{B}$ is an imposed uniform magnetic field. Thus, vorticity perturbations in the elastic and MHD flows evolve via damped Alfvén/shear waves, the damping being due to the fluid viscosity in both cases.

Next we consider the evolution of two dimensional inviscid disturbances in the shearing flow ($U(y)$) of an elastic fluid; the difference now being that the base-state elastic stress is no longer isotropic (given by $G\mathbf{I}$), but rather is given, at leading order, by $GA_{xx}\hat{x}\hat{x}$ with $A_{xx} \sim 2(\tau U')^2$. Thus, the shear waves now correspond to a pre-stressed medium and therefore propagate at a faster rate ($c = \sqrt{GA_{xx}/\rho} > \sqrt{G/\rho}$). In the MHD context, $B(y)$, will also be assumed to be non-uniform. The linear stability equations in terms of the normal displacement, ζ, for plane

parallel flows are given by:

$$\text{MHD,} \quad (\lambda_m, \nu \to 0)$$
$$\frac{d}{dy}\left[\{(U-c)^2 - 2EU'^2\}\frac{d\zeta}{dy}\right] = k^2\{(U-c)^2 - 2EU'^2\}\zeta \tag{4.35}$$
$$\text{Viscoelastic,} \quad (\tau^{-1}, \nu \to 0)$$
$$\frac{d}{dy}\left[\{(U-c)^2 - A^2\}\frac{d\zeta}{dy}\right] = k^2\{(U-c)^2 - A^2\}\zeta \tag{4.36}$$

where k is the streamwise wavenumber and $A = B(y)/\sqrt{\rho\mu_0}$ is the Alfvén wave speed and determined by the imposed magnetic field, $B(y)$. Despite its similarity with the MHD problem, it is worth noting that the viscoelastic case doesn't have the luxury of the shear wave speed being independently assigned; it is determined from the velocity-gradient profile once the base-state shearing flow is chosen.

It is evident that the above analogy would continue to exist even for swirling flows. Acheson [1973] gives the governing differential equation for 3D disturbances imposed on a swirling flow of a radially stratified (density) perfectly conducting magnetofluid with an imposed magnetic field, $\mathbf{B} = (0, B_\theta(r), B_z(r))$. If one considers the two dimensional homogeneous limit, we have the radial displacement ξ being governed by the following equation:

$$D\left[r^3 P_m D\xi\right] = r(m^2-1)P_m\xi, \tag{4.37}$$
$$\text{with} \quad P_m = \Sigma^2 - m^2\Omega_{\mathrm{B}}^2,$$

where the Alfvén wave speed is given by, $A(r) \equiv r\Omega_{\mathrm{B}} = B_\theta(r)/\sqrt{\rho\mu_0}$, and Σ is as defined in (4.24). The analogy is evident on comparing (4.24) and (4.37) although it is worth reiterating that the difference is that the Alfvén wave speed can be imposed independent of the base-state rotation rate via the magnetic field.

The purpose of the above exercise was to emphasize the analogy between two apparently disparate systems - the flow of a perfectly conducting magnetofluid and the shearing flow of a viscoelastic fluid in the absence of any relaxation. Although the analogy has been appreciated recently, a lot can nevertheless be achieved by adapting existing insights from one system to the other. One such instance has been in the study of the viscoelastic analogue of the celebrated magnetorotational instability (MRI) underlying the stability of accretion disks (Ogilvie & Potter [2008], Balbus & Hawley [1991]). The immense difficulty in performing experiments relevant to the MRI in the laboratory could be alleviated by studying the viscoelastic analog involving dilute polymer solutions in the relevant regime (Boldyrev *et al.* [2009]).

In chapter 2 we discussed at length the 2D continuous spectrum eigenfunctions for a Rankine vortex. On introduction of elasticity, with the approximation Re$\to\infty$ and De$\to\infty$, the continuous spectrum eigenfunctions will undergo modification; most importantly due to the shear wave singularities $P(r_c) = 0$. For E$\ll 1$, the eigenfunction is expected to remain largely similar to that of the inviscid one ((2.7)-(2.9)) but for the region $P(r) \ll 1$, centered about $\omega - m\Omega(r') = 0$, where elasticity is going to be dominant. Since $\omega - m\Omega(r') = 0$ is no longer a singularity of

(4.24), we introduce a boundary layer variable

$$\eta = \frac{r - r'}{\sqrt{2\mathrm{E}}} \tag{4.38}$$

and denote the boundary layer displacement and velocity as $\xi(r) = \tilde{\xi}(\eta)$ and $u_r(r) = \tilde{u}_r(\eta)$ respectively. (4.24) can then be written in the following reduced form as,

$$\frac{d}{d\eta}\left[(\eta^2 - 1)\frac{d\tilde{\xi}}{d\eta}\right] = 0 \tag{4.39}$$

$$\Rightarrow \qquad \tilde{u}_r(\eta) = \eta\left\{\mathcal{A}_1 + \mathcal{A}_2 \log\left|\frac{\eta - 1}{\eta + 1}\right|\right\} \tag{4.40}$$

The boundary condition imposed on the above solution is $\tilde{u}_r(\eta \to \infty) = u_r(r \to r'^{+}) = \tilde{u}_r(\eta \to -\infty) = u_r(r \to r'^{-})$. Thus, for $|r - r'| \ll \sqrt{\mathrm{E}}$ the continuous spectrum eigenfunction structure is given as,

$$\tilde{u}_r(\eta) = \frac{u_r(r')}{2}\eta \log\left|\frac{\eta + 1}{\eta - 1}\right| \tag{4.41}$$

whereas for $|r - r'| > \sqrt{\mathrm{E}}$, (2.7)-(2.9) would provide the leading order description of the eigenfunction. It should be noted that $\eta = \pm 1$ corresponds to the location of the shear wave singularities, $P(r_c) = 0$. This form of the eigenfunction will be revisited during the asymptotic analysis for the unstable mode in sections 4.6 and 4.7.

Though (4.41) accurately describes the leading order boundary layer structure, it lacks in identifying the elastic analog of the Kelvin mode and the continuous spectrum mode for E=0. As was already seen in chapter 2, the Kelvin mode and the continuous spectrum mode are distinguished by virtue of tangential velocity discontinuity or equivalently a jump in Du_r. The boundary layer structure (4.41) leads to $d\tilde{u}_r/d\eta \to 0$ as $\eta \to \pm\infty$. To identify the free and forced mode we need to find $\tilde{u}_r(\eta)$ to a higher order where $[d\tilde{u}_r(\eta)]_{-\infty}^{+\infty}$ is non-zero. Thus we have,

$$\begin{aligned}\tilde{u}_r(\eta) \quad = \quad & \frac{u_r(r')}{2}\eta \log\left|\frac{\eta + 1}{\eta - 1}\right| + \sqrt{\mathrm{E}}\eta\left[\mathcal{A}_3 + \left\{\mathcal{A}_4 + \frac{\eta}{2\sqrt{2}}\frac{u_r(r')\Omega''(r')}{\Omega'(r')}\right\}\log\left|\frac{\eta + 1}{\eta - 1}\right| - \right. \\ & \left. \frac{u_r(r')}{\sqrt{2}}\left\{\left(\frac{3}{r'} + \frac{\Omega''(r')}{\Omega'(r')}\right)\log(\eta^2 - 1) + \frac{\Omega''(r')}{\Omega'(r')}\frac{1}{\eta^2 - 1}\right\}\right] + O(\mathrm{E})\end{aligned} \tag{4.42}$$

For a Rankine vortex $\Omega''(r')/\Omega'(r') = -3/r'$ and thus 4.42 can be written as,

$$\tilde{u}_r(\eta) = \frac{u_r(r')}{2}\eta \log\left|\frac{\eta + 1}{\eta - 1}\right| + \sqrt{\mathrm{E}}\eta\left[\mathcal{A}_3 + \left\{\mathcal{A}_4 - \frac{3u_r(r')\eta}{2\sqrt{2}r'}\right\}\log\left|\frac{\eta + 1}{\eta - 1}\right| + \frac{3u_r(r')}{\sqrt{2}r'(\eta^2 - 1)}\right] + O(\mathrm{E}) \tag{4.43}$$

Now $[d\tilde{u}_r(\eta)]_{-\infty}^{+\infty} \neq 0$ and a choice of $\mathcal{A}_3^+$ and $\mathcal{A}_3^-$ leads to determine if there exists a forcing and thus a way for identifying the elastic analogs for Kelvin mode and the continuous spectrum modes. The above result serves as a starting point in showing how the choice of the continuous spectrum modes appear at a higher order in E and a detailed study needs to be carried out in the future for better understanding of continuous spectrum modes in elastic swirling flows.

4.4 Shear Wave Resonance Instability of a Vortex

Having examined the 2D viscoelastic CS-spectrum, we now study the instability of an elastic vortex column t two-dimensional (non-axisymmetric) disturbances both via a numerical approach, and using a matched asymptotic expansion technique. The unstable discrete mode in this case is found to coalesce with the continuous spectrum in the limit of a vanishingly small elasticity number. For purposes of simplicity, the analysis will be restricted to the case of a Rankine column with the angular velocity profile being given by, $\Omega(r) = \mathcal{H}(1-r) + \left(\frac{1}{r}\right)^2 \mathcal{H}(r-1)$; $\Omega'(r) = -2\frac{1}{r^3}\mathcal{H}(r-1)$. From the discussion in chapters 2 and 3, we know that a Rankine vortex is neutrally stable in the inviscid limit, and has both discrete and continuous spectra. For two dimensional disturbances the discrete spectrum is constituted of a single mode, the Kelvin mode, for every m. In section 4.2, we have already examined the modified continuous spectrum, associated with the ERE, and the elastic generalization of the Kelvin mode. Herein, we identify an unstable discrete mode that is purely elastic in origin.

Consider the ERE for the Rankine vortex configuration. Since the Rankine vortex offers a spatial separation of the vortical and straining regions, one may study the ERE in these regions separately; as noted above, the numerical investigation includes more general vorticity profiles, and serves to reinforce the usefulness of the analysis which is restricted to the Rankine vortex.

1. $r < 1$
   Solid body rotation is unaffected by elasticity and the solution for $r < 1$ is identical to the inviscid solution. In the interest of obtaining a normalized radial displacement, choose $u_r = \Sigma_0 r^{m-1}$ where $\Sigma_0 = \omega - m$. Thus $\xi = r^{m-1}$ and $\left.\frac{d\xi}{dr}\right|_{r=1-} = m-1$. Knowledge of the radial displacement field within the core allows the numerical integration to be restricted to the irrotational exterior with the appropriate boundary condition at the edge of the core.

2. $r > 1$
   By continuity of ξ across the vorticity interface ($r = 1$), we have $\left.\xi\right|_{r=1+} = \left.\xi\right|_{r=1} = 1$.
   Integrating (4.24) across $r = 1$, one obtains:

$$\left[r^3 P \frac{d\xi}{dr}\right]_{r=1-}^{r=1+} = 0 \tag{4.44}$$

$$\Rightarrow \quad \left\{\Sigma_0^2 - 8\mathrm{E}(m\Omega_0)^2\right\} \left.\frac{d\xi}{dr}\right|_{r=1+} - \Sigma_0^2 \left.\frac{d\xi}{dr}\right|_{r=1-} = 0 \tag{4.45}$$

$$\Rightarrow \quad \left.\frac{d\xi}{dr}\right|_{r=1+} = \frac{(m-1)(\omega-m)^2}{(\omega-m)^2 - 8m^2\mathrm{E}} \tag{4.46}$$

The radial displacement field in the exterior is governed by (4.24), which in expanded form, is given by:

$$D\left[r^3\left\{(\omega-m\Omega)^2 - 2m^2\mathrm{E}\Omega'^2\right\} D\xi\right] = r(m^2-1)\left\{(\omega-m\Omega)^2 - 2m^2\mathrm{E}\Omega'^2\right\}\xi \tag{4.47}$$

with the boundary conditions:

$$\xi\Big|_{r=1} = 1, \tag{4.48}$$

$$\frac{d\xi}{dr}\Big|_{r=1+} = \frac{(m-1)\,(\omega-m)^2}{(\omega-m)^2-8m^2\mathrm{E}}, \tag{4.49}$$

$$\xi \to 0, \quad \text{as } r\to\infty. \tag{4.50}$$

The terms in $(\omega-m\Omega)^2-2m^2\mathrm{E}\Omega'^2$ in (4.47) represent the interplay of inertia and elasticity. The regions in the flow domain where $(\omega-m\Omega)\sim\pm m\sqrt{2\mathrm{E}}\Omega'$, are the ones affected by elastic stresses. In the far-field, $r\gg 1$[3], clearly, elasticity is sub-dominant. Elasticity is, however, expected to make its presence felt in the straining region adjacent to the core ($r\approx 1$). For $r\approx 1$, a balance of the two terms above implies $(\omega-m)\sim\pm m\sqrt{8\mathrm{E}}$. Assuming, for the moment, a neutral mode one may obtain an estimate for the critical radius from this balance, which would be the region where elastic stresses associated within the mode would be localized. Linearizing the angular velocity about the critical radius, we find, $r_c\sim 1+O(\sqrt{\mathrm{E}})$, where elasticity becomes important at leading order. As already indicated, the physical mechanism of the instability involves a backward-traveling shear wave at the edge of the vortex core ($r\sim 1$) resonating with a forward traveling shear wave at $r=1+O(\sqrt{\mathrm{E}})$ for $\mathrm{E}\ll 1$. This suggests the introduction of a re-scaling corresponding to a boundary layer of thickness $O(\sqrt{\mathrm{E}})$. Rallison & Hinch [1995] first noted this re-scaling for the elastic instability in a submerged jet. Although things appear quite consistent, there is a hidden length-scale implicit in the boundary conditions that cannot be accounted by the $\sqrt{\mathrm{E}}$ re-scaling. This hidden length scale is the radial distance of the backward-traveling shear wave from the edge of the core; as will be seen later, this does not scale as $\sqrt{\mathrm{E}}$, but instead is transcendentally small.

Before proceeding with the details of the asymptotic analysis, we first examine the unstable mode numerically which also allows one an access to a wider range of E values. The breakdown of the numerics for small E serves as a natural motivation for the analysis that follows.

4.5 Numerical Calculations

The numerical issues in the limit of large Re and De, for the parallel flow analog of the vortex case considered here, are described in Miller [2005]. The exponentially small length scale mentioned above leads to the eigenvalue's transcendental dependence on the small parameter indicates that numerical evaluation needs to be done very carefully for $\mathrm{E}\ll 1$. Besides the presence of *exponential asymptotics*, the numerics is rendered more difficult by the fact that the marginal mode is now a singular neutral mode. This is quite unlike the classical inviscid problem where the marginal mode is a regular neutral mode. To ensure that we have indeed identified a true unstable mode and to distinguish it from the spurious ones, we study the problem numerically using three techniques.

The first method involves performing a standard spectral calculation, for the linear eigenvalue

[3] In taking $\mathrm{De}\to\infty$ we have ignored the isotropic part of the elastic stresses which become important in the far-field, and allow for the (radial) propagation of shear waves out to 'infinity'. This effect is therefore neglected in ERE.

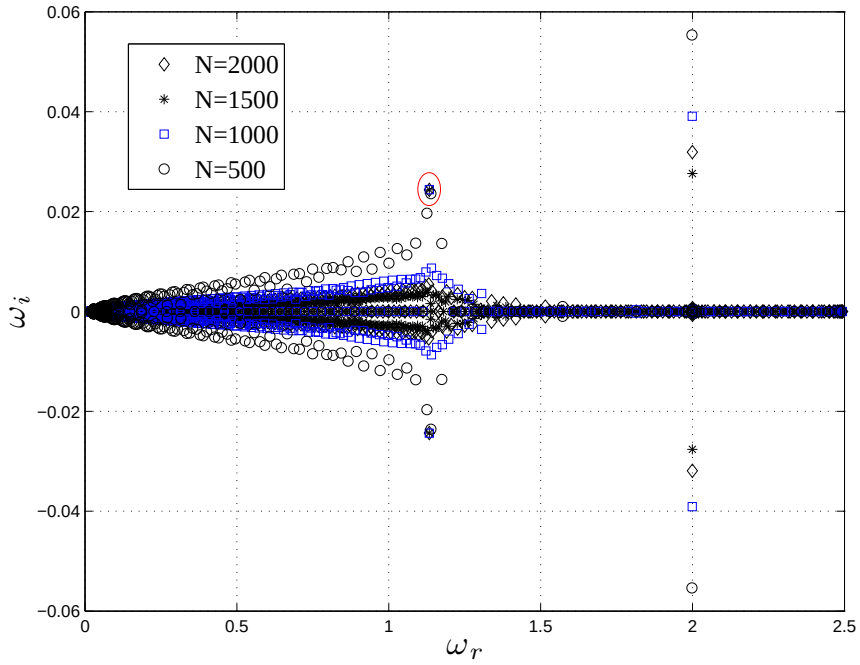

Figure 4.2: Collapse of 'ballooning' of spectrum with increasing N for a smooth vortex ($a = 0.95$, 3.27). The converged unstable mode is encircled.

problem given by (4.16)-(4.19) (in the limit Re,De$\to\infty$), based on a Chebyshev collocation (Trefethen [2000]). Aided by our knowledge of the continuous spectrum, we anticipate difficulties in the spectral technique. The spectral method obtains there entire eigenspectrum including the singular continuous spectra. Since the CSMs aren't C^∞, there is a 'ballooning' of the neutral spectrum for any finite number of collocation points; which, however, slowly collapses onto the real axis with increasing N (Figure 4.2) (Graham [1998]). This complicates the identification of the unstable mode, particularly in the limit of small E, as it remains engulfed in this 'balloon' for small values of N. One way of identifying the unstable mode relies on increasing N to sufficiently high values such that, the spurious imaginary part of the continuous spectrum vanishes, as the balloon collapses onto the real axis, while the true unstable mode converges to a location at a finite distance away from the real axis (see figure 4.2).

The second method involves a direct solution of the nonlinear eigenvalue problem (4.24) for ξ. The nonlinear eigenvalue problem is solved using a compound matrix method (Bridges & Morris [1984]), typically used to study spatial stability problems in the context of the Orr-Sommerfled equation. The essential idea involves writing the original non-linear eigenvalue problem as a higher dimensional linear one. Thus, (4.24) could be written as,

$$\begin{bmatrix} -\mathcal{C}_1 & -\mathcal{C}_2 \\ 1 & 0 \end{bmatrix} \begin{bmatrix} \xi_a \\ \xi_b \end{bmatrix} = \omega \begin{bmatrix} \mathcal{C}_0 & 0 \\ 0 & 1 \end{bmatrix} \begin{bmatrix} \xi_a \\ \xi_b \end{bmatrix}, \tag{4.51}$$

where
$$\xi_a = \omega\xi,\ \xi_b = \xi$$
$$\mathcal{C}_0 = D(r^3 D) - r(m^2-1)$$
$$\mathcal{C}_1 = -2mD(r^3\Omega D) + r(m^2-1)2m\Omega$$
$$\mathcal{C}_2 = D(r^3m^2(\Omega^2 - 2\mathrm{E}\Omega'^2)D) - r(m^2-1)m^2(\Omega^2 - 2\mathrm{E}\Omega'^2)$$

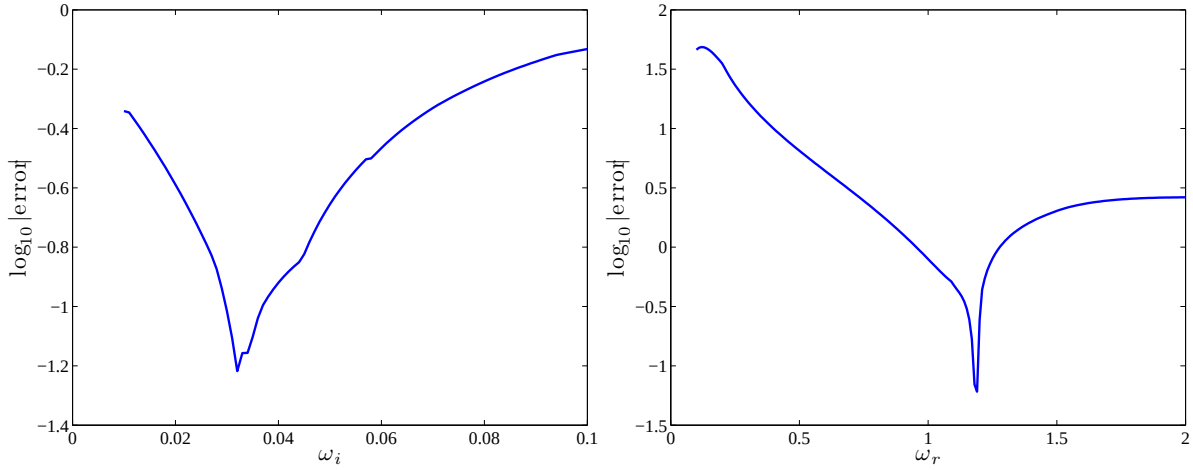

Figure 4.3: 'Error' for various values of $\omega_{i,r}$

and we proceed on to solve this equivalent higher dimensional linear eigenvalue problem.

The final method is a regular shooting method for the boundary value problem (4.24). This is done using the inbuilt BVP4C command in MATLAB. The trouble with the shooting method is, however, the extreme sensitivity to the initial guess for the eigenvalue, and this again happens due to the unstable mode lying in close proximity to the continuous spectrum. In the context of the submerged elastic jet instability with a governing equation of similar mathematical character, Miller [2005] suggests a 'carpet-bombing' technique to get a reasonably accurate guess for the value of eigenvalue. One of the boundary conditions is allowed to be an unknown and we call its difference from the true boundary condition as the 'error'. A complex ω grid is chosen and for every value of ω the unknown boundary condition and hence the 'error' is found. Figure 4.3 shows identification of the guess value for ω using the minimum of the absolute value of the 'error' .

All the three methods above yield mutually consistent results. The results from here on will be those computed using the third method which involves solving a boundary value problem with an initial guess obtained via a 'carpet-bombing' approach. Figure 4.4 shows the dependence of the wave-speed and growth-rate of the unstable mode on E for different values of m. Figure 4.4(b) highlights the dependence of the growth rate on the re-scaled azimuthal wave-number $m\sqrt{E}$, and there is expected collapse in the range where $m\sqrt{\mathrm{E}} \sim O(1)$ and m is sufficiently large. Figure 4.4(c) shows the transition of the wave-speed to the $1 - \sqrt{8\mathrm{E}}$ asymptote for small E, and figure 4.4(d) shows the comparison of increasingly refined asymptotic estimates for real par of the eigenvalue (predicted in section 4.7.4) with the numerical result. Since we do not yet have an expression for the growth-rate for the entire problem, figure 4.5 only shows the match of the numerically calculated growth-rate with (4.67), the expression obtained from the LHS problem (section 4.6). Note that the rather precipitous drop in growth rate for small E that owes its origin to the transcendental scaling. The eigenfunctions for both radial displacement and velocity can be seen in figure 4.6 and the twin peaks corresponding to the shear wave locations are clearly visible, and are reminiscent of the singularities at these locations for the CS-modes in the vicinity of the unstable mode (for the unstable mode there are no longer singularities,

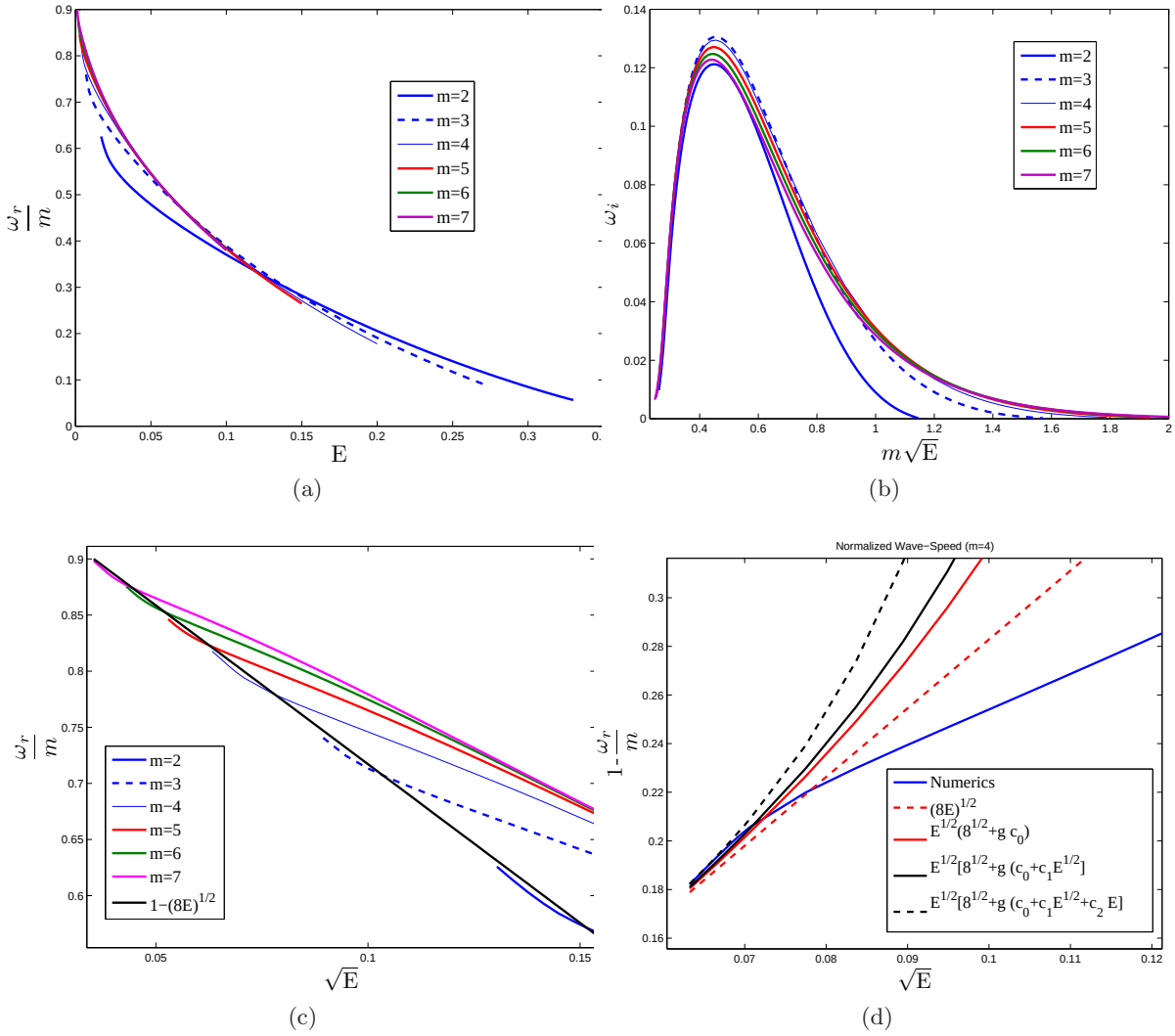

Figure 4.4: Dependence of the wave-speed (a) and growth-rate (b) on E for various values of m. In (c) the phase-speed is compared with the leading order asymptotic solution, $\omega_r = m(1-\sqrt{8E})$ (section 4.6), while in (d) comparisons are made with higher order asymptotic corrections

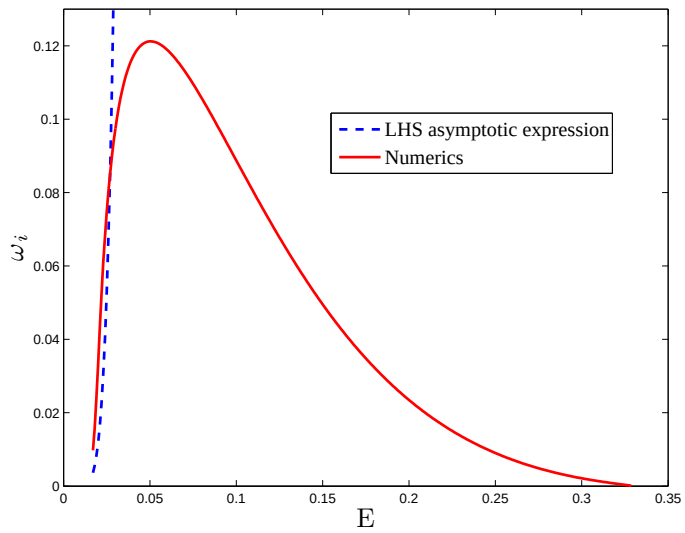

Figure 4.5: Comparison of numerically evaluated growth rate and the asymptotic expression obtained from LHS (m=2)

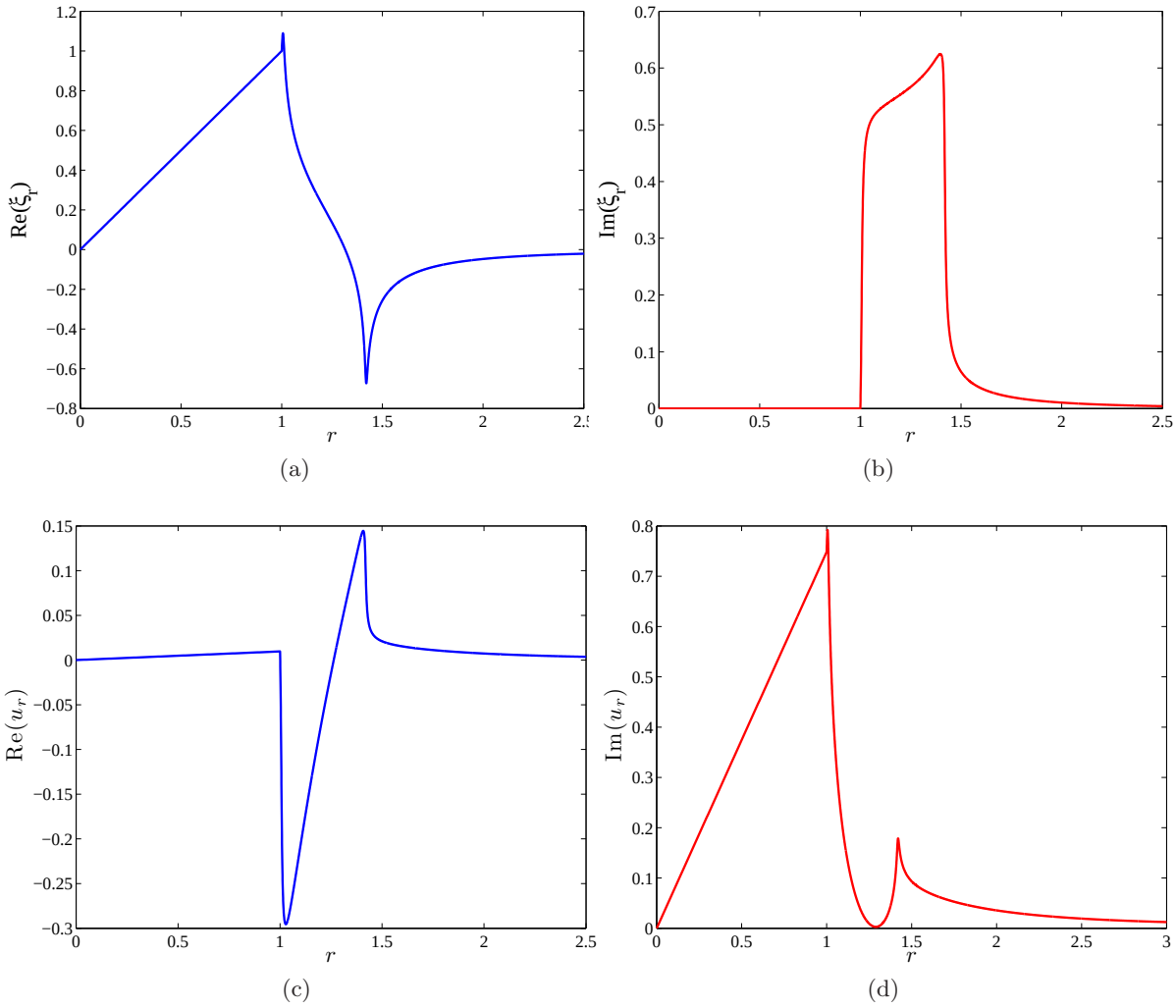

Figure 4.6: Radial displacement and velocity eigenfunctions for E=0.017, m=2.

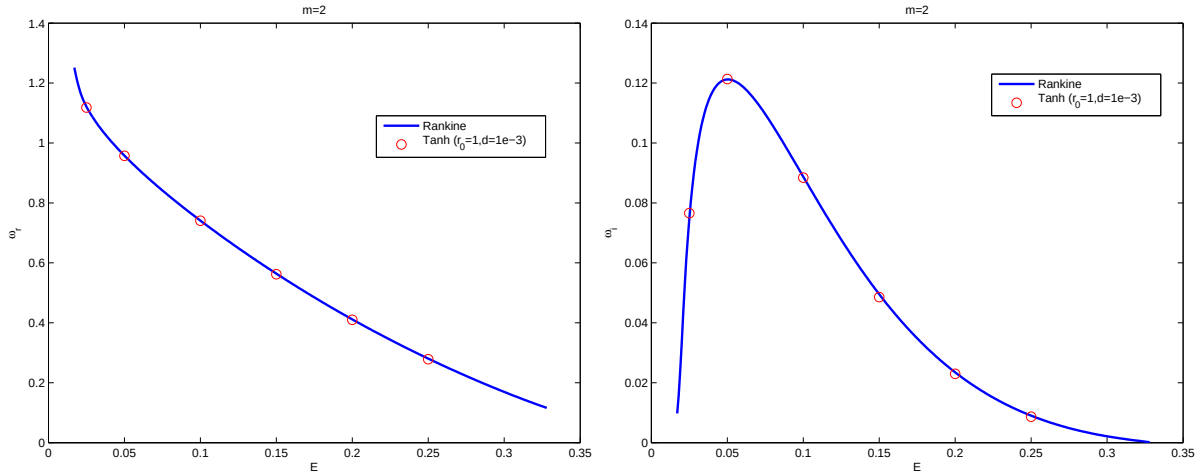

(a) (b)

Figure 4.7: Wave-speed and growth-rate comparisons for a smooth (4.52) and Rankine vortex ($a = 1, m = 2$ and $d = 10^{-3}$).

rather sharply peaked structures).

The numerical results so far have focussed on the Rankine vortex - a profile which has a discontinuity in the base-state angular velocity gradient, and therefore, in the hoop stress ($\overline{A}_{\theta\theta}$) profile. It could be argued that this discontinuity is the reason for the instability and a smoothened base-state vorticity profile will not support such exponentially growing modes. However, from our shear wave resonance argument, this seems unlikely. Indeed, from our knowledge of instabilities emanating via the resonant coupling of waves riding on sharp interfaces (for instance, the KH instability may be regarded as the resonance of Rossby waves riding on vorticity interface), a mere smoothening does not lead to a disappearance of the instability. For a smooth profile, one expects the transition width, the region over which the flow transitions from a rigid-body rotation to an irrotational straining one, to decide the fate of the instability. In particular, one expects the instability to persist for a smooth Rankine-like profile. Towards this end, we have examined the stability of a 'tanh' vorticity profile with the base-state vorticity being given by:

$$Z(r) = \frac{Z_0}{2}\left[1 - \tanh\left(\frac{r-a}{d}\right)\right] \tag{4.52}$$

Figure 4.7 shows the close comparison of growth-rate and wave-speed for a 'tanh' vortex with that of Rankine vortex, demonstrating the persistence of the elastic instability even for smooth vortices. As already mentioned the numerical approach in this case exploits the fact that elasticity plays no role in the region of solid body rotation, and one only needs to solve the governing equation in the irrotational exterior with appropriate boundary conditions at $r = 1$. For a smooth vortex the integration needs to be carried out over the entire domain. It would be of interest, in future, to conduct a more detailed investigation to determine the dependence of the instability characteristics on the width of the transition zone by considering a one-parameter family of vorticity profiles with the limiting member as the Rankine and the Lamb-Oseen profiles.

4.6 Asymptotics - LHS problem

To begin with, we need to understand why the re-scaling by $\sqrt{\mathrm{E}}$ does not work for the entire range of E. To do so, let us consider the irrotational region in the immediate neighbourhood of the core, $r-1 \ll 1$, in terms of re-scaled boundary layer coordinate, $x \to r = 1+\sqrt{\mathrm{E}}\,x$. We choose $\omega = m(1-a_1\sqrt{\mathrm{E}})$ where a_1 is an $O(1)$ constant. Using this transformation, and the local forms of Ω and Ω' in the boundary layer (4.47), at leading order, takes the form,

$$\frac{d}{dx}\left[\left\{(a_1-2x)^2-8\right\}\frac{d\xi}{dx}\right]=0 \tag{4.53}$$

The RHS of (4.47) has been discarded since it is asymptotically small for $m \sim O(1)$. (4.53) has solutions of the form,

$$\xi = c_1 + c_2 \log\left[\frac{2x-a_1-\sqrt{8}}{2x-a_1+\sqrt{8}}\right] \tag{4.54}$$

with the boundary conditions,

$$\xi\Big|_{x=0} = 1 \tag{4.55}$$

$$\frac{d\xi}{dx}\Big|_{x=0} = \sqrt{\mathrm{E}}\frac{(m-1)\,(\omega-m)^2}{(\omega-m)^2-8m^2\mathrm{E}} = \sqrt{\mathrm{E}}\frac{(m-1)\,a_1^2}{a_1^2-8} \tag{4.56}$$

$$\xi \to 0, \quad \text{as } x\to\infty \tag{4.57}$$

Since ξ, at leading order, should decay in the far-field (4.57), we have $c_1 = 0$. Applying the gradient boundary condition, (4.56), we have $c_2 = (m-1)a_1^2\sqrt{\mathrm{E}}/(8\sqrt{2})$. Next, considering (4.55), one obtains

$$\xi\Big|_{x=0} = \frac{(m-1)a_1^2\sqrt{\mathrm{E}}}{8\sqrt{2}}\log\left[\frac{a_1+\sqrt{8}}{a_1-\sqrt{8}}\right]=1 \tag{4.58}$$

Since $a_1 \sim O(1)$ the above relation can only be satisfied if,

$$a_1 = \sqrt{8}+2\sqrt{8}\,e^{-\frac{1}{m-1}\sqrt{\frac{2}{\mathrm{E}}}}a_2, \tag{4.59}$$

where a_2 is an $O(1)$ constant. Although we have seemingly added an exponentially small quantity to the expected $O(1)$ estimate, this addition is crucial in the normal displacement boundary condition. With the transcendentally small addition, the normal displacement gradient, given by (4.56), is found to be exponentially large quantity. This obviously contradicts the algebraic scaling assumed in (4.56)[4], and helps highlight the difficulty in performing an asymptotic analysis in the limit of small E; in particular, the requirement of *exponential asymptotics* (Boyd [1999]). Physically, the location $x = a_1+\sqrt{8}$ and $x = a_1-\sqrt{8}$ correspond, in re-scaled form, to the fore- and aft-moving shear wave singularities. Since $a_1-\sqrt{8} \sim e^{-\frac{1}{m-1}\sqrt{\frac{2}{\mathrm{E}}}}$, the implication is that the aft-travelling shear wave is separated from the edge of the core only by a transcendentally small

[4]The contradiction that arises is not an artifact of the order in which we choose to satisfy the boundary conditions.

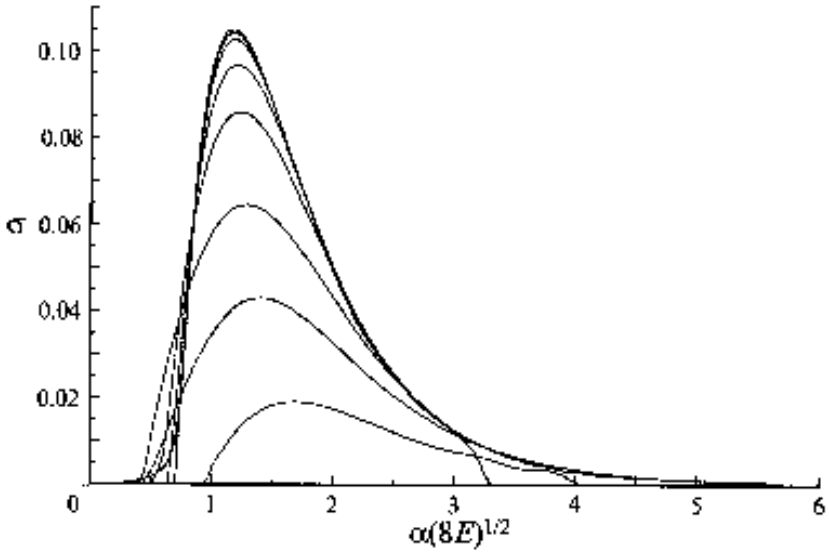

Figure 4.8: From Rallison & Hinch [1995] - "The growth rate $\sigma = \alpha c_i$ as a function of the rescaled wavenumber $\alpha(8\mathrm{E})^{1/2}$ for the varicose mode of an axisymmetric jet. The different curves are from the top for E = 0.0025, 0.005, 0.01, 0.025, 0.05, 0.1, 0.15 and 0.2.". The lack of collapse for small $\alpha(8\mathrm{E})^{1/2}$ must be noted, an indication for smaller-than-algebraic scaling.

amount. The mathematical character of the stability equations are identical for the vortex and parallel flow cases, and as evident in figure 4.8 for small rescaled wavenumber ($\alpha(8\mathrm{E})^{1/2} \ll 1$, α being the streetwise wavenumber), this is exactly the problem that plagues the analysis of purely elastic instability in a submerged jet (Rallison & Hinch [1995]).
To confirm the the requirement of *exponential asymptotics*, let us first consider an exactly soluble problem - the LHS of (4.47),

$$D\left[r^3\left\{(\omega - m\Omega)^2 - 2m^2\mathrm{E}\Omega'^2\right\}D\xi\right] = 0 \tag{4.60}$$

with boundary conditions (4.48)-(4.50). We refer to this as the LHS problem. The simplification will give us the leading-order behavior of the eigenvalue as the RHS enters in the asymptotics at a higher order. The solution of (4.60) which satisfies the boundary conditions (4.48) and (4.50) is,

$$\xi = \frac{\displaystyle\int_r^\infty \frac{dr'}{r'^3 P(r')}}{\displaystyle\int_1^\infty \frac{dr'}{r'^3 P(r')}}, \tag{4.61}$$

where, as defined before, $P(r) = (\omega - m\Omega(r))^2 - 2m^2\mathrm{E}\Omega'(r)^2$. On applying the boundary condition (4.49), we have the following dispersion relation:

$$\mathcal{D}(\omega, m; \mathrm{E}) \equiv 1 + (m-1)(\omega - m)^2 \int_1^\infty \frac{dr'}{r'^3 P(r')} = 0 \tag{4.62}$$

Before proceeding with a detailed analysis of the dispersion relation, we use a Nyquist method (Balmforth [1998]) to establish the presence of an unstable mode. Imagine a contour $\mathcal{C}$ in the

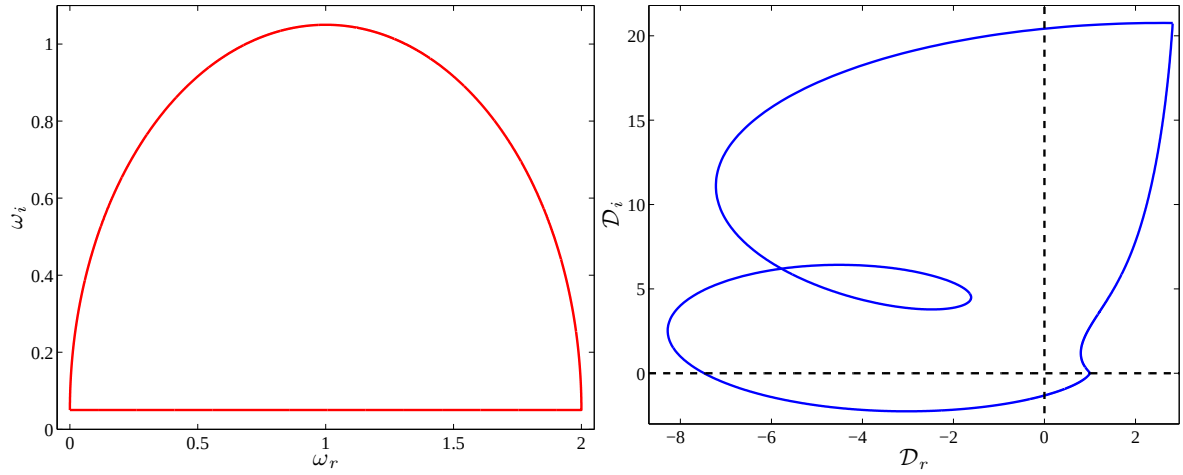

(a) Contour $\mathcal{C}$ in complex ω plane

(b) Contour $\mathcal{C}'$ in complex $\mathcal{D}$ plane

Figure 4.9: Diagnosis of the unstable elastic mode via the Nyquist method. $m = 2$, E=0.1

complex ω-plane (see figure 4.9a) mapped to the contour $\mathcal{C}'$ (see figure 4.9b) in the complex $\mathcal{D}$ plane via the mapping $\mathcal{D}(\omega)$. From the elastic version of Howard's semi-circle theorem for swirling flows, the contour $\mathcal{C}$ is chosen to be a suitably large semi-circle with the diameter an infinitesimal distance above the ω_r-axis. This ensures that an unstable mode, if it exists, would be contained inside $\mathcal{C}$. The choice of contour also avoids the branch-cut on the real-axis. The Nyquist method, which uses the idea of the winding number of an analytic function, states that the number of times $\mathcal{C}'$ loops the origin in the $\mathcal{D}$ plane equals the number of zeros of $\mathcal{D}(\omega, m; \mathrm{E})$. The existence of one or more such loops, as in figure 4.9b implies the presence of exponentially growing modes. Having confirmed that the LHS problem indeed allows for an unstable solution, we proceed to analyze the dispersion relation (4.62) in the limit of small E to obtain the scaling for the growth rate. (4.62), written out more explicitly after evaluation of the integral in closed form, takes the form

$$\mathcal{D}(\omega, m; \mathrm{E}) \equiv 1 + \frac{(m-1)f^2}{(\eta_1-\eta_2)(\eta_2-\eta_3)(\eta_3-\eta_1)} \{\eta_1(\eta_2-\eta_3)\log(1-\eta_1) + \eta_2(\eta_3-\eta_1)\log(1-\eta_2) + \eta_3(\eta_1-\eta_2)\log(1-\eta_3)\} = 0, \tag{4.63}$$

where $f = m/\omega - 1$ and $\eta_{1,2,3}$ are the roots of the cubic equation - $\eta(\eta-1-f)^2 - 8(1+f)^2\mathrm{E} = 0$. We make the *a priori* assumption of $f \ll 1$ but do not specify its smallness relative to E. This seems a reasonable assumption since we have already noted that the balance between elastic and inertial terms in P occurs when $\omega - m \sim O(\sqrt{\mathrm{E}})$. Knowing the exact expressions of $\eta_{1,2,3}$,

we expand them for small values of E and f:

$$\eta_1 = 1 + 2\sqrt{2\mathrm{E}} - 4\mathrm{E} + 10\sqrt{2}\mathrm{E}^{3/2} - 64\mathrm{E}^2 + f\left(1 + \sqrt{2\mathrm{E}} - 5\sqrt{2}\mathrm{E}^{3/2} + 64\mathrm{E}^2 + \ldots\right) + f^2\left(-\frac{\sqrt{\mathrm{E}}}{2\sqrt{2}} + \frac{15\mathrm{E}^{3/2}}{2\sqrt{2}} - 64\mathrm{E}^2 + \ldots\right) + \ldots, \tag{4.64}$$

$$\eta_2 = 8\mathrm{E} + 128\mathrm{E}^2 - 128f\mathrm{E}^2 + 128f^2\mathrm{E}^2 + \ldots, \tag{4.65}$$

$$\eta_3 = 1 - 2\sqrt{2\mathrm{E}} - 4\mathrm{E} - 10\sqrt{2}\mathrm{E}^{3/2} - 64\mathrm{E}^2 + f\left(1 - \sqrt{2\mathrm{E}} + 5\sqrt{2}\mathrm{E}^{3/2} + 64\mathrm{E}^2 + \ldots\right) + f^2\left(\frac{\sqrt{\mathrm{E}}}{2\sqrt{2}} - \frac{15\mathrm{E}^{3/2}}{2\sqrt{2}} - 64\mathrm{E}^2 + \ldots\right) + \ldots \tag{4.66}$$

and thus obtain asymptotic expression for f. The asymptotic expression for the eigenvalue ω is found to be,

$$\frac{\omega}{m} \sim 1 - \sqrt{\mathrm{E}}\left[\sqrt{8} + e^{-\frac{1}{m-1}\left(\sqrt{\frac{2}{\mathrm{E}}}-6\right)}\left\{2\sqrt{8} - 16\sqrt{\mathrm{E}} + 4\sqrt{8}\mathrm{E} - 128\mathrm{E}^{3/2}\log(32\mathrm{E}) - 64(3+4i\pi)\mathrm{E}^{3/2}\right\}\right] \tag{4.67}$$

Expectedly, $f \sim O(\sqrt{\mathrm{E}}) \ll 1$. The above expression highlights the transcendentally small nature of the growth rate ($\propto e^{-\frac{1}{m-1}\sqrt{\frac{2}{\mathrm{E}}}}$); specifically the dependence of the growth rate on E is given by, $\omega_i \sim O(\mathrm{E}^2 e^{-\frac{1}{m-1}\sqrt{\frac{2}{\mathrm{E}}}})$ in the limit $E \ll 1$. There will, of course be corrections to (4.67) from the neglected RHS terms, but the analysis in the next section shows that this correction is expected to only change the numerical pre-factor, but not the E scaling.

4.7 Complete asymptotics

The difficulty of dealing with a transcendentally small dependence on the small parameter could be bypassed by considering the case where $m\sqrt{\mathrm{E}} \sim O(1)$. The collapse of the curves in this parameter range, for various values of m (with $m^2 \gg 1$), was already noted in figure 4.4(b). The RHS of (4.47) then needs to be retained at leading order, and (4.53) takes the form:

$$\frac{d}{dx}\left[\left\{(a_1 - 2x)^2 - 8\right\}\frac{d\xi}{dx}\right] = \left\{(a_1 - 2x)^2 - 8\right\}\xi \tag{4.68}$$

in the elastic boundary layer, where we have assumed that $m^2 - 1 \approx m^2$, since $m \sim O(\mathrm{E}^{-1/2})$ and therefore, $m \gg 1$ for $\mathrm{E} \ll 1$. The above equation is a self-adjoint form of the confluent Heun equation (a spheroidal wave equation). Heun differential equations denote the class of ODEs with four regular singular points, one of them at infinity[5] (Ince [1956]). In the limit where one of the three singular points in the finite complex domain tends to infinity one obtains the confluent Heun equation with two regular singular points, and an irregular one at infinity [6]. The Frobenius exponents at the regular singular points have already been analyzed before;

[5] The more familiar hypergeometric class considers differential equations with three regular singular points.

[6] In the plane parallel flow context, Renardy [2008] has also noted the Heun form when studying stability of an axisymmetric jet with elasticity and inertia are dominant.

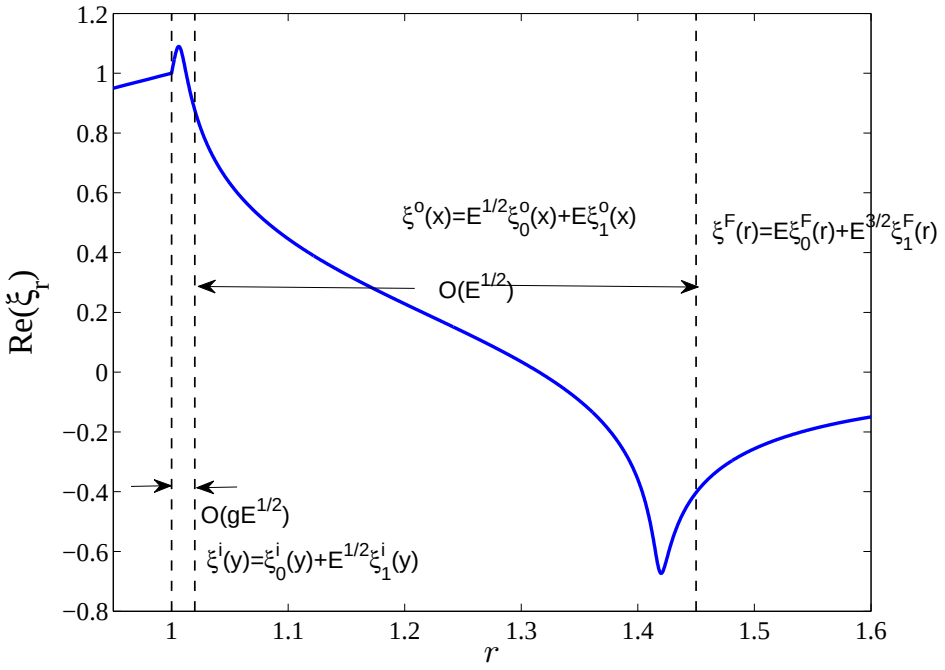

Figure 4.10: Boundary layer structure for radial displacement

these correspond, in the unscaled form, to $P(r_c) = 0$ (4.25); and physically, denote the shear-wave singularities. As noted by Rallison & Hinch [1995], recognizing (4.68) as a confluent Heun equation isn't particularly helpful from the perspective of obtaining closed form analytic solutions for $m\sqrt{\mathrm{E}} \sim O(1)$. In order to obtain some analytical insight into this problem, we therefore examine the limit $E \ll 1$ for $m \sim O(1)$ in this section. The transcendentally small growth rate expected in this limit necessitates a multiple boundary layer analysis. The asymptotic structure includes an inner boundary layer with $r - 1 \sim O(g\sqrt{\mathrm{E}})$ matching onto the boundary conditions at $r = 1$, the expected outer boundary layer with $r - 1 \sim O(\sqrt{\mathrm{E}})$, which in turn matches onto the outer region where $r - 1 \sim O(1)$. The introduction of the inner boundary layer implies that the outer $O(\sqrt{\mathrm{E}})$ boundary layer is no longer constrained to satisfy the boundary conditions at $r = 1$. This helps avoid the contradiction that arose in the naive approach.

The analytical approach follows the general principle of classical hydrodynamic stability in looking for an unstable mode in the vicinity of a neutral one (Lin [1961]). Although, in contrast to traditional theory, the neutral mode in this case is a singular one, and has a character already seen in the section on the 2D viscoelastic CS-spectrum. The approach adopted is thus generally applicable, and would therefore also be of use in the astrophysical analog of the problem. Figure 4.10 shows the different boundary layer regions in a numerically evaluated radial displacement eigenfunction. Based on the LHS problem, we assume the following expansion for the eigenvalue for the complete problem (including the RHS term):

$$\frac{\omega}{m} = 1 - \sqrt{\mathrm{E}}\left[\sqrt{8} + g\left\{c_0 + c_1\sqrt{\mathrm{E}} + c_2\mathrm{E} + c_{30}\mathrm{E}^{3/2}\log(32\mathrm{E}) + c_{31}\mathrm{E}^{3/2} + \ldots\right\}\right] \tag{4.69}$$

As will be seen, the fact that $g \sim e^{-\frac{1}{m-1}\sqrt{\frac{2}{\mathrm{E}}}}$ actually emerges from the detailed analysis below.

4.7.1 Far field- $r-1 \sim O(1)$

To begin with, we study the solution in the region where $r-1 \sim O(1)$. The radial displacement in this region is denoted by $\xi^F(r)$. Expanding P for small E, one obtains,

$$\begin{aligned} \frac{P}{m^2} &= \mathcal{S}_0 + \mathcal{S}_1\sqrt{\mathrm{E}} + \mathcal{S}_2\mathrm{E} + \ldots \qquad (4.70) \\ \text{where,} & \\ \mathcal{S}_0 &= \left(1-\frac{1}{r^2}\right)^2 \\ \mathcal{S}_1 &= -2\sqrt{8}\left(1-\frac{1}{r^2}\right) \\ \mathcal{S}_2 &= 8\left(1-\frac{1}{r^6}\right) \end{aligned}$$

This points to the following expansion of the eigenfunction,

$$\xi^F(r) = \mathrm{E}\,\xi_0^F(r) + \mathrm{E}^{3/2}\,\xi_1^F(r) + \mathrm{E}^2\,\xi_2^F(r) + \ldots \qquad (4.71)$$

where the $O(\mathrm{E})$ scaling of the leading order term is anticipated from the matching considerations between the different regions. As indicated in figure 4.10, the radial displacement is $O(1)$ only within the inner boundary layer, and is $O(\sqrt{\mathrm{E}})$ and $O(\mathrm{E})$ in the outer boundary layer, and outer regions respectively. Plugging the above expansion in (4.47), we collect terms of the same order and find the outer solution consistent with the far-field decay condition (4.50)

$\underline{O(\mathbf{E})}$

Equation - $\dfrac{d}{dr}\left[r^3 S_0 \dfrac{d\xi_0^F}{dr}\right] = 0$ with $\xi_0^F \to 0$ for $r \to \infty$,

$\Rightarrow\ \xi_0^F(r) = \dfrac{\mathcal{B}_0}{r^{m-1}(r^2-1)}.$

$\underline{O(\mathbf{E}^{3/2})}$

$\dfrac{d}{dr}\left[r^3\left\{S_0\dfrac{d\xi_1^F}{dr} + S_1\dfrac{d\xi_0^F}{dr}\right\}\right] = 0$ with $\xi_1^F \to 0$ for $r \to \infty$,

$\Rightarrow\ \xi_1^F(r) = \dfrac{2\sqrt{2}\mathcal{B}_0}{r^{m-1}(r^2-1)^2} + \dfrac{\mathcal{B}_1}{r^{m-1}(r^2-1)}.$

The far-field solution, to $O(\mathrm{E}^{3/2})$, is,

$$\xi^F(r) = \mathrm{E}\frac{\mathcal{B}_0}{r^{m-1}(r^2-1)} + \mathrm{E}^{3/2}\left\{\frac{2\sqrt{2}\mathcal{B}_0}{r^{m-1}(r^2-1)^2} + \frac{\mathcal{B}_1}{r^{m-1}(r^2-1)}\right\} + O(E^2). \qquad (4.72)$$

4.7.2 Outer boundary layer - $O(\sqrt{\mathbf{E}})$

Having found the structure of the solution for $r-1 \sim O(1)$, we now consider the $O(\sqrt{\mathrm{E}})$ boundary layer. Let us introduce a boundary layer coordinate (x) - $r = 1+\sqrt{\mathrm{E}}\,x$ and denote

the boundary layer displacement as $\xi(r) = \xi^o(x)$. In terms of the re-scaled coordinates, we have,

$$\frac{d}{dz}\left[\mathcal{Q}\frac{d\xi^o}{dz}\right] = \frac{2\mathrm{E}\mathcal{Q}(m^2-1)}{(1+\sqrt{2\mathrm{E}}(z+a_1/\sqrt{8}))^2}\xi^o, \tag{4.73}$$

where $z = \dfrac{2x-a_1}{\sqrt{8}}$. Further, $\mathcal{Q} = \dfrac{(1+\sqrt{2\mathrm{E}}(z+a_1/\sqrt{8}))^3 P}{m^2\mathrm{E}}$ is expanded as,

$$\mathcal{Q} = \mathcal{Q}_0 + \mathcal{Q}_1\sqrt{\mathrm{E}} + \mathcal{Q}_2\mathrm{E} + \ldots, \tag{4.74}$$

where,

$$\begin{aligned}
\mathcal{Q}_0 &= 8(z^2-1),\\
\mathcal{Q}_1 &= -12a_1(z^2-1) - 3\sqrt{2}(a_1^2-8)z,\\
\mathcal{Q}_2 &= 4(z^2-1)^2 + 3(a_1^2-88)(z^2-1) - 2\sqrt{2}a_1(a_1^2-24) - \frac{(a_1+\sqrt{8})^2}{16}(9a_1^2 - 4\sqrt{2}a_1 - 184).
\end{aligned}$$

This points to the following expansion of the eigenfunction,

$$\xi^o(z) = \sqrt{\mathrm{E}}\,\xi_0^o(z) + \mathrm{E}\,\xi_1^o(z) + \mathrm{E}^{3/2}\,\xi_2^o(z) + \ldots \tag{4.75}$$

Plugging the above expansion in (4.73), we collect terms of the same order. Note that neither the boundary conditions at r = 1, nor the far-field decay, are applicable to the outer boundary layer solution, and the unknown constants in the solutions below are entirely determined from the subsequent matching procedure.

$\underline{O(\sqrt{\mathbf{E}})}$

$$\frac{d}{dz}\left[\mathcal{Q}_0\frac{d\xi_0^o}{dz}\right] = 0,$$

$$\Rightarrow\ \xi_0^o(z) = \mathcal{G}_{10} + \mathcal{G}_{11}\log\left(\frac{z-1}{z+1}\right).$$

$\underline{O(\mathbf{E})}$

$$\frac{d}{dz}\left[\mathcal{Q}_0\frac{d\xi_1^o}{dz} + \mathcal{Q}_1\frac{d\xi_0^o}{dz}\right] = 0,$$

$$\Rightarrow\ \xi_1^o(z) = \mathcal{G}_{20} + \left(\mathcal{G}_{21} + \frac{3a_1}{2}\mathcal{G}_{11}\right)\log\left(\frac{z-1}{z+1}\right) - \frac{\mathcal{G}_{11}3\sqrt{2}(a_1^2-8)}{8(z^2-1)}.$$

$\underline{O(\mathbf{E}^{3/2})}$

$$\frac{d}{dz}\left[\mathcal{Q}_0\frac{d\xi_2^o}{dz} + \mathcal{Q}_1\frac{d\xi_1^o}{dz} + \mathcal{Q}_2\frac{d\xi_0^o}{dz}\right] = 2(m^2-1)\mathcal{Q}_0\xi_0^o,$$

$$\Rightarrow\ \xi_2^o(z) = \mathcal{G}_{30} + \left(\mathcal{G}_{31} - \frac{17}{2}\mathcal{G}_{11}\right)\log\left(\frac{z-1}{z+1}\right) + \frac{\mathcal{G}_{11}\left\{32(a_1-\sqrt{8}) - 7a_1(a_1^2-8) - 64(a_1+\sqrt{2}(z-1))\right\}}{4\sqrt{2}(z^2-1)} -$$

$$\frac{\mathcal{G}_{21}3(a_1^2-8)}{4\sqrt{2}(z^2-1)} + \frac{(m^2-1)}{3}\Big[\mathcal{G}_{10}\left\{z^2 - 2\log(z^2-1)\right\} + \mathcal{G}_{11}\Big\{-4z + \log(z-1)(z^2 + \log(256) - 4\log(z+$$

$$1)) - 8\mathrm{L}_2\Big(\frac{1-z}{2}\Big)\Big\}\Big],$$

where $\mathrm{L}_2(z) = -\displaystyle\int_0^z \frac{\log(1-t)}{t}dt$ is the dilogarithm function. As indicated above, $\mathcal{G}_{10}, \mathcal{G}_{11}, \ldots$

are constants determined via matching with the inner boundary layer and far-field. The $O(E^{3/2})$ solution includes the first contribution from the RHS terms in (4.47). The outer boundary layer solution to $O(\mathrm{E}^{3/2})$, is therefore given by:

$$\begin{aligned}\xi^o(z) &= \sqrt{\mathrm{E}}\left\{\mathcal{G}_{10}+\mathcal{G}_{11}\log\left(\frac{z-1}{z+1}\right)\right\}+\mathrm{E}\left\{\mathcal{G}_{20}+\left(\mathcal{G}_{21}+\frac{3a_1}{2}\mathcal{G}_{11}\right)\log\left(\frac{z-1}{z+1}\right)-\frac{\mathcal{G}_{11}3\sqrt{2}(a_1^2-8)}{8(z^2-1)}\right\}+\\ &\mathrm{E}^{3/2}\left[\mathcal{G}_{30}+\left(\mathcal{G}_{31}-\frac{17}{2}\mathcal{G}_{11}\right)\log\left(\frac{z-1}{z+1}\right)+\frac{\mathcal{G}_{11}\left\{32(a_1-\sqrt{8})-7a_1(a_1^2-8)-64(a_1+\sqrt{2}(z-1))\right\}}{4\sqrt{2}(z^2-1)}\right.\\ &-\frac{\mathcal{G}_{21}3(a_1^2-8)}{4\sqrt{2}(z^2-1)}+\frac{(m^2-1)}{3}\Big[\mathcal{G}_{10}\left\{z^2-2\log(z^2-1)\right\}+\mathcal{G}_{11}\Big\{-4z+\log(z-1)\\ &\left.(z^2+\log(256)-4\log(z+1))-8\mathrm{L}_2\Big(\frac{1-z}{2}\Big)\Big\}\Big]\Big]+O(\mathrm{E}^2\log(32E))\end{aligned} \tag{4.76}$$

Bearing in mind the matching to be done with the inner boundary layer ($z<1$), the multivaluedness of the logarithm needs to addressed. Invoking Lin's 'indentation rule', we regard the (singular) neutral mode as being the limit of an unstable mode, so that one obtains

$$\begin{aligned}\log(z-1) &= \log|z-1| \qquad z<1,\\ &= \log|z-1|+i\pi \quad z>1.\end{aligned} \tag{4.77}$$

Note that the existence of such a phase change across the critical radius has been proven in the framework of classical viscous theory (Drazin & Reid [1981]). It is quite likely that the effects of viscosity in the vicinity of critical layer again results in the same phase change as in the present case. However, the phase change is likely to be modified if the critical layer is governed by physics of a different kind.

4.7.3 Inner boundary layer - $O(g\sqrt{\mathrm{E}})$

Finally, we introduce an inner boundary layer in the irrotational region in the immediate neighbourhood of the vortex edge with, $r-1\sim O(g\sqrt{\mathrm{E}})$ with $g\ll 1$ for $\mathrm{E}\ll 1$. Defining a boundary layer coordinate by $r=1+g\sqrt{\mathrm{E}}\,y$ and denoting the inner boundary layer displacement as $\xi(r)=\xi^i(y)$, we have from (4.47)-(4.49):

$$\frac{d}{dy}\left[\mathcal{R}\frac{d\xi^i}{dy}\right]=\frac{g^2\mathrm{E}\mathcal{R}(m^2-1)}{(1+g\sqrt{\mathrm{E}}y)^2}\xi^i, \tag{4.78}$$

with $\mathcal{R} = (1 + g\sqrt{\mathrm{E}}y)^3 P/(m^2 g\mathrm{E})$ is expanded as:

$$\begin{aligned} \mathcal{R} &= \mathcal{R}_0 + \mathcal{R}_1\sqrt{\mathrm{E}} + \mathcal{R}_2\mathrm{E} + \mathcal{R}_{30}\mathrm{E}^{3/2}\log(32\mathrm{E}) + \mathcal{R}_{31}\mathrm{E}^{3/2} + \ldots, \qquad (4.79) \\ \text{where,} & \\ \mathcal{R}_0 &= 4\sqrt{2}(c_0 - 2y), \\ \mathcal{R}_1 &= 4\sqrt{2}(c_1 + 6\sqrt{2}y), \\ \mathcal{R}_2 &= 4\sqrt{2}c_2, \\ \mathcal{R}_{30} &= 4\sqrt{2}c_{30}, \\ \mathcal{R}_{31} &= 4\sqrt{2}c_{31}, \end{aligned}$$

In anticipation of the transcendental smallness, we assume $g\mathrm{E}^{-\alpha} \to 0$ as $\mathrm{E} \to 0$, $\forall\, \alpha > 0$.
The boundary conditions (4.48) and (4.49) now take the form:

$$\xi^i(y=0) = 1 \qquad (4.80)$$

$$\frac{d\xi^i}{dy}\Big(y=0\Big) = (m-1)\sqrt{\mathrm{E}}\left\{\frac{\sqrt{2}}{c_0} - \frac{\sqrt{2}c_1\sqrt{\mathrm{E}}}{c_0^2} + \frac{\sqrt{2}\left(c_1^2 - c_0c_2\right)\mathrm{E}}{c_0^3} - \frac{\sqrt{2}\left(c_1^3 - 2c_0c_1c_2 + c_0^2c_{31}\right)\mathrm{E}^{3/2}}{c_0^4} - \frac{\sqrt{2}c_{30}\mathrm{E}^{3/2}\log(32\mathrm{E})}{c_0^2} + \ldots\right\} \qquad (4.81)$$

Guided by the above expansions the boundary layer variable, $\xi^i(y)$, is expanded in the following manner:

$$\xi^i(y) = \xi_0^i(y) + \sqrt{\mathrm{E}}\,\xi_1^i(y) + \mathrm{E}\,\xi_2^i(y) + \mathrm{E}^{3/2}\,\xi_3^i(y) + \mathrm{E}^2\log(32\mathrm{E})\,\xi_{40}^i(y) + \mathrm{E}^2\,\xi_{41}^i(y) + \ldots \qquad (4.82)$$

where we note that the radial displacement is now $O(1)$. Plugging the above expansion in (4.78) and using the boundary conditions (4.80) and (4.81), we can collect terms and systematically find the inner boundary layer solution.

$\underline{O(1)}$

$$\frac{d}{dy}\left[\mathcal{R}_0\frac{d\xi_0^i}{dy}\right] = 0, \text{ with } \xi_0^i(y=0) = 1 \text{ and } \frac{d\xi_0^i}{dy}(y=0) = 0,$$
$$\Rightarrow\ \xi_0^i(y) = 1.$$

$\underline{O(\sqrt{\mathbf{E}})}$

$$\frac{d}{dy}\left[\mathcal{R}_0\frac{d\xi_1^i}{dy}\right] = 0, \text{ with } \xi_1^i(y=0) = 0 \text{ and } \frac{d\xi_1^i}{dy}(y=0) = \frac{\sqrt{2}(m-1)}{c_0},$$
$$\Rightarrow\ \xi_1^i(y) = -\frac{(m-1)}{\sqrt{2}}\log\left(\frac{c_0 - 2y}{c_0}\right).$$

$\underline{O(\mathbf{E})}$

$\frac{d}{dy}\left[\mathcal{R}_0\frac{d\xi_2^i}{dy}+\mathcal{R}_1\frac{d\xi_1^i}{dy}\right]=0$, with $\xi_2^i=0$ and $\frac{d\xi_2^i}{dy}=-\frac{\sqrt{2}(m-1)c_1}{c_0^2}$,

$\Rightarrow\ \xi_2^i(y)=-3(m-1)\log\left(\frac{c_0-2y}{c_0}\right)-\frac{(m-1)}{2}(\sqrt{2}c_1+6c_0)\left\{\frac{1}{c_0-2y}-\frac{1}{c_0}\right\}.$

$\underline{O(\mathbf{E}^{3/2})}$

$\frac{d}{dy}\left[\mathcal{R}_0\frac{d\xi_3^i}{dy}+\mathcal{R}_1\frac{d\xi_2^i}{dy}+\mathcal{R}_2\frac{d\xi_1^i}{dy}\right]=0$, with $\xi_3^i=0$ and $\frac{d\xi_3^i}{dy}=\frac{\sqrt{2}(m-1)(c_1-c_0c_2)}{c_0^3}$,

$\Rightarrow\ \xi_3^i(y)=-9\sqrt{2}(m-1)\log\left(\frac{c_0-2y}{c_0}\right)-\frac{(m-1)}{\sqrt{2}}(c_2+6\sqrt{2}c_1+36c_0)\left\{\frac{1}{c_0-2y}-\frac{1}{c_0}\right\}+$
$\frac{(m-1)}{2\sqrt{2}}(c_1+3\sqrt(2)c_0)^2\left\{\frac{1}{(c_0-2y)^2}-\frac{1}{c_0^2}\right\}.$

$\underline{O(\mathbf{E}^2\log(32\mathbf{E}))}$

$\frac{d}{dy}\left[\mathcal{R}_0\frac{d\xi_2^i}{dy}+\mathcal{R}_1\frac{d\xi_1^i}{dy}+\mathcal{R}_2\frac{d\xi_0^i}{dy}\right]=0$, with $\xi_{40}^i=0$ and $\frac{d\xi_{40}^i}{dy}=-\frac{\sqrt{2}(m-1)c_{30}}{c_0^2}$,

$\Rightarrow\ \xi_{40}^i(y)=-\frac{(m-1)}{\sqrt{2}}c_{30}\left\{\frac{1}{c_0-2y}-\frac{1}{c_0}\right\}.$

$\underline{O(\mathbf{E}^2)}$

Equation - $\frac{d}{dy}\left[\mathcal{R}_0\frac{d\xi_{41}^i}{dy}+\mathcal{R}_1\frac{d\xi_3^i}{dy}+\mathcal{R}_2\frac{d\xi_2^i}{dy}+\mathcal{R}_{31}\frac{d\xi_1^i}{dy}\right]=0$, with $\xi_{41}^i=0$ and
$\frac{d\xi_{41}^i}{dy}=-\frac{\sqrt{2}(m-1)(c_1^3-2c_0c_1c_2+c_0^2c_3)}{c_0^4}$,

$\Rightarrow\ \xi_{41}^i(y)=-54(m-1)\log\left(\frac{c_0-2y}{c_0}\right)-\frac{(m-1)}{\sqrt{2}}\{c_3+6\sqrt{2}c_2+54(c_1+3\sqrt{2}c_0)\}\left\{\frac{1}{c_0-2y}-\frac{1}{c_0}\right\}+$
$\frac{(m-1)}{2\sqrt{2}}\{2c_2(c_1+3\sqrt{2}c_0)+9\sqrt{2}(c_1+3\sqrt(2)c_0)^2\}\left\{\frac{1}{(c_0-2y)^2}-\frac{1}{c_0^2}\right\}-\frac{(m-1)}{3\sqrt{2}}(c_1+3\sqrt(2)c_0)^3\left\{\frac{1}{(c_0-2y)^3}-\frac{1}{c_0^3}\right\}$

Thus we have the inner boundary layer solution, to $O(\mathrm{E}^2)$, as:

$$\begin{aligned}\xi^i(y) \;=\;& 1-\sqrt{\mathrm{E}}\frac{(m-1)}{\sqrt{2}}\log\left(\frac{c_0-2y}{c_0}\right)-\mathrm{E}\left[3(m-1)\log\left(\frac{c_0-2y}{c_0}\right)+\frac{(m-1)}{2}(\sqrt{2}c_1+6c_0)\right.\\
&\left.\left\{\frac{1}{c_0-2y}-\frac{1}{c_0}\right\}\right]-\mathrm{E}^{3/2}\left[9\sqrt{2}(m-1)\log\left(\frac{c_0-2y}{c_0}\right)+\frac{(m-1)}{\sqrt{2}}(c_2+6\sqrt{2}c_1+36c_0)\right.\\
&\left.\left\{\frac{1}{c_0-2y}-\frac{1}{c_0}\right\}-\frac{(m-1)}{2\sqrt{2}}(c_1+3\sqrt(2)c_0)^2\left\{\frac{1}{(c_0-2y)^2}-\frac{1}{c_0^2}\right\}\right]-\mathrm{E}^2\log(32\mathrm{E})\frac{(m-1)}{\sqrt{2}}c_{30}\\
&\left\{\frac{1}{c_0-2y}-\frac{1}{c_0}\right\}-\mathrm{E}^2\left[54(m-1)\log\left(\frac{c_0-2y}{c_0}\right)+\frac{(m-1)}{\sqrt{2}}\{c_3+6\sqrt{2}c_2+54(c_1+3\sqrt{2}c_0)\}\right.\\
&\left\{\frac{1}{c_0-2y}-\frac{1}{c_0}\right\}-\frac{(m-1)}{2\sqrt{2}}\{2c_2(c_1+3\sqrt{2}c_0)+9\sqrt{2}(c_1+3\sqrt(2)c_0)^2\}\left\{\frac{1}{(c_0-2y)^2}-\frac{1}{c_0^2}\right\}+\\
&\left.\frac{(m-1)}{3\sqrt{2}}(c_1+3\sqrt(2)c_0)^3\left\{\frac{1}{(c_0-2y)^3}-\frac{1}{c_0^3}\right\}\right]+O(\mathrm{E}^{5/2}\log(32\mathrm{E}))\end{aligned}\tag{4.83}$$

The above solution satisfies both the boundary conditions at $y=0$, and further, needs to be matched to the solution in the outer boundary layer, which would then provide us with the

values of $c_0, c_1, \ldots$ required for obtaining the eigenvalue. Based on our LHS analysis we expect c_0 to be real, and thus, the multivalued-ness of the logarithm in (4.83) needs to be addressed. This would be essential in the matching region where we would consider $y \gg 1$. Invoking the 'indentation rule' once again, we have:

$$\begin{aligned} \log(c_0 - 2y) &= \log|c_0 - 2y| \qquad y < \frac{c_0}{2} \\ &= \log|c_0 - 2y| - i\pi \quad y > \frac{c_0}{2} \end{aligned} \tag{4.84}$$

Note that no information regarding the RHS (which is transcendentally small) has been used so far, and the above solution would therefore be identical to what one would obtain by constructing a similar inner boundary layer for the LHS problem.

4.7.4 Matching

With the inner, outer boundary layer and far-field solutions all obtained we proceed to derive the necessary constants via matching each of the solutions.

Far-field

First we expand the far-field solution for small values of $r-1$ and write it in terms of the outer boundary layer coordinate, $x = (r-1)/\sqrt{\mathrm{E}}$,

$\underline{r - 1 \ll 1}$

$$\begin{aligned} \xi^F \sim & \left\{\frac{\mathcal{B}_0}{2x} + O\left(\frac{1}{x^2}\right)\right\}\sqrt{\mathrm{E}} + \left\{\frac{1}{4}(1-2m)\mathcal{B}_0 + \frac{\mathcal{B}_1 - \sqrt{2}\mathcal{B}_0 m}{2x} + O\left(\frac{1}{x^2}\right)\right\}\mathrm{E} + \left\{\frac{\mathcal{B}_0(2m^2-1)}{8}x + \right. \\ & \left. \frac{1}{8}(2\mathcal{B}_1(1-2m) + \sqrt{2}\mathcal{B}_0(2m(m+1)-1)) + O\left(\frac{1}{x}\right)\right\}\mathrm{E}^{3/2} + \ldots \end{aligned} \tag{4.85}$$

Outer boundary layer

The outer boundary layer solution needs to be expanded both for large values of x, for matching with the far-field, and for small values, for matching with the inner boundary layer.

$\underline{x \gg 1}$

$$\begin{aligned} \xi^o \sim & \left\{\mathcal{G}_{10} - \frac{2\sqrt{2}\mathcal{G}_{11}}{x} + O\left(\frac{1}{x^2}\right)\right\}\sqrt{\mathrm{E}} + \left\{\mathcal{G}_{20} - \frac{2(6\mathcal{G}_{11} + \sqrt{2}\mathcal{G}_{21})}{x} + O\left(\frac{1}{x^2}\right)\right\}\mathrm{E} + \\ & \left\{\frac{\mathcal{G}_{10}(m^2-1)x^2}{6} + \frac{(2\mathcal{G}_{10} + 3\mathcal{G}_{11} - 2m^2(\mathcal{G}_{10} + 3\mathcal{G}_{11}))x}{3\sqrt{2}} + \Big(\mathcal{G}_{11} + \mathcal{G}_{30} + \right. \\ & \frac{m^2-1}{9}\left(2\mathcal{G}_{11}(2\pi^2 + 9 + 6(\log 2)^2) + \mathcal{G}_{10}(3 + \log 64)\right)\Big) + \frac{\sqrt{2}}{9x}\Big(9\mathcal{G}_{11} - 18\mathcal{G}_{31} + \\ & \left. 2(m^2-1)(6\mathcal{G}_{10} + \mathcal{G}_{11}(\log 64 - 25))\Big) + O\left(\frac{1}{x^2}\right)\right\}\mathrm{E}^{3/2} + \ldots \end{aligned} \tag{4.86}$$

$\underline{gc_0 \ll x \ll 1}$

$$\begin{aligned}\xi^o \;\sim\; & \Big\{\mathcal{G}_{10}+\mathcal{G}_{11}(\log\sqrt{8}+i\pi-\log x)\Big\}\sqrt{\mathrm{E}}+\Big\{\mathcal{G}_{20}+(3\sqrt{2}\mathcal{G}_{11}+\mathcal{G}_{21})(\log\sqrt{8}+i\pi-\log x)\Big\}\mathrm{E}+\\ & \Big\{9\mathcal{G}_{11}+\mathcal{G}_{30}-\frac{(17\mathcal{G}_{11}-2\mathcal{G}_{31})}{2}(\log\sqrt{8}+i\pi-\log x)-\frac{\mathcal{G}_{11}(m^2-1)}{18}(8\pi^2-3(8+20(\log 2)^2+\log 8)\\ & -6i\pi(1+\log 1024)+6(1+4i\pi+\log 16)\log x)-\frac{\mathcal{G}_{10}(m^2-1)}{3}(1-\log 2-2i\pi-2\log x)\Big\}\mathrm{E}^{3/2}+\ldots\end{aligned} \tag{4.87}$$

Inner boundary layer

The inner boundary layer solution is expanded for large values of y and written in terms of the outer boundary layer coordinate, $x = gy$,

$\underline{y >> 1}$

$$\begin{aligned}\xi^i \;\sim\; & 1-(m-1)\sqrt{\frac{\mathrm{E}}{2}}\left(\log\left|\frac{2}{c_0}\right|-\log g-i\pi+\log x\right)+(m-1)\mathrm{E}\Big\{3+\frac{c_1}{\sqrt{2}c_0}-3\Big(\log\left|\frac{2}{c_0}\right|-\log g-\\ & i\pi+\log x\Big)\Big\}+\frac{(m-1)\mathrm{E}^{3/2}}{4}\Big[\frac{12c_1}{c_0}-\sqrt{2}\left(\frac{c_1}{c_0}\right)^2+2\sqrt{2}\Big\{27+\frac{c_2}{c_0}-18\Big(\log\left|\frac{2}{c_0}\right|-\log g-i\pi+\\ & \log x\Big)\Big\}\Big]+(m-1)54\log g\,\mathrm{E}^2+\ldots\end{aligned} \tag{4.88}$$

On matching we obtain the following value of constants,

$$\begin{aligned}& g = e^{-\frac{1}{(m-1)}\sqrt{\frac{2}{\mathrm{E}}}}\\ & c_0 = 2\sqrt{8}e^{\frac{6}{m-1}},\; c_1 = 16(m-2)e^{\frac{6}{m-1}},\; c_2 = \frac{8\sqrt{2}}{9}e^{\frac{6}{m-1}}\left\{2(m^2-1)(\pi^2+12)+9(11m-10)\right\}\\ & \mathcal{G}_{10}=0,\;\mathcal{G}_{11}=\frac{m-1}{\sqrt{2}},\;\mathcal{G}_{20}=(m-1)(2m-1),\;\mathcal{G}_{21}=0,\\ & \mathcal{G}_{30}=\frac{2\sqrt{2}(m-1)}{9}\left\{9(2m-1)-(m^2-1)(\pi^2+3(\log 2)^2)\right\},\\ & \mathcal{G}_{31}=\frac{m-1}{\sqrt{2}}\left\{\frac{53}{2}-\frac{m^2-1}{3}(1+4i\pi+\log 16)\right\}\end{aligned}$$

We thus have the following asymptotic expression for the eigenvalue,

$$\begin{aligned}\frac{\omega}{m} \;=\; & 1-\sqrt{\mathrm{E}}\Big[\sqrt{8}+e^{-\frac{1}{(m-1)}\left(\sqrt{\frac{2}{\mathrm{E}}}-6\right)}\Big\{2\sqrt{8}+16(m-2)\sqrt{\mathrm{E}}+\frac{8\sqrt{2}}{9}\Big\{2(m^2-1)(\pi^2+12)+\\ & 9(11m-10)\Big\}\mathrm{E}+\ldots\Big\}\Big]\end{aligned} \tag{4.89}$$

The above expression gives us the modification of the LHS expression, (4.67). To the order analysed, is $O(\mathrm{E}^{3/2})$, (4.89) is purely real and doesn't have information about the growth-rate. The scaling of the growth rate, in the limit of small E, for the full problem must then be the same as that of the LHS problem ($O(\mathrm{E}^2)$); although the numerical pre-factor will not be the same. Since the numerics breaks down below a certain E (E$\approx$ 0.015 for $m = 2$), the analysis of the LHS problem, in particular, shows that the instability exists down to $E = 0$, and that there is no elastic threshold for instability.

4.8 Conclusions

In this chapter we identified a novel elastic instability for the Rankine vortex in a dilute polymer solution. The instability arises due to the resonance of elastic shear waves aided by the background shear in the irrotational exterior. The regime analyzed involves a leading order balance between inertia and elasticity and is governed by the elastic equivalent of the Rayleigh equation for swirling flows; momentum diffusion and relaxation of polymeric stresses for the disturbance is completely ignored. We proceed to numerically solve the elastic Rayleigh equation, and have also carried out a (multiple) boundary layer analysis in the limit of small E. The analysis helps extend the numerical results down to E=0, and the partial solution (the LHS problem) shows the absence of an elasticity threshold for instability; that is, the Rankine vortex appears to be unstable for any finite E. In the context of plane-parallel flows (e.g. - a submerged jet), it was believed that this purely elastic instability happened due to a discontinuity in base state shear, and would therefore be absent for smooth counterparts of such flows (Miller [2005]). In the present study in cylindrical geometry we have found that the instability persists even for smooth vorticity profiles - at least the 'intense' Rankine-like profiles. The study was entirely focussed on two dimensional disturbances and we anticipate more exciting physics to emerge when 3D effects are included.

Chapter 5

Optimal disturbances in stratified shear flow

The material in this chapter is done under the supervision of Prof. Rama Govindarajan.

5.1 Introduction

The interaction of stable stratification and mean shear plays a crucial role in problems of both engineering and geophysical interests (Turner [1973]). Classical inviscid stability theory states that a parallel mean velocity profile is stable to exponential disturbances if the Richardson number (Ri) is greater than 1/4 everywhere in the flow (Miles [1961]). Experiments and numerical simulations often belie this criterion (Farrell & Ioannou [1993a]). It is well known that algebraically growing disturbances can lead to transient amplification in shear flows, large enough for it to possibly undergo transition (Schmid & Henningson [2001]). The complexity of stratified shear flows stems from its ability to combine this transient amplification with propagating internal gravity waves (IGWs).

In this chapter we study the evolution of disturbances in a linearly density-stratified Couette flow. The initial value problem is solved asymptotically and the scope of algebraic growth is identified by subjecting the flow to localized buoyancy perturbations. An interesting analogy is noted between the three-dimensional lift-up effect in unstratified flows with two-dimensional algebraic instability present in the stratified case, normal vorticity being substituted by vorticity component along the mean vorticity. Next an optimal perturbation calculation is performed and dependence on stratification is studied. We also consider both temperature stratification in air and density stratification in water with relevance to heat and mass diffusion in atmosphere and ocean respectively. Another interesting feature which is also explored is the evolution of optimal energy ratio of potential energy to kinetic energy.

5.2 Problem formulation

We consider the stability of stratified fluid under the Bousinessq approximation (Spiegel & Veronis [1960]). The mean state is composed of a shear flow, $\overline{U}(z)$, present in an ambient density field, $\overline{\rho}(z)$. For non-dimensionalization we choose representative scales U_0, L_0 for velocity and length respectively. On linearization about the mean, the stability equations describing the

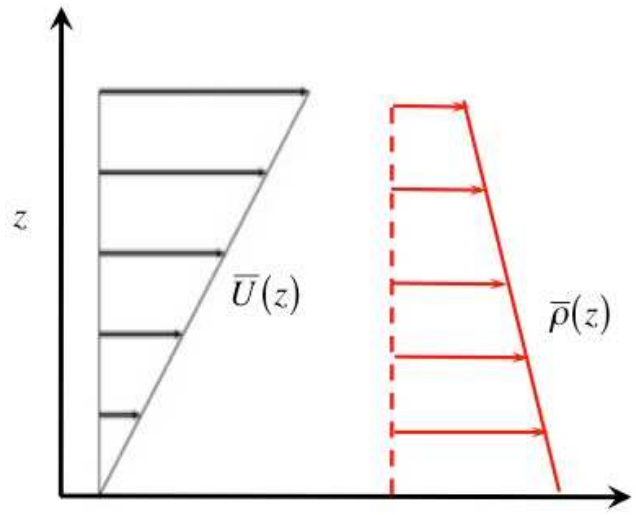

Figure 5.1: Flow Schematic

evolution of a three-dimensional velocity-density perturbation field could be written down as,

$$\left[\left(\frac{\partial}{\partial t}+\overline{U}\frac{\partial}{\partial x}\right)\nabla^2-\overline{U}''\frac{\partial}{\partial x}\right]w = -\mathrm{Ri}_0\nabla_H^2\rho+\frac{1}{\mathrm{Re}}\nabla^4 w \tag{5.1}$$

$$\left(\frac{\partial}{\partial t}+\overline{U}\frac{\partial}{\partial x}\right)\eta = -\overline{U}'\frac{\partial w}{\partial y}+\frac{1}{\mathrm{Re}}\nabla^2\eta \tag{5.2}$$

$$\left(\frac{\partial}{\partial t}+\overline{U}\frac{\partial}{\partial x}\right)\rho = \frac{N^2}{N_0^2}w+\frac{1}{\mathrm{Re\ Pr}}\nabla^2\rho \tag{5.3}$$

where w and η are the z-component of the velocity and vorticity perturbations respectively and ρ is the density perturbation. $\nabla_H^2=\frac{\partial^2}{\partial x^2}+\frac{\partial^2}{\partial y^2}$ is the horizontal laplacian. $N^2=-g\overline{\rho}'/\overline{\rho}_0$ is the Brunt-Väisälä frequency ($\overline{\rho}_0$ is chosen as the mean value of background density) and $N_0=\sqrt{g/L_0}$ is a reference value of this frequency. $\mathrm{Ri}_0=(N_0L_0/U_0)^2=\mathrm{Fr}^{-2}$ is a reference Richardson number (or inverse squared Froude number) whereas $\mathrm{Ri}=(NL_0/U_0)^2$ is the Richardson which captures the local variation of density. Viscous and diffusive effects are represented by the Reynolds number, $\mathrm{Re}=U_0L_0/\nu$ and Prandtl number, $\mathrm{Pr}=\nu/\kappa$. ν is the kinematic viscosity of the fluid and κ its thermal/mass diffusivity.

Assumption of normal mode form $f(x,y,z,t)=\hat{f}(z)e^{ik_x(x-ct)+ik_yy}$ for the inviscid, non-diffusive version of the system (5.1)-(5.3) gives us the celebrated Taylor-Goldstein-Haurwitz equation (Drazin & Reid [1981]),

$$(\overline{U}-c)\left[(\overline{U}-c)(\mathrm{D}^2-k^2)-\overline{U}''\right]\hat{w}+\mathrm{Ri}\ \hat{w}=0 \tag{5.4}$$

On incorporating viscous and diffusive dynamics we get,

$$\left[(\mathrm{D}^2-k^2)-ik_x\mathrm{RePr}(\overline{U}-c)\right]\left[(\mathrm{D}^2-k^2)^2-ik_x\mathrm{Re}\left\{(\overline{U}-c)(\mathrm{D}^2-k^2)-\overline{U}''\right\}\right]\hat{w}= k_x^2\mathrm{Pr\,Re}^2\mathrm{Ri}\,\hat{w} \tag{5.5}$$

$D = d/dz, k = \sqrt{k_x^2 + k_y^2}$.
Classical linear stability entails us solving the above equations for given boundary conditions as an eigenvalue problem. It is a well known fact that the Taylor-Goldstein-Haurwitz equation (5.4) is a singular equation similar to its homogenous counterpart - the Rayleigh equation. In addition (5.5) too is singular in the Pr$\rightarrow \infty$ limit even after inclusion of viscosity (finite Re). The singular nature of the equation isn't surprising as the Pr$\rightarrow \infty$ requires us dealing with $D\rho/Dt = 0$ i.e. density is conserved along streamlines and allowed to maintain arbitrarily cross-stream gradients. This singularity isn't as severe as its inviscid extension (Re,Pr $\rightarrow \infty$), in sense that all physically relevant quantities (velocity, vorticity) are regular at the location of singularity (Engevik [1974], Koppel [1964]).

5.3 Inviscid algebraic instabilities

(5.1)-(5.3) reveal an analogy between 3d stability of homogeneous shear flow and 2d stability of stratified shear flow. Without loss of generality let us consider uniform shear flow ($\overline{U} = z$). Let us consider normal mode of the form $e^{i(k_x x + k_y y)}$. Here onwards the hat decoration will be dropped and the context will elucidate whether we are dealing with f or $\hat{f}$. For 3d inviscid stability of homogeneous uniform shear flow the relevant equations are

$$\left(\frac{\partial}{\partial t} + ik_x\overline{U}\right)\nabla^2 w = 0 \tag{5.6}$$

$$\left(\frac{\partial}{\partial t} + ik_x\overline{U}\right)\eta = -ik_y\overline{U}'w \tag{5.7}$$

For 2d stability of stratified uniform shear flow in absence of diffusive and viscous effects we have,

$$\left(\frac{\partial}{\partial t} + ik_x\overline{U}\right)\rho = \frac{N^2}{N_0^2}w \tag{5.8}$$

$$\left(\frac{\partial}{\partial t} + ik_x\overline{U}\right)\xi = -ik_x \mathrm{Ri}_0\rho \tag{5.9}$$

where in 2d $\frac{\partial \xi}{\partial x} = \nabla^2 w$, ξ being the y component of perturbation vorticity (aligned along mean state vorticity).
(5.6)-(5.7) represent the classical Orr-Sommerfeld/Squire system which contains the celebrated algebraic instability - 'lift-up' (Ellingsen & Palm [1975], Landahl [1980]).

$$\eta = \eta_0(z)e^{-ik_x zt} - ik_y\overline{U}'\int_0^t w(z,t')e^{-ik_x z(t-t')}dt' \tag{5.10}$$

where η_0 is the initial normal vorticity. For streamwise independent perturbations ($k_x = 0$), $w(z,t) = w(z,0)$ and thus the normal vorticity increases linearly with time. For $k_x \neq 0$ the initial transient exhibits a linear growth before saturating. For the stratified case let us consider the toy problem where the background stratification is ignored but buoyancy perturbations are accounted for ($N^2 = 0$, $N_0^2 \neq 0 \Rightarrow \mathrm{Ri}_0 \neq 0$). It would probably not be unwise to draw parallels between buoyancy perturbations being advected by the flow and subsequently forcing the ξ, the

y component of perturbation vorticity, in the latter problem, with $\nabla^2 w$ (proportional to the wave-vector aligned vorticity component) being advected by the flow and subsequently forcing the evolution of normal vorticity, η, via w in the former. From (5.8)-(5.9) we have,

$$\xi = \xi_0(z)e^{-ik_x zt} - ik_x\rho_0(z)\mathrm{Ri}_0\, te^{-ik_x zt} \tag{5.11}$$

where ξ_0 is the initial y component of perturbation vorticity. This algebraic growth of ξ doesn't automatically imply algebraically growing perturbation energetics. The velocity fields, being integral and thus smoothening operations on the vorticity field, exhibit decaying long time asymptotics for smooth initial conditions of the form ($w \sim t^{-1}$ for $\rho_0 \neq 0$) consistent with the findings of Brown & Stewartson [1980] who studied this toy problem for the purpose of clarifying long time asymptotics of disturbances in stratified shear flow. The physics of this density initiated growth is different from that of 'lift-up'. The latter happens due to vertical transport of stream-wise momentum guided by mean flow momentum gradient ($\overline{U}' \neq 0$). The former happens due to the density field evolving uninhibited by the structure of the normal velocity field, w, but possessing the ability to force the normal velocity perturbations via buoyancy forcing. When $N^2 \neq 0$, w encounters resistance from the mean density gradient, thus reducing the 'resonant' buoyancy forcing of itself. This growth could be viewed as impulsive excitation of the system (a mass source forcing at $t = 0$) and the linear growth would happen even in a stratified system with no background flow. This can be seen from the short time expansion of the Green's function for disturbances in stratified medium (Voisin [1991]).

An idealized initial condition like a density sheet, $\rho_0 \propto \delta(z - z_0)$ (z_0 is a location in the flow domain), would be uninfluenced by the de-phasing process of background shear and thus allow for an algebraically growing velocity field and hence perturbation energy. This statement be easily checked by imposing a density sheet initial condition proxy in the form of a sharply localized density perturbation. If the initial condition has an extent of $O(\sqrt{\delta})$ then destructive interference of the initial condition would happen over a time-scale of $O(\delta^{-1/2})$, a period during which the linear growth would be observed and energy would attain a maximum value proportional to $O(\delta^{-1})$. A suitable density sheet proxy is a Gaussian density perturbation distribution, as one can appropriately approach a delta function as $\delta \to 0$. Thus the solution of (5.11) with the initial condition

$$\xi_0(z) = 0,\ \ \rho_0(z) = \frac{\mathcal{C}}{2\sqrt{\pi\delta}}e^{-(z-z_0)^2/4\delta} \tag{5.12}$$

can be written down as,

$$w = k_x^2\mathrm{Ri}_0\,\mathcal{C}t\int_{-1}^{1}\rho_0(z')\mathcal{G}^0(z,z')e^{-ik_x z't}dz' \tag{5.13}$$

where, $$\mathcal{G}^0(z,z') = -\frac{\sinh k_x(1-z)\sinh k_x(1+z')\mathcal{H}(z-z') + \sinh k_x(1+z)\sinh k_x(1-z')\mathcal{H}(z'-z)}{k_x\sinh k_x}$$

$$\Rightarrow w = -k_x\mathrm{Ri}_0\,\mathcal{C}\,\frac{\sinh k_x(1-z)\mathcal{G}_1^0 + \sinh k_x(1+z)\mathcal{G}_2^0}{4\sinh k_x}t\,e^{-ik_x z_0 t} \tag{5.14}$$

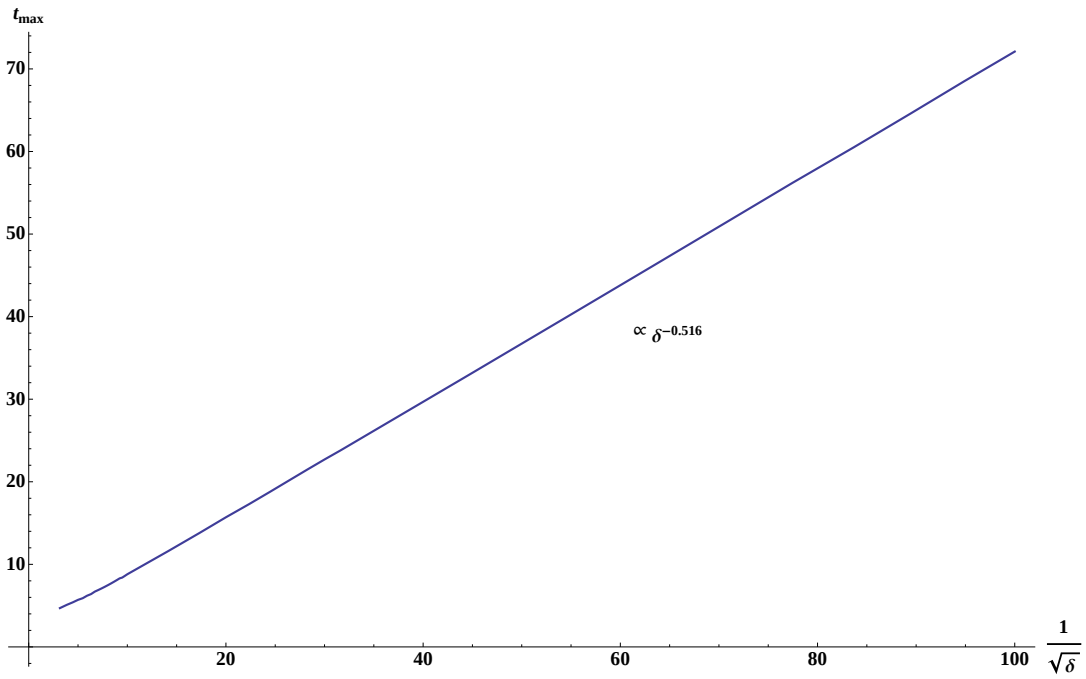

Figure 5.2: Duration of linear growth of velocity field for initial conditions given by equation 5.12 for different width of the initial condition

where

$$\begin{aligned}
\mathcal{G}_1^0 &= e^{-k_x^2(i+t)^2\delta+k_x(1+z_0)}\left(\text{Erf}\left[\frac{1+z_0-2ik_x\delta(i+t)}{2\sqrt{\delta}}\right]+\text{Erf}\left[\frac{z-z_0+2ik_x\delta(i+t)}{2\sqrt{\delta}}\right]\right)- \\
&\quad e^{-k_x^2(i-t)^2\delta-k_x(1+z_0)}\left(\text{Erf}\left[\frac{1+z_0+2ik_x\delta(i-t)}{2\sqrt{\delta}}\right]+\text{Erf}\left[\frac{z-z_0-2ik_x\delta(i-t)}{2\sqrt{\delta}}\right]\right) \\
\mathcal{G}_2^0 &= e^{-k_x^2(i-t)^2\delta+k_x(1-z_0)}\left(\text{Erf}\left[\frac{1-z_0-2ik_x\delta(i-t)}{2\sqrt{\delta}}\right]-\text{Erf}\left[\frac{z-z_0-2ik_x\delta(i-t)}{2\sqrt{\delta}}\right]\right)- \\
&\quad e^{-k_x^2(i+t)^2\delta-k_x(1-z_0)}\left(\text{Erf}\left[\frac{1-z_0+2ik_x\delta(i+t)}{2\sqrt{\delta}}\right]-\text{Erf}\left[\frac{z-z_0+2ik_x\delta(i+t)}{2\sqrt{\delta}}\right]\right)
\end{aligned}$$

For $\delta << 1$ and $t < 1/\sqrt{\delta}$, the solution would have the following asymptotic form,

$$w \sim -k_x \text{Ri}_0 \mathcal{C} \frac{\sinh k_x(1-z)\sinh k_x(1+z_0)\mathcal{H}(z-z_0)+\sinh k_x(1+z)\sinh k_x(1-z_0)\mathcal{H}(z_0-z)}{\sinh k_x} t\, e^{-ik_x z_0 t} \tag{5.15}$$

identical to the response due to a density sheet. On the contrary for $\delta << 1$ and $t >> 1/\sqrt{\delta}$, the decay is $O(t^{-1})$ in confirmation with Brown & Stewartson [1980].

On solving (5.8)-(5.9) for $N^2 = 0$ and initial conditions given by (5.12) we plot the duration of growth and maximum energy attained as a function of δ in figures 5.2-5.6. The numerical solutions confirm the argued scaling. We have shown this previously with Rahul Bale (Bale [2009]).

Having explained the dynamics using a toy model the immediate question that arises is - how far would this feature persist with background stratification? Would a intensely localized initial condition produce an algebraic growth for short times if $N^2 \neq 0$? If yes, would the growth be

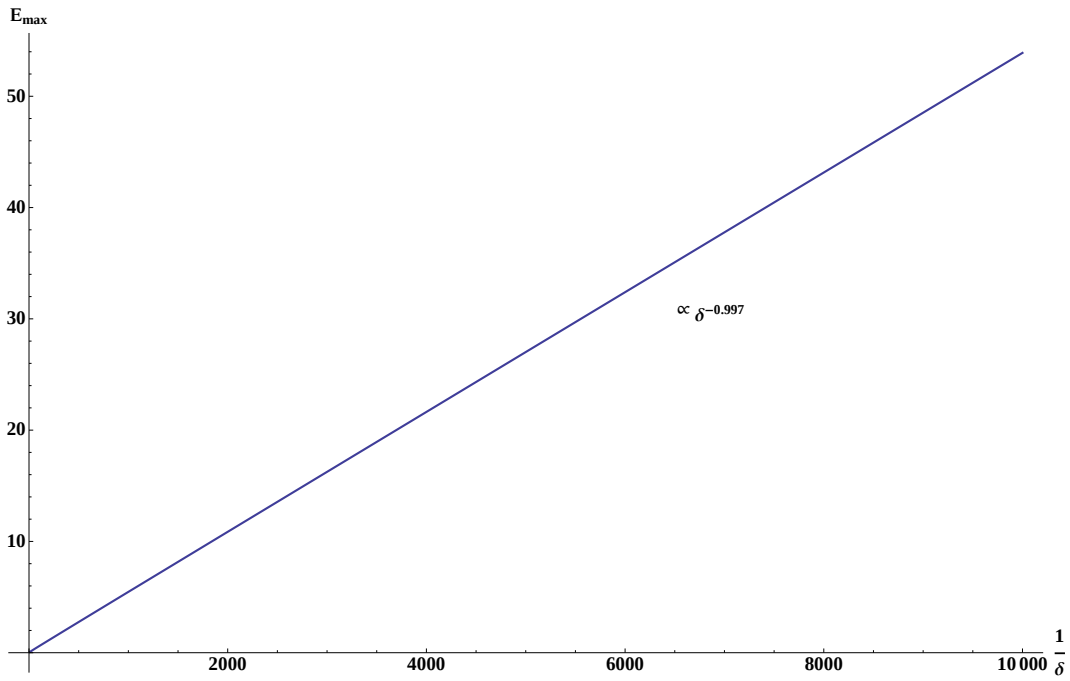

Figure 5.3: Maximum energy attained for initial conditions given by (5.12) for different width of the initial condition

linear, sub-linear or super-linear? The last scenario seems unlikely based on the inhibitive effect of background stratification but answers to the above questions demand a thorough analysis. On Laplace-transforming (5.8)-(5.9) and solving for w provides with the following expression,

$$w = \frac{1}{2\pi i}\int_{\gamma-i\infty}^{\gamma+i\infty}\int_{-1}^{1}\left[\frac{i\xi_0(z')}{(s+ik_xz')} + \frac{k_xRi\rho_0(z')}{(s+ik_xz')^2}\right]\mathcal{G}(z,z';s)dz'ds \tag{5.16}$$

where

$$\mathcal{G}(z,z';s) = \sqrt{(s+ik_xz)(s+ik_xz')}\frac{\{K_n(\Lambda_>)I_n(\Lambda_{z'}) - I_n(\Lambda_>)K_n(\Lambda_{z'})\}\{K_n(\Lambda_<)I_n(\Lambda_z) - I_n(\Lambda_<)K_n(\Lambda_z)\}}{K_n(\Lambda_1)I_n(\Lambda_{-1}) - I_n(\Lambda_1)K_n(\Lambda_{-1})}$$
$$n = \sqrt{\frac{1}{4} - \mathrm{Ri}},\ \Lambda_z = -i(s+ik_xz),\ \Lambda_{z'} = -i(s+ik_xz'),\ \Lambda_1 = -i(s+ik_x),\ \Lambda_{-1} = -i(s-ik_x)$$
$$\Lambda_> = \Lambda_1 H(z-z') + \Lambda_{-1}H(z'-z),\ \Lambda_< = \Lambda_{-1}H(z-z') + \Lambda_1 H(z'-z) \tag{5.17}$$

γ in the above Bromwich integral is chosen so as to encompass all the singularities of the solution in the transform space. Though a closed-form solution to the above inversion is not known, approximate forms of it have been obtained while working in various limits. A large number of studies have focussed on calibrating the long time asymptotics and as mentioned before, Brown & Stewartson [1980] put a lid to several such attempts (some erroneous). Here we will try extending our finding of algebraic instability by focusing on short time transients. Figure 5.5 depicts the singularities to be dealt with while performing the inverse Laplace transform. The Green's function, $\mathcal{G}(z,z';s)$ has simple poles at $s = s_n$ corresponding to internal gravity waves modified by shear (present only for Ri$>1/4$, figure 5.4) and algebraic branch-cuts at $s = -ik_xz$ and $s = -ik_xz'$ (a mobile one). An observation of the form of the initial condition which convolves with the Green's function would convince that $s = -ik_xz'$ is the more severe initial

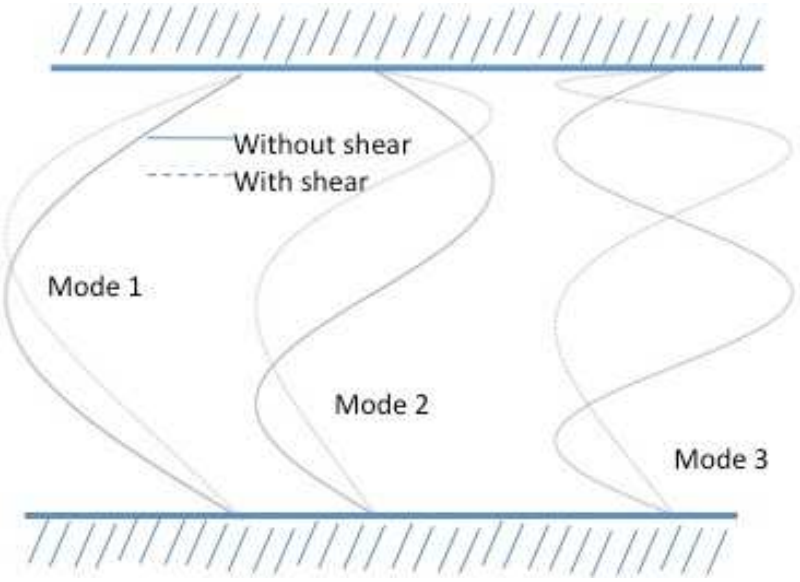

Figure 5.4: Sheared Internal Gravity Waves (uniform shear)

condition and would be primarily responsible for depicting initial transients. In the vicinity of $s = -ik_x z'$ we could approximate the Green's function as,

$$\mathcal{G}(z, z'; s) \sim (s + ik_x z')^{-n+\frac{1}{2}} g(z, z') \tag{5.18}$$

where, $$g(z, z') = -\frac{i^n \Gamma(n)}{2^{1-n}} \frac{\sqrt{ik_x(z-z')} I_n(\Lambda_>) \left\{K_n(\Lambda_<) I_n(k_x(z-z')) - I_n(\Lambda_<) K_n(k_x(z-z'))\right\}}{K_n(\Lambda_1) I_n(\Lambda_{-1}) - I_n(\Lambda_1) K_n(\Lambda_{-1})}$$

Now for a density sheet initial condition $\rho_z = \mathcal{C}\,\delta(z - z_0)$ the velocity field from (5.16) can be written down after performing the inverse Laplace transform as,

$$w(z,t) = \frac{k_x \mathrm{Ri}\, \mathcal{C}\, g(z, z_0)}{\Gamma(\frac{3}{2} + n)} e^{-ikz_0 t} t^{\frac{1}{2}+n} \tag{5.19}$$

Thus in presence of background stratification, the perturbation velocity field grows sub-linearly in response to a density sheet initial condition (Ri→0 recovers the linear growth).
Similar to the toy model, here too a smooth initial condition will exhibit $t^{1/2+n}$ growth initially before settling into the familiar $t^{-3/2+n}$ asymptotic decay (Booker & Bretherton [1967]). Figure 5.6 shows that numerical evaluation[1] of (5.8) and (5.9) for a localized density initial condition and a comparison to the predicted behavior of kinetic energy, $E \sim t^{2n+1}$.
The study with the toy model and the transient analysis for the entire problem revealed several interesting features but we need to explore the algebraic instabilities in stratified shear systems beyond the restrictive initial conditions we have considered so far. A common approach for such global analysis is the optimal perturbation methodology.

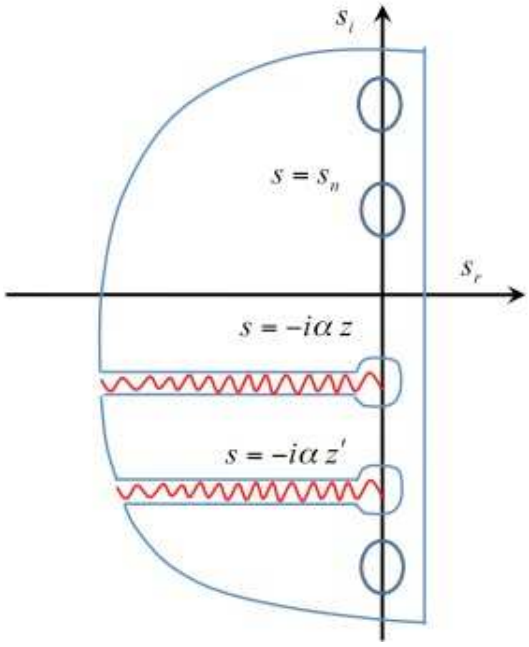

Figure 5.5: Bromwich contour with the singularities - branch cuts at $s = -i\alpha z, -i\alpha z$ and poles at $s = s_n$ (location of sheared gravity waves, absent for Ri<1/4)

5.4 Optimal Perturbation Analysis

The objective functional to be optimized (maximized in the present problem) is the total energy normalized by its initial value.

$$\mathrm{G}_{\max} = \frac{E(k_x, k_y; t)}{E(k_x, k_y; 0)} \tag{5.20}$$

where

$$E(k_x, k_y; t) = \frac{1}{2k^2} \int_{-1}^{1} (-w^*.\nabla w + \eta^*.\eta + \mathrm{Ri} k^2 \rho^* \rho) dz \tag{5.21}$$

The optimal perturbation approach involves scanning over the space of all initial conditions and finding the one which provides us with the maximum energy amplification. This can be done using two popular techniques - the singular value decomposition (SVD) technique (Schmid & Henningson [2001]) and the power iteration technique (Corbett & Bottaro [2000]). Both involve solving the following equation,

$$\frac{\partial \mathbf{q}}{\partial t} = \mathbf{A}\mathbf{q} \tag{5.22}$$

[1]For the numerical calculation, the spatial discretization is done using the Chebyshev spectral collocation method (Trefethen [2000]) and the time integration is carried out using the MATLAB software command ODE45, based on an explicit Runge-Kutta formula with adaptive step-sizes.

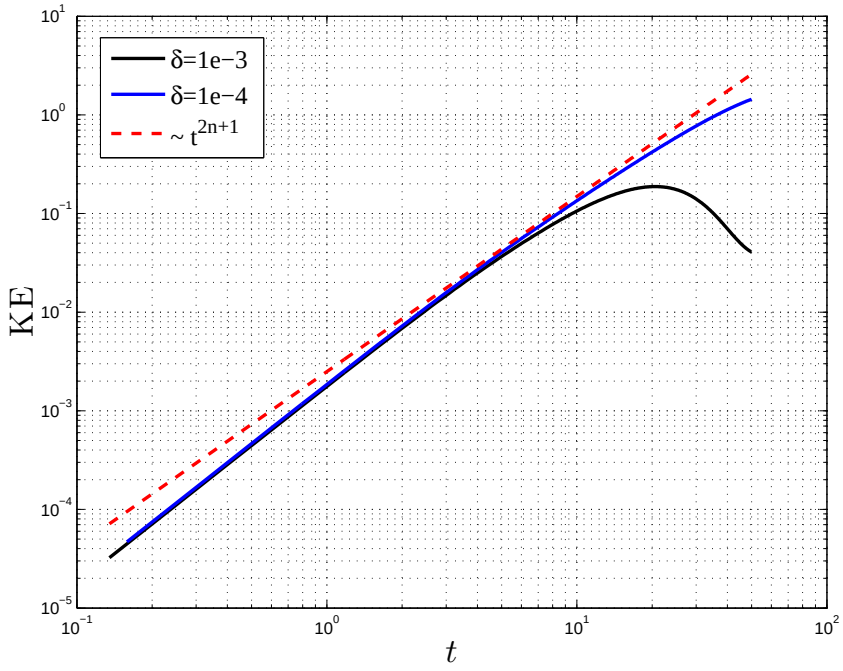

Figure 5.6: Kinetic energy evolution for initial conditions given by (5.12) (width - $\delta = 1e-3, 1e-4$) and its comparison with asymptotic estimate (Ri=0.1, $k_x = 1$)), when $N \neq 0$.

$\mathbf{q} = [w\ \eta\ \rho]^T$,with the given boundary conditions. Where, $\mathbf{A} = \mathbf{M}^{-1}\mathbf{L}$

$$\mathbf{M} = \begin{bmatrix} \mathrm{D}^2 - k^2 & 0 & 0 \\ 0 & 1 & 0 \\ 0 & 0 & 1 \end{bmatrix} \tag{5.23}$$

$$\mathbf{L} = \begin{bmatrix} \mathrm{L}_{OS} & 0 & k^2\mathrm{Ri}_0 \\ -ik_y\overline{U}' & \mathrm{L}_{SQ1} & 0 \\ \dfrac{N^2}{N_0^2} & 0 & \mathrm{L}_{SQ2} \end{bmatrix} \tag{5.24}$$

$$\mathrm{L}_{OS} = -ik_x\overline{U}(\mathrm{D}^2 - k^2) + ik_x\overline{U}'' + \frac{1}{Re}(\mathrm{D}^2 - k^2)^2 \tag{5.25}$$

$$\mathrm{L}_{SQ1} = -ik_x\overline{U} + \frac{1}{\mathrm{Re}}(\mathrm{D}^2 - k^2) \tag{5.26}$$

$$\mathrm{L}_{SQ2} = -ik_x\overline{U} + \frac{1}{\mathrm{Re\ Pr}}(\mathrm{D}^2 - k^2) \tag{5.27}$$

The power iteration technique has been made more rigorous and versatile by developing it from the perspective of Lagrangian formulation (Guégan [2007]). It is a generalized method to find optimal perturbations, and is applicable even for non-linear problems (scenario where SVD and eigenfunction expansion based techniques do not work). For linear systems the power iteration technique is particularly useful when one deals with unbounded systems. Unbounded shear flows have viscous continuous spectrum and SVD, which involved expanding over a finite basis of eigenfunctions, may underestimate the energy amplification by not appropriately capturing the contribution from the viscous continuous spectrum (Guégan *et al.* [2006]). For bounded systems (the present case being one) SVD is more suited than power iteration due to computational efficiency. Though we have performed calculations using both techniques - results presented

have been done using a SVD analysis. In the present chapter we will restrict the detailed parameter space that is accessible we will fix Re=500.

5.4.1 2D optimal perturbations

Figure 5.7 shows the variation of G_{max}, the optimal streamwise wavenumber ($k_{x,opt}$) and the optimal time (T_{opt}) with stratification (Ri). The dominant mechanism of energy amplification in 2D is the Orr mechanism and it involves titling of wave fronts by background shear and the Reynolds stress aiding in energy transfer from the mean flow to the perturbations. Stratification resists vertical motion and that translates to the inhibition of energy amplification by the Orr mechanism. This is easily seen for Pr=1 (figure 5.7(a)). But interestingly when the density field remains frozen and only gets stirred by the diffusive velocity field (Pr=700,7000) then for an initial range of Ri, the stratified cases exhibit more amplification than the unstratified case, see Figure 5.7(b), confirming that this amplification results from momentum diffusion in the absence of mass diffusion. Both $k_{x,opt}$, T_{opt} (figures 5.7(c)-(d)) show a clear demarcation of dynamics at Ri$\approx$ 0.25. For a uniformly stratified Couette flow, according to inviscid theory, Ri= 0.25 indicates the onset of sheared IGWs. At any Ri greater than this value, the dynamics is going to be largely influenced by IGWs. This is clearly observed in figure 5.7(d) where the T_{opt} perfectly scales with $Ri^{-0.5}$, and is thus just a measure of the inverse of N, the Brunt-Väisälä frequency. We may thus ask whether this is true algebraic growth.

Since we deal with a global quantity like G_{max}, an important feature in the context of stratified shear flows which is often overlooked in the optimal perturbation calculations is the 'energy partitioning' i.e. the ratio PE/KE (PE is the potential energy and KE the kinetic energy). In figure 5.8 the temporal evolution of the total energy and its two components is shown for optimal initial condition excitations for various values of Ri and Pr. For weak stratification, the momentum forcing describes the total energy evolution almost till optimal time beyond which the buoyancy component sustains it. For strong stratification, IGWs set in and the energy evolution is described both via momentum and buoyancy forcing. The maximum energy amplification occurs during the maximum of PE. One can guess, with increasing stratification, the initial forcing will transition from a purely momentum one to increasingly more buoyant one (figure 5.9(a)). But at the optimal instant this ratio saturates with increasing stratification (figure 5.9(b)).

5.4.2 3D optimal perturbations

In 3D the dominant transient growth mechanism is the 'lift-up' effect. As already discussed this involves redistribution of momentum by fluid parcel traveling vertically. Stratification once again reduces transient amplification as seen in figure 5.10(a). Comparing with 2D results it initially appears surprising that k_x, k_y and T_{opt}, none of them exhibits a transition at Ri=0.25. This becomes clear when one realizes that 'lift-up' effect dictates $k_{x,opt} \to 0$ as Ri$\to$ 0. Thus for small Ri, with vanishing streamwise dependence, the vertical velocity and buoyancy equation

can be reduced from (5.22)-(5.24) as,

$$\frac{\partial}{\partial t}(\mathrm{D}^2 - k_y^2)w = k_y^2 \mathrm{Ri}_0 \rho \tag{5.28}$$

$$\frac{\partial}{\partial t}\rho = \frac{N^2}{N_0^2} w \tag{5.29}$$

$$\Rightarrow \quad \frac{\partial^2}{\partial t^2}(\mathrm{D}^2 - k_y^2)w = k_y^2 \mathrm{Ri} w \tag{5.30}$$

The above system supports IGWs for any non-zero Ri; by considering $k_x = 0$ the role of shear has been removed. This is confirmed from the optimal perturbation calculations - T_{opt} scales with the buoyancy time scale ($\sim \mathrm{Ri}^{-0.5}$) (figure 5.10(d)) and the amplification which depends on the optimal time as T_{opt}^2, scales as O(Ri^{-1})(figure 5.10(a)).

An interesting quantity to study via optimal perturbation calculation is the obliqueness of the optimal initial condition. The obliqueness is measured as $\theta = \tan^{-1}(k_{y,\mathrm{opt}}/k_{x,\mathrm{opt}})$. In the unstratified case, the initial condition is almost streamwise independent ($k_{x,\mathrm{opt}}$ =35/Re for Couette flow). With increasing stratification the initial condition becomes increasingly oblique (5.11).

Unlike 2D, in 3D the optimal forcing is momentum dominated as can be seen from the PE/KE ratio at the initial instant and also the optimal time (figure 5.12).

5.5 Conclusions

Evolution of non-modal disturbances in stratified shear flows is studied in the present chapter. First an analogy with unstratified 'lift-up' effect is drawn for 2D stratified shear flow. Algebraic growth occurs in 2D stratified shear flows for localized buoyancy forcing and comparisons are made with numerical solutions.

Next the focus is shifted to optimal perturbation calculations. Both 2D and 3D optimal perturbations in stratified shear flows are studied. The focus is on how various optimal quantities, , vary with stratification (Ri). Stratification suppresses the transient amplification in both 2D and 3D because of its resistance to any vertical motion, crucial for both Orr mechanism and 'lift-up' effect. There occurs an exception in 2D when the mass diffusion is neglected and stratified cases could lead to larger amplification than the unstratified case.

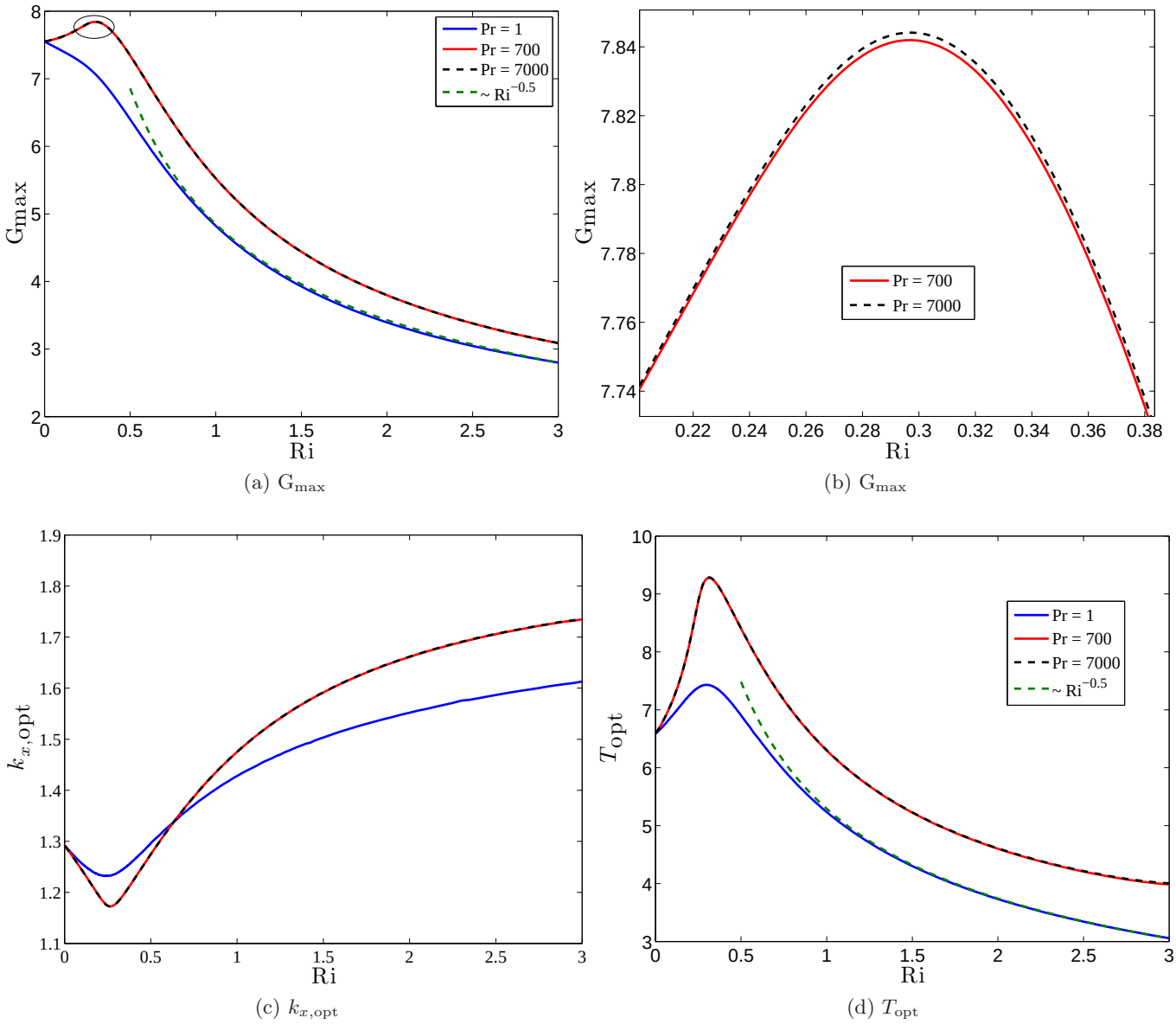

(a) G_{max} (b) G_{max}

(c) $k_{x,opt}$ (d) T_{opt}

Figure 5.7: Dependence of optimal G_{max}, $k_{x,opt}$ and T_{opt} on stratification (Ri) for various values of Pr. (b) is a zoomed in version of (a) highlighting the larger values for Pr=7000 over that of Pr=700

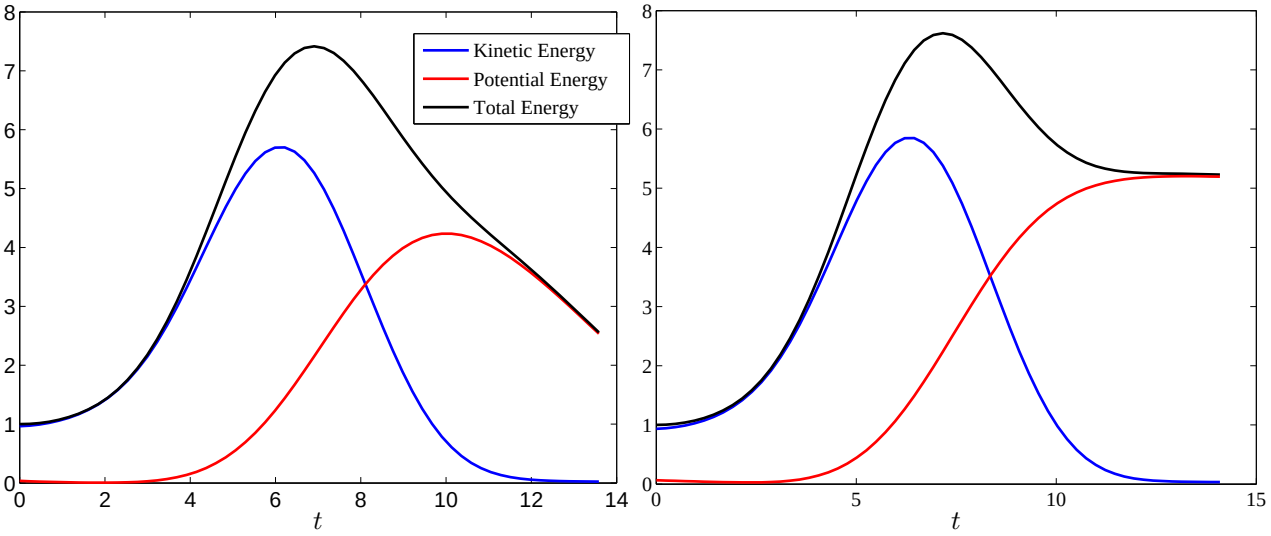

(a) Ri=0.1, Pr=1

(b) Ri=0.1, Pr=700

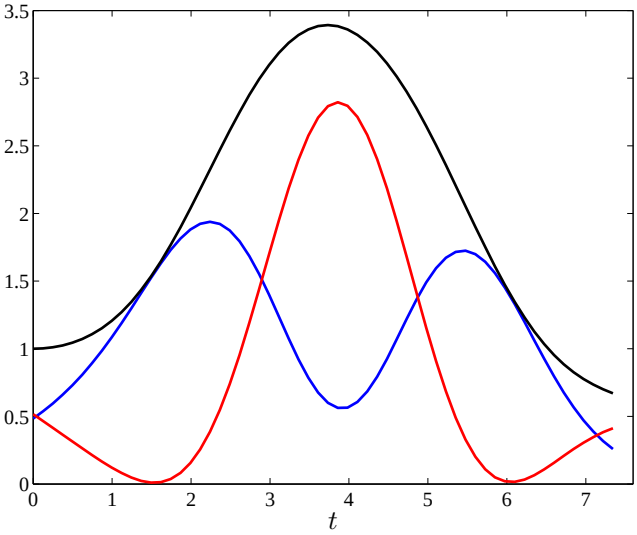

(c) Ri=2, Pr=1

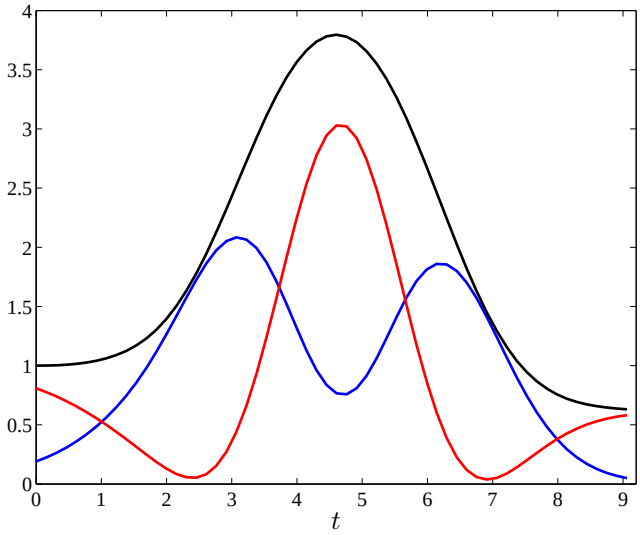

(d) Ri=2, Pr=700

Figure 5.8: Temporal evolution of kinetic, potential and total energy for various values of Ri and Pr for an excitation corresponding to optimal initial condition and optimal T

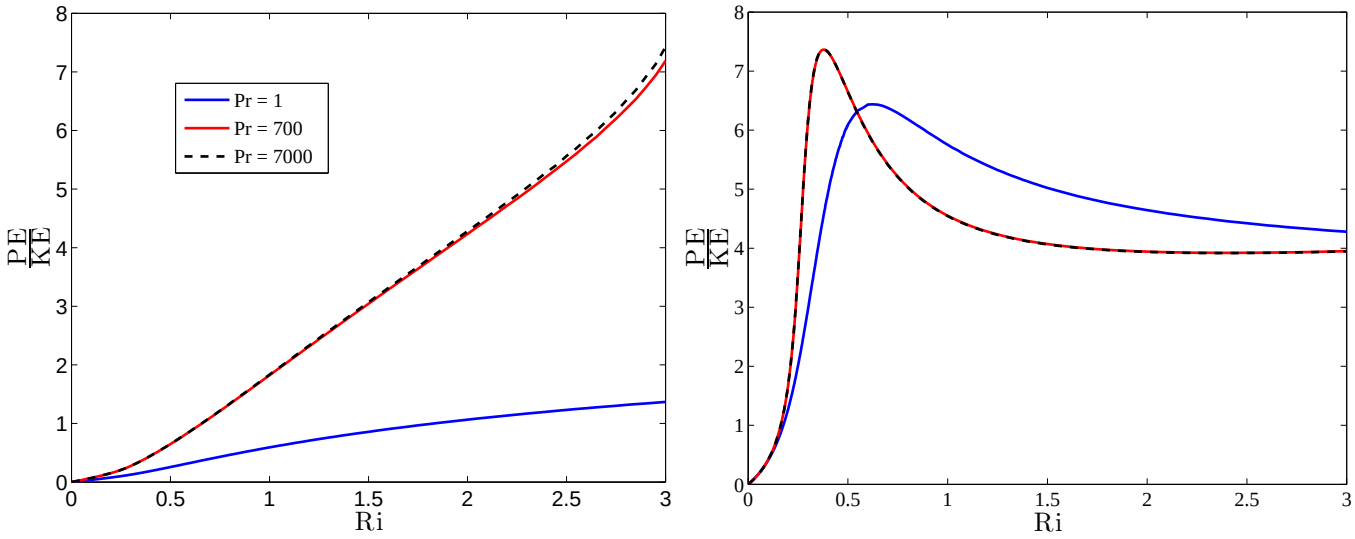

(a) $t = 0$ (b) $t = T_{\text{opt}}$

Figure 5.9: Variation of 'energy partitioning' (PE/KE) on stratification (Ri) at the initial instant (a) and optimal time (b)

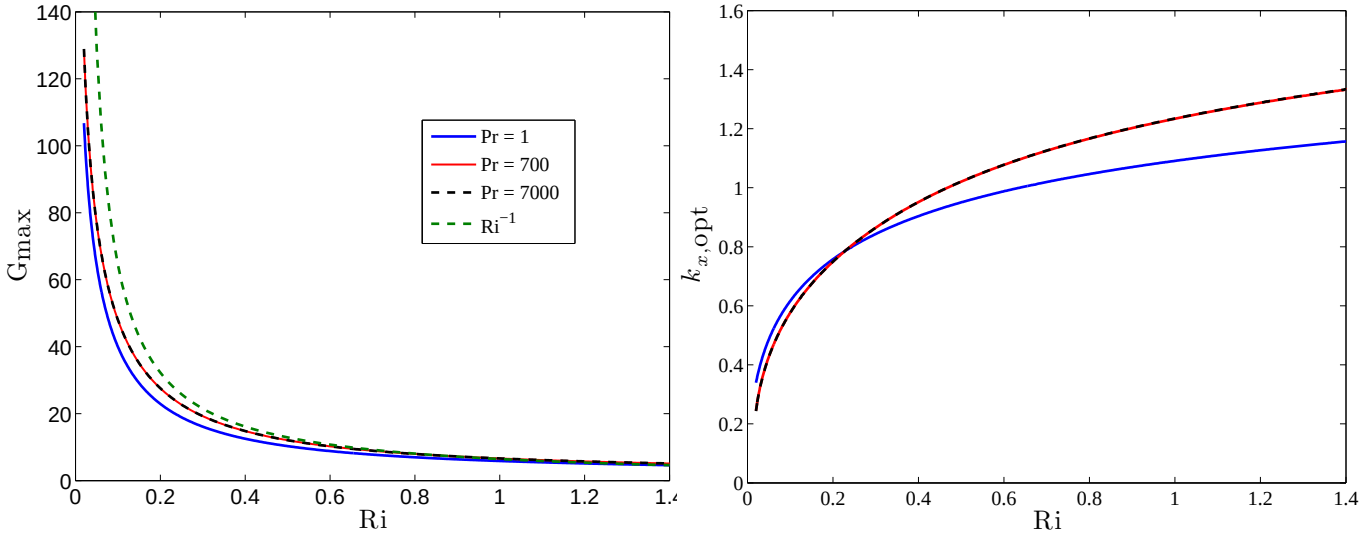

(a) $\mathrm{G_{max}}$

(b) $k_{x,\mathrm{opt}}$

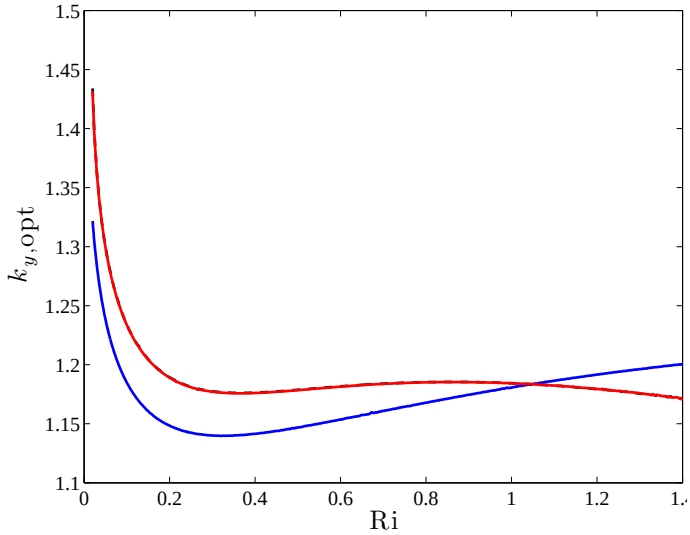

(c) $k_{y,\mathrm{opt}}$

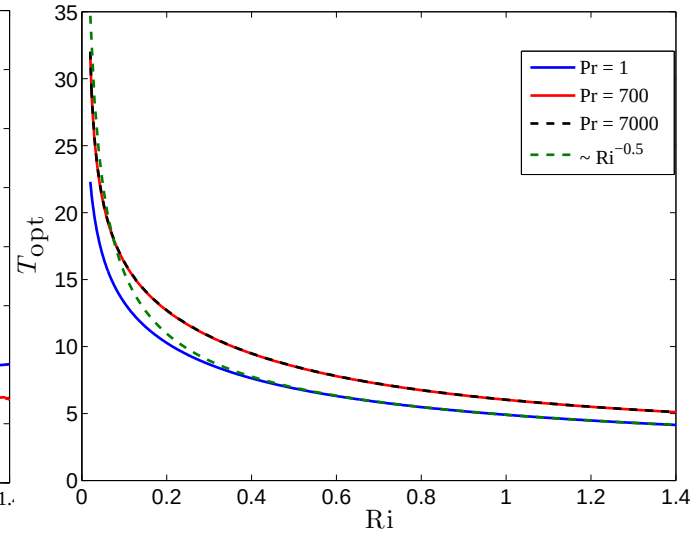

(d) T_{opt}

Figure 5.10: Dependence of optimal $\mathrm{G_{max}}$, $k_{x,\mathrm{opt}}$, $k_{y,\mathrm{opt}}$ and T_{opt} on stratification (Ri) for various values of Pr.

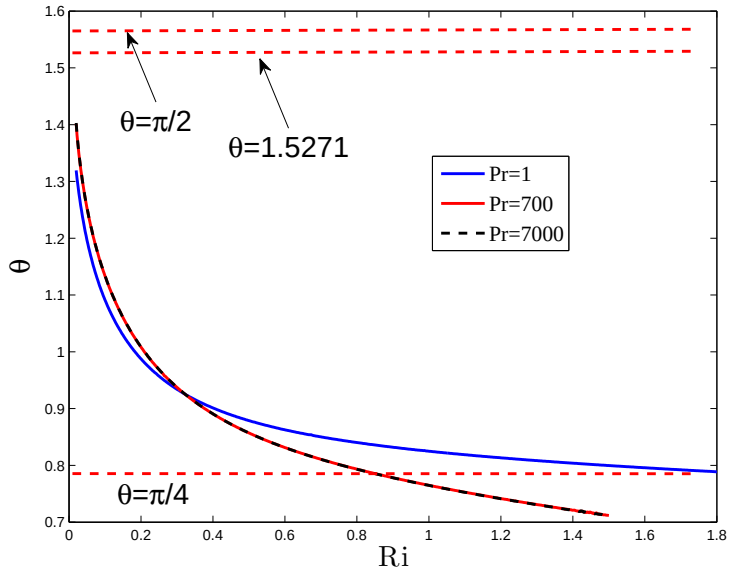

Figure 5.11: Variation of obliqueness of the optimal perturbation with stratification. $\theta = 1.5271$, for $k_{x,\mathrm{opt}} = 35/\mathrm{Re}, k_y = 1.6$, is the optimal obliqueness for unstratified Couette flow.

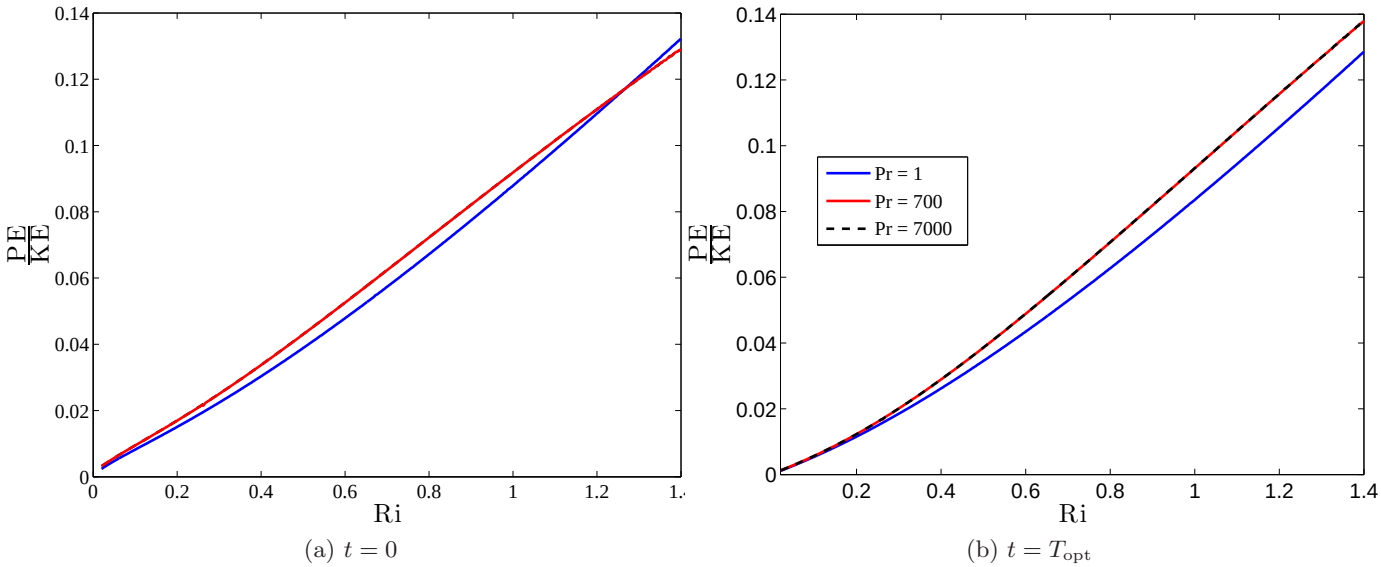

(a) $t = 0$ (b) $t = T_{\mathrm{opt}}$

Figure 5.12: Variation of 'energy partitioning' (PE/KE) on stratification (Ri) at the initial instant (a) and optimal time (b)

Chapter 6

Normal mode interpretation of 'lift-up' effect

6.1 Introduction

The non-modal behavior of infinitesimal disturbances in shear flows is attributed mathematically to the non-normal nature of the underlying linear stability operator (Schmid & Henningson [2001]). The two dominant physical mechanisms for non-modal behavior, leading to short-time algebraic growth, are the Orr mechanism and the lift-up effect. A Reynolds-stress-based argument, that allows for a transfer of energy between the mean flow and an imposed perturbation, is usually offered as an explanation for the Orr mechanism (for instance, see Farrell [1987];Pradeep & Hussain [2006]). For the lift-up effect, which comes into play only in the presence of an added spanwise variation of an imposed perturbation, the common explanation is based on the redistribution of mean-flow momentum in the transverse direction; for instance, one finds a mention of this basic mechanism in Benney & Lin [1960]. The mechanism may be best understood for purely spanwise disturbances in which case the wall normal disturbance velocity is time independent, and transports ('lifts up') the mean momentum, riding on its gradient, to produce a streamwise disturbance velocity that grows linearly in time (Schmid & Henningson [2001]).

Albeit more cumbersome, a perturbation-vorticity-based stretching/tilting mechanism may also used to explain the phenomenon and lends more insight. This complementary vortex-tilting based explanation, for a single spanwise-directed Fourier mode, is illustrated in figure 6.1. In this picture, the lift-up effect arises because the vertical shear in the mean vorticity direction, due to the spanwise variation in the vertical perturbation velocity ($\partial\hat{u}_y/\partial z$: representative of a 'roll' initial condition), tilts the mean vorticity ($-\overline{U}'$), producing a linearly growing wall-normal perturbation vorticity ($\hat{w}_y$: representative of the vorticity field of a growing streak); note that a general roll initial condition (as opposed to the single Fourier mode in figure 6.1) would have an associated $\partial\hat{u}_z/\partial z$, and would therefore also stretch the base-state vorticity at linear order. Now, there is an additional linearly growing streamwise perturbation vorticity field ($\hat{w}_x$) generated due to $\hat{w}_y$ being tilted by the mean shear ($\overline{U}'$), but this is exactly cancelled by the tilting of the base-state vorticity ($-\overline{U}'$) due to the spanwise variation of the streamwise perturbation velocity ($\partial\hat{u}_x/\partial z$ induced by $\hat{w}_y$). As a result, only the growing streak survives. Such a cancellation, however, occurs only for plane parallel flows where the base-state velocity gradient and vorticity are given by $+\overline{U}'$ and $-\overline{U}'$, respectively. This is no longer the case for curvilinear (vortical) flows, and the latter vortex stretching-tilting mechanism noted above persists in these cases (chapter 3). This latter mechanism for algebraic growth has been referred as the 'anti lift-up' effect in the context of axisymmetric vortices (Antkowiak & Brancher [2004]). In fact, the traditional lift-up effect is vanishingly small in regions of negligible base-state vorticity,

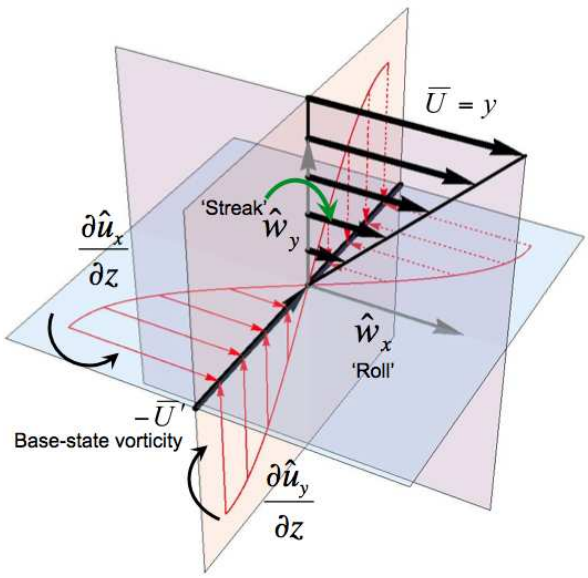

Figure 6.1: Algebraic growth in shear flow associated with a spanwise 'roll' Fourier mode into a 'streak' Fourier mode.

being identically zero for the limiting case of an irrotational flow induced by a point vortex. Finally, we note that although Ellingsen & Palm [1975] and Landahl [1980] are often credited as being the first to offer an explanation for the 'lift-up' effect based on a solution of the initial value problem, the possibility of algebraic growth of general disturbances in shear flows, due to the presence of a *Jordan block* structure in the linear stability operator, can be found even earlier in Arnol'd [1972].

Both the algebraic growth mechanisms discussed above are essentially of an inviscid origin with viscosity only leading to an eventual decay of the perturbation kinetic energy on a time scale that, in convective units, is proportional to the Reynolds number (Schmid & Henningson [2001]). Thus, there must exist an alternate interpretation of the algebraic growth, in plane parallel shearing flows, in terms of the known dynamics of the inviscid continuous spectra associated with the Rayleigh operator (Case [1960];Sazonov [1996]; chapter 2). Such an interpretation is most easily seen for the Orr mechanism in two dimensions. While the original IVP analyses describing the Orr mechanism in Couette flow (for instance, see Farrell [1987]) were in terms of Kelvin modes (Fourier modes with a time-dependent wave vector that is turned by the ambient linear flow), an equivalent description may be given in terms of a convected superposition of CS-modes; for two-dimensional perturbations, these modes are flow aligned vortex sheets (Case [1960]). In the Kelvin mode interpretation, the temporal dynamics of the kinetic energy may be divided into growth and decay phases corresponding to the (planar) wavefronts of the Fourier mode having upstream and downstream inclinations, respectively. The shearing flow turns the wavefronts from the former to the latter orientation, and the instant of maximum kinetic energy corresponds to vertical or gradient-aligned wavefronts. In the equivalent CS-mode interpretation, as shown in figure 6.2, one considers the action of a shearing flow on an ensemble of vortex-sheet CS-modes staggered in the upstream direction. The greater the degree of upstream staggering, the smaller is the degree of coherence (in phase) in the gradient direction, and the smaller is the

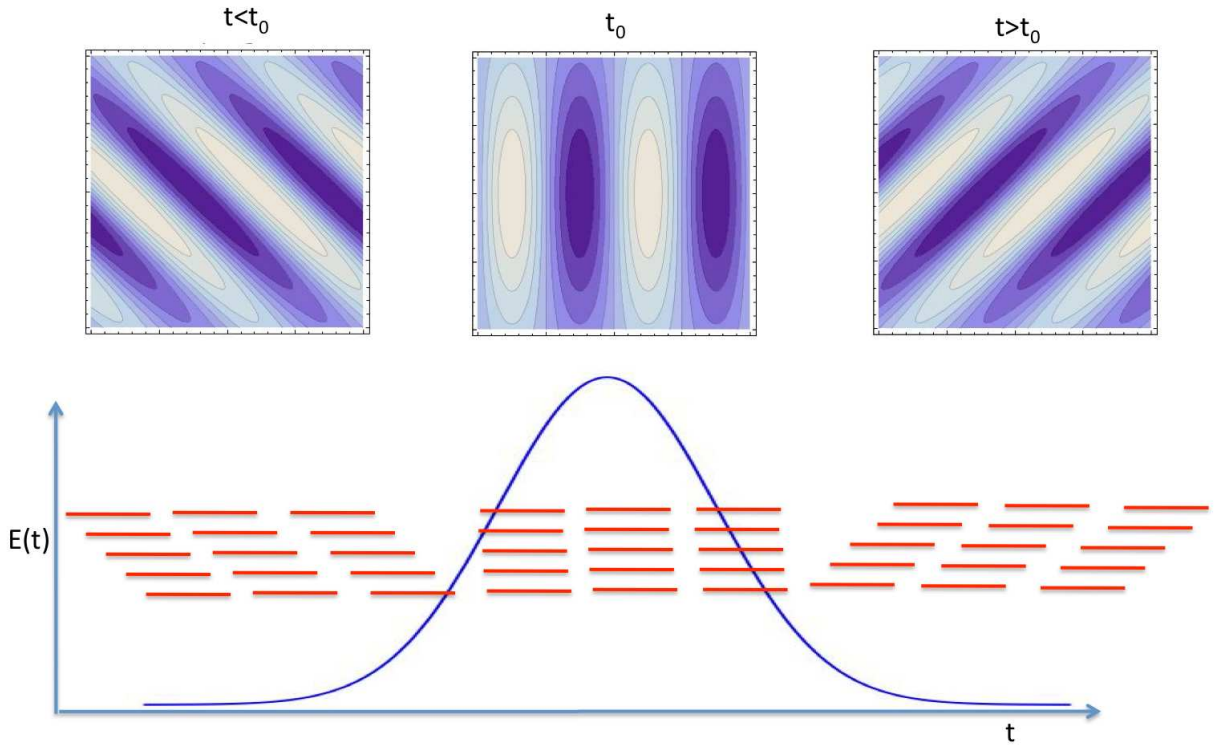

Figure 6.2: Schematic illustrating Orr mechanism via tilting of an upstream oriented initial condition by background shear. The top array of figures represent the perturbation streamfunction at its initial instant and its subsequent evolution. The bottom array represents the temporal evolution of kinetic energy with superimposed on it stacks of Case vortex sheets, an eigenmode, used to represent the flow at various instants of its evolution.

initial kinetic energy. The differential convection due to shear brings the vortex sheets into phase-alignment, and the instant of maximum coherence in the transverse direction corresponds to the maximum kinetic energy. Further convection by shear causes the vortex sheets to progressively de-cohere, leading to a decrease in the kinetic energy for later times. Although not necessary, the superposition of phase-aligned vortex sheet may be such as to reproduce a single Kelvin mode, in which case the two interpretations are coincident. Further, the kinetic energy decays as $O(t^{-2})$ for long times in the inviscid limit, and this may be seen by noting that the motion for long times is primarily along the horizontal, and the kinetic energy therefore scales as $O[k_y(t)]^2\psi$ with ψ being the stream function and $k_y(t)$ being the (time-dependent) inverse length scale in the gradient direction. Since the vorticity field does not decay in the inviscid case, we have $k_y^2(t)\psi \sim O(1)$ with $k_y \sim O(t)$ for long times.

To the best of our knowledge, there exists no modal explanation for the inviscid lift-up effect along the above lines; in particular, a modal representation of the growth that arises due to a purely spanwise perturbation when there can be no contribution due to the Orr mechanism, and more generally, for any three-dimensional perturbation when the growth is no longer solely due to the Orr mechanism. A modal explanation for the lift-up effect is attributed to the non-normality of the operator and the resulting non-orthogonality of the discrete viscous modes. In the present work we attempt to offer an explanation for the lift-up effect based on the inviscid eigenmodes, and argue that this is preferrable to the existing explanation (Schmid & Henningson [2001]) for large Reynolds number (Re) since the individual viscous modes do not have sensible limits for $Re \to \infty$. This chapter is organized as follows. In section 6.2 the problem is formulated for a base-state corresponding to an arbitrary plane-parallel shear flow. Herein, the choice of a wave-vector aligned coordinate system, instead of the usual flow-aligned one, allows one to simplify the normal mode analysis. Next, in section 6.3, based on the existing knowledge of the 3D CS-modes for Couette flow (Sazonov [1996]) and the 2D CS-modes for non-linear shear flows (Balmforth & Morrison [1995a]), the two families of CS-eigenfunctions, for a non-linear shear flow, are obtained. This then leads the required modal superposition for an arbitrary initial condition that then exhibits the possibility of algebraic instability in the form of the 'lift-up' effect. Since exponentially unstable modes are not responsible for the 'lift-up' effect, the analysis above is initially developed for a non-inflectional smooth velocity profile in which case the spectrum is absolutely continuous (which automatically excludes any discrete modes; see Lin [1955];Fadeev [1971]); later, the superposition is generalized to accommodate inflectional velocity profiles by allowing for additional discrete modes. The inviscid modal interpretation of the 'lift-up' effect given here is complementary to the existing interpretation via non-orthogonal viscous discrete modes, although the relation between the two is non-trivial. Thus, section 6.5 is devoted to a discussion of the connection between an inviscid eigenmode and the discrete viscous modes, for large but finite Re, in the context of the analytically soluble problem of Couette flow. Section 6.6 concludes by summarizing the main findings of this communication.

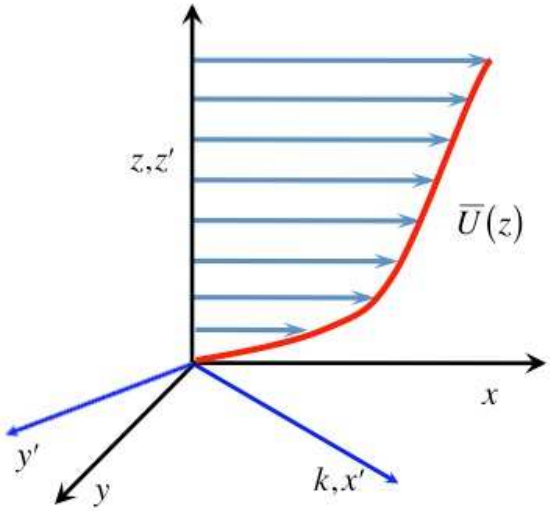

Figure 6.3: Shear flow in the flow aligned and wave-vector aligned coordinate systems

6.2 Problem formulation

Let us consider a 3D Fourier mode imposed on a shear flow, with the base-state velocity profile $\overline{U}(z)$, in a wave-vector-aligned coordinate system (x', y', z) instead of the usual flow-aligned coordinate system (x, y, z) with x, y and z in the latter case corresponding, respectively, to the flow, gradient and vorticity directions of the base-state. Since the flow and vorticity directions are homogeneous, the wave-vector, $\boldsymbol{k} \equiv (k_x, k_y)$, lies in the flow-vorticity plane, and the Fourier mode has the general form $F(z)e^{i[(k_x x + k_y y) + ct]}$. The aforementioned coordinate systems are related by a rotation about the z-axis as shown in figure 6.3. If ϕ be the angle made by $\boldsymbol{k}$ with the flow direction, the relevant relations between the coordinates are given by:

$$k_x = k\cos\phi, \qquad k_y = k\sin\phi, \qquad k_{x'} = k = \sqrt{k_x^2 + k_y^2}, \tag{6.1}$$

$$u_{x'} = u_x\cos\phi + u_y\sin\phi, \qquad u_{y'} = u_y\cos\phi - u_x\sin\phi, \qquad u_z' = u_z. \tag{6.2}$$

The linearized equations of motion for the perturbation velocity components, and the different components of the perturbation vorticity field, in the flow-aligned and wave-vector-aligned coordinate systems, are summarized in table 6.1, where D is used to denote d/dz.

Table 6.1: Relevant equations in the flow-aligned and wave-vector-aligned coordinate systems

Momentum Equation	
Flow aligned	Wave-vector aligned
$ik_x(\overline{U}-c)u_x + u_z\overline{U}' = -ik_x p$	$ik_x(\overline{U}-c)u_{x'} + u_z\overline{U}'\cos\phi = -ikp$
$ik_x(\overline{U}-c)u_y = -ik_y p$	$ik_x(\overline{U}-c)u_{y'} - u_z\overline{U}'\sin\phi = 0$
$ik_x(\overline{U}-c)u_z = -Dp$	$ik_x(\overline{U}-c)u_z = -Dp$
$ik_x u_x + ik_y u_y + Du_z = 0$	$iku_{x'} + Du_z = 0$
Vorticity Components	
Flow aligned	Wave-vector aligned

$w_z = ik_x u_y - ik_y u_x$	$w_z = iku_{y'}$
$w_x = ik_y u_z - Du_y$	$w_{x'} = -Du_{y'}$
$w_y = Du_x - ik_x u_z$	$w_{y'} = Du_{x'} - iku_z$
$(D^2 - k^2)u_z = ik_y w_x - ik_x w_y$	$(D^2 - k^2)u_z = -ikw_{y'}$

In wave-vector-aligned coordinates, one can write down a system of equations for the normal velocity (u_z) and vorticity fields ($w_z = ik_x u'_y$) equivalent to the Rayleigh-Squire system known for the flow aligned coordinate system (the structure of the finite Re analog of the Rayleigh-Squire system, the Orr-Sommerfeld-Squire system, is discussed in detail in Schmid & Henningson [2001]):

$$ik(\overline{U} - c)w_{y'} = -\overline{U}'' u_z, \tag{6.3}$$

$$ikk_x(\overline{U} - c)u_{y'} = \overline{U}' k_y u_z, \tag{6.4}$$

where we note from table 6.1 that $w_{y'}$ is related to the normal velocity perturbation as $-ikw_{y'} = (D^2 - k^2)u_z$. The Rayleigh equation for $w_{y'}$, the component of vorticity normal to $\boldsymbol{k}$, remains identical to that for two-dimensional perturbations with $\boldsymbol{k}$ along the flow axis. The system (6.3)-(6.4) supports two families of CS-modes, and for a non-inflectional velocity profile which supports a purely continuous spectrum, it will be shown by construction that these two families constitute a complete set of (singular) eigenfunctions capable of representing an arbitrary initial vorticity distribution. One of the families arises from the homogeneous solution of the Rayleigh equation, with the resulting normal velocity field forcing the Squire equation; these are the Rayleigh or, as we shall term them, the Λ_1 modes. The second family is a homogeneous solution of (6.4), the Squire equation, and therefore has a velocity field restricted to the flow-vorticity plane. These Squire modes will be termed the Λ_2 modes in what follows. The latter nomenclature is motivated by our identification of these families with the structure of the two independent CS-mode families known for the case of a Rankine vortex (chapter 2); although, there is an additional discrete spectrum in the vortex case. In general, there are differences in detail with regard to the structure of vorticity (and velocity) field associated with the Λ_1 and Λ_2 families for the parallel flow and vortex cases, but there arises an exact analogy in the two-dimensional limit between Couette flow and the Rankine vortex. As already mentioned, for the parallel flow case, this limit corresponds to the wave vector being in the flow-gradient plane, and for the vortex case, the limit corresponds to the absence of any modulation in the imposed perturbation along the axis of rotation.

For the inviscid limit considered here, the shear flow is considered to be bounded between $z = -1$ and $z = +1$, and this may be done without any loss in generality since the structure of the inviscid continuous spectrum remains qualitatively unaltered regardless of whether the domain is bounded or unbounded. There is a certain loss of generality for the viscous case, that is, when Re is large but still finite. On one hand, introducing an unbounded (semi-infinite) domain for velocity profiles, that approach a uniform flow at infinity, leads to the appearance of a viscous continuous spectrum for the Orr-Sommerfeld equation which consists of eigenfunctions

that oscillate finitely rather than decay at infinity; this was originally found in the context of the Blasius profile and is a general feature of Blasius-like profiles in a semi-infinite domain (Mack [1976];Murdock & Stewartson [1977]). In contrast, for velocity profiles that asymptote to a finite shear at infinity, for instance, unbounded Couette flow, the existence of viscous eigenfunctions is crucially reliant on the presence of boundaries, and there is indeed no discrete spectrum in these cases in the absence of boundaries. The crucial role of boundaries in the latter case leads to a non-trivial relation between the inviscid CS-modes for a given flow, analyzed in sections 6.3.1 and 6.3.2, and the viscous modes for large but finite Re for the same flow. In particular, each CS-mode may be sensibly interpreted only as the limiting form of a viscous wavepacket for $Re \to \infty$; the individual viscous eigenmodes do not approach sensible limiting forms in the inviscid limit. This relationship is examined in some detail in section 6.5. Now, we proceed with the construction of the singular eigenfunctions, associated with the Λ_1 and Λ_2 families, in the inviscid limit.

6.3 The CS-spectrum of the linearized Euler equations

6.3.1 The Λ_1 family - Inclined Case vortex sheets

From (6.3), the solution for $w_{y',k}$ (the subscript k has been added to denote that the quantities considered are for a single Fourier mode) is seen to contain two contributions - a localized vortex sheet component corresponding to the homogeneous solution and a non-local PV-singular component. This is identical to the structure of the 2D CS-modes originally identified by Case [1959] in the context of perturbations to the electron velocity distribution as governed by the Vlasov equation, and discussed in more detail and in the specific context of inviscid hydrodynamic stability by Balmforth & Morrison [1995a]. Thus, a Λ_1 CS-mode is characterized by:

$$w_{y',k} = -\mathcal{C}_1\delta(z-z_c) + \mathcal{P}\frac{i}{k}\frac{\overline{U}'' u_{z,k}}{(\overline{U}-c)}, \tag{6.5}$$

$$u_{y',k} = \mathcal{P}\frac{k_y \overline{U}' u_{z,k}}{ikk_x(\overline{U}-c)}. \tag{6.6}$$

Here, $\overline{U}(z_c) = c$ with z_c denoting the critical level where the fluid in the base-state travels at the same speed as the perturbation. We note that, unlike the 2D CS-modes, there is now an additional component of velocity perpendicular to $\boldsymbol{k}$, that is, along the y' direction. This component is PV-singular and arises from (6.4) due to the tilting of the base-state vorticity field by the normal component of the perturbation velocity field. The Λ_1 mode has thus PV-singular velocity and vorticity fields in contrast to 2D perturbations wherein the velocity profile only has a discontinuity in slope across the critical level. Since the PV-singularity in the velocity field arises from vortex-tilting and not from a base-state vorticity gradient, it persists even for Couette flow as first shown by Sazonov (1996). For the case of Couette flow, the PV-singular term in the vorticity field vanishes, however, and the vorticity eigenmode is exactly a vortex sheet; thus, (6.5) represent the generalization of the Case vortex-sheets, originally found by Case (1960) for 2D perturbations, to the case of an inclined wavevector. The above is also unlike

the 3D CS-modes for vortical flows wherein, as illustrated for the case of a Rankine vortex, the PV-singular contribution is absent in the velocity field due to the irrotational nature of the base-state (chapter 2). Since $u_{z,k} = (D^2 - k^2)^{-1}(-ikw_{y',k})$, we have the following expression for the normal component of the perturbation velocity associated with $w_{y',k}$ in (6.5):

$$u_{z,k}(z;z_c) = -ik\mathcal{C}_1\mathcal{G}(z;z_c) + \mathcal{P}\int_{-1}^{1}\frac{\mathcal{G}(z;z')\overline{U}''(z')u_{z,k}(z;z')}{\overline{U}(z') - \overline{U}(z_c)}dz', \tag{6.7}$$

where

$$\mathcal{G}(z;z_c) = -\frac{\sinh k(1-z_>)\sinh k(1+z_<)}{k\sinh 2k}, \tag{6.8}$$

is the Greens function of the one-dimensional Laplacian for the bounded domain, $z\,\epsilon\,[-1,1]$, under consideration, with $z_<(z_>)$ denoting the smaller (larger) of z and z_c. It is the explicit form for the Greens function that is sensitive to the domain being bounded or unbounded; the general character of the perturbation vorticity and velocity fields characterizing the Λ_1 CS-modes remains unaltered, however. Finally, on normalizing the total y'-vorticity component associated with a given Λ_1 mode:

$$\int_{-1}^{1} w_{y',k}(z';z_c)dz' = \Sigma_1, \tag{6.9}$$

one may characterize each Λ_1 CS-mode by the following expressions for the vorticity and velocity fields:

$$w^{\Lambda_1}_{y',k}(z;z_c) = \left\{\Sigma_1 - \frac{i}{k}\mathcal{P}\int_{-1}^{1}\frac{\overline{U}''(z')u^{\Lambda_1}_{z,k}(z';z_c)}{\overline{U}(z') - \overline{U}(z_c)}dz'\right\}\delta(z-z_c) + \mathcal{P}\frac{i}{k}\frac{\overline{U}''u^{\Lambda_1}_{z,k}(z;z_c)}{\overline{U}(z) - \overline{U}(z_c)}, \tag{6.10}$$

$$u^{\Lambda_1}_{z,k}(z;z_c) = -ik\Sigma_1\mathcal{G}(z;z_c) + \int_{-1}^{1}\overline{U}''(z')u^{\Lambda_1}_{z,k}(z';z_c)\frac{\mathcal{G}(z;z') - \mathcal{G}(z;z_c)}{\overline{U}(z') - \overline{U}(z_c)}dz', \tag{6.11}$$

$$u^{\Lambda_1}_{y',k}(z;z_c) = \mathcal{P}\frac{k_y\overline{U}'u^{\Lambda_1}_{z,k}(z;z_c)}{ikk_x(\overline{U}-c)}. \tag{6.12}$$

Note that normalization based on Σ_1 above assumes the total vorticity associated with the eigenmode to be non-zero. This may not alway be the case. As seen in chapter 2, for the Rankine vortex, that there exist Λ_1-modes in with zero net vorticity, one expects a similar situation for parallel flows with kinked velocity profiles (for instance, see Sazonov [1989]); in the analysis here, we will neglect these instances, regarding them as exceptional.

6.3.2 The Λ_2 family - Squire jets

The Λ_2 CS-modes are homogeneous solutions of the Squire equation with $u_{y',k}$ being the only non-zero velocity component. The Squire operator in (6.4) is just the multiplication operator, and $u_{y',k}$ must therefore be a delta function; hence, the alternate name of a 'Squire jet'. Note that since $w_{y',k} = u_{z,k} = 0$, the Rayleigh equation is trivially satisfied in these cases. Thus, we

have a Λ_2 CS-mode being characterized by the following velocity and vorticity fields:

$$u^{\Lambda_2}_{y',k}(z;z_c) = \Sigma_2\delta(z-z_c), \tag{6.13}$$
$$w^{\Lambda_2}_{z,k}(z;z_c) = ik\Sigma_2\delta(z-z_c), \tag{6.14}$$
$$w^{\Lambda_2}_{x,k}(z;z_c) = -\Sigma_2\delta'(z-z_c). \tag{6.15}$$

The normalization $\Sigma_2 = \int_{-1}^{1} u^{\Lambda_2}_{y',k}(z';z_c)dz'$ may be interpreted as the volume flux per (half) wavelength associated with each mode. As shown originally by Case (1960) for Couette flow, and later by Balmforth and Morrison (1995) for a general non-linear shearing flow, an arbitrary vortical perturbation in two dimensions (that is, with the perturbation velocity field restricted to the xz plane) may be expressed as a superposition of the Λ_1 CS-modes alone. Thus, the Λ_2-modes come into play only for a perturbation that includes a spanwise variation. Although written down in the above explicit form for the first time by Sazonov (1996) for the specific case of Couette flow, the infinitesimally localized perturbation velocity field implies that the evolution only depends on the local velocity gradient at the critical level, and therefore, (6.13)-(6.15) remain solutions of the linearized equations of motion for an arbitrary non-linear velocity profile.

As is usually the case for CS-modes, quantities such as perturbation kinetic energy associated with individual modes are not well defined since they involve products of generalized functions (Gel'fand & Shilov [1964], Vanneste [1996]). There are no difficulties, however, if one considers the evolution of sufficiently smooth initial conditions, since in these cases, one would always deal with a packet of CS-modes instead of an individual one. With the Λ_1 and Λ_2 families defined as above, in the next section, we proceed with the formulation of the modal superposition, and thence, a modal description of the lift-up effect.

6.4 The modal representation of a vortical initial condition

6.4.1 A general initial condition

The determination of the arbitrary time evolution of a general initial velocity field $\hat{\mathbf{u}}(\mathbf{x},0)$ may be reduced to the problem of the evolution of a single Fourier mode in the wave-vector aligned coordinate system in the following manner. We have,

$$\begin{aligned}\hat{\mathbf{u}}(\mathbf{x},t) &= \int_{-\infty}^{\infty} dk_x dk_y \mathbf{u}_k(z,t)e^{i(k_x x+k_y y)} \\ &= \int_{-\infty}^{\infty} dk_x dk_y \left\{u_{x,k}(z,t)\hat{\mathbf{x}} + u_{y,k}(z,t)\hat{\mathbf{y}} + u_{z,k}(z,t)\hat{\mathbf{z}}\right\} e^{i(k_x x+k_y y)},\end{aligned}$$

in terms of the Fourier modes in the space-fixed coordinate system. In terms of the velocity components in the wave-vector-aligned coordinate system, one obtains:

$$\begin{aligned}\hat{\mathbf{u}}(\mathbf{x},t) = \int_{-\infty}^{\infty} dk_x dk_y \Bigg[&\left\{\frac{i}{k}Du_{z,k}(z,t)\cos\phi - u_{y',k}(z,t)\sin\phi\right\}\hat{\mathbf{x}} + \\ &\left\{u_{y',k}(z,t)\cos\phi + \frac{i}{k}Du_{z,k}(z,t)\sin\phi\right\}\hat{\mathbf{y}} + u_{z,k}(z,t)\hat{\mathbf{z}}\Bigg] e^{i(k_x x+k_y y)}\end{aligned} \tag{6.16}$$

It is clear from (6.16) that a description of $u_{z,k}(z,t)$ and $u_{y',k}(z,t)$ for a given $\boldsymbol{k}$, in terms of a superposition over the singular eigenfunctions of the aforementioned Λ_1 and Λ_2 families, would lead to the required modal representation for an arbitrary $\hat{\mathbf{u}}(\mathbf{x},t)$ via a Fourier integral. Hence, we now examine the evolution of a single Fourier mode that, at the initial instant, has a vertical structure given by $(w_{y',k}(z,0), u_{y',k}(z,0)) \equiv (\mathscr{Q}_1(z), \mathscr{Q}_2(z))$. This choice of perturbation fields is motivated by the structure of the Λ_2 family; specifically, the fact that the Λ_2-eigenmodes have $w_{y',k} = 0$ which, as shown below, allows one to arrive at the modal superposition in a simple sequential manner. The continuity equation, and the kinematic relation between stream function between vorticity, may be used to obtain the remaining disturbance velocity fields in terms of the two given perturbation fields. The choice of perturbation fields above is in contrast to the usual choice of the wall-normal velocity $(u_{z,k})$ and the wall-normal vorticity fields $(w_{z,k})$ (for instance, see Schmid & Henningson [2001]). However, the two choices may be readily related: $u_{z,k}(z,0)$ is related to $w_{y',k}(z,0)$ via the Poisson equation, so $i/k(D^2 - k^2)u_{z,k} = \mathscr{Q}_1$; and $w_{z,k}(z,0) = ik\mathscr{Q}_2(z)$ (see table 6.1).

To construct the ensemble of the Λ_i-modes $(i = 1, 2)$ that reproduce the above initial condition, for a fixed $\boldsymbol{k}$, we exploit the fact that the Λ_2 family is devoid of $w_{y'}$. As a result, one may construct the required modal superposition by first determining the superposition of Λ_1-modes required to represent $w_{y',k}(z,0) \equiv \mathscr{Q}_1(z)$, the mathematical statement of this superposition being given by

$$\mathscr{Q}_1(z) = \int_{-1}^{1} A^{\Lambda_1}(z') w^{\Lambda_1}_{y',k}(z;z') dz', \tag{6.17}$$

where $A^{\Lambda_1}(z')$ is the unknown amplitude distribution that needs to be determined. Provided one knows A^{Λ_1}, the vorticity field $w_{y',k}$, at an arbitrary time instant, follows immediately on convecting each of the Λ_1-mode with the base-state velocity at its critical level. Thus,

$$w_{y',k}(z,t) = \int_{-1}^{1} A^{\Lambda_1}(z') w^{\Lambda_1}_{y'}(z;z') e^{-ik_x \overline{U}(z')t} dz', \tag{6.18}$$

with an analogous equation for $u_{z,k}(z,t)$. Using (6.5) with $z_c = z'$ for $w^{\Lambda_1}_{y'}(z;z')$ in (6.18), one obtains the following Cauchy integral equation (Gakhov [1990]) to be solved for $A^{\Lambda_1}(z)$:

$$\mathscr{Q}_1(z) = A^{\Lambda_1}(z)\left\{\Sigma_1 - \frac{i}{k}\mathcal{P}\int_{-1}^{1} \frac{\overline{U}''(z') u^{\Lambda_1}_z(z;z')}{\overline{U}(z') - \overline{U}(z)} dz'\right\} - \frac{i}{k}\overline{U}''(z)\mathcal{P}\int_{-1}^{1} \frac{A^{\Lambda_1}(z') u^{\Lambda_1}_z(z;z')}{\overline{U}(z') - \overline{U}(z)} dz', \tag{6.19}$$

where the kernel has a PV-singularity. The solution of an analogous integral equation in plasma physics, that arose from the Vlasov equation governing, was originally accomplished by Case [1959] in terms of the solution of a Riemann-Hilbert problem in the complex plane (Gakhov [1990]); solutions of similar integral equations arising in the context of both parallel shearing flows (Balmforth & Morrison [1995a]) and vortical flows (appendix B) have also been obtained. We refer the reader to these references for details of the solution procedure, and write down the

final expression for $A^{\Lambda_1}(z)$ directly:

$$A^{\Lambda_1}(z) = \frac{1}{\epsilon_{\mathrm{R}}^2 + \epsilon_{\mathrm{L}}^2}\left[\epsilon_{\mathrm{R}}\mathscr{Q}_1 - \frac{\epsilon_{\mathrm{L}}\overline{U}'}{u_z(z;z)}\mathcal{P}\int_{-1}^{1}\frac{u_z^{\Lambda_1}(z;z')\mathscr{Q}_1(z')}{\overline{U}(z')-\overline{U}(z)}dz'\right], \tag{6.20}$$

where

$$\epsilon_{\mathrm{R}} = \Sigma_1 - \frac{i}{k}\mathcal{P}\int_{-1}^{1}\frac{\overline{U}''(z')u_z^{\Lambda_1}(z;z')}{\overline{U}(z')-\overline{U}(z)}dz', \tag{6.21}$$

$$\epsilon_{\mathrm{L}} = -\frac{i\pi}{k}\frac{\overline{U}''(z)u_z^{\Lambda_1}(z;z)}{\overline{U}'(z)}. \tag{6.22}$$

It is important to note that, although the solution via the Riemann-Hilbert problem achieves the formal inversion, thereby expressing the amplitude distribution of the CS-modes in terms of the initial vorticity distribution, the explicit analytical forms for the actual eigenmodes will, for a general velocity profile, require a numerical solution. As shown by Balmforth and Morrison (1995), in the context of 2D perturbations, this may be accomplished by writing the velocity components u_z and $u_{x'}$ in terms of a scalar streamfunction (since $u_{y'}$ denotes a uniform flow orthogonal to $\boldsymbol{k}$) which satisfies a regular Fredholm integral equation (rather than the singular Cauchy integral equation above). For Couette flow, of course, the perturbation velocity fields are available in closed form.

Since each of the Λ_1-modes has an associated $u_{y',k}(z)$ (6.12), the Λ_1-superposition needed to reproduce an initial $w_{y',k}(z,0)$ would also generate a $u_{y'}$ contribution given by $\int_{-1}^{1}A^{\Lambda_1}(z')u_{y'}^{\Lambda_1}(z;z')dz'$ at the initial instant. Thus, the superposition of the Λ_2-modes needs to reproduce the difference between the initial $u_{y'}(z,0) \equiv \mathscr{Q}_2(z)$ and that corresponding to the Λ_1-superposition above. One may write:

$$\begin{aligned}\mathscr{Q}_2(z) &= \int_{-1}^{1}A^{\Lambda_1}(z')u_{y',k}^{\Lambda_1}(z;z')dz' + \int_{-1}^{1}A^{\Lambda_2}(z')u_{y',k}^{\Lambda_2}(z;z')dz',\\ &= \frac{\overline{U}'(z)k_y}{ikk_x}\mathcal{P}\int_{-1}^{1}\frac{A^{\Lambda_1}(z')u_z^{\Lambda_1}(z;z')}{\overline{U}(z)-\overline{U}(z')}dz' + A^{\Lambda_2}(z),\end{aligned} \tag{6.23}$$

where we have used the expression for $u_{y',k}^{\Lambda_1}$ from (6.12), and the fact that $u_{y',k}^{\Lambda_2}$ is just a delta function. Thus,

$$A^{\Lambda_2}(z) = \frac{1}{\Sigma_2}\left[\mathscr{Q}_2(z) - \frac{\overline{U}'(z)k_y}{ikk_x}\mathcal{P}\int_{-1}^{1}\frac{A^{\Lambda_1}(z')u_z^{\Lambda_1}(z;z')}{\overline{U}(z)-\overline{U}(z')}dz'\right], \tag{6.24}$$

where A^{Λ_1} is known from (6.20). Combining (6.23) and (6.24), and accounting for the convection of the Λ_2-modes with the base-state velocities at the individual critical levels, we have the following expression for the arbitrary time evolution of $u_{y',k}(z,t)$:

$$u_{y',k}(z,t) = \mathscr{Q}_2(z)e^{-ik_x\overline{U}(z)t} + \frac{\overline{U}'(z)k_y}{k}\int_{-1}^{1}A^{\Lambda_1}(z')u_z^{\Lambda_1}(z;z')\frac{e^{-ik_x\overline{U}(z')t}-e^{-ik_x\overline{U}(z)t}}{ik_x(\overline{U}(z)-\overline{U}(z'))}dz' \tag{6.25}$$

Equation (6.18) with $w_{y',k}^{\Lambda_1}$ replaced by $u_{z,k}^{\Lambda_1}$, together with (6.25), yield the modal superposition

for a single $\boldsymbol{k}$. Now, one may use (6.16)

$$u_{z,k}(z,t) = \int_{-1}^{1} A^{\Lambda_1}(z')u_z^{\Lambda_1}(z;z')e^{-ik_x\overline{U}(z')t}dz', \tag{6.26}$$

where as already mentioned $(u_{x,k}(z,0), u_{y,k}(z,0), u_{z,k}(z,0)) = \mathbf{u}_k(z,0)$ represents the initial condition's Fourier transform and $u_z^{\Lambda_1}(z;z')$ and $A^{\Lambda_1}(z)$ are given by (6.11) and (6.20) respectively with $\mathscr{Q}_1 = i/k(D^2-k^2)u_{z,k}(z,0)$ (without loss of generality assume $\Sigma_1 = 1$). This provides the expression for arbitrary time evolution of the perturbation velocity field,

$$\begin{aligned}\hat{\mathbf{u}}(\mathbf{x},t) &= \int_{-\infty}^{\infty} dk_x dk_y e^{i(k_x x+k_y y)}\left[\left\{\hat{\mathbf{x}}ik^{-1}\cos\phi\, D + \hat{\mathbf{y}}ik^{-1}\sin\phi\, D + \hat{\mathbf{z}}\right\}u_{z,k}(z,t)+\right.\\ &\left.\{-\hat{\mathbf{x}}\sin\phi + \hat{\mathbf{y}}\cos\phi\}\, u_{y',k}(z,t)\right] \qquad (6.27)\\ &= \int_{-\infty}^{\infty} dk_x dk_y e^{i(k_x x+k_y y)}\\ &\left[\left\{\hat{\mathbf{x}}ik^{-1}\cos\phi\, D + \hat{\mathbf{y}}ik^{-1}\sin\phi\, D + \hat{\mathbf{z}}\right\}\int_{-1}^{1} A^{\Lambda_1}(z')u_z^{\Lambda_1}(z;z')e^{-ik_x\overline{U}(z')t}dz' + \right.\\ &\{-\hat{\mathbf{x}}\sin\phi + \hat{\mathbf{y}}\cos\phi\}\left\{(u_{y,k}(z,0)\cos\phi - u_{x,k}(z,0)\sin\phi)\, e^{-ik_x\overline{U}(z)t} + \right.\\ &\left.\left.\frac{\overline{U}'(z)k_y}{k}\int_{-1}^{1} A^{\Lambda_1}(z')u_z^{\Lambda_1}(z;z')\frac{e^{-ik_x\overline{U}(z')t} - e^{-ik_x\overline{U}(z)t}}{ik_x(\overline{U}(z)-\overline{U}(z'))}dz'\right\}\right] \qquad (6.28)\end{aligned}$$

6.4.2 Transient growth for a 'Roll' initial condition

Considering the superposition for a fixed $\boldsymbol{k}$, we note that, for a vanishingly small streamwise wavenumber, (6.25) reduces to:

$$\begin{aligned}u_{y'}(z,t) &= u_{y'}(z,0) + \overline{U}'(z)\left[t\, u_z(z,0) - \frac{ik_x t^2}{2}\int_{-1}^{1} A^{\Lambda_1}(z')u_z^{\Lambda_1}(z;z')\left\{\overline{U}(z') + \overline{U}(z)\right\}dz' + O(k_x^2t^3)\right],\\ &= u_{y'}(z,0) + \overline{U}'(z)t\left[u_z(z,0) - \frac{ik_x t}{2}\left\{u_z(z,0)\overline{U}(z) + \int_{-1}^{1} A^{\Lambda_1}(z')u_z^{\Lambda_1}(z;z')\overline{U}(z')dz'\right\} + O(k_x t)^2\right],\end{aligned} \tag{6.29}$$

where

$$u_z(z,0) = \int_{-1}^{1} A^{\Lambda_1}(z')u_z^{\Lambda_1}(z;z')dz'.$$

Thus, the relevant (dimensionless) small parameter in (6.29) is $k_x\bar{U}_c t$, $\bar{U}_c$ being a characteristic velocity scale, and not k_x alone. The expression (6.29) evidently depicts an algebraic instability over a time-scale $t \ll O(k_x\bar{U}_c)^{-1}$. For times of $O(k_x\bar{U}_c)^{-1}$, all terms in the above series expansion become comparable and the resulting mutual cancellation leads to a saturation of the initial algebraic growth. Physically, this is indicative of differential convection leading to decoherence (phase-mixing) for long-times. For $k_x = 0$, that is, a perfectly spanwise-aligned initial condition, the role of shear in phase-mixing becomes redundant and the algebraic growth

persists for all times, with

$$u_{y'}(z,t) = u_x(z,t) = u_x(z,0) + \overline{U}'(z)t\, u_z(z,0), \tag{6.30}$$

where we have used that the y'-axis now coincides with the flow direction for a spanwise perturbation. Thus, the algebraic instability for three-dimensional disturbances in shear flows is contained in the modal superposition of the Λ_i eigenfunctions.

In order to obtain a clearer picture of the instablity, we consider the manner in which the modal superposition in (6.25) reproduces a given a 'roll' initial condition with the velocity field restricted to the (x', z') plane. We further simplify the physical picture by restricting ourselves to Couette flow with $\overline{U}''(z) = 0$, in which case the $w_{y'}$-component of a Λ_1 mode reduces to a delta function; there is no real loss of generality, since as is evident from (6.30), it is the velocity gradient and not the vorticity gradient that is responsible for the algebraic instability. The two-dimensional nature of the roll implies that the only non-zero vorticity component in the initial condition is $w_{y'}(z,0)$. This initial field may readily be formed by a stack of Λ_1 modes with the amplitude of a particular mode being proportional to the value of $w_{y'}(z,0)$ at its critical level, the location of the $w_{y'}$-vortex sheet (note that, except, for 2D perturbations, the vorticity field associated with a Λ_1-mode remains three-dimensional, and the term vortex-sheet here refers only to the delta function in $w_{y'}$). Each of the Λ_1-modes, however, also has a PV-singular $u_{y'}$ field not present in the initial condition. Thus, the $u_{y'}$ field generated by the Λ_1-superposition must be precisely cancelled out by an appropriate superposition of Squire jets. Since the jet refers to a delta-function $u_{y'}$ field, the amplitude of each Squire jet must equal the magnitude but be opposite in sign to the local $u_{y'}$ induced by the Λ_1-superposition. The precise cancellation in $u_{y'}$ can only happen at $t = 0$, and for subsequent times, the differential convection of the CS-modes and the resulting incomplete cancellation will lead to a growing $u_{y'}$ (streak). Figure **??** illustrates the above picture for the simplistic case where the initial roll is the velocity field in the (x', z') plane associated with a single Λ_1 mode. For any finite k_x, eventual de-coherence in the vertical direction will terminate this growth. But, as the initial condition approaches a spanwise alignment, the phase-mixing becomes infinitely slow. Thus, the 'lift-up' effect, in a modal approach, may be interpreted as the result of the differential convection of a flow-aligned superposition of the Λ_1 vortex sheets and the and the corresponding ensemble of Squire jets. Finally, we note that that (6.30) is valid even for non-linear velocity profiles with a non-trivial base-state vorticity gradient. Thus, the argument above holds in these cases too, except that the details of the superposition become complicated; for instance, the amplitude $A^{\Lambda_1}(z)$, instead of obeying a trivial relation, $\mathscr{Q}_1$ ($A^{\Lambda_1}(z')\Sigma_1 = \mathscr{Q}_1$), as for a plane Couette flow, is now determined by an integral equation instead (see (6.20)).

6.4.3 Inclusion of discrete modes

The expressions (6.26-6.25) for evolution of a general initial condition via Λ_1 and Λ_2 families can be modified for inflectional velocity profiles, to accommodate discrete modes using the formulation of Case [1959]. The discrete modes, $u_{zn}(z; c_n)$, with eigenvalues c_n are solution of

the equation

$$(D^2 - k^2)u_{zn} - \frac{\overline{U}''}{(\overline{U} - c_n)}u_{zn} = 0 \tag{6.31}$$

satisfying the dispersion relation

$$1 - \frac{i}{k}\int_{-1}^{1} \frac{\overline{U}''(z')u_{zn}(z;c_n)}{\overline{U}(z') - c_n}dz' = 0 \tag{6.32}$$

$\epsilon_{\mathrm{R}}^2 + \epsilon_{\mathrm{L}}^2$ which previously had no zeros in the complex plane for non-inflectional velocity profiles (6.20)-(6.22); for an inflectional velocity profile leads to the above dispersion relation.
In (6.26)-(6.25) the expressions for $u_{z,k}(z,t)$ and $u_{y',k}(z,t)$ are now modified as,

$$u_{z,k}(z,t) = \sum_n a_n u_{zn}(z;c_n)e^{-ik_x c_n t} + \int_{-1}^{1} A^{\Lambda_1}(z')u_z^{\Lambda_1}(z;z')e^{-ik_x\overline{U}(z')t}dz', \tag{6.33}$$

$$\begin{aligned} u_{y',k}(z,t) = {} & (u_{y,k}(z,0)\cos\phi - u_{x,k}(z,0)\sin\phi)\, e^{-ik_x\overline{U}(z)t} + \\ & \frac{\overline{U}'(z)k_y}{k}\int_{-1}^{1} A^{\Lambda_1}(z')u_z^{\Lambda_1}(z;z')\frac{e^{-ik_x\overline{U}(z')t} - e^{-ik_x\overline{U}(z)t}}{ik_x(\overline{U}(z) - \overline{U}(z'))}dz' + \\ & \frac{\overline{U}'(z)k_y}{k}\sum_n a_n u_{zn}(z;c_n)\frac{e^{-ik_x c_n t} - e^{-ik_x\overline{U}(z)t}}{ik_x(\overline{U}(z) - c_n)}, \end{aligned} \tag{6.34}$$

where $A^{\Lambda_1}(z)$ is now modified as

$$A^{\Lambda_1}(z) = \frac{1}{\epsilon_{\mathrm{R}}^2 + \epsilon_{\mathrm{L}}^2}\left[\epsilon_{\mathrm{R}}\mathscr{R}_1 - \frac{\epsilon_{\mathrm{L}}\overline{U}'}{u_z(z;z)}\mathcal{P}\int_{-1}^{1}\frac{u_z^{\Lambda_1}(z;z')\mathscr{R}_1(z')}{\overline{U}(z') - \overline{U}(z)}dz'\right] \tag{6.35}$$

$$\mathscr{R}_1 = \frac{i}{k}(D^2 - k^2)\left\{u_{z,k}(z,0) - \sum_n a_n u_{zn}(z;c_n)\right\} \tag{6.36}$$

$$a_n = \frac{\displaystyle\int_{-1}^{1}\frac{\mathscr{Q}_1(z)u_{zn}(z;c_n)}{(\overline{U}(z) - c_n)}dz}{\displaystyle\frac{i}{k}\int_{-1}^{1}\left\{\frac{u_{zn}(z;c_n)}{(\overline{U}(z) - c_n)}\right\}^2\overline{U}''(z)dz} \tag{6.37}$$

ϵ_{R} and ϵ_{L} is given by the expressions (6.21)-(6.22) and $\mathscr{Q}_1 = i/k(D^2 - k^2)u_{z,k}(z,0)$.

6.5 Representation of an inviscid eigenmode in terms of viscous discrete modes

The earlier sections have led to the identification of the 'lift-up' effect in terms of a modal superposition of the inviscid singular eigenfunctions. In the viscous case, the lift-up effect, and transient growth in general, is typically attributed to the non-orthogonality of underlying

(discrete) eigenfunctions for large Re of the system of equations,

$$\left[\left\{\frac{\partial}{\partial t}+\overline{U}\frac{\partial}{\partial x}\right\}\nabla^2-\overline{U}''\frac{\partial}{\partial x}-\frac{1}{Re}\nabla^4\right]u_z = 0 \tag{6.38}$$

$$\left[\frac{\partial}{\partial t}+\overline{U}\frac{\partial}{\partial x}-\frac{1}{Re}\nabla^2\right]w_z = -\overline{U}'\frac{\partial u_z}{\partial y} \tag{6.39}$$

Written in normal mode form, the solution of 6.38 and the associated solution of 6.39 are termed as the Orr-Sommerfeld eigenmodes while the unforced solutions of 6.39 ($u_z = 0$) constitute the Squire eigenmodes (Schmid & Henningson [2001]). Interestingly, a modal superposition argument also appears on page 106-107 in Schmid & Henningson [2001]. For instance, we quote a brief passage from this description '. Unlike the inviscid problem, the explicit form of the viscous eigenmodes involved in such a superposition is, of course, not known in general owing to the intractability of the Orr-Sommerfeld equation. But, it is nevertheless worthwhile delving into the relation between the inviscid modal superposition described here, and the large Re-limit of the viscous modal superposition detailed in Schmid & Henningson [2001]. As will be seen below, the relation is not trivial owing to fundamental differences between the inviscid spectrum and the large-Re viscous spectrum.

Though the solutions of (6.38) and (6.39) are known for few elementary velocity profiles, $\overline{U}(z)$, the spectral analysis gets easily unwieldy and an effort to address the connection between inviscid and viscous spectra almost always goes unanswered. Thus the evolution of an initial condition via inviscid singular eigenfunctions and that as a superposition of viscous discrete modes with inclusion of diffusion needs to be analyzed via a model problem. The model problem adopted here is the advection-diffusion equation,

$$\frac{\partial\tilde{\phi}}{\partial t}+\overline{U}(z)\frac{\partial\tilde{\phi}}{\partial x}=\nu\nabla^2\tilde{\phi} \tag{6.40}$$

If ∇^2 is interpreted as a three dimensional Laplacian then (6.40) is the Squire equation (homogeneous part of 6.39), where $\tilde{\phi} = w_z$. Though analytically tractable for some nonlinear shear flows, we would consider $\overline{U}(z) = \dot{\gamma}z$. With the linear shear flow assumptions, (6.40) also mimics the Orr-Sommerfeld equation (6.38) with $\tilde{\phi} = \nabla^2 u_z = \partial_y w_x - \partial_x w_y$. As the spectral properties of (6.40) remain qualitatively unaltered with the introduction of three dimensionality, we would restrict our attention to 2D and consider monochromatic disturbances of the form, $\tilde{\phi}(x,z,t) = \phi(z,t)e^{ik_x x}$. Thus (6.40) reduces to,

$$\frac{\partial\phi}{\partial t}+ik_x\dot{\gamma}z\phi=\nu\left(\frac{\partial^2\phi}{\partial z^2}-k_x^2\phi\right) \tag{6.41}$$

Considering k_x^{-1} to be a characteristic length scale and thus a Reynolds number defined as $Re = \dot{\gamma}(\nu k^2)^{-1}$, the non-dimensional equation is,

$$\frac{\partial\phi}{\partial t}+iz\phi=\frac{1}{Re}\left(\frac{\partial^2\phi}{\partial z^2}-\phi\right) \tag{6.42}$$

We have chosen to denote the dimensional and non-dimensional quantities by the same variable, leaving it to the context to distinguish the two.

Let us consider an initial condition of a vortex sheet, $\phi(z,0)=\delta(z-z_1)$. In absence of diffusion (Re$=\infty$), a vortex sheet is an eigenmode; a member of the singular continuous spectrum. Thus the imposed vortex sheet evolves unaltered with the fluid local velocity at $z=z_1$, $\tilde{\phi}(z,t)=\delta(z-z_1)e^{i(x-z_1t)}$. With the inclusion of diffusion, the vortex sheet is unable to preserve itself and its evolution is given by the Green's function, $\mathcal{G}$, of the advection-diffusion operator

$$\frac{\partial \mathcal{G}}{\partial t}+iz\mathcal{G}-\frac{1}{Re}\left(\frac{\partial^2\mathcal{G}}{\partial z^2}-\mathcal{G}\right)=\delta(z-z_1)\delta(t) \tag{6.43}$$

$$\Rightarrow \qquad \mathcal{G}(z,t)=\sqrt{\frac{Re}{4\pi t}}\exp\left[-\frac{it(z+z_1)}{2}-\frac{t}{Re}\left(\frac{t^2}{12}+1\right)-\frac{(z-z_1)^2Re}{4t}\right] \tag{6.44}$$

The above Green's function has been found for an infinite domain ($|z|<\infty$). For a bounded/semi-infinite domain the Green's function can be easily modified by method of images (Kevorkian [2000]). In the limit of Re$\to\infty$, $\mathcal{G}$ reduces to a convected vortex sheet $\delta(z-z_1)e^{-iz_1t}$; the inviscid eigenmode. In an unbounded geometry infinitesimal perturbations in a linear shear flow can also be expanded in terms of convected Fourier modes, plane-wave solutions (Monin & Yaglom [1997]),

$$\mathcal{G}(z,t)=\frac{1}{2\pi}\int_{-\infty}^{\infty}\exp\left[i\{-zt+k_z(z-z_1)\}-\frac{1}{Re}\left\{\left(1+k_z^2\right)t-k_zt^2+\frac{t^3}{3}\right\}\right]dk_z \tag{6.45}$$

Once again it can be seen from the above expression that the convected Fourier modes reduce to the inviscid eigenmode for $Re\to\infty$. Now the final connection that needs to be made is in terms of the viscous spectrum of (6.42). Assuming $\phi(z,t)=\Phi(z)e^{-ic_nt}$ the relevant eigenvalue equation is,

$$\frac{d^2\Phi}{dz^2}=\{iRe(z-c_n)+1\}\Phi \tag{6.46}$$

The above differential equation has solutions in terms of Airy functions (Ai(z) and Bi(z)) and for a semi-infinite domain with boundary conditions $\Phi(0)=0$ and $\Phi\to 0$ as $z\to\infty$, only Ai(z) needs to be considered [1]. For the geometry considered the viscous eigenvalues are given by,

$$c_n=-\frac{\mathrm{ai}_n}{(iRe)^{1/3}}+\frac{1}{iRe} \tag{6.47}$$

where ai_n is the n-th zero of the Airy function, Ai(z). For large n the asymptotic form of the eigenvalue is,

$$c_n\sim\left[\left\{\frac{3\pi(4n-1)}{8}\right\}^2\frac{1}{iRe}\right]^{1/3}+\frac{1}{iRe} \tag{6.48}$$

Figure 6.4 depicts the spectrum for Re=100 with the comparison between the numerically evaluated eigenvalues (6.47) and its asymptotic approximations (6.48). As the asymptotic ex-

[1] For nonlinear shear flows, where analytical solutions cannot be found, spectral properties can be studied for Re$\gg 1$ using a WKB approach.

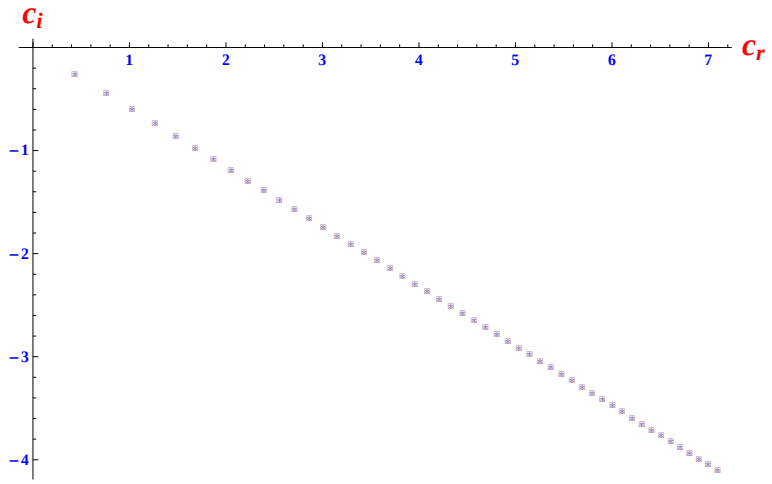

Figure 6.4: Viscous spectrum for semi-infinite Couette flow ($0 \leqslant z < \infty$) for Re=100. '$*$' - (6.47), '$\square$' - (6.48).

pression indicates, with increasing Re the spectrum emerges as a ray at an angle of $\pi/6$ with the real axis. One would recall that for a bounded Couette flow ($|z| < 1$), the spectrum forms a Y-shaped 'spectral tie' (Reddy *et al.* [1993]). With increasing Re the viscous spectrum becomes invariant in shape (one can always find an eigenvalue in a particular region of the ray if we fix $n^2 \sim O(Re)$) and does not approach the real line - the inviscid continuous spectrum - in a continuous fashion. On tracking an individual mode with $Re \gg 1$, it is observed that the mode migrates towards the origin, thus confirming a known fact that there is no direct correspondence between an individual viscous mode and an inviscid continuous spectra mode. Instead a connection needs to be made between a (infinite) collection of viscous discrete modes and an inviscid continuous spectrum mode [2].

Realizing the non self-adjoint nature of (6.46) and using the properties of the orthogonality relations with the adjoint solutions we have,

$$\delta(z - z_1) = \sum_{n=1}^{\infty} \frac{(iRe)^{1/3}\mathrm{Ai}\left[(iRe)^{1/3}\left\{z - c_n + \frac{1}{iRe}\right\}\right]\mathrm{Ai}\left[(iRe)^{1/3}\left\{z_1 - c_n + \frac{1}{iRe}\right\}\right]}{\mathrm{Ai}'\left[(iRe)^{1/3}\left\{-c_n + \frac{1}{iRe}\right\}\right]^2} \tag{6.49}$$

The above relation represents an inviscid eigenmode, a vortex sheet, as a linear superposition of the viscous discrete modes. Thus the Green's function can now be represented via the viscous

[2] The converse connection between a superposition of inviscid continuous spectrum modes and a viscous discrete mode has been studied in the context of exponentially damped linear response of dissipation-less systems - Landau poles/quasi-modes (Balmforth [1998], Ng & Bhattacharjee [2004]).

discrete spectrum as,

$$\mathcal{G}(z,t) = \sum_{n=1}^{\infty} \frac{(iRe)^{1/3}\mathrm{Ai}\left[(iRe)^{1/3}\left\{z - c_n + \frac{1}{iRe}\right\}\right]\mathrm{Ai}\left[(iRe)^{1/3}\left\{z_1 - c_n + \frac{1}{iRe}\right\}\right]}{\mathrm{Ai}'\left[(iRe)^{1/3}\left\{-c_n + \frac{1}{iRe}\right\}\right]^2} e^{-ic_n t} \tag{6.50}$$

Between the Green's function given in (6.50) and (6.44), only the former is constrained to vanish at $z = 0$ but the difference between the two is exponentially small for $Re \gg 1$.
Using this model problem it is shown how the evolution of a inviscid eigenmode in presence of diffusion can be understood via a superposition of viscous discrete modes.

6.6 Conclusion

In this chapter we have shown the modal interpretation of the 'lift-up' effect. This involved identifying the two inviscid continuous spectra for a plane parallel shear flow in section 6.3 - the wave-vector aligned version of Case vortex sheets (6.3.1) and the purely 3D Squire jets (6.3.2). After representing an arbitrary initial condition via an eigenfunction expansion of these two families, it was shown how a 'roll' initial condition leads to algebraic instability. The formulation was then expanded to include discrete modes (6.4.3). Finally in section 6.5 a connection was made between an inviscid continuous spectrum mode with that of a collection of viscous discrete modes, for the simple case of semi-infinite Couette flow. This was done to show how the existing modal interpretation of the 'lift-up' effect in terms of non-orthogonal viscous discrete modes is in harmony with the explanation presented in this note in terms of the inviscid continuous spectra.

Chapter 7

Conclusion and Future Work

This thesis has focussed on the study of the singular eigenfunctions in various problems of hydrodynamic stability with special attention to those involving rotation, stratification and elasticity. Detailed conclusions have already been provided at the end of individual chapters. Herein, a summary is provided with a few topics that will be studied in the future.

The complete inviscid spectrum for a Rankine vortex was obtained in chapter 2. It is well known that a Rankine vortex has a discrete spectrum. These regular modes by themselves are eponymously known as the Kelvin modes, and do not form a complete set. The analysis obtained the relevant continuous spectra consisting of singular eigenfunctions that were necessary to form a complete set. A modal superposition, involving both the discrete and the continuous spectra, is arrived at for describing evolution of an arbitrary initial vorticity field. The analysis of the continuous spectrum modes is then extended to vortices with smooth vorticity profiles. While in 2D, the modal superposition may be written down as the solution of a Riemann-Hilbert problem, in 3D an approximate analysis is performed by borrowing analogies from stratified shear flows. In particular, it is shown that the 3D continuous spectrum modes of a smooth vortex, like those of a stratified shear flow, require a 'finite-part' interpretation (Lighthill [1958], Gel'fand & Shilov [1964]).

The Cauchy initial value problem for a Rankine vortex was analyzed in chapter 3, both in 2D and 3D. The completeness of the modal approach is shown by proving the equivalence of the modal superposition result obtained in chapter 2 to the solution of the initial value problem. The IVP approach reiterates the importance of the continuous spectrum in acting as a mediator between external vortical disturbances and the vortex column, a fact crucial in early stages of vortex - turbulent field interactions. The growth-rate spectra for both vortex sheet and vortex 'ribbon' (initial conditions, at the resonant locations) were obtained. The comparison of these spectra with those obtained in numerical studies on more realistic vorticity profiles (e.g., the Lamb Oseen profile), and for finite Re ($\sim 10^4$), are encouraging, and clearly emphasize the importance of resonant interaction, in the short-term algebraic growth phase.

The singular eigenfunctions studied in chapters 2 and 3 were for neutrally-stable inviscid columnar vortices and were responsible for algebraic instabilities in these systems. In chapter 4 a novel elastic instability (exponential) in a Rankine vortex was identified, a situation relevant to vortices in dilute polymer solutions. Here, the unstable discrete mode emerges from a singular neutral continuous spectrum mode. The instability arises due to the resonance of elastic shear waves aided by the background shear in the irrotational exterior. The analyzed regime involves a balance between inertia and elasticity, with the viscous effects being asymptotically

small and is governed by the elastic equivalent of the Rayleigh equation for swirling flows; both momentum diffusion and the relaxation of polymeric stresses for the disturbance are ignored. The elastic Rayleigh equation was solved numerically and via the method of matched asymptotic expansions in the limit of small E. The analysis helps extend the numerical results down to E=0; the partial solution (the so-called LHS problem) shows the absence of an elasticity threshold for instability. The numerical study also confirmed that the instability persists even for smooth vorticity profiles - the 'intense' ones.

After mentioning the various possibilities of algebraic growths in flows with continuous spectrum, in chapter 5 an optimal perturbation calculation was performed for stratified shear flows. The optimal calculations confirmed the common belied that stratification due to its strong dislike for any vertical mention, suppresses transient growth in shear flows. But if one considers the density field to be non-diffusive and only be stirred by a viscous velocity field, then weak stratification could result in enhanced transient growth in comparison to the unstratified case. It was also shown that once the onset of internal gravity waves occur, the optimal time is determined directly by the Brunt-Väisälä frequency of the background flow. The optimal partitioning of energy in kinetic and potential energy in the initial condition and also its optimal obliqueness in 3D was studied.

Several intriguing questions and future directions have emerged from the present study. Some of them are -

1. An interesting extension of the present analysis would be to examine the continuous spectrum for a vortex ring. A vortex ring unlike a vortex column is non-isochronous (the angular velocity is not constant).The analysis of the 2D CS-modes of a vortex column are the axisymmetric continuous spectrum modes of the ring. Further, due to the non-isochronous property of a vortex ring the core eigenmodes are no longer degenerate as in the case of a column,and these modes have been examined by (Kopiev & Chernyshev [1997]). However, the axisymmetric CS-modes with vorticity outside the core, and inside irrotational fluid envelope, are yet to be examined. The entire 3D core continuous spectrum is still unresolved. Interestingly for certain members of the Fraenkel-Norbury family there exists an irrotational region of fluid around the toroidal vortex ring, called the vortex envelope, which propagates with the ring (Batchelor [1967]). There would also exist another family of continuous spectrum eignemodes which are toroidal vortex sheets concentric with the vortex ring, an extension of the singular eigenmodes for the vortex column investigated in the present work.

2. The 2D *quasi-mode* of a smooth vortex has been examined in detail before and we have revisited some of these results in this thesis in the context of the modal representation. A study has been undertaken to systematically map the 3D *quasi-modes* of vortices with Rankine-like vorticity profiles ('intense' vortices); in particular, the dependence of their decay rates on both the vorticity and vorticity gradient(jump) in the base state. In parallel,the quasi-modes associated with the stratified shear flow analog of the Rankine vortex will be studied.

3. The growth-rate spectrum calculations, in the context of the IVP of a Rankine vortex, have been done for initial conditions of zero width (analytically), and for transversely coherent initial conditions of a finite width (numerically). For a more consistent comparison with numerical simulations of realistic vortices, one needs to also account for resonance and vortex stretching-tilting processes for an upshear-tilted initial condition. This will help establish the relative importance of resonance, vortex stretching-tilting and the Orr mechanism in the algebraic growth phase.

4. Even for finite De and Re, the viscoelastic stability equations are singular and have continuous spectra. Although stress diffusion is often proposed as a means to make the spectrum purely discrete, and thus avoid the discomfort of dealing with singular eigenfunctions, a second possibility is related to a nonlinear spring model for the polymer molecule (for instance, a FENE-P model). A nonlinear critical layer analysis, where the complete FENE-P model is considered in the critical layer, needs to be undertaken,and one needs to study the effect of the finite extensibility within the critical layer on modal growth rates.

5. Recent experiments on the swirling flow of elastic liquids also motivate the study of the the 3D perturbations of a vortex column in presence of both inertia and elasticity. A first step in this regard would be the study of axisymmetric oscillations/instabilities of a vortex column.

Appendix A

Vessel Modes

In the modal analysis treatments we obtained the Kelvin modes from the generalized continuous spectrum modes by setting the amplitude of the second vortex sheet to 0. The reader might have noticed there exists, both in 2D and 3D, cases where the amplitude of second vortex sheet becomes infinite. A closer analysis would reveal that the perturbation velocity field inside the second vortex sheet becomes infinitely stronger than the exterior field. This special class of modes we label as *vessel modes*, as they have a confining effect on the perturbation velocity field.

2D Vessel Modes

For 2D continuous spectrum modes we have from equation 2.16 the amplitude of second vortex sheet as,

$$A(r_f) = \frac{2m\left[1 - m\left(1 - \frac{1}{r_f^2}\right)\right]}{\left[(m-1)r_f^m - mr_f^{m-2} + \frac{1}{r_f^m}\right]}$$

For $m = 1$, independent of r_f, the amplitude $A(r_f)$ becomes infinite. The constants c_1, c_2 and d, needed to determine the interior velocity field (inside the second vortex sheet), are all proportional to $A(r_f)$. Hence the perturbation velocity field disappears, for $r > r_f$, for all continuous spectrum modes. In 2D $m = 1$ Kelvin mode corresponds to a linear translation of the vortex core. Let us assume the perturbation velocity field, $|\tilde{u}| = \epsilon|U_{\text{mean}}|$, where U_{mean} is the velocity field of the base state rankine vortex. If one considers the velocity field inside the vortex core (assume the angular velocity and radius of the vortex core both to be unity),

$$|U_{\text{mean}} + \epsilon\tilde{u}| = \sqrt{r^2 - 2\epsilon r d\sin(\theta - \omega t) + (\epsilon d)^2} \tag{A.1}$$

Though $\epsilon \ll 1$ is the premise of linear stability theory, we plot the total velocity field at several instants of time for $\epsilon = 1$ to provide an exaggerated view of the dynamics. One can observe from figure A.1 that the velocity field is identical to that of a offset rankine vortex placed inside a cylindrical container. The centre of the vortex (zero velocity) goes around clockwise in a circle with the centre of the unperturbed rankine vortex as its centre. Thus the second vortex sheet for $m = 1$ continuous spectrum modes acts like a rigid wall. It ensures disappearance of perturbation velocity field outside the second vortex sheet and clockwise rotation of the vortex core.

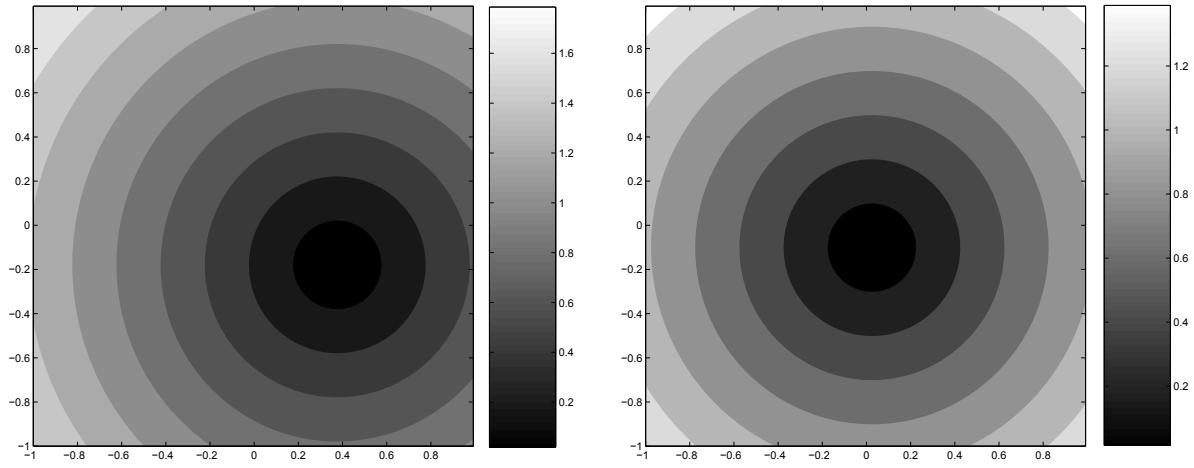

(a) $t = 1$ (b) $t = 3$

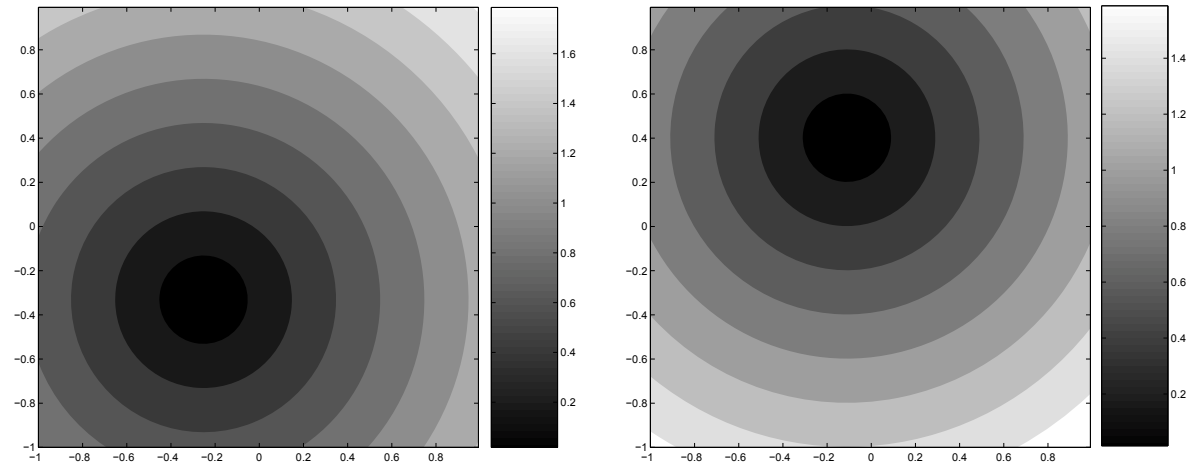

(c) $t = 5$ (d) $t = 10$

Figure A.1: Time evolution of mean (solid-body rotation) and perturbation velocity field inside the vortex core for a $m = 1$ continuous spectrum mode. The cylindrical vortex sheet is placed at $r_f = 1.5$. The mean and perturbation are assumed to be of the same order ($\epsilon = 1$).

3D Vessel Modes

For 3D continuous spectrum modes we have from equation 2.59 the amplitude of second vortex sheet as,

$$A_1(r_f) = \frac{M}{k\{K'_m(kr_f)N - I'_m(kr_f)M\}}$$

where,

$$M = g^2\beta a J'_m(\beta a)K_m(ka) + 2mg\Omega_0 J_m(\beta a)K_m(ka) + (4\Omega_0^2 - g^2)J_m(\beta a)kaK'_m(ka)$$
$$N = g^2\beta a J'_m(\beta a)I_m(ka) + 2mg\Omega_0 J_m(\beta a)I_m(ka) + (4\Omega_0^2 - g^2)J_m(\beta a)kaI'_m(ka)$$

As discussed before the zeroes of M corresponds to the Kelvin modes. The question here is what does the singularities of $A_1(r_f)$ or equivalently zeroes of $K'_m(kr_f)N - I'_m(kr_f)M$ correspond to? Based on the analysis for 2D vessel modes one could guess that these correspond to the 3D modes of vibration of a rankine vortex inside a container. This indeed can be proved immediately. Similar to the unbounded case, for rankine vortex inside a container of radius r_f, the velocity field can be written as,

$\underline{r < a}$

$$\hat{u}_z = dJ_m(\beta r) \tag{A.2}$$
$$\hat{u}_r = -\frac{i}{kr}\frac{gd}{g^2 - 4\Omega_0^2}\left\{2m\Omega_0 J_m(\beta r) + g\beta r J'_m(\beta r)\right\} \tag{A.3}$$

$\underline{r_f > r > a}$

$$\hat{u}_z = c_1 K_m(kr) + c_2 I_m(kr) \tag{A.4}$$
$$\hat{u}_r = -i\{c_1 K'_m(kr) + c_2 I'_m(kr)\} \tag{A.5}$$

Without loss of generality, we choose $d = 1/J_m(\beta a)$. Enforcing continuity of $\hat{u}_z$ across the core, $r = a$ and $\hat{u}_r(r_f) = 0$ at the cylinder wall one obtains,

$$c_1 = \frac{I'_M(kr_f)}{K_m(ka)I'_m(kr_f) - I_m(ka)K'_m(kr_f)} \tag{A.6}$$
$$c_2 = -\frac{K'_M(kr_f)}{K_m(ka)I'_m(kr_f) - I_m(ka)K'_m(kr_f)} \tag{A.7}$$

Enforcing continuity of radial velocity across the vortex core (equations A.3, A.5-A.7),

$$K'_m(kr_f)N - I'_m(kr_f)M = 0 \tag{A.8}$$

The above equation gives the dispersion relation for three-dimensional vibrations of a vortex column confined inside a cylinder of radius r_f. Like the unbounded problem the bounded problem too has denumerably infinite number of discrete modes. From figure A.2 one observes that the continuous spectrum mode frequency $\omega_{NK} = m\Omega(r_f)$ corresponding to the second vortex sheet location r_f, intersects the discrete modes of a rankine vortex inside a cylinder of radius r_f at discrete locations in k-space. Thus for each continuous spectrum mode (r_f), for every m, there exist denumerably infinite values of k such that the perturbation velocity field

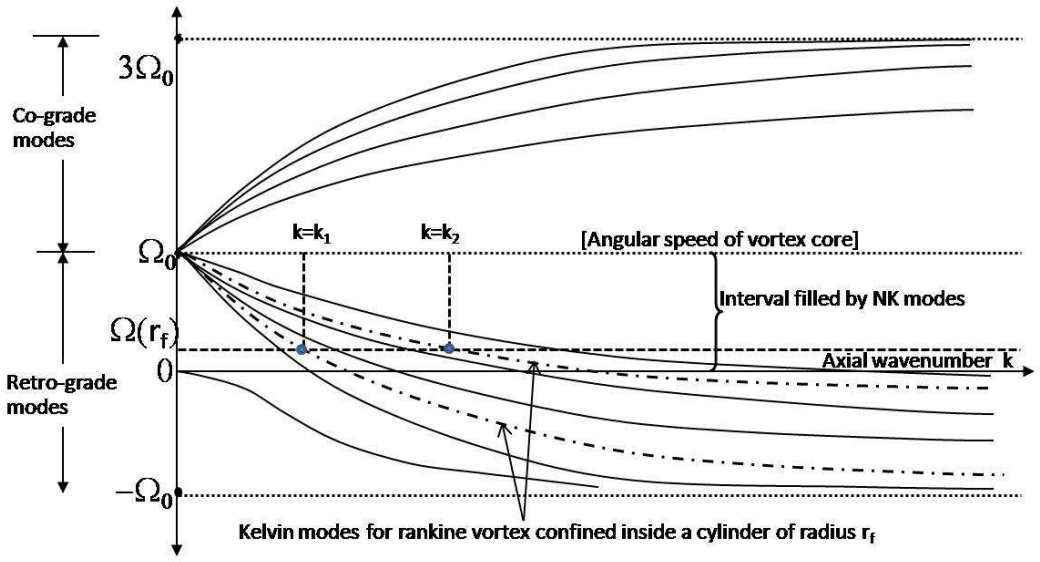

Figure A.2: Schematic of dispersion curves for rankine vortex for $m = 1$. The continuous lines represent dispersion curves for unbounded rankine vortex whereas the dash-dot lines are dispersion curves for rankine vortex confined in a container of radius r_f

for $r > r_f$ is identically zero and the interior velocity field is that of a confined rankine vortex. Similarly for every ordered pair (m, k) there exists a denumerably infinite number of continuous spectrum modes whose frequency and velocity field matches with that of a confined rankine vortex.

Appendix B

Riemann-Hilbert problem for a smooth vortex

To obtain the CS-mode amplitude distribution, $\Pi(r_f)$, corresponding to an initial condition of the form $w_{z0}(r)e^{im\theta}$, we will follow the framework developed by Balmforth & Morrison [1995a] for parallel shear flows. The integral equation that needs to be solved (see (2.118) in section 2.3.1) is given by

$$w_{z0}(r)e^{im\theta} = \int_0^\infty \Pi(r_f)\hat{w}_z^{\mathrm{CSM}}(r;r_f)e^{im\theta}dr_f, \tag{B.1}$$

and, on using (2.115) for $\hat{w}_z^{\mathrm{CSM}}(r;r_f)$, (B.1) takes the form

$$w_{z0}(r) = \left[1+\mathcal{P}\int_0^\infty \frac{1}{r'}\frac{DZ(r')\hat{\psi}^{\mathrm{CSM}}(r';r)}{\Omega(r')-\Omega(r)}dr'\right]\Pi(r) - \frac{DZ(r)}{r}\mathcal{P}\int_0^\infty \frac{\hat{\psi}^{\mathrm{CSM}}(r;r_f)}{\Omega(r)-\Omega(r_f)}\Pi(r')dr'. \tag{B.2}$$

Equation (B.2) is formulated as a Riemann-Hilbert problem by defining the following two sectionally analytic functions:

$$\mathbf{\Phi} = \frac{1}{2\pi i}\mathcal{P}\int_0^\infty \frac{1}{r'}\frac{DZ(r')\hat{\psi}^{\mathrm{CSM}}(r';r)}{\Omega(r')-\Omega(r)}dr', \tag{B.3}$$

$$\mathbf{\Psi} = \frac{1}{2\pi i}\mathcal{P}\int_0^\infty \frac{\Pi(r')\hat{\psi}^{\mathrm{CSM}}(r';r)}{\Omega(r')-\Omega(r)}dr', \tag{B.4}$$

where r is now regarded as a complex variable, and Φ and Ψ are analytic except when $r\,\epsilon\,[0,\infty)$. From the Sokhotski-Plemelj formulae [Gakhov [1990]], one has the following expressions for the limiting values of these functions for r approaching the positive real axis through complex-valued sequenes with positive $(+)$ and negative $(-)$ imaginary parts:

$$\mathbf{\Phi}^{\pm} = \pm\frac{1}{2}\frac{DZ(r)\hat{\psi}^{\mathrm{CSM}}(r;r)}{r\Omega'(r)} + \frac{1}{2\pi i}\mathcal{P}\int_0^\infty \frac{1}{r'}\frac{DZ(r')\hat{\psi}^{\mathrm{CSM}}(r';r)}{\Omega(r')-\Omega(r)}dr', \tag{B.5}$$

$$\mathbf{\Psi}^{\pm} = \pm\frac{1}{2}\frac{\Pi(r_f)\hat{\psi}^{\mathrm{CSM}}(r;r)}{\Omega'(r)} + \frac{1}{2\pi i}\mathcal{P}\int_0^\infty \frac{\Pi(r')\hat{\psi}^{\mathrm{CSM}}(r';r)}{\Omega(r')-\Omega(r)}dr'. \tag{B.6}$$

Using (B.5) and (B.6), (B.2) may be written as,

$$\frac{\hat{\psi}^{\mathrm{CSM}}(r;r)w_{z0}(r)}{\Omega'(r)} = \epsilon^+\mathbf{\Psi}^+ - \epsilon^-\mathbf{\Psi}^-, \tag{B.7}$$

where $\epsilon^+ = 1+2\pi i\mathbf{\Phi}^+$ and $\epsilon^- = 1+2\pi i\mathbf{\Phi}^-$. Further, if one defines another sectionally analytic function:

$$\mathbf{Q} = \frac{1}{2\pi i}\int_0^\infty \frac{w_{z0}(r')\hat{\psi}^{\mathrm{CSM}}(r';r)}{\Omega(r')-\Omega(r)}dr' \tag{B.8}$$

with the limiting values

$$\mathbf{Q}^{\pm} = \pm\frac{1}{2}\frac{\hat{\psi}^{\mathrm{CSM}}(r;r)w_{z0}(r)}{\Omega'(r)} + \frac{1}{2\pi i}\mathcal{P}\int_0^{\infty}\frac{w_{z0}(r')\hat{\psi}^{\mathrm{CSM}}(r';r)}{\Omega(r')-\Omega(r)}dr', \tag{B.9}$$

then (B.7) takes the form

$$\mathbf{Q}^{+} - \mathbf{Q}^{-} = \epsilon^{+}\mathbf{\Psi}^{+} - \epsilon^{-}\mathbf{\Psi}^{-}, \tag{B.10}$$

$$\Rightarrow \mathbf{Q}^{+} - \epsilon^{+}\mathbf{\Psi}^{+} = \mathbf{Q}^{-} - \epsilon^{-}\mathbf{\Psi}^{-}. \tag{B.11}$$

It is clear that the function $\mathbf{Q}-\epsilon\mathbf{\Psi}$ is analytic even for $r\,\epsilon\,(0,\infty)$. In the absence of regular discrete modes, as is the case for a monotonically decreasing base-state vorticity profile, this function is, in fact, analytic on the entire complex plane. In accordance with Liouville's theorem, it must therefore be a constant. Moreoever, since $\mathbf{Q}-\epsilon\mathbf{\Psi}\to 0$ for $|r|\to\infty$, we have $\mathbf{Q}=\epsilon\mathbf{\Psi}=0$, or $\mathbf{\Psi}=\frac{\mathbf{Q}}{\epsilon}$. One may now write

$$\begin{aligned}
\Pi(r) &= \frac{\Omega'(r)}{\hat{\psi}^{\mathrm{CSM}}(r;r)}(\mathbf{\Psi}^{+}-\mathbf{\Psi}^{-}),\\
&= \frac{\Omega'(r)}{\hat{\psi}^{\mathrm{CSM}}(r;r)}\left[\frac{\mathbf{Q}^{+}}{\epsilon^{+}}-\frac{\mathbf{Q}^{-}}{\epsilon^{-}}\right],\\
&= \frac{\Omega'(r)}{\epsilon^{+}\epsilon^{-}\hat{\psi}^{\mathrm{CSM}}(r;r)}\left[\left(\frac{\epsilon^{+}+\epsilon^{-}}{2}\right)\frac{\hat{\psi}^{\mathrm{CSM}}(r;r)w_{z0}(r)}{\Omega'(r)}-\left(\frac{\epsilon^{+}-\epsilon^{-}}{2\pi i}\right)\mathcal{P}\int_0^{\infty}\frac{w_{z0}(r')\hat{\psi}^{\mathrm{CSM}}(r';r)}{\Omega(r')-\Omega(r)}dr'\right],\\
\Rightarrow \Pi(r) &= \frac{1}{\epsilon_{\mathrm{R}}^2+\epsilon_{\mathrm{L}}^2}\left\{\epsilon_{\mathrm{R}}w_{z0}(r)-\frac{\epsilon_{\mathrm{L}}}{\pi}\mathcal{P}\frac{\Omega'(r)}{\hat{\psi}^{\mathrm{CSM}}(r;r)}\int_0^{\infty}\frac{w_{z0}(r')\hat{\psi}^{\mathrm{CSM}}(r;r')}{\Omega(r')-\Omega(r)}dr'\right\}.
\end{aligned} \tag{B.12}$$

where $\epsilon_{\mathrm{R}}=(\epsilon^{+}+\epsilon^{-})/2$ and $\epsilon_{\mathrm{L}}=(\epsilon^{+}-\epsilon^{-})/2i$.

Appendix C

Constants for smooth vortex eigenfunctions

$$R_1 = ik^2 S_c A_0 \left[\frac{m}{k^2 r_c}\epsilon \,\mathrm{sgn}(r-r_c) + \frac{Z_c}{m\Omega_c'}\,\mathrm{sgn}(r-r_c)\right] \tag{C.1}$$

$$R_2 = ik^2 S_c B_0 \left[\frac{m}{k^2 r_c}(1-\epsilon)\,\mathrm{sgn}r - r_c) + \frac{Z_c}{m\Omega_c'}\,\mathrm{sgn}(r-r_c)\right] \tag{C.2}$$

$$R_3 = ik^2 S_c A_0 \left[\frac{m\epsilon}{k^2 r_c}\left(1-\frac{\alpha_1}{r_c}\right) + \frac{m}{k^2 r_c^2} + \left(\frac{m}{k^2 r_c} + \frac{Z_c}{m\Omega_c'}\right)\alpha_1 + \frac{2Z_c'\Omega_c' - Z_c\Omega_c''}{2m\Omega_c'}\right] + \frac{S_c'}{S_c} R_1 \,\mathrm{sgn}(r-r_c) \tag{C.3}$$

$$R_4 = ik^2 S_c B_0 \left[\frac{m(1-\epsilon)}{k^2 r_c}\left(\beta_1 - \frac{1}{r_c}\right) + \frac{m}{k^2 r_c^2} + \left(\frac{m}{k^2 r_c} + \frac{Z_c}{m\Omega_c'}\right)\beta_1 + \frac{2Z_c'\Omega_c' - Z_c\Omega_c''}{2m\Omega_c'}\right] + \frac{S_c'}{S_c} R_2 \,\mathrm{sgn}(r-r_c) \tag{C.4}$$

$$R_5 = iS_c A_0 \frac{m}{r_c}\,\mathrm{sgn}(r-r_c)\left\{\epsilon\left(\alpha_2 - \frac{\alpha_1}{r_c} + \frac{1}{r_c^2}\right) + 2\left(\alpha_2 - \frac{1}{r_c^2}\right)\right\} + \frac{S_c'}{S_c}\left(R_3\,\mathrm{sgn}(r-r_c) - \frac{S_c'}{S_c}R_1\right) + \frac{R_1 S_c''}{2S_c} \tag{C.5}$$

$$Q_1 = \frac{i}{k}\left[\epsilon A_0\,\mathrm{sgn}(r-r_c) + \frac{im}{r_c}R_1\right] \tag{C.6}$$

$$Q_2 = \frac{i}{k}\left[(1-\epsilon)B_0\,\mathrm{sgn}(r-r_c) + \frac{im}{r_c}R_2\right] \tag{C.7}$$

$$Q_3 = \frac{i}{k}\left[(1+\epsilon)\alpha_1 A_0 + \frac{1}{r_c^2}\left\{r_c(A_0 + imR_3) - imR_1\,\mathrm{sgn}(r-r_c)\right\}\right] \tag{C.8}$$

$$Q_4 = \frac{i}{k}\left[(2-\epsilon)\beta_1 B_0 + \frac{1}{r_c^2}\left\{r_c(B_0 + imR_4) - imR_2\,\mathrm{sgn}(r-r_c)\right\}\right] \tag{C.9}$$

$$Q_5 = \frac{i}{k}\left[(2+\epsilon)\alpha_2 A_0 + \frac{1}{r_c^3}\left\{r_c^2\left\{A_0\alpha_1\,\mathrm{sgn}(r-r_c) + im\left(R_5 + \frac{R_1 S_c''}{2S_c}\right)\right\} - r_c\,\mathrm{sgn}(r-r_c)\left\{A_0 + imR_3\right\} + 2imR_1\right\}\right] \tag{C.10}$$

where,

$$S_c = \frac{r_c^2}{m^2 + (kr_c)^2},\ S_c' = \frac{2m^2 r_c}{(m^2+(kr_c)^2)^2},\ S_c'' = \frac{2m^2(m^2 - 3(kr_c)^2)}{(m^2+(kr_c)^2)^3}$$

Appendix D

Analysis of singularities present in the 3D initial value problem

Equations 3.46 and 3.47 have several singularities but not all of them contribute to the solution in temporal domain after one performs the inverse Laplace transform. For the inverse Laplace transform one can adopt a contour as shown in figure D.1. The singularity $s = s_n$ are zeros of

$$\Delta = \frac{K'_m(ka)}{kaK_m(ka)} + \frac{J'_m(k\xi a)}{k\xi aJ_m(k\xi a)} + \frac{2im\Omega_0}{(k\xi a)^2(s + im\Omega_0)}$$

They are simple poles and constitute the discrete spectrum of vibrations of a vortex column, the 3D Kelvin modes. $F_3(0)$ has a pole at $s = -im\Omega$. The pole is of order 2 in presence of radial vorticity initial conditions. It comprises the continuous spectrum modes. To have a careful look at the singularities $s = -im\Omega_0, -i(m \pm 2)\Omega_0$ equations 3.46 and 3.47 are rewritten as

$$\underline{r < a}$$

$$\hat{u}_z = \frac{\displaystyle\int_a^\infty r' K_m(kr') F_3(0) dr' \Big/ (ka)^2 K_m(ka) - \int_0^a r' J_m(k\xi r') F_1(0) dr' \Big/ (k\xi a)^2 J_m(k\xi a) + P}{\Delta} \frac{J_m(k\xi r)}{J_m(k\xi a)} + \left[g(r) - g(a) \frac{J_m(k\xi r)}{J_m(k\xi a)} \right]$$

$$\underline{r > a}$$

$$\hat{u}_z = \frac{\displaystyle\int_a^\infty r' K_m(kr') F_3(0) dr' \Big/ (ka)^2 K_m(ka) - \int_0^a r' J_m(k\xi r') F_1(0) dr' \Big/ (k\xi a)^2 J_m(k\xi a) + P}{\Delta} \frac{K_m(kr)}{K_m(ka)} + \left[h(r) - h(a) \frac{K_m(kr)}{K_m(ka)} \right]$$

As $s \to -i(m \pm 2)\Omega_0$, $\xi \to 0$. Instead of performing the inverse transform in entirety we can explore the analyticity of the expressions above as $\xi \to 0$ by investigsting the necessary asymptotic forms. For $\xi \ll 1$,

$$\frac{J_m(k\xi r')}{(k\xi a)^2 J_m(k\xi a)} \sim O\left(\frac{1}{\xi^2}\right), \qquad \Delta \sim O\left(\frac{1}{\xi^2}\right), \qquad P \approx F_2(0)|_{r=a} \sim O\left(\frac{1}{\xi^2}\right)$$

Thus the velocity field expression outside the vortex core is analytic at $s \to -i(m \pm 2)\Omega_0$. Since the velocity field inside and outside the core cannot have different modal contributions the same can be said about the interior velocity field. To prove this one needs to consider the behaviour of $g(r)$ as $\xi \to 0$. Though $Y_m(k\xi r)$ present in $g(r)$ is singular as $\xi \to 0$ the relevant product $J_m(k\xi r')Y_m(k\xi r)$ is analytic for all $m \neq 0$. For $m = 0$, $Y_0(k\xi r)$ has a logarithmic singularity but the combined term,

$$J_0(k\xi r')Y_0(k\xi r) - Y_0(k\xi r')J_0(k\xi r)$$

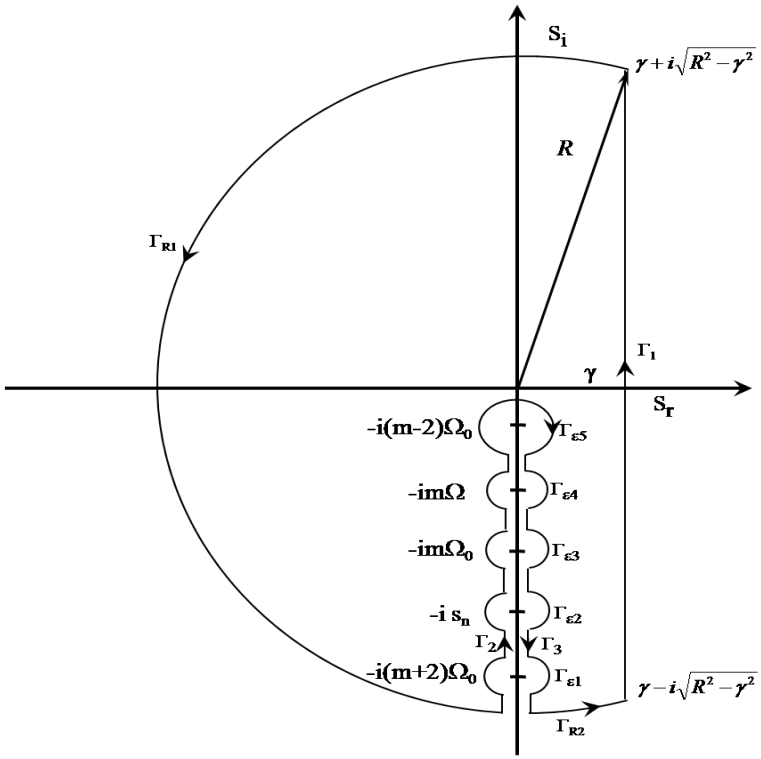

Figure D.1: Contour of integration depicting the singularities present in equations 3.46 and 3.47.

has a cancelling of the individual branch-cut contribution and thus is analytic as $\xi \to 0$.
The singularity $s = -im\Omega_0$ appears both as an essential singularity and a simple pole. Its importance stems from the fact that it serves as the accumulation point of the Kelvin modes. The latter form of the singularity owes its origin to accounting for vorticity perturbation in the exterior (the one present in P via $F_4(0)\Big|_{r=a}$). It is quite straightforward that the simple pole at $s = -im\Omega_0$ does have a contribution. To simplify matters let us focus on the exterior flow field and if we overlook the essential singularity we need to perform the following inverse transform,

$$\mathcal{L}^{-1}\frac{i}{ka}\frac{F_4(0)\Big|_{r=a}}{\Delta}\frac{K_m(kr)}{K_m(ka)} \tag{D.1}$$

Unlike poles and branch cuts, it is clearly not obvious whether the essential singularity will have a contribution to the inverse Laplace transform or not.
To consider the effect of essential singularity, $s = -im\Omega_0$, let us consider the interior velocity field,

$$\begin{aligned}
\tilde{u}_z &= \mathcal{L}^{-1}f(s) \\
&= \frac{1}{2\pi i}\left(\oint_{\Gamma_{\epsilon 2}} + \oint_{\Gamma_{\epsilon 3}} + \oint_{\Gamma_{\epsilon 4}}\right) f(s)e^{st}ds \\
\text{where, } f(s) &= \frac{\dfrac{\displaystyle\int_a^\infty r'K_m(kr')F_3(0)dr'}{(ka)^2K_m(ka)} - \dfrac{\displaystyle\int_0^a r'J_m(k\xi r')F_1(0)dr'}{(k\xi a)^2J_m(k\xi a)} + P}{\Delta}\frac{J_m(k\xi r)}{J_m(k\xi a)} + \left[g(r) - g(a)\frac{J_m(k\xi r)}{J_m(k\xi a)}\right]
\end{aligned}$$

The integrals over the contour $\Gamma_{\epsilon 2}$ and $\Gamma_{\epsilon 4}$ provides the contribution due to the discrete and the continuous spectrum respectively (refer figure D.1). To investigate the contribution of the essential singularity we need to evaluate the integral over the contour $\Gamma_{\epsilon 3}$. On performing the following change of variables, $is = m\Omega_0 + \epsilon e^{i\phi}$,

$$\oint_{\Gamma_{\epsilon 3}} f(s)e^{st}ds = H_1 + H_2$$

$$H_1 = \epsilon \int_0^{2\pi} \frac{\displaystyle\int_a^\infty r' K_m(kr')F_3(0)dr' \Big/ (ka)^2 K_m(ka) - \int_0^a r' J_m(k\xi r')F_1(0)dr' \Big/ (k\xi a)^2 J_m(k\xi a)}{\Delta} + P \frac{J_m(k\xi r)}{J_m(k\xi a)} e^{-i(m\Omega_0+\epsilon e^{i\phi})t+i\phi} d\phi$$

$$H_2 = \epsilon \int_0^{2\pi} \left[g(r) - g(a)\frac{J_m(k\xi r)}{J_m(k\xi a)} \right] e^{-i(m\Omega_0+\epsilon e^{i\phi})t+i\phi} d\phi$$

where, $\xi^2 = -1 + \dfrac{4\Omega_0^2}{\epsilon^2} e^{-2i\phi}$

we let $\epsilon \to 0$ through a sequence which does not tread the zeros of $\Delta, s = s_n$. As $\epsilon \to 0$ (the radial 'wave-number' $\xi \to \pm\infty$), $F_2(0), F_3(0)$ and $F_4(0)$ remain bounded where as $F_1(0) \sim \xi^2 ik\tilde{\omega}_z(0)/(2\Omega_0)$. Consider a bessel function, $J_m(z)$. The principal asymptotic form of $J_m(z)$ as $|z| \to \infty$ varies from an oscillatory decay $\sqrt{2/(\pi z)}\cos(z - m\pi/2 - \pi/4)$ to an exponential growth (when z is purely imaginary). Since the exponent of exponential growth is independent of the order of bessel function, the ratio of two bessel functions of different order but same argument, $J_m(z)$ and $J_n(z)$, remains bounded for $|z| \gg 1$. For the limit under consideration $J'_m(z) \sim J_{m-1}(z)$ and hence $\Delta \sim K'_m(ka)/(kaK_m(ka))$. Thus,

$$\lim_{\epsilon\to 0} H_1 = \frac{kaK_m(ka)}{K'_m(ka)} \left[\int_a^\infty \frac{r' K_m(kr')F_3(0)G_1 dr'}{(ka)^2 K_m(ka)} - \frac{\displaystyle\int_0^a r' G_2 ik\tilde{\omega}_z(0)dr'}{2\Omega_0(ka)^2} + PG_1 \right] e^{-im\Omega_0 t}$$

$$\text{where, } G_1 = \lim_{\epsilon\to 0} \epsilon \int_0^{2\pi} \frac{J_m\left(\frac{2\Omega_0 kr}{\epsilon}e^{-i\phi}\right)}{J_m\left(\frac{2\Omega_0 ka}{\epsilon}e^{-i\phi}\right)} e^{i\phi} d\phi \sim \lim_{\epsilon\to 0} \epsilon \int_0^{2\pi} \sqrt{\frac{a}{r}} \frac{\cos\left(\frac{2\Omega_0 kr}{\epsilon}e^{-i\phi} - \frac{m\pi}{2} - \frac{\pi}{4}\right)}{\cos\left(\frac{2\Omega_0 ka}{\epsilon}e^{-i\phi} - \frac{m\pi}{2} - \frac{\pi}{4}\right)} e^{i\phi} d\phi$$

$$G_2 = \lim_{\epsilon\to 0} \epsilon \int_0^{2\pi} \frac{J_m\left(\frac{2\Omega_0 kr}{\epsilon}e^{-i\phi}\right) J_m\left(\frac{2\Omega_0 kr'}{\epsilon}e^{-i\phi}\right)}{\left(J_m\left(\frac{2\Omega_0 ka}{\epsilon}e^{-i\phi}\right)\right)^2} e^{i\phi} d\phi$$

$$\sim \lim_{\epsilon\to 0} \epsilon \int_0^{2\pi} \frac{a}{\sqrt{rr'}} \frac{\cos\left(\frac{2\Omega_0 kr}{\epsilon}e^{-i\phi} - \frac{m\pi}{2} - \frac{\pi}{4}\right) \cos\left(\frac{2\Omega_0 kr'}{\epsilon}e^{-i\phi} - \frac{m\pi}{2} - \frac{\pi}{4}\right)}{\cos^2\left(\frac{2\Omega_0 ka}{\epsilon}e^{-i\phi} - \frac{m\pi}{2} - \frac{\pi}{4}\right)} e^{i\phi} d\phi$$

Thus both G_1 and G_2 approach 0 as $\epsilon \to 0$. Since P ($F_4(0)\Big|_{r=a}$ to be precise) has a pole at $s = -im\Omega_0$, PG_1 doesn't vanish as $\epsilon \to 0$. An easier way to find its contribution would be to find the inverse of $\Delta^{-1} J_m(k\xi r)/J_m(k\xi a)$, which would involve only the discrete Kelvin modes, the inverse of $-i/(ka)F_4(0)\Big|_{r=a}$ and then perform the convolution (equations 3.54-3.55). The argument for lack of contribution of the essential singularity in H_2 proceeds in identical manner

and requires us dealing again with integrals G_1 and G_2.

Appendix E

Velocity field due to a periodic cylindrical vortex sheet and its relation to that of a vortex ring

The velocity field induced by a cylindrical vortex sheet can be computed using Biot-Savart law. Moreover we will also show how the expression can be used to compute the velocity field due to a vortex ring. Consider a periodic cylindrical vortex sheet threaded by azimuthal vortex lines, $\omega_\theta = V_0 e^{ikz}\delta(r - r_1)$. By Biot-Savart law the expression for induced velocity field at point $(x', 0, z')$is,

$$\begin{aligned} \boldsymbol{u} &= \frac{1}{4\pi}\int \frac{\boldsymbol{\omega}\wedge\boldsymbol{r'}}{r'^3}dV \\ &= \frac{1}{4\pi}\int_{\partial\Omega} V_0 e^{ikz}\frac{\hat{\boldsymbol{\theta}}\wedge\boldsymbol{r'}}{r'^3}dS \end{aligned}$$

Here, $\partial\Omega$ is the surface of the vortex sheet and $\boldsymbol{r'} = (x' - r_1\cos\theta)\,\hat{\boldsymbol{x}} - r_1\sin\theta\,\hat{\boldsymbol{y}} + (z' - z)\,\hat{\boldsymbol{z}}$. If one defines $\eta = z' - z$ then expression for velocity field could be rewritten as,

$$\boldsymbol{u} = \frac{V_0 r_1 e^{ikz'}}{\pi}\int_0^\pi\int_0^\infty \frac{(r_1 - x'\cos\theta)\cos k\eta\hat{\boldsymbol{z}} - i\eta\sin k\eta\cos\theta\hat{\boldsymbol{x}}}{(r_1^2 + x'^2 + \eta^2 - 2r_1x'\cos\theta)^{3/2}}d\eta\,d\theta \tag{E.1}$$

Using the following representation of modified Bessel function of second kind (Abramowitz & Stegun [1965])

$$K_\nu(xw) = \frac{\Gamma(\nu+\frac{1}{2})(2w)^\nu}{\sqrt{\pi}x^\nu}\int_0^\infty \frac{\cos xt}{(t^2+w^2)^{\nu+\frac{1}{2}}}dt$$

we can compute the inner η integral,

$$\boldsymbol{u} = \frac{V_0 r_1 e^{ikz'}}{\pi}\int_0^\pi \left[(r_1 - x'\cos\theta)\frac{|k|}{d}K_1(|k|d)\hat{\boldsymbol{z}} - i\cos\theta\; kK_0(|k|d)\hat{\boldsymbol{x}}\right]d\theta \tag{E.2}$$

The $k = 0$ special limit (same-signed vortex lines) gives us a constant axial flow inside the sheet and quiescent fluid outside. This is the fluid-dynamical analogoue to the magnetic field induced by an infinite solenoid (Batchelor [1967]). To compute the velocity field for any arbitrary k, we need to use Graf's generalisation of Neumann's addition theorem for Bessel functions (Watson

[1927]),

$$K_\nu(\zeta)\cos\nu\psi = \sum_{m=-\infty}^{\infty} K_{\nu+m}(A)I_m(a)\cos m\theta \qquad \text{for, } |ae^{\pm i\theta}| < |A|$$

$$\text{where, } \zeta = \sqrt{A^2+a^2-2Aa\cos\theta} \qquad \text{and } \tan\psi = \frac{a\sin\theta}{A-a\cos\theta}$$

Expanding the integrand in equation E.2 in the above series one can immediately obtain the expression for velocity field,

$$\underline{r<a}$$
$$\boldsymbol{u} = V_0 r_1 e^{ikz}[|k|K_1(|k|r_1)I_0(|k|r)\hat{\boldsymbol{z}} - ikK_1(|k|r_1)I_1(|k|r)\hat{\boldsymbol{r}}] \tag{E.3}$$
$$\underline{r>a}$$
$$\boldsymbol{u} = V_0 r_1 e^{ikz}[-|k|K_0(|k|r)I_1(|k|r_1)\hat{\boldsymbol{z}} - ikK_1(|k|r)I_1(|k|r_1)\hat{\boldsymbol{r}}] \tag{E.4}$$

We have replaced z' by z and since the velocity field is axisymmetric we have replaced x' by r. The vorticity field for a vortex ring is given as,

$$\omega_{\theta,ring} = \Gamma\delta(r-r_1)\delta(z) = \frac{\Gamma}{2\pi}\int_{-\infty}^{\infty}\delta(r-r_1)e^{ikz}dk = \frac{\Gamma}{2\pi}\int_{-\infty}^{\infty}\omega_{\theta,sheet}\,dk \tag{E.5}$$

$\omega_{\theta,sheet} = \delta(r-r_1)e^{ikz}$ is the vorticity field of a periodic cylindrical vortex sheet of unit strength ($V_0 = 1$). Since $\omega_{\theta,ring}$ has a linear functional dependence on $\omega_{\theta,sheet}$ we have,

$$\boldsymbol{u}_{ring} = \frac{\Gamma}{2\pi}\int_{-\infty}^{\infty}\boldsymbol{u}_{sheet}\,dk \tag{E.6}$$

Using equations E.3 and E.4 (for $V_0 = 1$) in equation E.6 we obtain the following form of axial velocity field (the velocity-field is two-dimensional),

$$\begin{aligned} u_{ring,z} &= \frac{\Gamma r_1}{\pi}\int_0^\infty k\cos kz\; K_1(kr_1)I_0(kr)dk && r<a \\ &= -\frac{\Gamma r_1}{\pi}\int_0^\infty k\cos kz\; K_0(kr)I_1(kr_1)dk && r>a \end{aligned}$$

If we define,

$$\Pi_{in} = \int_0^\infty k\cos kz\; K_0(kr_1)I_0(kr)dk$$
$$\Pi_{out} = \int_0^\infty k\cos kz\; K_0(kr)I_0(kr_1)dk$$

then,

$$\begin{aligned} u_{ring,z} &= -\frac{\Gamma r_1}{\pi}\frac{\partial\Pi_{in}}{\partial a} && r<a \\ &= -\frac{\Gamma r_1}{\pi}\frac{\partial\Pi_{out}}{\partial a} && r>a \end{aligned}$$

Kirchhoff in 1853 obtained the following relation for integrals of Bessel functions (Watson [1927]),

$$\Pi_{in} = \int_0^\infty \cos kz \; K_0(kr_1) I_0(kr) dk = \int_0^{\pi/2} \frac{d\theta}{\sqrt{z^2 + (r+r_1)^2 - 4r_1 r \sin^2\theta}} = \Pi_{out} = \Pi \tag{E.7}$$

which provides us with the following relation,

$$u_{ring,z} = -\frac{\Gamma r_1}{\pi} \frac{\partial \Pi}{\partial a} \qquad \text{everywhere} \tag{E.8}$$

Since,

$$\Pi = \int_0^{\pi/2} \frac{d\theta}{\sqrt{z^2 + (r+r_1)^2 - 4r_1 r \sin^2\theta}} = \frac{p}{2\sqrt{r r_1}} K(p) \qquad \text{where, } p = 2\sqrt{\frac{r r_1}{z^2 + (r+r_1)^2}} \tag{E.9}$$

$K(p)$[1] is the complete elliptic integral of first kind. Combining equations E.8 and E.9 we have,

$$u_{ring,z} = \frac{\Gamma p}{4\pi r_1} \sqrt{\frac{r_1}{r}} \left[K(p) - \frac{2-p^2}{2(1-p^2)} E(p) + \frac{r_1}{2r} \frac{p^2}{1-p^2} E(p) \right] \tag{E.10}$$

The expression thus obtained is the exact expression for velocity field induced due to a vortex ring. The radial component of velocity is,

$$u_{ring,r} = \frac{\Gamma p}{4\pi r_1} \frac{z}{r_1} \left(\frac{r_1}{r} \right)^{3/2} \left[-K(p) + \frac{2-p^2}{2(1-p^2)} E(p) \right] \tag{E.11}$$

[1] Here, the definition of complete elliptic integral is the one adopted in Whittaker & Watson [1927]

$$K(x) = \int_0^{\pi/2} \frac{d\phi}{\sqrt{1 - x^2 sin^2\phi}}, \qquad E(x) = \int_0^{\pi/2} \sqrt{1 - x^2 sin^2\phi}\, d\phi$$

Appendix F

Oscillations of a Hollow Vortex

The stability of a hollow vortex column or a cylindrical vortex sheet, has been of interest to fluid dynamicists for a long time. The earliest work on the linearized dynamics of a hollow vortex can be traced to Lord Kelvin's seminal 1880 paper (Kelvin [1880]). He studied oscillations of a 'coreless' vortex that might serve as a model for a gaseous core surrounded by irrotational fluid. Waves on a coreless vortex are cylindrical analogues of surface gravity waves with centrifugal force rather than gravity providing the necessary restoring action. Such vortices were fundamental to Kelvin's theory of vortex atoms. In a letter to Professor G. F. FitzGerald (Kelvin [1889]) he wrote,

"I have quite confirmed one thing I was going to write to you (in continuation with my letter of October 26), viz. that rotational vortex cores must be absolutely discarded, and we must have nothing but irrotational revolution and vacuous cores. So not to speak of my little piece of coreless vortex work ('Vibrations of a Columnar Vortex,' *Proc. R.S.E.*, March 1,1880), Hicks' Paper, 'On the Steady Motion and small vibrations of a Hollow Vortex,' *Transactions Roy. Society*, 1884), will be the beginning of the Vortex Theory of ether and matter, if it is ever to be a theory."

'Coreless' vortices, as the name suggests ignores the core inertia and thus are not particularly useful in the geophysical context. Rather vortices with quiescent or almost irrotational cores (but inertial) are more suited as models for geophysical coherent structures. The eigenmodes of a cylindrical vortex sheet with a quiescent core was analyzed by Rotunno [1978]. Besides correcting inconsistency in previous literature, the author also mentions that multiple vortex phenomena in tornadoes could arise due to instability of cylindrical vortex sheet. Stability calculations for more realistic profiles of a vortex with a vorticity deficit in the core have also been studied in the context of tornadoes (Gall [1983]) and tropical cyclones (Kossin *et al.* [2000]). In the context of plasma physics Smith & Rosenbluth [1990] studied such an inflectional electron density (vorticity equivalent) profile and noted that, for $m = 1$, the vortex exhibits an algebraic instability with the streamfunction growing as $O(\sqrt{t})$.

In order to characterize the temporal response of a hollow vortex column, and to analyze the possibility of inviscid resonances as for the Rankine case considered in the text, we revisit the results obtained by Rotunno [1978]. The author found that a cylindrical vortex sheet, of radius a and the exterior fluid slipping past the quiescent core with an angular velocity Ω_0, supports two waves for every m and k having the following complex frequencies:

$$\omega_{3D} = m\Omega_0 k a I'_m(ka)K_m(ka) \pm i\Omega_0 ka\sqrt{I'_m(ka)K'_m(ka)\{1 - m^2 K_m(ka)I_m(ka)\}}$$

The modes $m = 1$ and 2 exhibit purely oscillatory behaviour for all wavenumbers. While $\forall m \geq 3$, there exists a critical wave-number k_c, which demarcates the unstable solutions from

the oscillatory ones. An estimate for k_c can be written as, $k_c \sim \frac{m}{2a}\sqrt{m^2-4}$. In the limit $k \to 0$, the dispersion relation simplifies to

$$\omega_{2D} = \frac{m\Omega_0}{2} \pm i\frac{\Omega_0}{2}\sqrt{m(m-2)} \tag{F.1}$$

In 2D, $m = 1$ has a pure translation mode (ω_{2D}) similar to that of a vortex column and another wave that rotates with the angular velocity of the sheet, Ω_0, and also rides on it (critical radius is at a). Thus in the linear framework it is an infinitesimal strengthening of the vortex sheet. These waves do not propagate energy and thus their three-dimensional counterparts have vanishing group velocity in the limit $k \to 0$. It is evident from (F.1) that there is a degeneracy for $m = 2$ implying an $O(t)$ algebraic growth for all time if the excitation is by a vortex sheet located at an arbitrary location. If the perturbation sheet is stationed at $\sqrt{2}a$, the critical radius, then the resonance mechanism would generate a $O(t^2)$ growth of the radial velocity field.

Due to similarity with the analysis for a vortex column, we omit the detailed expression for 3D perturbation velocity for an arbitrary initial vorticity forcing. Instead a canonical excitation is chosen, that of an arbitrarily stationed cylindrical vortex sheet, $\omega_\theta = -kr_1V_0/m\ \delta(r - r_1)e^{i(kz+m\theta)}$, $\omega_z = V_0\delta(r-r_1)e^{i(kz+m\theta)}$ $(r_1 > a)$. The axial velocity perturbations will thus obey the following evolution equations,

$\underline{r < a}$

$$\tilde{u}_z = \mathscr{C}\left\{\frac{-\alpha_1(\omega_1)e^{-i\omega_1 t}}{(\omega_1-\omega_2)(\omega_1-im\Omega_1)} + \frac{\alpha_1(\omega_2)e^{-i\omega_2 t}}{(\omega_1-\omega_2)(\omega_2-im\Omega_1)} + \frac{-\alpha_1(-im\Omega_1)e^{-im\Omega_1 t}}{(\omega_1-im\Omega_1)(\omega_2-im\Omega_1)}\right\}\frac{I_m(kr)}{I_m(ka)} \tag{F.2}$$

$\underline{r_1 > r > a}$

$$\tilde{u}_z = \mathscr{C}\left\{\frac{-\alpha_2(\omega_1)e^{-i\omega_1 t}}{(\omega_1-\omega_2)(\omega_1-im\Omega_1)} + \frac{\alpha_2(\omega_2)e^{-i\omega_2 t}}{(\omega_1-\omega_2)(\omega_2-im\Omega_1)} + \frac{-\alpha_2(-im\Omega_1)e^{-im\Omega_1 t}}{(\omega_1-im\Omega_1)(\omega_2-im\Omega_1)}\right\}\frac{K_m(kr)}{K_m(ka)} + \mathscr{C}I_m(ka)\left\{\frac{I_m(kr)}{I_m(ka)} - \frac{K_m(kr)}{K_m(ka)}\right\}e^{-im\Omega_1 t} \tag{F.3}$$

$\underline{r > r_1}$

$$\tilde{u}_z = \mathscr{C}\left\{\frac{-\alpha_2(\omega_1)e^{-i\omega_1 t}}{(\omega_1-\omega_2)(\omega_1-im\Omega_1)} + \frac{\alpha_2(\omega_2)e^{-i\omega_2 t}}{(\omega_1-\omega_2)(\omega_2-im\Omega_1)} + \frac{-\alpha_2(-im\Omega_1)e^{-im\Omega_1 t}}{(\omega_1-im\Omega_1)(\omega_2-im\Omega_1)}\right\}\frac{K_m(kr)}{K_m(ka)} + \mathscr{C}\left\{\frac{I'_m(kr_1)}{K'_m(kr_1)}K_m(ka) - I_m(ka)\right\}\frac{K_m(kr)}{K_m(ka)}e^{-im\Omega_1 t} \tag{F.4}$$

where, $\alpha_1(\omega) = -\omega(\omega - m\Omega_0)I_m(ka)$, $\alpha_2(\omega) = -\omega^2 I_m(ka) + \Omega_0^2 ka I'_m(ka)$ and $\mathscr{C} = \dfrac{V_0}{m}(kr_1)^2K'_m(kr_1)$. Thus besides the well-studied exponentially unstable modes for axial wavenumbers $k < k_c$ and $m \geq 3$, there could also be algebraic growth for a hollow vortex. Similar to a vortex column, a $\tilde{\omega}_r$ intial distribution would also lead to a $O(t^2)$ growth in velocity perturbations for a hollow vortex.

Appendix G

Dini expansion of $I_0(kr)$

For the axisymmetric case the dispersion relation reduces to,

$$\begin{aligned} & \frac{J_0'(\beta_n)}{\beta_n J_0(\beta_n)} + \frac{K_0'(k)}{kK_0(k)} = 0 \\ \Rightarrow \quad & \frac{\beta_n J_1'(\beta_n)}{J_1(\beta_n)} - \frac{kK_1'(k)}{K_1(k)} = 0 \end{aligned}$$

The latter form will enable us to borrow results of Dini expansion of a function in $(0, 1)$ (Watson [1927]). If

$$\begin{aligned} f(r) &= \sum_{n=1}^{\infty} b_n J_1(\beta_n r) \quad \text{where,} \quad b_n = \frac{2\beta_n^2 \int_0^1 x f(x) J_1(\beta_n x) dx}{(\beta_n^2 - 1) J_1^2(\beta_n) + \beta_n^2 J_1'^2(\beta_n)} \\ f(r) + r f'(r) &= \sum_{n=1}^{\infty} b_n \beta_n r J_0(\beta_n r) \end{aligned}$$

On choosing $f(r) = I_1(kr)$,

$$\begin{aligned} I_0(kr) &= \sum_{n=1}^{\infty} b_n \xi_n J_0(\beta_n r) = 2 \sum_{n=1}^{\infty} B_n^{(-1)} \frac{1}{k^2 K_0(k)} \frac{J_0(\beta_n r)}{J_0(\beta_n)} \frac{1}{i\omega_n} \\ \Rightarrow I_0(kr) &= \sum_{b \pm 1} \sum_{n=1}^{\infty} B_n^b \frac{1}{k^2 K_0(k)} \frac{J_0(\beta_n r)}{J_0(\beta_n)} \frac{1}{i\omega_n} \end{aligned}$$

References

Ablowitz, M. J. & Fokas, A. S. 2003 *Complex variables: Introduction and applications*. Cambridge University Press.

Abramowitz, M. & Stegun, I. A. 1965 *Handbook of mathematical functions with formulas, graphs and mathematical tables*. Dover.

Acheson, D.J. 1973 Hydromagnetic wavelike instabilities in a rapidly rotating stratified fluid. *J. Fluid Mech.* **61**, 609–624.

Antkowiak, A. 2005 *Dynamique aux temps courts d'un tourbillon isolé*. PhD thesis, Université Paul Sabatier.

Antkowiak, A. & Brancher, P. 2004 Transient growth for the lamb-oseen vortex. *Phys. Fluids* **16**, L1–L4.

Antkowiak, A. & Brancher, P. 2007 On vortex rings around vortices: an optimal mechanism. *J. Fluid Mech.* **578**, 295–304.

Aref, H. & Flinchem, E. P. 1984 Dynamics of vortex filament in shear flow. *J. Fluid Mech.* **144**, 477–497.

Arendt, S., Fritts, D. & Andreassen, Ø. 1997 The initial value problem for kelvin vortex waves. *J. Fluid Mech.* **344**, 181.

Arnol'd, V.I. 1972 Notes on the three-dimensional flow pattern of a perfect fluid in the presence of a small perturbation of the initial velocity field. *Journal of Applied Mathematics and Mechanics* **36**, 236–242.

Arora, K. & Khomami, B. 2005 The influence of finite extensibility on the eigenspectrum of dilute polymeric solutions. *J. Non-Newtonian Fluid Mech.* **129**, 56–60.

Azaiez, J. & Homsy, G.M. 1994 Linear stability of free shear flow of viscoelastic liquids. *J. Fluid Mech.* **268**, 37–69.

Balbus, S. A. & Hawley, J. F. 1991 A powerful local shear instability in weakly magnetized disks. i. linear analysis. *The Astrophysical Journal* **376**, 214–222.

Bale, R. 2009 *Algebraic instability and transient growth in stratified shear flows*. MS (Engg.) thesis, Jawaharlal Nehru Centre for Advanced Scientific Research.

Balmforth, N.J. 1998 Stability of vorticity defects in viscous shear. *J. Fluid Mech.* **357**, 199–224.

Balmforth, N.J. & Morrison, P.J. 1995a *Singular eigenfunctions for shearing fluids I.*. Institute for Fusion studies, University of Texas, Austin, Report No. 692.

Balmforth, N.J., Smith, S.G. Llewellyn & Young, W.R. 2001 Disturbing vortices. *J. Fluid Mech.* **426**, 95–133.

Banks, W.H.H., Drazin, P.G. & Zaturska, M.B. 1976 On the normal modes of parallel flow of inviscid stratified fluid. *J. Fluid Mech.* **75**, 149–271.

Bassom, A.P. & Gilbert, A.D. 1998 The spiral wind-up of vorticity in an inviscid planar vortex. *J. Fluid Mech.* **371**, 109–140.

Batchelor, G.K. 1967 *Introduction to fluid dynamics.*. Cambridge University Press.

Bayly, B. J., Orszag, S. A. & Herbert, T. 1988 Instability mechanisms in shear-flow transition. *Annu. Rev. Fluid Mech.* **20**, 359–391.

Bender, C.M. & Orszag, S.A. 1999 *Advanced mathematical methods for scientists and engineers.*. Springer.

Benney, D.J. & Bergeron, R.F. 1969 A new class of nonlinear waves in parallel flows. *Studies in App. Math.* **48**, 181–204.

Benney, D.J. & Lin, C. C. 1960 On the secondary motion induced by oscillations in a shear flow. *Phys. Fluids* **3**, 656–657.

Bhave, A. V., Armstrong, R. C. & Brown, R. A. 1991 Kinetic theory and rheology of dilute, nonhomogeneous polymer solutions. *J. Chem. Phys.* **95**, 2988–3000.

Bird, R. B., Armstrong, R. C. & Hassager, O. 1987 *Dynamics of polymeric liquids. Volume 1 - Fluid Mechanics.*. John Wiley and Sons.

Boldyrev, S., Hunyh, D. & Pariev, V. 2009 Analog of astrophysical magnetorotational instability in a couette-taylor flow of polymer fluids. *Phys. Rev. Lett.* **80**, 066310 (1–4).

Booker, J. R. & Bretherton, F. P. 1967 The critical layer for internal gravity waves in a shear flow. *J. Fluid Mech.* **27**, 513–539.

Boyd, J.P. 1999 The devil's invention: asymptotic, superasymptotic and hyperasymptotic series. *Acta Applicandae Mathematicae* **56**, 1–98.

Bridges, T.J. & Morris, P.J. 1984 Differential eigenvalue problems in which the parameter appears nonlinearly. *J. Comput. Phys.* **55**, 437–460.

Briggs, R.J., Daugherty, J.D. & Levy, R.H. 1970 Role of landau damping in crossed-field electron beams and inviscid shear flow. *Phys. Fluids* **13**, 421.

Broadbent, F.P. 1967 The time-dependent motion due to a cylinder moving in an unbounded rotating or stratified fluid. *J. Fluid Mech.* **28**, 545–570.

Brown, S. N. & Stewartson, K. D. 1980 On the algebraic decay of disturbances in a stratified linear shear flow. *J. Fluid Mech.* **100**, 811–816.

Case, K.M. 1959 Plasma oscillations. *Ann. Phys. (N.Y.)* **7**, 349–364.

Case, K.M. 1960 Stability of inviscid plane couette flow. *Phys. Fluids* **3**, 143.

Chandrasekhar, S. 1961 *Hydrodynamic and hydromagnetic stability*. Dover.

Charru, F. 2011 *Hydrodynamic instabilities*. Cambridge University Press.

Chomaz, J. M. 2005 Global instabilities in spatially developing flows: non-normality and nonlinearity. *Annu. Rev. Fluid Mech.* **37**, 357–392.

Coleman, B. D. & Noll, W. 1961 Foundations of linear viscoelasticity. *Rev. Mod. Phys.* **33**, 239–249.

Corbett, P. & Bottaro, A. 2000 Optimal perturbations for boundary layers subject to stream-wise pressure gradient. *Phys. Fluids* **12**, 120–130.

Craik, A. D. D. 1985 *Wave Interactions and Fluid Flows*. Cambridge University Press.

Craik, A. D. D. 2004 The origins of water wave theory. *Annu. Rev. Fluid Mech.* **36**, 1–28.

Craik, A. D. D. 2005 George gabriel stokes on water wave theory. *Annu. Rev. Fluid Mech.* **37**, 23–42.

Criminale, W.O., Lasseigne, D.G. & Jackson, T.L. 2001 Vortex perturbation dynamics. *Stud. App. Maths.* **98**, 99–120.

Davidson, P.A. 2001 *An introduction to magnetohydrodynamics*. Cambridge University Press.

Dikii, L.A. 1960 The stability of plane-parallel flows of an ideal fluid. *Sov. Phys. Dokl.* **135**, 1179–1182.

Drazin, P.G. & Reid, W.H. 1981 *Hydrodynamic stability*. Cambridge University Press.

Drazin, P.G., Zaturska, M.B. & Banks, W.H.H. 1979 On the normal modes of parallel flow of inviscid stratified fluid. part 2. unbounded flow with propagation at infinity. *J. Fluid Mech.* **95**, 681–705.

Eliassen, A., Hoiland, E. & Riis, E. 1953 *Two-dimensional perturbation of a flow with constant shear of a stratified fluid.*. Inst. Weather and Climate Res., Oslo, publ. no. 1.

Ellingsen, T. & Palm, E. 1975 Stability of linear flow. *Phys. Fluids* **18**, 487–488.

Engevik, L. 1971 A note on a stability problem in hydrodynamics. *Acta Mechanica* **12**, 143–153.

Engevik, L. 1974 The stream function within the critical layer of a shear flow in a stratified and incompressible fluid. *Acta Mechanica* **19**, 169–178.

Fabre, D. 2002 *Instabilités et instationnarités dans les tourbillons: Application aux sillages avions.*. PhD thesis, Université Paris VI.

Fabre, D. & Le Dizès, S. 2008 Viscous and inviscid centre modes in the linear stability of vortices: the vicinity of the neutral curves. *J. Fluid Mech.* **603**, 1–38.

Fabre, D., Sipp, D. & Jacquin, L. 2006 Kelvin waves and the singular modes of the lamb oseen vortex. *J. Fluid Mech.* **551**, 235–274.

Fadeev, L.D. 1971 On the theory of the stability of stationary plane-parallel flows of an ideal fluid. *Zapiski Nauch. Semin. Leningrad. Otdel. Matemat. Instit. Akad. Nauk SSSR* **21**, 164–172.

Farrell, B.F. 1984 Modal and non-modal baroclinic waves. *J. Atmos. Sci.* **41**, 668–673.

Farrell, B.F. 1987 Developing disturbances in shear. *J. Atmos. Sci.* **45**, 2191–2199.

Farrell, B.F. 1989 Optimal excitation of baroclinic waves. *J. Atmos. Sci.* **46**, 1193–1206.

Farrell, B.F. & Ioannou, P. J. 1993a Transient development of perturbations in stratified shear flow. *J. Atmos. Sci.* **50**, 2201–2214.

Farrell, B.F. & Ioannou, P. J. 1993b Stochastic forcing of the linearized navier-stokes equations. *Phys. Fluids.* **5**, 2600–2609.

Ferziger, J. H. 1965 Completeness property of solutions of the relaxation problem in kinetic theory. *Phys. Fluids.* **8**, 426–431.

Friedman, B. 1990 *Principles and techniques of applied mathematics*. Dover.

Fukumoto, Y. 2003 The three-dimensional instability of a strained vortex tube revisited. *J. Fluid Mech.* **14**, 463.

Gakhov, F.D. 1990 *Boundary value prolems*. Dover.

Gall, R.L. 1983 A linear analysis of the multiple vortex phenomenon in simulated tornadoes. *J. Atmos. Sci.* **40**, 2010.

Gel'fand, I.M. & Shilov, G.E. 1964 *Generalized Functions, Vol. 1 - Properties and Operations*. Academic Press.

Gorodtsov, V. & Leonov, A. 1967 On a linear instability of a plane parallel couette flow of viscoelastic fluids. *J. Appl. Math. Mech.* **31**, 289–299.

Gorshkov, K.A., Ostrovsky, L.A. & Soustova, I.A. 2000 Perturbation theory for rankine vortices. *J. Fluid Mech.* **404**, 1–25.

Graham, M. D. 1998 Effect of axial flow on viscoelastic taylor-couette instability. *J. Fluid Mech.* **360**, 341–374.

Graves, L.P., McWilliams, J.C. & Montgomery, M.T. 2006 Vortex evolution due to straining: a mechanism for dominance of strong, interior anticyclones. *Geophys. & Astrophys. Fluid Dyn.* **100**, 151–183.

Greenspan, H.P. 1968 *The Theory of Rotating Fluids*. Cambridge University Press.

Groisman, A. & V.Steinberg 2000 Elastic turbulence in a polymer solution flow. *Nature* **405**, 53–55.

Grosch, C.E. & Salwen, H. 1978 The continuous spectrum of the orr-sommerfeld equation. part i. the spectrum and the eigenfunctions. *J. Fluid Mech.* **87**, 33–54.

Guégan, A. 2007 *Optimal perturbations in swept leading-edge boundary layers.*. PhD thesis, École polytechnique Laboratoire d'hydrodynamique (LadHyX).

Guégan, A., Schmid, P. J. & Huerre, P. 2006 Optimal energy growth and optimal control in swept hiemenz ßow. *J. Fluid Mech.* **566**, 11–45.

Guinn, T.A. & Schubert, W.H. 1993 Hurricane spiral bands. *J. Atmos. Sci.* **50**, 3380–3403.

Haj-Hariri, H. & Homsy, G.M. 1997 Three-dimensional instability of viscoelastic elliptic vortices. *J. Fluid Mech.* **353**, 357–381.

Hardin, J.C. 1982 The velocity field induced by a helical vortex filament. *Phys. Fluids* **25**, 1949–1952.

Heaton, C.J. 2007a Centre modes in inviscid vortex flows, and their application to the stability of the batchelor vortex. *J. Fluid Mech.* **576**, 325–348.

Heaton, C.J. 2007b Optimal growth of the batchelor vortex viscous modes. *J. Fluid Mech.* **592**, 495–505.

Heaton, C.J. & Peake, N. 2006 Algebraic and exponential instability of inviscid swirling flow. *J. Fluid Mech.* **565**, 279–318.

Heaton, C.J. & Peake, N. 2007 Transient growth in vortices with axial flow. *J. Fluid Mech.* **587**, 271–301.

Held, I.M. 1985 Pseudomomentum and the orthogonality of modes in shear flows. *J. Atmos. Sci.* **42**, 2280–2288.

Hinch, E.J. 1995 *Perturbation methods.*. Cambridge University Press.

Hirota, M., Tatsuno, T. & Yoshida, Z. 2003 Degenerate continuous spectra producing localized secular instability - an example in a non-neutral plasma. *J. Plasma Physics* **69**, 397–412.

Howard, L.N. 1962 Note on a paper of john w. miles. *J. Fluid Mech.* **10**, 509–512.

Howard, L.N. & Gupta, A.S. 1962 On the hydrodynamic and hydromagnetic stability of swirling flows. *J. Fluid Mech.* **14**, 463.

Huerre, P. 2000 *Open shear flow instabilities. In 'Perspectives in Fluid Dynamics: A Collective Introduction to Current Research' (ed. G. K. Batchelor, H. K. Moffatt and M. G. Worster)..* Cambridge University Press.

Huerre, P. & Rossi, M. 1998 *Hydrodynamic instabilities in open flows. In 'Hydrodynamics and Nonlinear Instabilities' (ed. C. Godreche and P. Manneville)..* Cambridge University Press.

Ince, E.L. 1956 *Ordinary differential equations*. Dover.

Kelbert, M. & Sazonov, I. 1996 *Pulses and other wave processes in fluids*. Kluwer.

Kelvin, Lord 1880 Vibrations of a columnar vortex. *Phil. Mag.* **10**, 155.

Kelvin, Lord 1889 On the stability and small oscillation of a perfect liquid full of nearly straight coreless vortices. *Proc. R. Irish Acad.* **1**, 340.

Kerswell, R.R. 2002 Elliptical instability. *Annu. Rev. Fluid Mech.* **34**, 83.

Kevorkian, J. 2000 *Partial Differential Equations: Analytical Solution Techniques*. Springer.

Kopiev, V.F. & Chernyshev, S.A. 1997 Vortex ring eigen-oscillations as a source of sound. *J. Fluid Mech.* **341**, 19–57.

Koppel, D. 1964 On the stability of a thermally stratified fluid under the action of gravity. *J. Math. Phys.* **5**, 963–982.

Kossin, J.P., Schubert, W.H. & Montgomery, M.T. 2000 Unstable interactions between a hurricane's primary eyewall and a secondary ring of enhanced vorticity. *J. Atmos. Sci.* **57**, 3893.

Kupferman, R. 2005 On the linear stability of plane couette flow for an oldroyd-b fluid and its numerical approximation. *J. Non-Newton. Fluid Mech.* **127**, 169–190.

Lamb, H. 1932 *Hydrodynamics*. Dover.

Landahl, M.T. 1980 A note on an algebraic instability of inviscid parallel shear flows. *J. Fluid Mech.* **98**, 243–251.

Landau, L. D. & Lifshitz, E. M. 1987 *Fluid Mechanics.*. Pergamon Press.

Lansky, I.M., O'Neil, T.M. & Schecter, D.A. 1997 A theory of vortex merger. *Phys. Rev. Lett.* **79**, 1479–1482.

Larson, R.G. 1988 *Constitutive equations for polymer melts and solutions*. Butterworths.

Larson., R.G. 1992 Instabilities in viscoelastic flows. *Rheologica Acta* **31**, 213–263.

Larson, R.G. 1999 *The structure and rheology of complex fluids*. Oxford University Press.

Larson, R.G., Shaqfeh, E.S.G. & Muller, S.J. 1990 A purely elastic instability in taylor-couette flow. *J. Fluid Mech.* **218**, 573–600.

Le Dizès, S. 2000 Non-axisymmetric vortices in two-dimensional flows. *J. Fluid Mech.* **406**, 175–198.

Le Dizès, S. 2004 Viscous critical-layer analysis of vortex normal modes. *Studies in App. Math.* **112**, 315.

Le Dizès, S. & Billant, P. 2009 Radiative instability in stratified vortices. *Phys. Fluids* **21**, 096602.

Le Dizès, S. & Fabre, D. 2007 Large-reynolds-number asymptotic analysis of viscous centre modes in vortices. *J. Fluid Mech.* **585**, 153–180.

Le Dizès, S. & Lacaze, L. 2005 Non-axisymmetric vortices in two-dimensional flows. *J. Fluid Mech.* **542**, 69–96.

Leibovich, S., Brown, S.N. & Patel, Y. 1986 Bending waves on inviscid columnar vortices. *J. Fluid Mech.* **173**, 595–624.

Leibovich, S. & Ma, H.Y. 1983 Soliton propagation on vortex cores and the hasimoto soliton. *Phys. Fluids.* **26**, 3173–3179.

Lessen, M., Singh, P.J. & Paillet, F. 1974 The stability of a trailing line vortex. part i. inviscid theory. *J. Fluid Mech.* **63**, 753–763.

Lighthill, M.J. 1958 *An introduction to Fourier analysis and generalized functions*. Cambridge University Press.

Lin, C.C. 1955 *The theory of hydrodynamic stability*. Cambridge University Press.

Lin, C.C. 1961 Some mathematical problems in the theory of the stability of parallel flows. *J. Fluid Mech.* **10**, 430–438.

Lumley, J. L. 1969 Drag reduction by additives. *Annu. Rev. Fluid Mech.* **1**, 367–384.

Lumley, J. L. 1973 Drag reduction in turbulent flow by polymer additives. *J. Polym. Sci. Macromol. Rev.* **7**, 263–290.

Mack, L. M. 1976 A numerical study of the temporal eigenvalue spectrum of the blasius boundary layer. *J. Fluid Mech.* **73**, 497–520.

Marshall, J.S. 1997 The flow induced by periodic vortex rings wrapped around a columnar vortex core. *J. Fluid Mech.* **345**, 1–30.

Maslowe, S. 1986 Critical layers in shear flows. *Annu. Rev. Fluid Mech.* **18**, 405–432.

Maslowe, S. & Nigam, N. 2008 The nonlinear critical layer for kelvin modes on a vortex with a continuous velocity profile. *SIAM J. Appl. Math.* **68**, 825–843.

Matsubera, M. & Alfredsson, P.H. 2001 Disturbance growth in boundary layers subjected to free-stream turbulence. *J. Fluid Mech.* **430**, 149–168.

Mayer, E.W. & Powell, K.G. 1992 Viscous and inviscid instabilities of a trailing vortex. *J. Fluid Mech.* **245**, 91–114.

McWilliams, J.C. 1984 The emergence of isolated coherent vortices in turbulent flow. *J. Fluid Mech.* **146**, 21.

McWilliams, J.C., Graves, L.P. & Montgomery, M.T. 2003 A formal theory for vortex rossby waves and vortex evolution. *Geophys. & Astrophys. Fluid Dyn.* **97**, 275–309.

Melander, M.V. & Hussain, F. 1993 Coupling between a coherent structure and fine-scale turbulence. *Phys. Rev. E* **48**, 2669–2689.

Melander, M.V. & Hussain, F. 1994 Core dynamics on a vortex column. *Fluid Dyn. Res.* **13**, 1–37.

Michalke, A. & Timme, A. 1967 On the inviscid instability of certain twodimensional vortextype flows. *J. Fluid Mech.* **29**, 647–666.

Miles, J. W. 1961 On the stability of heterogeneous shear flows. *J. Fluid Mech.* **402**, 349–378.

Miller, J.C. 2005 *Shear flow instabilities in viscoelastic fluids.*. PhD thesis, Cambridge University Press.

Miyazaki, T. & Hunt, J.C.R. 2000 Linear and nonlinear interactions between a columnar vortex and external turbulence. *J. Fluid Mech.* **402**, 349–378.

Moet, H., Laporte, F., Chevalier, G. & Poinsot, T. 2005 Wave propagation in vortices and vortex bursting. *Phys. Fluids* **17**, 054109–1–15.

Monin, A. S. & Yaglom, A. M. 1997 *Statistical Fluid Mechanics, The Mechanics of Turbulence, New English edition vol. 1, Chapters 2 and 3.*. NASA Ames, Stanford University.

Montgomery, M.T. & Kallenbach, R.J. 1997 A theory of vortex rossby-waves and its application to spiral bands and intensity changes in hurricanes. *Q. J. R. Meteorol. Soc.* **123**, 435–465.

Morozov, A.N. & van Saarloos, W. 2005 Subcritical finite-amplitude solutions in plane couette flow of visco-elastic fluids. *Phys. Rev. Lett.* **95**, 024501–1–4.

Murdock, J. W. & Stewartson, K. 1977 Spectra of the orr-sommerfeld equation. *Phys. Fluids* **20**, 1404–1411.

Ng, C.S. & Bhattacharjee, A. 2004 Complete spectrum of kinetic eigenmodes for plasma oscillations in a weakly collisional plasma. *Phys. Rev. Lett.* **92**, 065002(1–4).

Ogilvie, G.I. & Potter, A.T. 2008 Magnetorotational-type instability in couette-taylor flow of a viscoelastic polymer liquid. *Phys. Rev. Lett.* **100**, 074503(1–4).

Ogilvie, G.I. & Proctor, M.R.E. 2003 On the relation between viscoelastic and magnetohydrodynamic flows and their instabilities. *J. Fluid Mech.* **476**, 389–409.

Orr, W.McF. 1907 Stability or instability of the steady motions of a perfect liquid and of a viscous liquid. part i: A perfect liquid. *Proc. R. Irish Acad.* **A27**, 9–68.

Pedlosky, J. 1964 An intial value problem in the theory of baroclinic instability. *Tellus* **16**, 12–17.

Phan-Thein, N. 1985 Cone and plate flow of the oldroyd-b fluid is unstable. *J. Non-Newtonian Fluid Mech.* **17**, 3744.

Pradeep, D.S. & Hussain, F. 2006 Transient growth of perturbations in a vortex column. *J. Fluid Mech.* **550**, 251.

Pradeep, D.S. & Hussain, F. 2010 Vortex dynamics of turbulence-coherent structure interaction. *Theoretical and Computational Fluid Dynamics* **24**, 265–282.

Rallison, J.M. & Hinch, E.J. 1995 Instability of a high-speed submerged elastic jet. *J. Fluid Mech.* **288**, 311–324.

Rayleigh, Lord 1945 *Theory of Sound, Vol. II*. Dover.

Reddy, S.C., P.J.Schmid & D.S.Henningson 1993 Pseudospectra of the orr-sommerfeld operator. *SIAM J. Appl. Math.* **53**, 15–47.

Renardy, M. 1992 A rigorous stability proof for plane couette flow of an upper convected maxwell fluid at zero reynolds number. *Eur. J. Mech. B* **11**, 511–516.

Renardy, M. 2008 Stability of viscoelastic shear flows in the limit of high weissenberg and reynolds numbers. *J. Non-Newtonian Fluid Mech.* **155**, 124–129.

Rotunno, R. 1978 A note on the stability of a cylindrical vortex sheet. *J. Fluid Mech.* **87**, 761.

Saffman, P.G. 1992 *Vortex Dynamics*. Cambridge University Press.

Sazonov, I.A. 1989 Interaction of continuous spectrum waves with each other and discrete spectrum waves. *Fluid Dynamics Research* **4**, 586.

Sazonov, I.A. 1996 Evolution of three-dimensional wave packets in the couette flow. *Izv., Atmos. Ocean. Phys.* **32**, 21–28.

Schecter, D.A., Durbin, D.H.D., Cass, A.C., Dritscoll, C.F., Lansky, I.M. & O'Neil, T.M. 2000 Inviscid damping of asymmetries on a two-dimensional vortex. *Phys. Fluids* **12**, 2397.

Schecter, D.A. & Montgomery, M.T. 2003 On the symmetrization rate of an intense geophysical vortex. *Dyn. Atmos. Oceans* **37**, 55–88.

Schmid, P.J. & Henningson, D.S. 2001 *Stability and transition in fluid flows*. Springer.

Schmid, P. J. 2007 Nonmodal stability theory. *Annu. Rev. Fluid Mech.* **39**, 129–162.

Shaqfeh, E.S.G. 1996 Purely elastic instabilities in viscometric flows. *Annu. Rev. Fluid Mech.* **28**, 129–185.

Sheshadri, A. 2010 *Vortex column oscillations*. JNCASR SRFP report.

Shrira, V.I. & Sazonov, I.A. 2001 Quasi-modes in boundary-layer-type flows. part 1. inviscid two-dimensional spatially harmonic perturbations. *J. Fluid Mech.* **446**, 133–171.

Shrira, V.I. & Sazonov, I.A. 2003 Quasi-modes in boundary-layer-type flows. part 2. large-time asymptotics of broadband inviscid small-amplitude two-dimensional perturbations. *J. Fluid Mech.* **488**, 245–282.

Smith, G.B. II & Montgomery, M.T. 1995 Vortex axisymmetrization: Dependence on azimuthal wave-number or asymmetric radial structure changes. *Q. J. R. Meteorol. Soc.* **121**, 1615–1650.

Smith, R.A. & Rosenbluth, M.N. 1990 Algebraic instability of hollow electron columns and cylindrical vortices. *Phys. Rev. Lett.* **64**, 649.

Spalart, P.R. 1998 Airplane trailing vortices. *Annu. Rev. Fluid Mech.* **30**, 107.

Spiegel, E.A. & Veronis, G. 1960 On the boussinesq approximation for a compressible fluid. *The Astrophysical Journal* **131**, 441–447.

Stokes, J.R., Graham, L.J.W., Lawson, N.J. & Boger, D.V. 2001 Swirling flow of viscoelastic fluids. part 1. interaction between inertia and elasticity. *J. Fluid Mech.* **429**, 67–115.

Subramaniam, G. & Nott, P.R. 2011 The fluid dynamics of swimming microorganisms and cells. *Journal of the Indian Institute of Science* **91**, 383–413.

Subramanian, G. 2011 *Microhydrodynamics with applications to multiphase flow.*. http://desktop.jncasr.ac.in/uploaded/sganesh/Stokesian_Suspensions_6.pdf.

Tabor, M. & de Gennes, P.G. 1986 A cascade theory of drag reduction. *Europhys. Lett.* **2**, 519–522.

Taylor, G.I. 1931 Effect of variation in density on the stability of superposed streams of fluid. *Proc. Roy. Soc. A* **132**, 499–523.

Townsend, A.A. 1956 *The Structure of Turbulent Shear Flow*. Cambridge University Press.

Trefethen, L.N. 2000 *Spectral Methods in MATLAB*. SIAM.

Trefethen, L.N., Trefethen, A.E., Reddy, S.C. & Driscoll, T.A. 1993 Hydrodynamic stability without eigenvalues. *Science* **261**, 578–583.

Turner, J.S. 1973 *Buoyancy effects in fluids*. Cambridge University Press.

Vallis, G.K. 2006 *Atmospheric and oceanic fluid dynamics*. Cambridge University Press.

Van Kampen, G. 1955 On the theory of stationary waves in plasmas. *Physica* **51**, 949–963.

Vanneste, J. 1996 Rossby wave interaction in a shear flow with critical levels. *J. Fluid Mech.* **323**, 317–338.

Voisin, B. 1991 Internal wave generation in uniformly stratified fluids. part 1. greens function and point source. *J. Fluid Mech.* **231**, 439–480.

Watson, G.N. 1927 *Theory of Bessel functions*. Cambridge University Press.

White, C.M. & Mungal, M.G. 2008 Mechanics and prediction of turbulent drag reduction with polymer additives. *Annu. Rev. Fluid Mech.* **40**, 235–256.

Whittaker, E.T. & Watson, G.N. 1927 *A Course of Modern Analysis*. Cambridge University Press.

Widnall, S. 1975 The structure and dynamics of vortex filaments. *Annu. Rev. Fluid Mech.* **7**, 141.

Wilson, H., Renardy, M. & Renardy, Y. 1999 Structure of the spectrum in zero reynolds number shear flow of the ucm and oldroyd-b liquids. *J. Non-Newton. Fluid Mech.* **80**, 251–268.

Yarin, A.L. 1997 On the mechanism of turbulent drag reduction in dilute polymer solutions: Dynamics of vortex filaments. *J. Non-Newtonian Fluid Mech.* **69**, 137–153.

Yih, C.S. 1980 *Stratified flows*. Academic Press.